



**UNIVERSITÄT
BAYREUTH**

Faculty of Mathematics, Physics and Informatics within the program of the
Graduate School for Mathematics and Natural Sciences (BayNAT)

**Synthesis of glutathione analogues to investigate the
enzymatic mechanism of phytochelatase by
fluorescence spectroscopy**

Dissertation

Approved by the University of Bayreuth

to obtain the degree

Doctor of natural sciences (Doctor rerum naturalium)

Submitted by

Oxana Kempf

born in Obninsk, USSR

Bayreuth 2022

The presented doctoral thesis was prepared under supervision of Dr. habil. Elisa Bombarda.

This is a full reprint of the dissertation submitted to obtain the academic degree of Doctor of Natural Sciences (Dr. rer. nat.) and approved by the Faculty of Mathematics, Physics and Informatics within the program of the Graduate School for Mathematics and Natural Sciences (BayNAT) of the University of Bayreuth.

Date of submission: 01.07.2022

Date of scientific colloquium: 04.11.2022

Acting Director: Prof. Dr. Hans Kepler

Doctoral Committee:

Dr. habil. Elisa Bombarda

1st reviewer

Prof. Dr. Rainer Schobert

2nd reviewer

Prof. Dr. Carlo Unverzagt

chairman

Prof. Dr. Matthias Breuning

member of the committee

Dedicated to my too early deceased father

“The time for action is now. It’s never too late to do something”

Antoine de Saint-Exupery

„Imagination is more important than knowledge“

„Life is like riding a bicycle. To keep your balance, you must keep moving“

Albert Einstein

Table of content

Abstract	7
Zusammenfassung	9
Abbreviations.....	11
1. Spectroscopic methods relevant for this work	13
1.1. Perrin-Jablonski Diagram.....	14
1.2. UV- Vis Absorption Spectroscopy	16
1.3. Fluorescence Spectroscopy	17
1.3.1. FRET	19
1.4. NMR Spectroscopy	20
2. Phytochelatin synthase and its substrate	24
2.1. Phytochelatin Synthase	24
2.2. Glutathione and its major Functions	26
2.3. Fluorogenic Probes.....	28
2.3.1. Dabcyl as Dark Quencher	30
3. Organic Synthesis of Peptides	33
3.1. Protecting Groups Strategy	33
3.2. Condensation Reagents for Amide Bond Formation.....	34

4. Overview of the Publications.....	37
4.1. List of Publications	37
4.2. Motivation and Synopsis.....	37
Publication [P1] HydrodabcyI: a Superior Hydrophilic Alternative to the Dark Fluorescence Quencher DabcyI.....	42
Publication [P2] Chemoselective Attachment of the Water-soluble Dark Quencher HydrodabcyI to Amino Groups in Peptides and Preservation of its Spectroscopic Properties over a wide pH Range.	43
Publication [P3] Structural and biophysical Analysis of the Phytochelatin- Synthase-like Enzyme from Nostoc sp. shows that its Protease Activity is sensitive to the Redox State of the Substrate.	44
Publication [P4] Modular synthesis of glutathione analogues to study peptidase reactions in vitro and in vivo.	46
4.3. Description of the own Contribution	49
5. Outlook	54
6. Conference Contribution as a Part of this Dissertation	56
7. Other Publications and Research Contribution outside this Dissertation	57
Acknowledgment	58
References	59
Appendix	69

Abstract

Phytochelatase (PCS) is an enzyme ubiquitous in the plant kingdom and present in numerous species of fungi and animals but not in vertebrates. It can act both as a peptidase, by cleaving off the glycine from glutathione (GSH), and as transpeptidase, by transferring the remaining γ -glutamyl-cysteine (γ EC) dipeptide onto another GSH molecule. This reaction forms the so-called phytochelatins (PCs) which play an important role in heavy metal detoxification and metal homeostasis. In addition to synthesis of PCs, PCS has also been discussed to be involved in other processes such as xenobiotic catabolism. The enzymatic mechanism has not yet been characterized in detail. Prokaryotic PCS-like enzymes show homology to the catalytic N-terminal domain of eukaryotic PCS and display mainly peptidase activity. However, mechanistic understanding is lacking and their natural functions are even less evident. The substrate of PCS is GSH, which is ubiquitous in almost all living organisms and it is the most abundant non-protein thiol in mammalian cells. Its main functions are redox activity including the constitution of the cytosolic redox buffer and redox signalling, being nucleophile for the detoxification of electrophilic toxins and cofactor for the biosynthesis of eicosanoids, steroids and iron-sulphur clusters.

In the present work, we set out to study in detail the enzymatic mechanism of the PCS-like enzyme from the cyanobacterium *Nostoc* (NsPCS) using spectroscopic methods, such as NMR, absorbance and fluorescence. Since appropriately labelled GSH derivatives as substrate analogues were not commercially available, we developed an efficient modular reaction system based on a protection group pattern that allows us to produce various derivatives of GSH. The synthesis starts from three natural amino acids each of which featuring three functional groups. The protected building blocks can be synthesized and coupled in large laboratory scale with good to excellent yields. In order to study the peptidase reaction of PCS, we synthesized a double chromophore-labelled derivative (i.e., a fluorogenic GSH probe) containing a donor-acceptor pair suitable for FRET-based fluorescence experiments. As donor, we used the commercially available bimane, which can be easily linked to the cysteine- thiol. Since the widely used quencher dabcyI is very poorly soluble in water, which is the natural medium for biological systems, we developed the hydroxylated derivative hydrodabcyI. In detailed characterization studies, we showed its superiority over the parent compound with respect to water solubility and absorption properties. As an application of the double chromophore-labelled GSH derivative, we carried out different experiments for monitoring the peptidase activity of NsPCS by increase of fluorescence.

When studying enzyme kinetics, non-cleavable substrate analogues are important to distinguish between catalysis and binding. In addition, such derivatives often act as inhibitors which can be also of pharmacological importance. We addressed this aspect by additionally preparing derivatives containing three different non-cleavable peptide bond isomers of the bond between cysteine and glycine, namely the N-methylated amide, the reduced CH₂ amino group and a ketone.

For structural characterization of NsPCS, we presented three crystal structures. Two structures were obtained from the wild-type enzyme crystallized in presence and absence of its substrate GSH. Unexpectedly, the structure obtained with GSH showed the acyl-enzyme intermediate, i.e., the γ EC dipeptide bound as thioester to the active site cysteine. The novel discovery was the presence of a second GSH molecule in this complex, bound *via* disulphide to the γ EC dipeptide. A third structure was obtained from the catalytically inactive cysteine-to-serine mutant, which was found to co-crystallize in complex with GSH without addition of GSH to the crystallization buffer. Kinetics studies measured by NMR and fluorescence confirmed on the one hand the catalytic cleavage of reduced GSH. In presence of oxidized GSSG on the other hand, stoichiometric conversion of the enzyme into the acyl-enzyme intermediate occurred leaving the complex unable for further transformations. This result infers the biological significance of PCS as a redox sensor and also implies the evolutionary emergence of phytochelatins having potentially formed at first spontaneously by an intramolecular S-N-acyl shift on the blocked acyl-enzyme intermediate.

In summary, we provide novel aspects concerning the enzymatic mechanism and function of NsPCS obtained by crystallography and NMR spectroscopy. For kinetic studies on NsPCS with fluorescence spectroscopy, we synthesized a fluorogenic probe based on its substrate GSH. The practical modular synthesis of GSH-analogues that we have developed is extremely helpful in the investigation of PCS and is expected to boost studies of many other GSH-dependent enzymes. As a part of the fluorogenic probe, we synthesized a novel water-soluble universal dark quencher hydrodabcyI, which was even patented due to its general utility.

Zusammenfassung

Phytochelatine Synthase (PCS) ist ein Enzym, welches in vielen Arten aus den Reichen der Pflanzen, Pilze und Tiere vorkommt. PCS kann sowohl Glycin von Glutathion (GSH) abspalten (Peptidase-Aktivität), als auch das resultierende γ -Glutamyl-Cystein Dipeptid (γ EC) auf ein anderes GSH- Molekül übertragen (Transpeptidase-Aktivität). Diese Reaktion bildet die sogenannten Phytochelatine, welche eine wichtige Rolle für Schwermetallentgiftung und Metallhomöostase spielen. Zusätzlich zur Synthese von Phytochelatinen hat PCS auch noch weitere Funktionen wie der Abbau von Glutathion S-Konjugaten. Der katalytische Mechanismus ist noch nicht vollständig aufgeklärt. Prokaryotische PCS-like-Proteine besitzen eine Sequenzhomologie zu der N-terminalen katalytischen Domäne von eukaryotischen PCS. Sie zeigen hauptsächlich Peptidase-Aktivität aber ihre biologische Funktion ist noch weniger eindeutig. Das Substrat von PCS ist GSH, welches ubiquitär in fast allen lebenden Organismen vorkommt und der häufigste nicht-Protein-Thiol in Säugetieren ist. Seine Hauptfunktionen sind Redoxaktivität inklusive der Rolle als cytosolischer Redox-Puffer und Redox-Signalisation; der Thiol ist Nucleophil für die Entgiftung von elektrophilen Toxinen und GSH agiert als Kofaktor in der Biosynthese von Eicosanoiden, Steroiden und Eisen-Schwefel-Komplexen.

Für die vorliegenden Studien haben wir den enzymatischen Mechanismus des PCS-like-Enzyms aus dem Cyanobacterium *Nostoc* (NsPCS) mithilfe spektroskopischer Methoden wie Absorption, Fluoreszenz und NMR untersucht. Weil passende Chromophor-markierte GSH-Derivate als Substratanaloga nicht kommerziell erhältlich waren, haben wir ein modulares System entwickelt, um verschiedene GSH-Derivate zu synthetisieren. Dabei gingen wir aus von drei Aminosäure-Hauptbausteinen, die jeweils drei funktionelle Gruppen enthalten. Die geschützten Bausteine können in großem Labor- Maßstab und in guten bis hervorragenden Ausbeuten synthetisiert, selektiv entschützt und gekoppelt werden. Um die Peptidase-Reaktion von PCS zu untersuchen, haben wir ein doppelt Chromophor- markiertes fluorogenes GSH-Derivat synthetisiert, welches ein Donor-Akzeptor-Paar für FRET-basierte Fluoreszenzmessungen enthält. Als Donor haben wir das kommerziell erhältliche Biman verwendet, welches leicht mit dem Thiol des Cysteins gekoppelt werden kann. Da der kommerziell erhältliche und häufig als Fluoreszenzlöcher eingesetzte Azofarbstoff Dabcyl sehr schlecht in Wasser löslich ist, haben wir mit Hydrodabcyl ein hydroxyliertes Derivat entwickelt. In detaillierten Charakterisierungsstudien haben wir dessen Vorteile gegenüber dem Mutterchromophor Dabcyl im Hinblick auf Wasserlöslichkeit und Absorptionsverhalten aufgezeigt. Wir beschrieben in verschiedenen Experimenten die Anwendung des fluorogenen

GSH-Derivates für die Quantifizierung der Peptidase-Aktivität von PCS durch Zunahme der Fluoreszenz.

Für die Untersuchung von Enzymkinetik sind nicht spaltbare Substratanaloga wichtig, um Bindung von Katalyse einzeln zu analysieren. Solche Analoga wirken zusätzlich oft als Inhibitor und können dadurch auch pharmakologische Bedeutung erlangen. Wir haben diesen Aspekt in unsere Synthesen eingebracht durch die Herstellung von Derivaten, die anstatt der Bindung zwischen Cys und Gly drei unterschiedliche nicht-spaltbare Peptidbindungsisostere enthalten, nämlich das N-methylierte Amid, die reduzierte CH₂-Aminogruppe und das Keton.

In einer weiteren Publikation werden drei Kristallstrukturen von NsPCS präsentiert. Das Wildtypenzym wurde kristallisiert mit und ohne sein Substrat GSH. Unerwarteter Weise zeigte die Struktur, die mit GSH erhalten wurde, das Acyl-Enzym-Zwischenprodukt, d.h. das γ EC-Dipeptid bildet einen Thioester mit dem katalytisch aktiven Cys. Die neue Entdeckung war aber die Präsenz eines zweiten GSH-Moleküls im selben Komplex, welches über eine Disulfidbrücke am γ EC-Dipeptid gebunden war. Die dritte Kristallstruktur wurde von einer katalytisch inaktiven Cys-zu-Ser-Mutante von NsPCS erhalten, die interessanterweise mit GSH ko-kristallisierte, ohne Zugabe von GSH zum Kristallisationspuffer. Kinetikmessungen mittels NMR und Fluoreszenz bestätigten die katalytische Spaltung von reduziertem GSH. In Gegenwart von oxidiertem GSSG jedoch, erfolgte die quantitative Umsetzung des Enzyms zu einem stabilen Acyl-Enzym-Zwischenprodukt, welches nicht weiter reagierte. Dieses Ergebnis legte die biologische Bedeutung von PCS als Redox-Sensor nahe und lieferte auch einen Hinweis auf die evolutionäre Entstehung von Phytochelatinen, die sich erstmals spontan durch eine intramolekulare S-N-Acylverschiebung am blockierten Acyl-Enzym-Zwischenprodukt gebildet haben könnten.

Zusammenfassend werden neue Aspekte betreffend des enzymatischen Mechanismus und der Funktion von NsPCS vorgestellt, die mittels Protein-Kristallstruktur und NMR-Spektroskopie erhalten wurden. Um Kinetikstudien von NsPCS mittels Fluoreszenzspektroskopie zu ermöglichen, wurde eine fluorogene Sonde auf Basis des Substrates GSH synthetisiert. Die modulare Synthese von GSH-Analoga, die wir entwickelt haben, ist sehr hilfreich für Untersuchungen an PCS und kann auch die Studien an vielen anderen GSH-abhängigen Enzymen vorantreiben. Als Teil dieser fluorogenen Sonde haben wir einen neuen wasserlöslichen universellen Fluoreszenzlöcher synthetisiert, welcher aufgrund seiner allgemeinen Nützlichkeit sogar patentiert wurde.

Abbreviations

A	acceptor
ATR	attenuated total reflectance
Bn	benzyl
Boc	<i>tert</i> -Butyl-oxy-carbonyl
Boc ₂ O	Di- <i>tert</i> -Butyl-dicarbonat
br	bright signal
BuLi	<i>n</i> -Butyllithium
C ^q	quaternary carbon atom
D	donor
d	doublet
DCC	N,N'-Dicyclohexylcarbodiimide
DCM	dichlormethane
dd	doubled dublett
DMAP	N,N-Dimethylaminopyridine
DMF	N,N-Dimethylformamide
dq	doubled quartet
EDC*HCl	1-ethyl-3-(3-dimethylaminopropyl)carbodiimid- hydrochloride
EI	elektron ionisation
Eq	equivalent
Et	ethyl
Et ₂ O	diethylether
EtOAc	ethyl acetate
EtOH	ethanol
Fmoc	fluorenyl-methoxy-carbonyl
FRET	fluorescence resonance energy transfer
GSH	glutathione
h	hour
HOBT	1-hydrohybenzotriazole
HONSu	N-hydroxysuccinimide
HV	high vacuum
Hz	Hertz
IC	Internal Conversion
IR	infrared

ISC	Intersystem Crossing
<i>J</i>	coupling constant
Lit.	literature
m	multiplett
min	minute
mL	milliliter
mmol	millimol
MS	mass spektrometrie
NEt ₃	triethylamin
NMR	nuclear magnetic resonance
PCS	phytochelatine synthase
PCs	phytochelatins
ppm	parts per million
Q	quencher
q	quartett
qn	quintett
r.t.	room temperature
R _f	retention faktor
s	singulett
T	temperature
<i>t</i>	<i>tert</i>
t	triplett
T ₃ P	2,4,6-Tripropyl-1,3,5,2,4,6-trioxatriphosphorinane-2,4,6-trioxide
<i>t</i> Bu	<i>tert</i> -Butyl
TFA	trifluoroacetic acid
THF	tetrahydrofurane
TIPS	triisopropylsilyl
TLC	thin layer chromatography
TMS(E)	trimethyl-silyl(ethyl)
UV	ultraviolett
γEC	γ-Glutamyl-Cysteine
λ _{em}	emission wavelanght

1. Spectroscopic methods relevant for this work

Spectroscopy is a branch of physics, which studies the interactions between electromagnetic radiation and matter as a function of wavelength or frequency, i.e., energy. In molecular spectroscopy the matter consists in molecules. From the interpretation of electromagnetic spectra, information can be obtained about the structure of molecules or interactions between them¹. The energy of electromagnetic radiation is inversely proportional to its wavelength and is described by the equation (1):

$$E = h \cdot \nu = h \cdot \frac{c}{\lambda} \quad (1)$$

Where, E is the energy of the light, h is the Planck's constant (elementary quantum of action $6.62607004 \cdot 10^{-34} \text{ m}^2 \cdot \text{kg} \cdot \text{s}^{-1}$), ν is the frequency, c is the velocity of light (the distance light travels in vacuum $299792458 \text{ m} \cdot \text{s}^{-1}$) and λ is the wavelength.

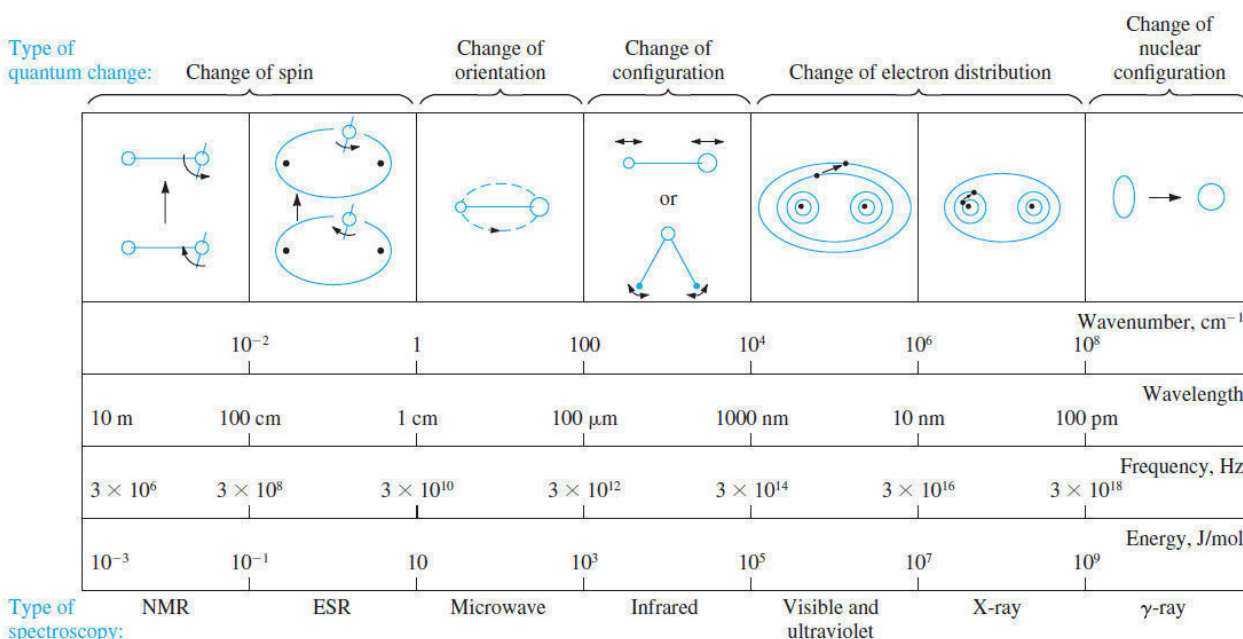


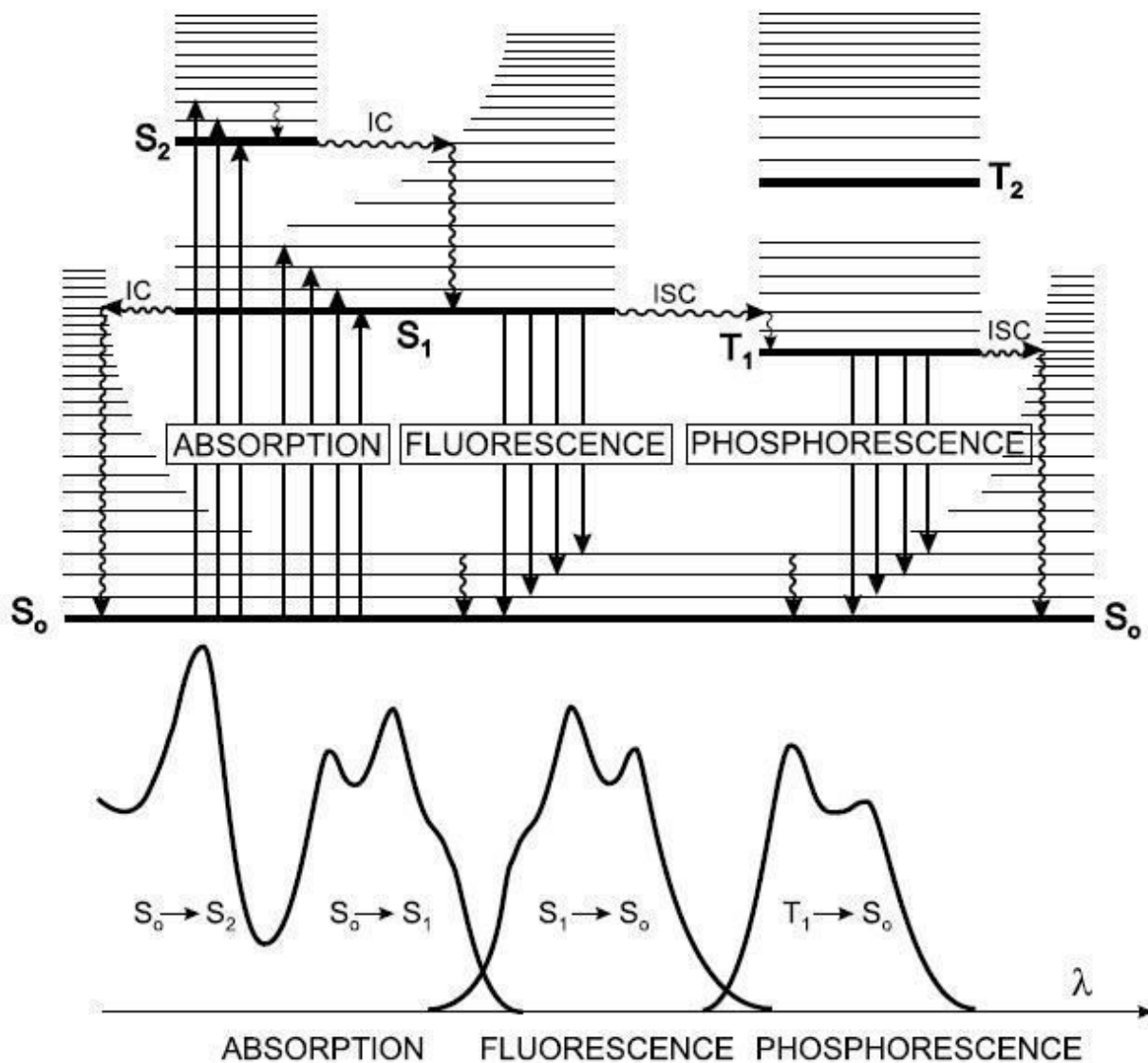
Figure 1. The electromagnetic spectrum and related spectroscopic techniques². The change of orientation is also called rotation and the change of configuration is also called vibration. The change of electron distribution concerns the transitions of electrons between different orbitals.

Figure 1 shows an overview of the electromagnetic radiation classified according to the energy content and the associated molecular processes at the basis of the different spectroscopic techniques. Spectroscopic methods in the region of visible, ultraviolet (UV) and infrared (IR) radiation are usually called optical methods even if the human eye is not sensitive to UV or IR radiation³.

Depending on the nature of the interaction of the electromagnetic irradiation with the matter, spectroscopy is divided in different types. The types that have been used in this work are: absorption (commonly in UV-Vis), emission (e.g. fluorescence), elastic scattering or reflection (e.g. X-ray crystallography), and nuclear spectroscopy (e.g. NMR)⁴. Nowadays, spectroscopy has important and powerful applications in physics, chemistry, astronomy, biology and medicine. During my work, I was actively involved in the experiments in which absorption, fluorescence and NMR spectroscopy played a central role. Therefore, these techniques are described in the following sections with more details.

1.1. Perrin-Jablonski Diagram

The specific effects of the interaction of UV/Vis-light with molecules concerning absorbance, fluorescence and phosphorescence can be illustrated in the Perrin-Jablonski diagram (Figure 2). For these processes the electronic states and associated vibrational energy levels of a molecule as well as the transitions between them are represented schematically.



CHARACTERISTIC TIMES	
absorption	10^{-15} s
vibrational relaxation	10^{-12} - 10^{-10} s
lifetime of the excited state S_1	10^{-10} - 10^{-7} s → fluorescence
intersystem crossing	10^{-10} - 10^{-8} s
internal conversion	10^{-11} - 10^{-9} s
lifetime of the excited state T_1	10^{-6} -1 s → phosphorescence

Figure 2. Perrin-Jablonski diagram to visualize absorbance, fluorescence and phosphorescence. The electronic singlet states are noted by S_0 (ground state), S_1 (first excited state) and S_2 (second excited state); the triplet excited states are noted with T_1 and T_2 . Horizontal lines show transition between vibrational levels. In addition, the spectra associated to each process are sketched in the central part and the characteristic timescales are given in the box at the bottom⁵.

At room temperature, the electrons of most of the molecules exist in the lowest vibrational level of the ground electronic state (S_0). After absorption of the photon, the electron rises to higher energy levels (excited states S_1 and S_2); this process is very fast (10 fs). The electron can then

return to the lowest energy S_0 by radiative, e.g., fluorescence, phosphorescence, and non-radiative processes, e.g., vibrational relaxation, Internal Conversion (IC), Intersystem Crossing (ISC). After excitation to a higher vibrational level of S_2 , the lowest vibrational excited electronic state S_2 can be reached through non-radiative vibrational-relaxation process. The Internal Conversion (IC) is a non-radiative transition between two excited states with spin conservation, e.g., from the lowest vibrational in S_2 to a vibrational level of the same energy in S_1 . The excess of vibrational energy is dissipated as heat without emission of photons due to collision of the molecule with solvent molecules to reach the lowest vibrational level of S_1 . Intersystem Crossing (ISC) involves instead a reversion of the electronic spin. In this case, the electron passes through a non-radiative transition from the lowest vibrational excited singlet state into a vibrational level with the same energy in the triplet state. ISC is theoretically forbidden, but the spin-orbit coupling can be large enough to make it possible.

1.2. UV-Vis Absorption Spectroscopy

In absorption spectroscopy, the amount of light absorbed by molecules is measured by quantification of the radiation that is transmitted through the sample (Figure 3).

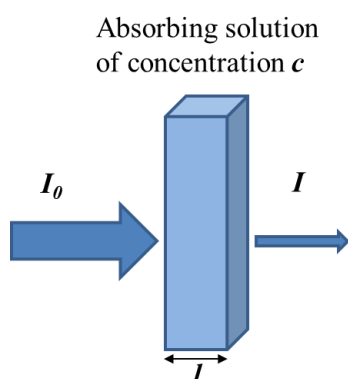


Figure 3. Schematic representation of the principle of absorbance measurement. The larger arrow on the left represents a higher incident light intensity I_0 and the smaller arrow on the right represents the lower intensity of the light I transmitted by the solution. The optical path length of the light in the solution is l and the concentration of absorbing molecules in the solution is c [picture freely modified from Skoog al. ³].

From the transmittance T of a solution, the absorbance A can be calculated with a logarithmic dependence, described in equation (2):

$$A = -\log T = -\log \frac{I(\lambda)}{I_0} = \log \frac{I_0}{I(\lambda)} \quad (2)$$

T can also be expressed as the quotient of the light intensity before passing the sample I_0 and the wavelength dependent measured intensity after passing through a sample $I(\lambda)$.

This measured intensity depends also on the concentration and the nature of the absorbing molecule as described by Lambert-Beer's law, which is the basic rule for absorption spectroscopy:

$$I(\lambda) = I_0 \cdot e^{-\varepsilon(\lambda) \cdot c \cdot l} \quad (3)$$

where ε is the attenuation coefficient also called molar absorbance ($M^{-1} \cdot cm^{-1}$), c is the molar concentration (M). Depending on those parameters, the absorbance of light can also be written as follows:

$$A(\lambda) = \log\left(\frac{I_0}{I(\lambda)}\right) = \varepsilon(\lambda) \cdot c \cdot l \quad (4)$$

In UV-Vis spectroscopy, the phenomenon of absorbance at the molecular level is caused by the transition of electrons from a lower-energy state to a higher energy (excited) state. A photon is absorbed, if the energy of radiation equals the difference in energy between two energy levels.

If the absorption of a molecule takes place in the UV/Vis region, the molecule is called chromophore.

1.3. Fluorescence Spectroscopy

The emission of the light from any substance is called generally luminescence. There are many different types of luminescence, depending on the excitation source. When the energy is provided by light, we deal with photoluminescence. Photoluminescence can be divided in two different types: fluorescence and phosphorescence. The radiative transition from the lowest vibration excited singlet state to the ground state $S_1 \rightarrow S_0$ with emission of a photon is called *Fluorescence*. The radiative transition from the lowest triplet state T_1 to the ground state S_0 with emission of a photon is called *phosphorescence*. The time spent in the excited state is called lifetime τ^5 . In contrast to phosphorescence (time range μs to s), the fluorescence lifetime is shorter (in the range of ps to ns)⁶.

A fluorescent molecule is called fluorophore. Typical fluorophores are aromatic compounds. In general fluorescence is observed at larger wavelengths than the ones used to excite the fluorophore. This principle is called Stokes shift. As can be seen in the Jablonski diagram (Figure 2), an electron excited to a higher vibrational level of the excited state S_1 relaxes very fast to the lowest vibrational level of S_1 . Fluorescence occurs when the excited electron returns from S_1 to the ground state S_0 . In analogy to the excitation process, the electron can return to higher vibrational levels and loose the energy by transfer of thermal energy to the surrounding until the lowest vibrational level is reached. This vibrational relaxation causes the emitted light

to possess less energy in comparison to absorbed light and thus a longer wavelength. Besides these main effects, excitation energy can be lost due to solvent effects, complex formation, excited-state reactions or energy transfer.

Fluorescence spectral data are characterised by excitation and emission spectra. A fluorescence emission spectrum is a plot of the fluorescence intensity in function of the wavelength (nm). The emission spectrum is generated by excitation of the fluorophore at a single wavelength (usually at maximum of absorption) while scanning through the emission wavelengths. An excitation spectrum is generated by scanning through the absorption spectrum of a fluorophore while recording the emission intensity at a single wavelength (usually at maximum of emission intensity). In general, the fluorescence spectrum is independent of the excitation wavelength, since excitation to higher excited states or higher vibrational levels of S_1 leads to a rapid loss of energy (ps) and the molecule reaches the lowest vibrational level of S_1 from where fluorescence occurs. For most fluorophores the emission spectra are symmetrical to the band from the S_0 to the S_1 of the excitation spectra, but not to the total absorption spectrum (Figure 4).

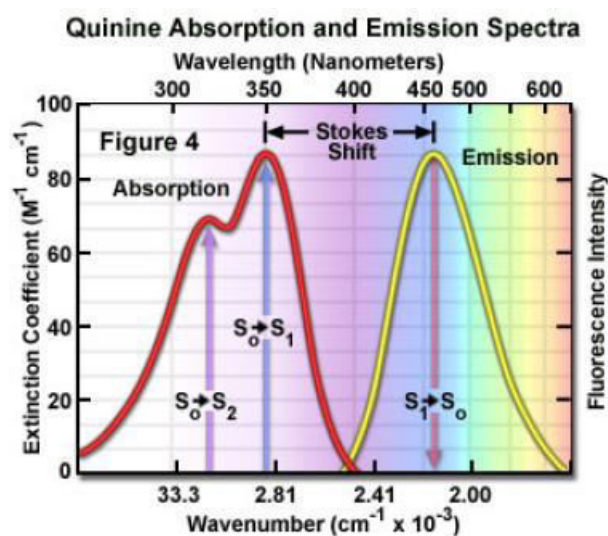


Figure 4. Mirror-image principle and, measured absorbance and emission spectra of Quinine⁷.

This effect is called mirror image principle and is based on the Franck-Condon principle⁶, which takes into account the probability of transitions from the S_0 ground state to different vibrational levels of S_1 (Figure 2). In other words, (1) some transitions are more probable leading to a higher intensity and vice versa. The vibrational energy levels of S_0 have comparable spacing according to S_1 and the distribution of the electrons over these vibrational levels after excitation to S_1 is the same as the distribution after return to S_0 . For this reason, the structure of the emission spectrum displays mirror symmetry to the absorption spectrum and is specific for each molecule.

The fluorescence quantum yield (Φ) quantifies the efficiency of the fluorescence process and is therefore an important characteristic of the fluorophore. This value is defined as the ratio of the number of emitted photons to the number of absorbed photons:

$$\Phi = \frac{\text{Emitted photons}}{\text{Absorbed photons}} \quad (5)$$

Fluorescence is very sensitive to the local environment around the fluorophore and solvent polarity, which makes it a very versatile tool, with many applications in biochemistry and medicine, *in vitro* and *in vivo*.

1.3.1. FRET

Resonance energy transfer (RET) is a physical phenomenon describing a non-radiative transfer of energy from the excited state of a donor (D) molecule to the ground state of the acceptor (A) chromophore through long-range dipole-dipole interactions (Figure 5a). In contrast to the donor, the acceptor molecule is not necessarily fluorescent. After absorbing the photon (in blue) the donor molecule is excited, but instead of emitting fluorescence (in green) the donor energy is transferred (dashed line) to the acceptor chromophore, which becomes excited by following fluorescence (in red). The energy is transferred by resonance and no photon emission/reabsorption occurs. Accordingly, in the widespread acronym FRET the letter F should not stay for “Fluorescence”, but for T. Förster, who provided the quantitative description of the mechanism of energy transfer in case of very weak coupling. Among the different mechanisms of the RET, Förster resonance energy transfer (FRET) is the most common in solution.

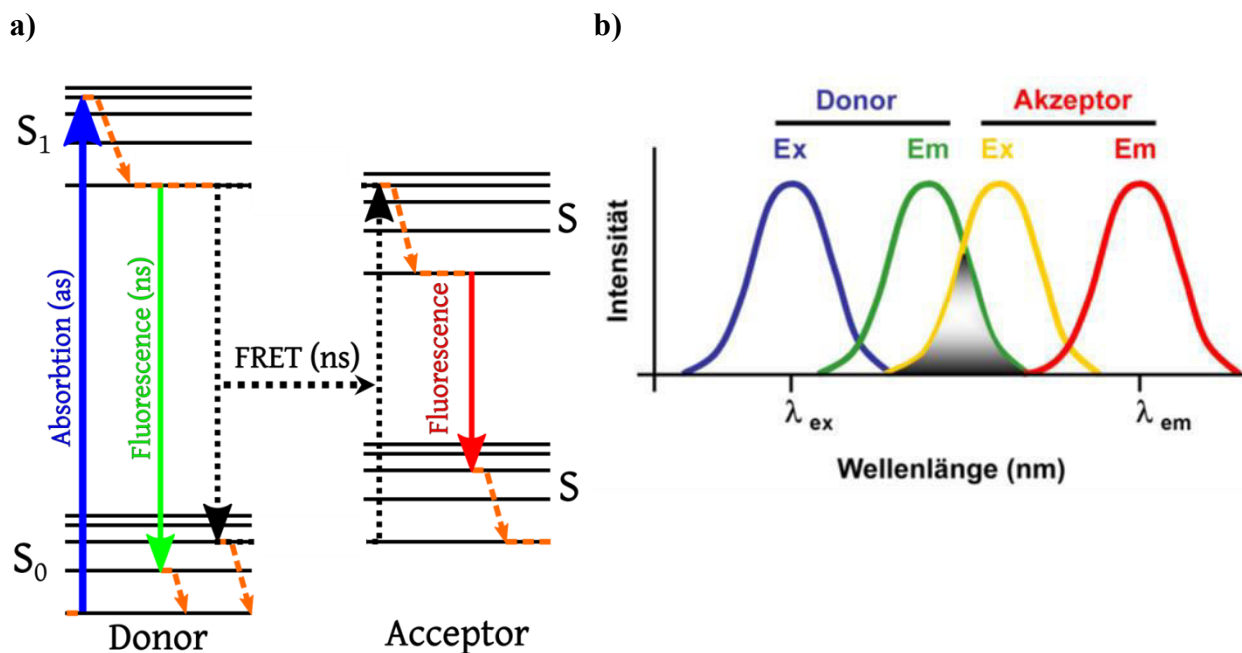


Figure 5. a) The principle of RET as a Jablonski diagram⁸ and **b)** the general conditions for RET⁹, which can only occur if the emission spectrum of the donor (in green) overlaps with the excitation spectrum of acceptor (in yellow), the overlap is shown in grey.

The essential condition for RET is the overlap of the absorption spectrum of A with the emission spectrum of D (Figure 5b), such a pair of molecules is called donor/acceptor pair. RET from donor to acceptor depends on a distance of typically 10 to 100 Å. Relative orientation of transition dipoles of donor/acceptor pair is another important aspect and should be approximately parallel for efficient transfer.

In FRET the rate of energy transfer ($k_T(r)$) from the donor to an acceptor is:

$$k_T(r) = \frac{1}{\tau_D} \left(\frac{R_0}{r} \right)^6 \quad (6)$$

where r is the distance between D and A, τ_D is lifetime of the donor in absence of the acceptor FRET, R_0 is the Förster distance¹⁰ at which the half of energy is transferred. The Förster distance is in the range 10 to 90 Å, which is comparable in size to biological macromolecules and the thickness of biological membranes. Therefore, changes of distance due to conformational changes or to the binding of a substrate can be extensively studied by FRET¹¹. The application area of FRET is broad, including biochemical experiments, biomedical diagnostics, DNA analysis, optical imaging and drug discovery.

1.4. NMR Spectroscopy

Nuclear Magnetic Resonance Spectroscopy (NMR) is a very powerful technique to analyse the structure of small molecules or even macro molecules (usually until 35 kDa¹²). The principle of

NMR will be explained in this chapter on the example of ^1H -NMR. Experimentally, the important prerequisite is the application of two magnetic fields. In the ground state without influence of a magnetic field, all spins of the protons are oriented randomly into all directions. When the sample is placed into the strong and permanent magnetic field (B_{ext} in Figure 6) generated by a superconducting electric coil, all spins are aligning either parallel or antiparallel to B_{ext} . Then, a weak magnetic field in the radio-frequency range is induced as a short pulse by the transmitter coil (induction). This pulse is able to excite the protons spinning with a resonant frequency resulting in spin reversion. After the pulse, the spin of the excited protons is returning to the ground state (relaxation). The liberated energy by the relaxation is recorded by the detector coil as free induction decay (FID). The relaxation frequency of each proton in the FID is converted by Fourier Transformation to depict the intensity of the induction signals as a function of the respective frequencies in a conventional ^1H -NMR spectrum¹³ (Figure 6).

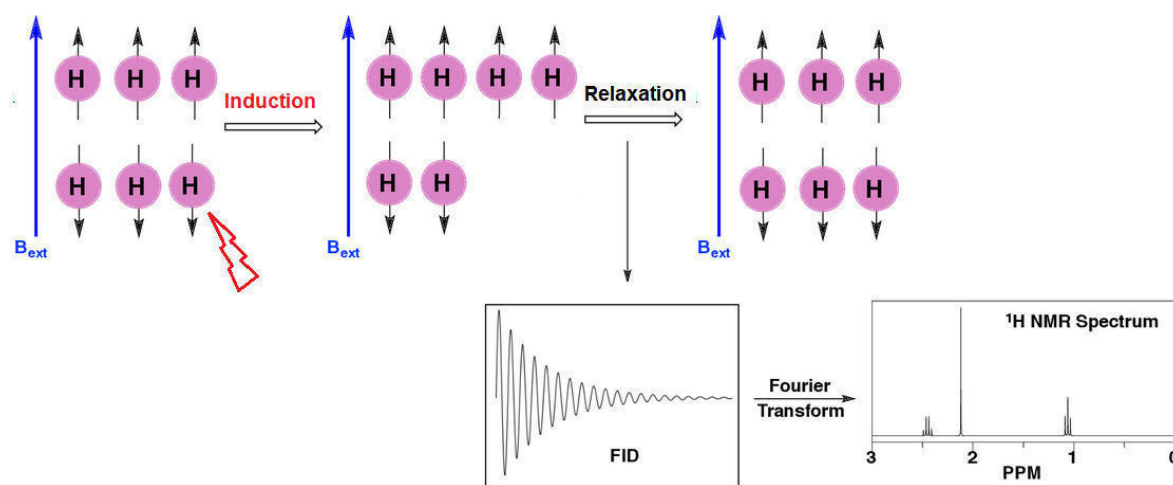


Figure 6. Schematic representation of the generation of ^1H -NMR spectra [picture freely modified from Mazumder et al.¹³]

The intensity is depending on the number of the excited protons and can be quantified from the spectrum *via* the area (integral) under the corresponding peak. The frequency of each signal on the x-axis is commonly expressed as the chemical shift δ in ppm (parts per million), in order to display a value independent from the spectrometer frequency. The chemical shift is the central metric for substance characterization. δ is not an absolute value, but determined relatively to the peak of the reference substance tetramethylsilane (TMS), which is standardized to 0 ppm. The reason why the protons display different chemical shifts resides in the type of its electronic surrounding. The electron density of neighbouring functional groups is shielding the excited proton from the pulse field resulting in different chemical shifts (Figure 7) depending on the ability of groups to donate (shielding) or to withdraw (deshielding) electron density.

Deshielded protons are thus more sensitive to excitation, i.e., showing resonance at lower field (“downfield shift”) than more shielded ones (“upfield shift”).

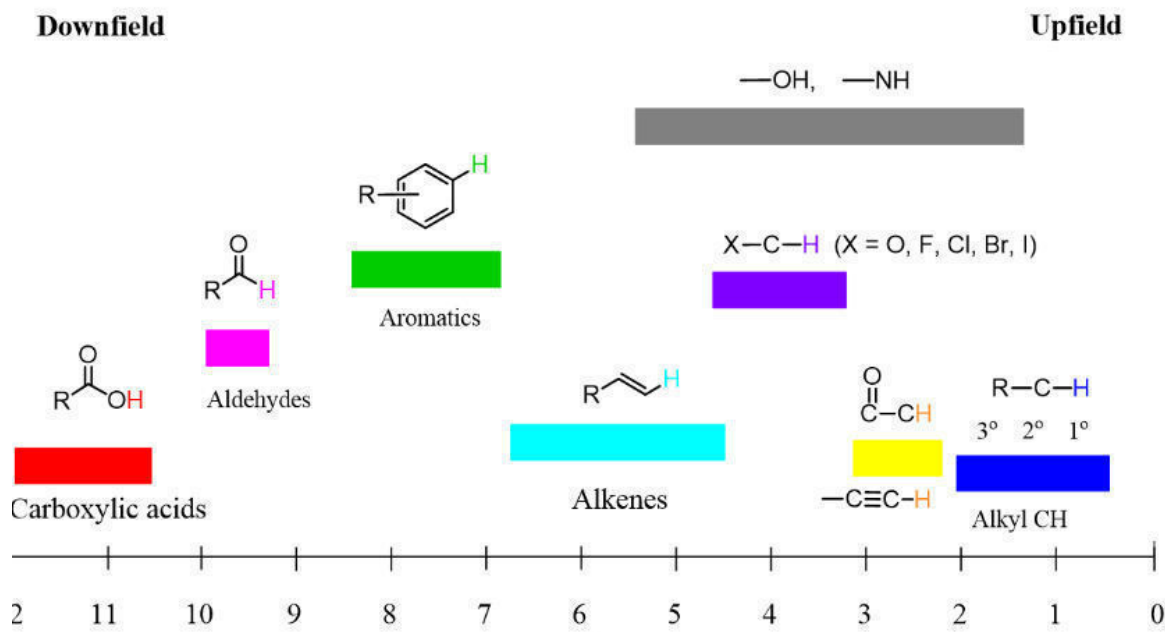


Figure 7. Chemical shift of proton signal according to the neighbouring functional groups¹⁴.

Each proton generates its own magnetic field influencing its neighbours through spin-spin coupling (J coupling). The field of each neighbouring proton is either parallel to the external field resulting in stronger field acting on the respective excited proton ($B_{\text{ext}} + B_{\text{neighbour}}$) or antiparallel to the external field thus decreasing its intensity ($B_{\text{ext}} - B_{\text{neighbour}}$). The interaction between the respective excited proton and one neighbour can be quantified by the difference between the two signals resulting from resonance at $B_{\text{ext}} + B_{\text{neighbour}}$ and $B_{\text{ext}} - B_{\text{neighbour}}$. This splitting of signals is called multiplicity. In general, the actual field influencing an excited proton is the sum of the fields of all neighbours n plus the pulse field resulting in a multiplicity $n+1$.

Since NMR spectra are usually recorded in solution and the solvent is present in much higher concentrations than the analysed substance, the large solvent signal would often cover signals from the analysed substance. In order to measure only the analysed molecule in solution, but not the solvent, deuterated solvents are used for ^1H -NMR spectroscopy. The reason is that only nuclei with a total spin number $\neq 0$ are detectable by NMR spectroscopy. Analogously to ^1H , other atoms with unpaired numbers of protons are commonly analysed by NMR, such as ^{13}C , ^{31}P , or ^{15}N . For a detailed analysis and a better resolution of complex molecules, 2D NMR experiments can be performed. In general, 2D NMR experiments correlate proton with proton or proton with carbon spectra. Analogously to the J-coupling, the 2D correlations are based on

the magnetic interactions between different protons. Besides being a crucial tool for analysing the structure of the small molecules during organic synthesis and to determine the tertiary structure of proteins from multiple 2D spectra, NMR can be used to study enzymatic kinetics^{15,16}, as it will be illustrated in this work.

2. Phytochelatin synthase and its substrate

2.1. Phytochelatin Synthase

Enzymes are proteins which catalyse specific reactions. In general, a chemical reaction consists in the conversion of reactants into products. In case of enzymatic reactions, the reactant is called substrate of that specific enzyme. Enzymes catalysing the hydrolysis of peptide bonds have been originally called proteases. This term is nowadays often replaced by the more evocative term “peptidase”. Accordingly, the term peptidase will be used in this work.

Phytochelatin synthase (PCS) is an important member of the papain-like cysteine peptidase family characterized by a catalytic triad consisting of three amino acid residues: cysteine, histidine and aspartate (asparagine in papain). The catalytic triad is highly conserved because it is crucial for the enzymatic activity¹⁷.

PCS is found in several eukaryotic organisms. It is ubiquitous in the plant kingdom¹⁸ and PCS genes have been found in yeasts and some invertebrates such as nematodes¹⁹, but not in vertebrates. PCS is able to synthesise thiol-rich non-ribosomal peptides, the so-called phytochelatins. Since phytochelatins have a strong capacity for metal complexation, they are important biomolecules for the detoxification of heavy metals like Cd²⁺, As³⁺, Hg²⁺, Pb²⁺ and homeostasis of essential metals like Zn²⁺, Cu²⁺, Fe²⁺^{20,21,22,23}.

The substrate of PCS is the tripeptide glutathione γ -Glu-Cys-Gly (GSH), where PCS specifically cleaves the peptide bond between cysteine and glycine. This reaction takes place by nucleophilic attack of the active-site cysteine thiol to the carbonyl atom of the cysteine in GSH (right upper corner in Figure 8a). By releasing glycine, the remaining γ -glutamyl cysteine dipeptide (γ -EC) is bound to the active-site cysteine thiol forming a thioester (acylation of the enzyme). The similarity to cysteine peptidases²⁴ seems to be obvious at the first glance, but the function of PCS is more complex.

In addition to the hydrolysis of GSH, PCS can transfer the γ -EC dipeptide onto another GSH molecule. This transpeptidase activity generates the phytochelatins (PCs, Figure 8b) with the general structure $(\gamma\text{-GluCys})_n\text{Gly}$, where n is usually not more than 5, but can be between 2 and 11²⁵. Due to the presence of different GSH analogues in some plant species, corresponding PC derivatives exist, where glycine is replaced by serine²⁶, glutamate²⁷, glutamine²⁸, or β -alanine²⁹.

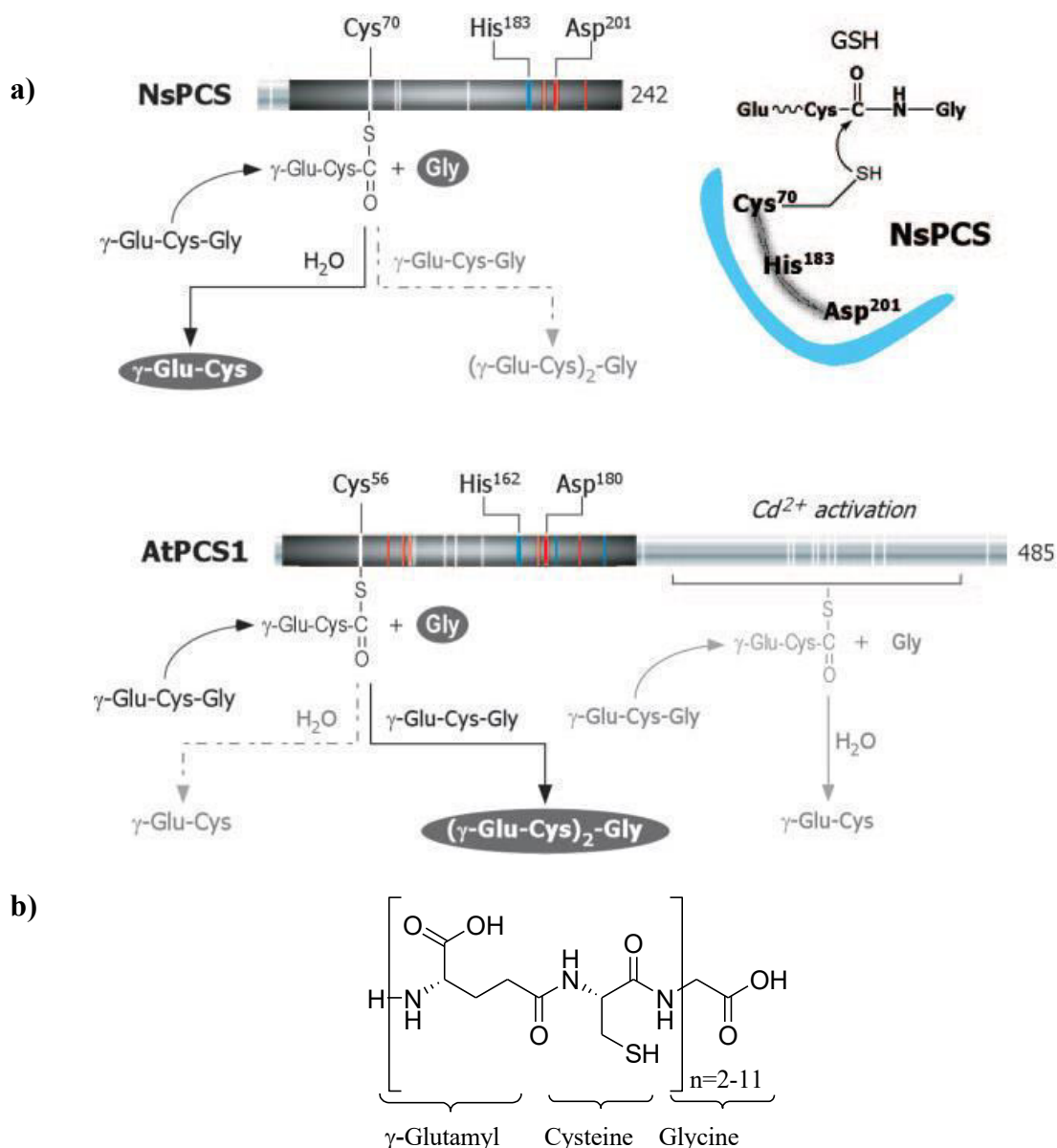


Figure 8. a) Comparison between PCS-like enzyme from cyanobacterium *Nostoc* (*NsPCS*, upper) and PCS enzyme from *Arabidopsis thaliana* (*AtPCS1* down). *NsPCS* and *AtPCS1* are similar in N-terminal domain with the catalytic triad consisting of the amino acids Asp, His and Cys-70. The dark arrows show the main catalytic activities, for *NsPCS* peptidase and for *AtPCS1* transpeptidase activity³⁰; **b)** The general structure of phytochelatins (PCs).

Eukaryotic PCS enzymes contain a conserved N-terminal catalytic domain and a more variable C-terminal domain (*AtPCS1*, Figure 8a) which has regulatory function involved in the Cd^{2+} activation of PCs synthesis³¹. This regulatory function is still not completely characterized, since truncated proteins lacking the C-terminal domain still possess Cd^{2+} dependent transpeptidase activity¹⁷, yet with a lower rate. After all studies, the dual enzymatic activity remains still subject of controversial discussions^{32,33,34} and waits for more detailed characterization.

In prokaryotes, proteins have been found, which show a sequence homology to the N-terminal domain of PCS, but lack the C-terminal domain. The 22-36 % sequence identity and around

50 % sequence similarity are quite low, but no other proteins have been found with a significant homology. Consequently, a phylogenetic and functional correlation was inferred leading to the denomination of PCS-like enzymes. In the present work, we concentrate on the PCS-like enzyme from the cyanobacterium *Nostoc* (NsPCS), which contains among the conserved residues the catalytic triad consisting of Cys70, His183 and Asp201 as confirmed by crystal structures³⁵. PCS-like enzymes are able to cleave the glycine from glutathione, but produce oligomeric phytochelatins only at very low rate, if at all therefore the transpeptidase activity is still debated^{30,32,36,37}. Even though the activity of NsPCS was reported to be independent from the presence of heavy metals³⁸, another prokaryotic PCS from the cyanobacterium *Geitlerinema sp.* was recently shown to form phytochelatins in presence of cadmium, yet with a very low rate compared to plant PCS³². Since PCS-like enzymes are structurally simpler and exhibit mainly peptidase activity, they are a basic model to start mechanistic investigations.

2.2. Glutathione and its major Functions

Glutathione (GSH) is a ubiquitous peptide in almost all living organisms and it is the most abundant non-protein thiol in mammalian cells. It consists of three essential amino acids L-glutamic acid, L-cysteine and glycine (Figure 9.a). The two latter amino acids are connected by a proteinogenic peptide bond. A special characteristic of GSH is the non-proteinogenic pseudo peptide bond between the γ carboxyl group of glutamate and the amino group of cysteine. This pseudo peptide bond prevents GSH from uncontrolled degradation by cytosolic proteases and can only specifically be attacked by enzymes involved in regulated GSH metabolic processes such as γ -glutamyltranspeptidase, γ -glutamylcyclotransferase 1 and the fungi-specific DUG enzyme³⁹. Another important chemical characteristic is the formation of a dimeric derivative (GSSG, Figure 9.b) linked through a disulphide bridge as a result of oxidation of the cysteine thiol.

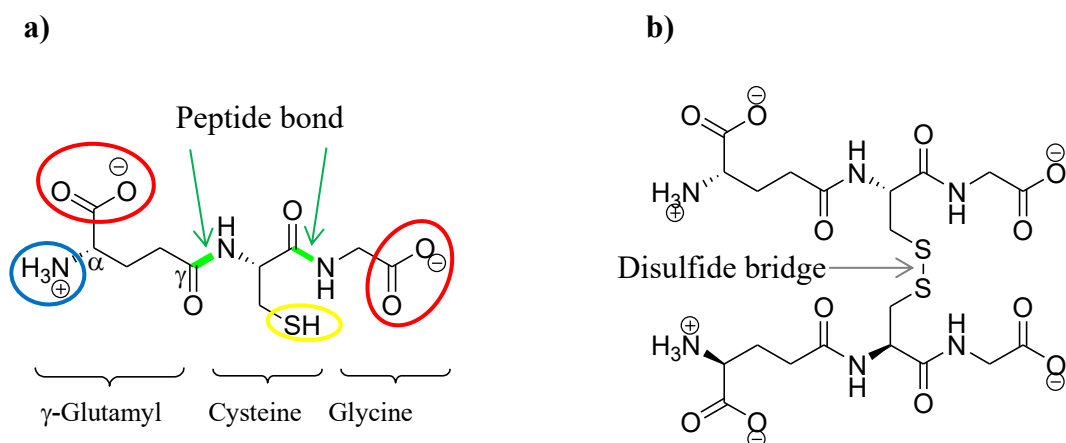


Figure 9. Chemical structure of glutathione: **a)** reduced form (GSH) and **b)** oxidised form (GSSG). Functional groups: thiol in yellow circle, carboxylate groups in red circle, amino group in blue circle. Peptide bonds are marked by green lines.

GSH is involved in many different important biological processes⁴⁰ and it acts both independently and as enzyme cofactor. Concerning the chemical reactivity, functions can be summarized on the one hand under the term “redox activity” and, on the other hand, under the action of the thiol as nucleophile. “Redox activity” includes the constitution of the cytosolic redox buffer (GSH/GSSG), antioxidant capacities against reactive oxygen (ROS) or nitrogen (RNS) species as well as redox signalling⁴¹. The thiol is an important nucleophile both for the detoxification of electrophilic toxins and in the biosynthesis of eicosanoids, steroids and iron-sulphur clusters⁴². Concerning the biochemical role, several enzymes act specifically on GSH in antioxidant defence and xenobiotic metabolism⁴³. GSH also operates as cofactor for enzymes and participates in many pathways of primary metabolism⁴⁴. For instance, modulation of GSH associated with regulation of redox-sensitive transcription factors such as nuclear factor kappa B (NF- κ B) providing a significant impact on neuroinflammation. In this respect, recent studies showed significant impact of GSH redox imbalance on autism pathology⁴⁵. Moreover, GSH can also store or transport nitric oxide⁴⁶, which is important for a number of physiological processes, such as neurotransmission or muscle contraction. Furthermore, GSH is a reserve form of cysteine, because due to the metal affinity of cysteine, its thiol is more oxidation-sensitive than the one in GSH⁴⁷.

In addition to GSH as precursor for phytochelatin serving as metal chelators, GSH itself is capable of stable metal ion binding and thus plays an important role in metal homeostasis. Its thiol group has a particularly high affinity for the metal cations Cd^{2+} , Cu^{2+} , Zn^{2+} , Hg^{2+} , Ag^+ , As^{3+} and Pb^{2+} ⁴⁸.

From above presented various examples, the landmark importance of GSH for all biological systems providing additional interest for investigations on PCS enzymes specifically acting on GSH as substrate.

2.3. Fluorogenic Probes

Fluorescence spectroscopy is widely used for monitoring biochemical events *in vitro* and *in vivo*. In order to detect fluorescence, a fluorescent molecule is necessary to report about the phenomenon of interest. Some biomolecules exhibit intrinsic fluorescence, such as nucleic acids or some proteins. Fluorescent molecules occurring naturally in proteins are the aromatic amino acids tryptophane, tyrosine and phenylalanine or cofactors such as NADH, flavins, derivatives of pyridoxyl and chlorophyll⁶. If the studied event does not involve an intrinsic fluorophore or the latter is not affected by the studied event, an extrinsic fluorophore can be used to generate a fluorescent probe, among them dansyl, fluorescein, rhodamine and many others. The biochemical effect is measured by change of fluorescence (intensity, wavelength, etc.) which can be quantified in response to different factors, for example change of pH, hydrophobicity or ionic strength. Alternatively, a fluorogenic probe can be used⁶. In contrast to standard fluorescent probes, fluorogenic probes are particular non- or weakly fluorescent molecules (“off”), which are getting fluorescent (“on”) after a biochemical event (e.g., enzymatic cleavage). Consequently, this biochemical event can be quantified by measuring the off-on transition. A fluorogenic probe can either be singly-labelled or doubly-labelled. In the first case, the fluorescence is generated from a pre-fluorescent state by the observed event, which requires a direct involvement of the chromophore in the reaction. In order to improve the strategy, doubly-labelled probes are developed containing two covalently bound chromophores. Depending on the strategy, the second chromophore besides the reporter can be either another fluorophore or a quencher. In the first case, decrease of the fluorescence from the reporter and increase of the fluorescence from the second fluorophore can be monitored; nevertheless, there is always a need for optical filters and complex data analysis. The use of a dark quencher instead of a second fluorophore can be very efficient and solve all these inconvenients⁴⁹. A dark quencher is a chromophore that reduces the intensity of fluorescence from the reporter fluorophore while returning, after excitation, to the ground state by non-radiative relaxation. For this reason, it shows no fluorescence. The quenching mechanism can be divided in two types, namely dynamic and static quenching (Figure 10). Dynamic quenching occurs by non-radiative energy transfer between the reporter fluorophore and the quencher through the weak coupling between them (e.g., FRET). Static or so-called contact quenching occurs through the

formation of ground state complex of reporter and quencher through the strong coupling between them, with the formation of intramolecular dimer.

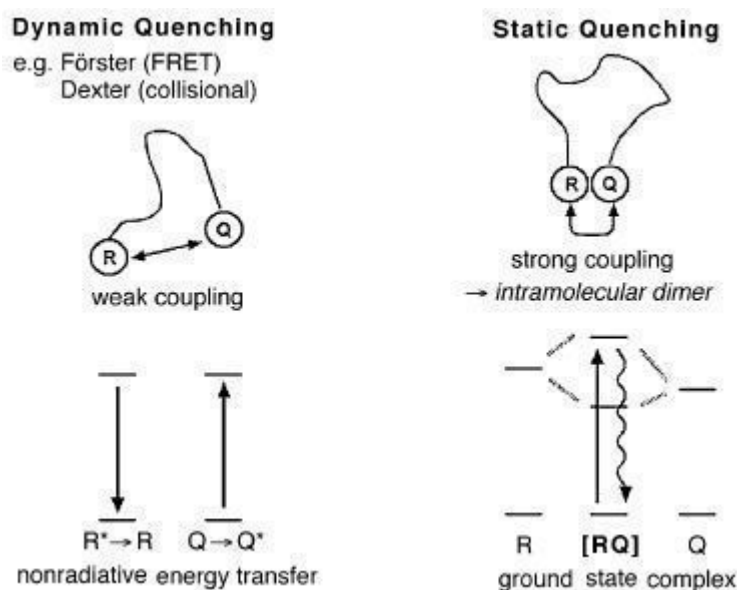


Figure 10. Two types of quenching mechanism: dynamic quenching and static quenching, where R is fluorescence reporter and Q is fluorescence quencher, R^* and Q^* are in excited state [picture freely modified from Johansson et al.⁴⁹].

In fluorogenic probes, the most frequently described mechanism for fluorescence quenching is FRET, but static quenching can also contribute. The application of a doubly-labelled fluorogenic probes is a very powerful tool and generally used to design probes for monitoring enzyme activity⁴⁹, which concerns in most cases an enzymatic cleavage of the substrate. In the closed form of fluorogenic probe, the close proximity of a fluorescent donor molecule to a quencher leads to a decrease of the signal (Figure 11.). The enzymatic cleavage of the substrate generates so-called open form of the fluorogenic probe, where the spatial separation of fluorescent donor and quencher results in an increase of fluorescence.



Figure 11. Schematic representation of an assay for the enzymatic cleavage of a doubly-labelled fluorogenic probe equipped with fluorescent reporter (green circle) and fluorescence quencher (black circle) [picture freely modified from Kempf et al.⁵⁰].

Since the first step of the enzymatic activity of PCS is a peptidase reaction, the application of a doubly-labelled fluorogenic probes is a suitable option for investigating this process. In a previous study, the FRET principle has already been used for enzymatic activity tests of cysteine proteases⁵¹.

2.3.1. Dabcyl as Dark Quencher

The azobenzene derivative 4-(*N,N*-Dimethylamino)azobenzene-4'-carboxylic acid, commonly known as dabcyl⁵² (**1**) is a popular azo dye and dark quencher (Figure 12). Dabcyl is characterized by an absorption maximum at 475 nm and a quenching range from 400-550 nm. These properties permit its use in fluorogenic probe⁵³ as acceptor in combination with many donor fluorescent dyes such as 5-((2'-aminoethyl) amino) naphthalene-1-sulfonic acid (EDANS) ($\lambda_{em} = 490$ nm), carboxyfluorescein (FAM) ($\lambda_{em} = 520$ nm) and many others⁵⁴.

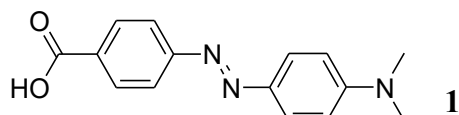


Figure 12. Chemical structure of dabcyl.

Azobenzene derivatives are a class of aromatic azo dyes with a core structure consisting of two phenyl rings connected through a -N=N- double bond (azo group) where each nitrogen atom carries a non-bonding electron pair (Figure 13). Azobenzene is used as a model molecule for compounds containing a diarylazo moiety.

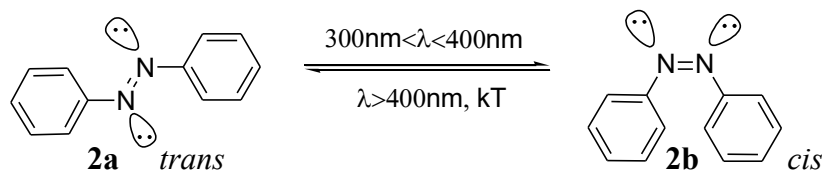


Figure 13. *Trans-cis* photoisomerization of azobenzene [picture freely modified from Chevalier et al. ⁵⁵].

An important process studied on azobenzene is the *cis-trans* photoisomerization around the -N=N- bond which is characterised by the equilibrium between the thermodynamically stable *trans* isomer **2a** and the *cis* isomer **2b**⁵⁶. Photoisomerization from the *trans* into the *cis* isomer occurs under UV light irradiation. The return process can be mediated either by visible light or, in the absence of light, by thermal isomerization to the more stable *trans* form. Among different proposed mechanisms for this isomerization process only two are most commonly accepted namely rotation and inversion⁵⁷. Rotation requires disruption of the π bond of the diazo -N=N- group to allow rotation around the σ bond; inversion occurs by turning around of a nitrogen lone pair and spin around the C-N bond (Figure 14).

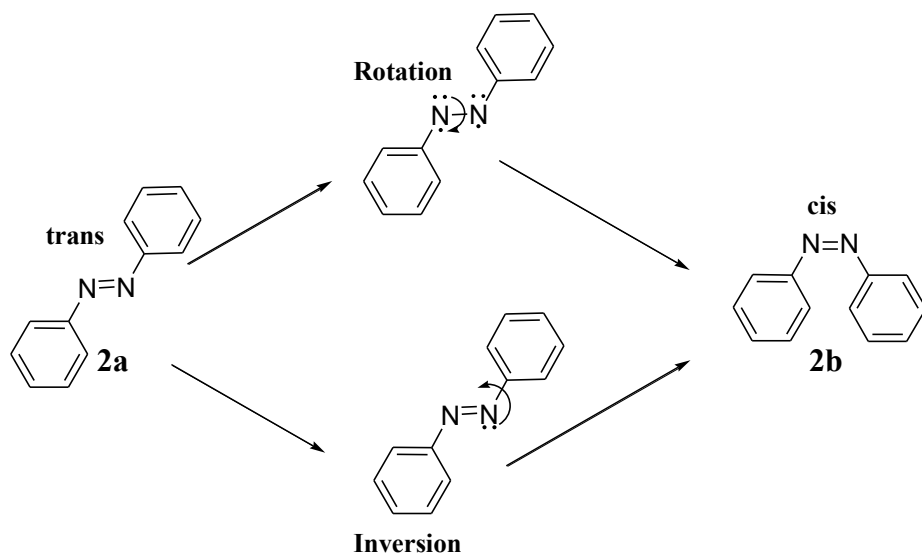


Figure 14. Proposed mechanisms for azobenzene isomerization⁵⁷.

Both mechanisms have been confirmed by experimental data, which are, in some cases, explained by a combination of both^{56, 58}. DabcyI belongs to the group of push-pull substituted azobenzene derivatives, which are characterized by a mesomeric charge delocalization⁵⁹ over each two resonance structures **1a/b** and **1c/d**, respectively (Figure 15). Structure **1b** shows that the diazo bond has partial σ character, allowing easy rotation at low energy. For this reason, isomerization requires only disruption of a partial π bond and rotation is the dominating mechanism⁶⁰.

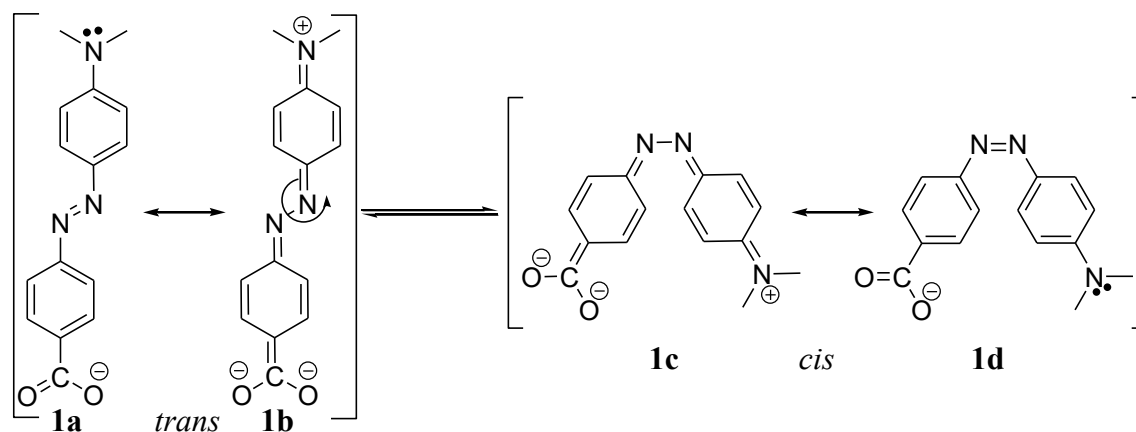


Figure 15. Cis-trans isomerization of dabcyI is facilitated by rotation around the diazo N-N bond with partial σ bond character because of mesomeric charge delocalization.

An important characteristic of chromophores based on the azobenzene scaffold is the absence or the low level of emitted fluorescence caused by non-radiative deactivation of the excited states⁵⁵. This characteristic is an important prerequisite for their use as fluorescence quencher. One process contributing to this phenomenon of fluorescence quenching is the *cis-trans* photoisomerization of azobenzene derivatives. The photoisomerization of chromophores as a

non-radiative process has been shown to compete with fluorescence by comparing the fluorescence of two similar fluorophores⁶¹. The system which was unable to effect isomerization was always fluorescent independently of solvent or temperature, whereas the isomerizing chromophore showed significantly stronger fluorescence at lower temperature and in more viscous solvents, i.e., conditions where isomerization is known to be disfavoured. For this reason, photoisomerization was described as a self-quenching mechanism. Consequently, the *cis-trans* isomerization, facilitated by the push-pull system of dabcy1, is probably the main reason for its efficient quenching properties. Besides the photoisomerization, other non-radiative processes may also contribute to the relaxation to the ground state, for example intermolecular energy transfer *via* π - π stacking between the aromatic rings of the chromophore⁶².

Due to its advantageous spectroscopic properties and simple synthesis, dabcy1 is a very popular dark quencher and is employed for numerous biochemical applications, such as monitoring of enzymatic activity⁶³, real-time fluorescence PCR⁶⁴, biosensing and bioimaging⁵⁵ and it was even recently used as quencher in fluorogenic probes for SARS-CoV-2 detection⁶⁵.

3. Organic Synthesis of Peptides

Peptides are heterooligomers or heteropolymers, where the carboxyl group of each amino acid is connected with the amino group of the next one *via* peptide bond. The number of amino acids can vary from two to several dozens. The molecular mass limit is set at 6000 Da; molecules over this limit are considered as proteins⁶⁶.

Peptide synthesis can be performed either in solution or using solid-phase methods. For large scale industrial production, a combination of both can be used as well. Solid-phase synthesis has become a more and more attractive tool for synthesis of longer peptides⁶⁷, but the expensive resin solid matrix is usually not regenerated and is thus not economic for small peptides. The advantages of classical solution phase techniques are low cost, high flexibility and the intermediates can be isolated and characterised at each step. For these reasons, all syntheses in the present work have been carried out in solution.

3.1. Protecting Groups Strategy

Peptides consist of amino acids each containing at least two, more often three functional groups. For selective chemical transformations, functional groups which are not meant to take part in a certain reaction need to be protected to avoid the formation of unwanted side products.

Due to the enormous variety of existing protecting groups for amino acids⁶⁸, in the following section we focus only on those used in the present work (Figure 16).

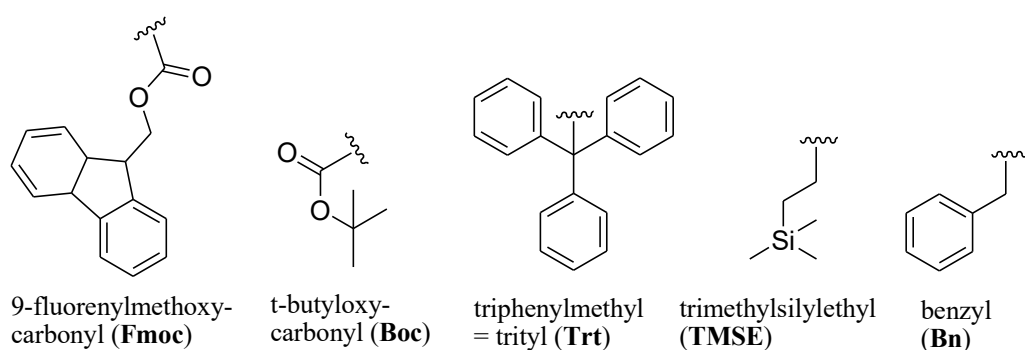


Figure 16. Amino acid protecting groups used in this work.

The **Boc** and **Fmoc** groups belong to the alkyl-oxycarbonyl family, the most common protection for amino compounds. Two advantages are characteristic for this family. Firstly, protection can be carried out in aqueous solvent mixtures offering their employment in the first step of functionalizing native amino acids which are very polar. Secondly, the deprotection proceeds often quantitatively without reversible re-protection due to the irreversible loss of carbon dioxide. Alkyl-oxycarbonyl groups are most often used for amino protection forming a

carbamate, but can also be attached to alcohols in anhydrous solvents. In this case, the functional group is called carbonate instead of carbamate.

The **trityl group (Trt)** can be used for amino groups, carboxylic acids and thiols. Under acidic conditions, they form a stabilized carbocation as well during protection and deprotection. Upon activation with Lewis acids, the reagent trityl chloride generates the trityl cation which is attacked by the nucleophilic groups thus protecting them. Deprotection under with Brønsted acids proceeds *via* the same intermediate cation.

Silyl groups (e. g. TMSE) are mostly used for alcohol protection. Carboxylic silyl esters are not sufficiently stable for preparative purposes. An exception is the trimethylsilylethyl group containing a silicium-carbon instead of a silicium-oxygen bond rendering its ester conveniently stable for isolation while offering the selective and mild deprotection with fluoride which is a strong advantage of all silyl groups.

Benzyl groups are used for alcohol or amino groups and can quantitatively be deprotected *via* catalytic hydrogenation, e.g., with palladium as catalyst and gaseous hydrogen as reactant, but are not suitable for sulphur-containing molecules, since the sulphur is inactivating the metal catalyst.

Setting up a protecting group strategy requires the choice of conditions for protection and deprotection steps to proceed selectively without destabilizing neighbouring protecting groups in the same molecule. The selective protection/ deprotection of one protecting group under conditions which do not interfere with the other groups (i.e., the other groups remain stable) is referred to as orthogonality. The two most common classes of protecting groups with respect to chemical reactivity are acid-labile (e.g., *tert*-butyl derivatives) and base-labile (e.g., Fmoc) groups, which are orthogonal to each other. If it is necessary to have a third orthogonal group to be deprotected without deprotecting the groups of the other two classes, a silyl group can be used. Due to their affinity for fluoride, silyl groups can be selectively removed without deprotecting acid- or base- labile groups. In addition to chemical reactivity, protecting groups facilitate isolation and purification of highly polar biomolecules by decreasing polarity and thus increasing the solubility in organic solvents and facilitating chromatography.

3.2. Condensation Reagents for Amide Bond Formation

Amide bond formation between carboxyl and amino groups is an endergonic process, which requires a condensation reagent to generate a spontaneous reaction between the activated acid derivative and the amino group (Figure 17).

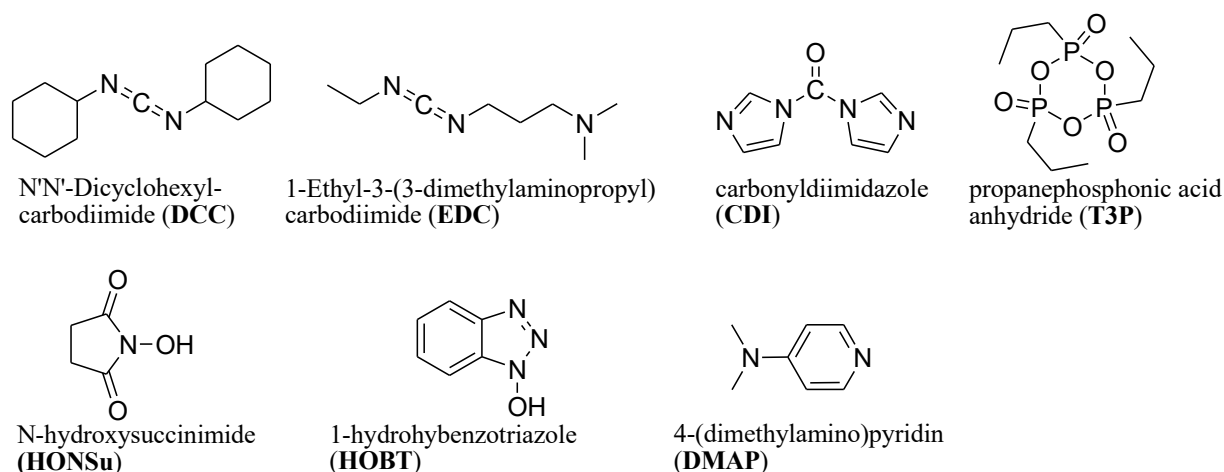


Figure 17. Condensation reagents for peptide bond formation.

Commonly used condensation reagents are carbodiimides such as N,N'-dicyclohexylcarbodiimide (DCC)⁶⁹. The formed by-product dicyclohexylurea often causes problems during purification which can be avoided with the water-soluble derivative 1-ethyl-3-(3-dimethylaminopropyl)carbodiimide (EDC).

The reaction cascade starts with activation of the carbodiimide by protonation through the carboxylic acid (Figure 18.). The corresponding carboxylate then attacks the carbodiimide to form an O-acyl isourea, which is not sufficiently electrophilic to be attacked rapidly by amino groups.

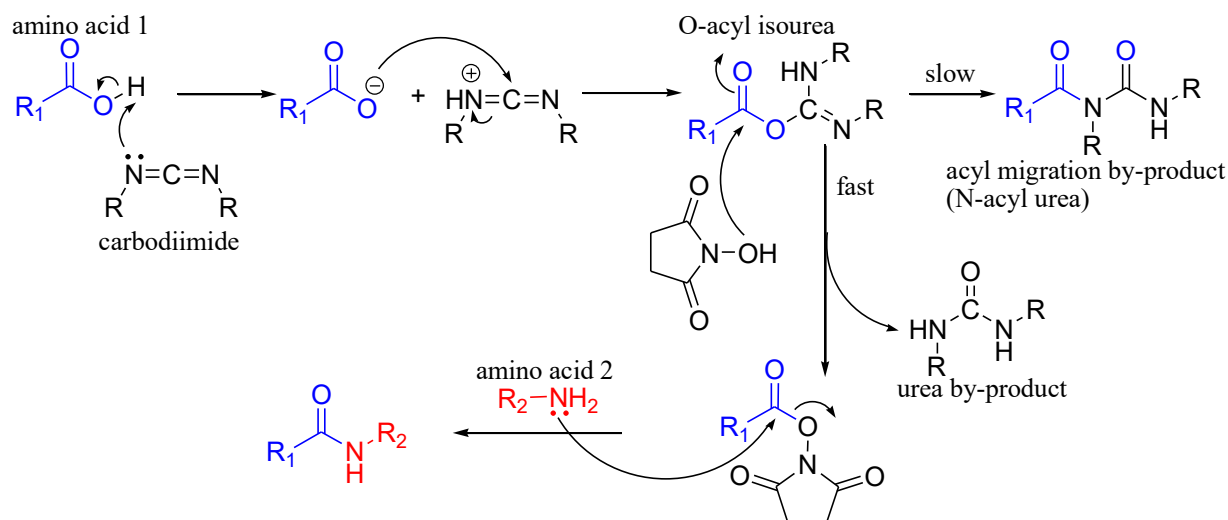


Figure 18. General mechanism for amide bond formation with carbodiimide and N-hydroxy-succinimide (HONSu).

Without a catalyst, the slowly occurring rearrangement to the stable N-acyl urea can compete with the attack by the amino group and thus lower the yield. For this reason, catalysts containing highly nucleophilic alcohol groups such as N-hydroxy-succinimide (HONSu) or 1-hydroxy-benzotriazole (HOBT) are used to form a second activated carbonyl derivative, the so-

called active ester. The latter is then attacked by the amino group forming the peptide bond and liberating the catalyst. Since alcohols are less nucleophilic than amino groups, the HONSu active ester would not be sufficiently electrophilic to compete with the acyl migration. For the formation of esters, DMAP is used as catalyst instead, forming a highly electrophilic positively charged amide intermediate (Steglich esterification⁷⁰).

Instead of carbodiimides, carbonyldiimidazole (CDI) can be used to generate alternatively a mixed anhydride as the first reactive intermediate. Subsequent formation of an activated imidazole amide under CO₂ extrusion allows direct attack by the amino group without additional catalyst.

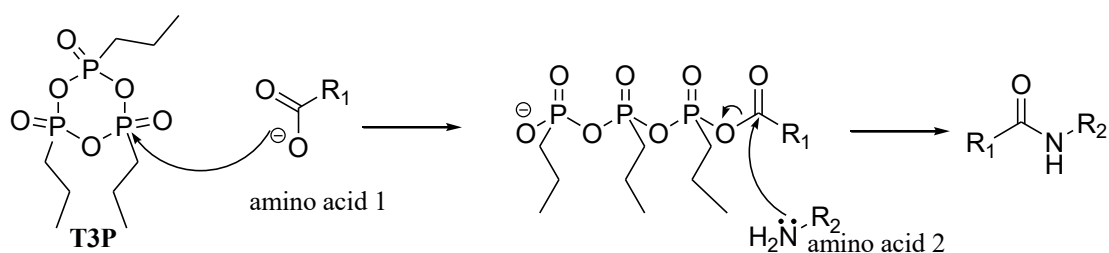


Figure 19. Mechanism of activation by propanephosphonic acid anhydride (T3P) of the carboxyl group of amino acid for coupling with amino group of another amino acid.

During the last twenty years propanephosphonic acid anhydride (T3P)⁷¹ became a very popular condensation reagent (Figure 19). Its advantages are fast reaction (only 30 minutes), mild conditions at 0°C and water soluble by-products thereby providing clean crude products in almost quantitative yield with low rate epimerization. The mechanism involves formation of the mixed anhydride which readily reacts with amino groups without additional catalyst. Because of these advantages, the peptide bonds in the present work were formed mainly in presence of T3P.

4. Overview of the Publications

4.1. List of Publications

P1: Kempf O., Kempf K., Schobert R., Bombarda* E. – HydrodabcyI: A Superior Hydrophilic Alternative to the Dark Fluorescence Quencher DabcyI. *Anal. Chem.*, **2017**, *89*, 11893-11897. <https://doi.org/10.1021/acs.analchem.7b03488>.

Patent: Kempf O., Bombarda E., Kempf K., Ullmann G.M., Schobert R. – HydrodabcyI. International patent WO 2016/083611 A1, issued 02.06.2016; (US Patent 25.05.2017; EU Patent 24.07.2018).

P2: O. Kempf, G.M. Ullmann, R. Schobert, K. Kempf*, E. Bombarda*. – Chemoselective attachment of the water-soluble dark quencher hydrodabcyI to amino groups in peptides and preservation of its spectroscopic properties over a wide pH range. *ACS Omega*, **2021**, *6*, 32896-32903. <https://doi.org/10.1021/acsomega.1c04891>.

P3: F. J. Gisdon, C. G. Feiler, O. Kempf, J. M. Förster, J. Haiss, Wulf Blankenfeldt, G. Matthias Ullmann, Elisa Bombarda*. – Structural and biophysical analysis of the phytochelatin-synthase-like enzyme from *Nostoc* sp. shows that its protease activity is sensitive to the redox state of the substrate. *ACS Chemical Biology*, **2022**, *17*, 883-897. <https://doi.org/10.1021/acscchembio.1c00941>.

P4: O. Kempf, O. Stemmann, R. Schobert, K. Kempf*, E. Bombarda*. – Modular Synthesis of Glutathione analogues to study peptidase reactions *in vitro* and *in vivo*. Manuscript close to submission.

4.2. Motivation and Synopsis

Phytochelatin synthase (PCS) is known to play an essential role in detoxification/homeostasis of a wide range of heavy metals in plants and other organisms¹⁷. In plants, phytochelatins (PCs) are produced in response to heavy metals since PCS activity was shown to be very low in the absence of heavy metals⁷². During the past years, the role of PCs for heavy metal detoxification has still attracted scientific interest. In times of growing population, the development of new agricultural solutions becomes more and more urgent. Cultivation or phytoremediation of contaminated soil represents an interesting perspective when giving a closer look on PCS of culture crops such as *Oryza sativa* (Rice)⁷³ and *Zea mays* (corn)⁷⁴.

PCS genes are widely found in various eucaryotic organisms, but for most of them, heavy metal detoxification does not seem to be sufficient for explaining the presence of

phytochelatins. Consequently, there is still a mystery about other functions of PCS in addition to the importance of the synthesis of phytochelatins. Recently, Hematy et al.⁷⁵ identified PEN4/AtPCS1 as a player in preinvasive immune responses against fungal pathogens. Other results suggest that PCS of the human pathogenic flatworm *Schistosoma mansoni* participates both in metal homeostasis and xenobiotic metabolism rather than metal detoxification. Consequently, PCS may be part of a global stress response in the worm. Because humans do not have PCS, this enzyme is of particular interest as a drug target against schistosomiasis⁷⁶. In addition to its functions, the enzymatic mechanism of PCS and the influence of metals in particular remain still controversially discussed⁷⁷ and a quantitative characterisation is lacking.

Prokaryotic PCS-like proteins are a reasonable starting point for mechanistic studies, since these enzymes are structurally and mechanistically simpler performing mainly peptidase reactions. Their biological functions, however, are even less evident, since phytochelatins are produced only at a very low rate, if at all. For these reasons, we decided to focus on the mechanistic characterization of the PCS-like enzyme from the cyanobacterium *Nostoc* sp. (NsPCS). We studied its catalysis using different spectroscopic methods such as NMR, absorbance and fluorescence measurements. Since appropriately labelled GSH analogues are not commercially available, the development of an organic synthesis strategy is one of the main tasks of the present work.

In addition to the importance of PCS, also its substrate GSH is of huge scientific interest itself, since it plays very important roles in all living cells. Although the main function of GSH concerns protection against oxidative stress, GSH is also involved in cell signalling⁴¹ including autophagy and viral infection. A recent hypothesis linked an endogenous deficiency of GSH to serious manifestations and death in COVID-19 patients⁷⁸.

The combination of the general importance of both PCS and GSH is the main motivation for the present work. On the one hand, PCS is scientifically interesting due to its various functions, most of which are still not completely characterized. On the other hand, synthetic strategies for GSH derivatives can be valuable for numerous applications due to the multifunctionality of GSH.

The present cumulative dissertation comprehends four publications [**P1** to **P4**] describing the results of the work on the thesis: “Synthesis of glutathione analogues to investigate the enzymatic mechanism of phytochelatin synthase by fluorescence spectroscopy”. In addition, the newly developed chromophore hydrodabcyI is a very promising dark quencher and was therefore patented⁷⁹.

Our strategy for the investigations on PCS is based on fluorescence spectroscopy. Since natural GSH does not contain a chromophore, we designed a fluorogenic probe based on a GSH analogue labelled with a donor-acceptor pair in order to monitor the peptidase reaction of NsPCS (Figure 20) [P4].

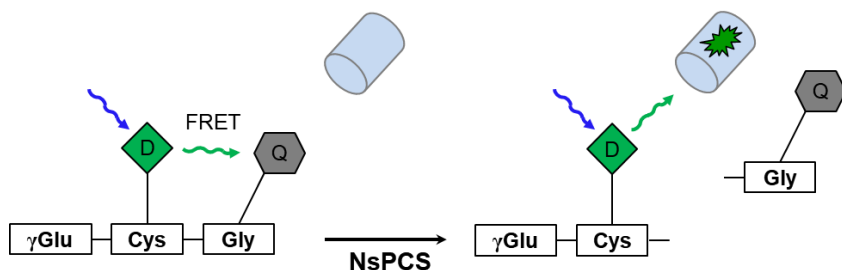


Figure 20. Schematic view of the FRET-based experiment to monitor the peptidase activity of NsPCS with GSH⁸⁰.

When the glutathione is intact, the fluorescence of donor is drastically reduced by the proximity of the quencher. Upon cleavage by NsPCS, restoring of the donor fluorescence can then be monitored in time-course experiments, providing the cleavage kinetics (Figure 21) [P4(d)].

Theoretical calculations based on the crystal structures described in publication [P3] showed that the GSH binding site has a high positive potential, indicating that the overall negative charge of GSH is important for binding to PCS. Coherently, the results reveal possible hydrogen bond interactions of the glutamyl-moiety with Arg232, Asn170 through its α -carboxylate group and with Asp225 through its α -amino group. Furthermore, the carboxylate group of the glycyl-moiety seems to interact with Arg173 (Figure 21). Contrarily, the thiol group of the cysteinyl-moiety does not interact with the enzyme. These prerequisites suggest that carboxyl group of the Gly residue, unlike the thiol, is not to be used for attaching a fluorescence label.

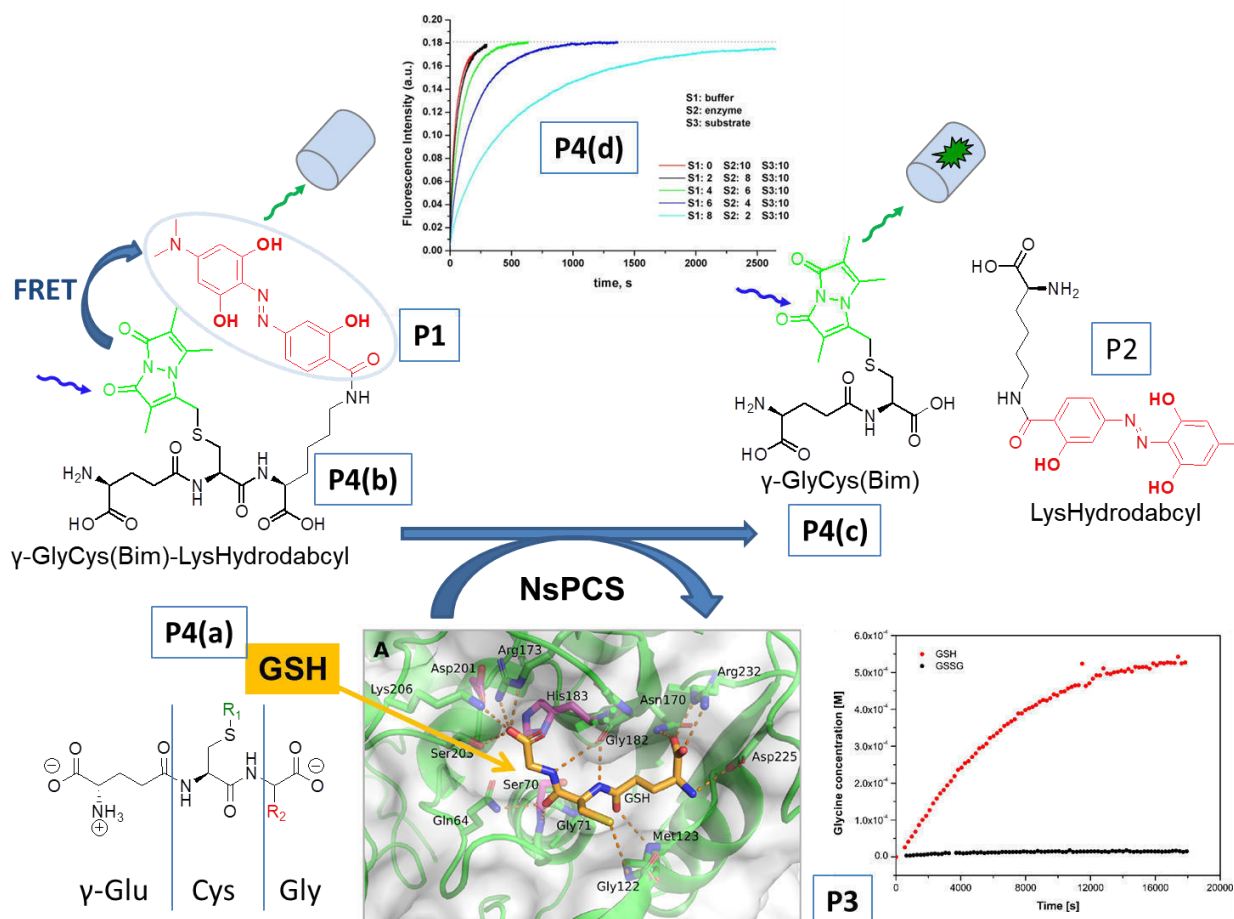


Figure 21. Schematic view of this work with reference to the four publications (P1 to P4). Different aspects of publication P4 are indicated as “P4(a) to P4(d)”. Possible hydrogen bond network of GSH (in yellow) in the binding pocket of NsPCS in the crystal structure C70-NsPCS⁸¹.

According to the above considerations, the fluorogenic probe was designed as follows. The donor chromophore was bound to the thiol-group (Figure 21, R₁ in green), the acceptor was linked to the side chain of lysine, which replaced the natural glycine during the synthesis of (Figure 21, R₂ in red) [P4(a)]. Mono-bromo-bimane was chosen as the donor chromophore, since it has already been used in previous physiological studies⁸² and can be easily coupled with the thiol group [P4(a)]. Dabsyl was already shown to be a suitable acceptor for bimane⁸³, but the coupling to an amino group in the substrate would lead to a formation of a sulfone amide (Figure 22), which contains two oxygens and a sulphur atom creating a sterically demanding electron density in direct vicinity of the substrate, and was not further considered.

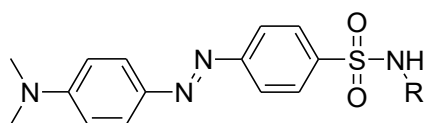


Figure 22. Chemical structure of dabsyl coupled to amino group of amino acid.

Instead, the similar dark quencher⁸⁴ dabcyI (Figure 12) carries a carboxyl in place of the sulfonyl group, generating a sterically less demanding amide after coupling to an amino group in the substrate.

Since appropriate derivatives of GSH are not commercially available, the modular synthesis for several GSH analogues based on a tailored protecting group strategy was developed and applied for the synthesis of a fluorogenic probe [P4]. As expected, the fluorescence of bimane in the complete fluorogenic probe was drastically reduced due to the closeness of the quencher. According to the plan, the cleavage of this substrate by NsPCS led to an increase in fluorescence. However, the detailed analysis of the spectroscopic experiments supported by ¹H-NMR measurements showed only incomplete conversion of the substrate indicating that the enzyme gets inhibited. This inhibition effect was attributed to the hydrophobicity of dabcyI preventing the cleaved lysine-dabcyI fragment to be released into water. In another experiment, inhibition by the lysine-dabcyI fragment was confirmed by incomplete cleavage of natural GSH followed by NMR spectroscopy. Prompted by this finding, we developed a new hydrophilic dark quencher, named hydrodabcyI [P1]. Indeed, the analogous NMR experiment confirmed complete cleavage of natural GSH after preincubation of the enzyme with the lysine-hydrodabcyI fragment. In publication [P1], we characterized hydrodabcyI and presented a proof-of-concept illustrating the superiority of hydrodabcyI over dabcyI. Due to its potential for broad applications in biochemical systems, where the natural environment is water, hydrodabcyI was patented.

Since its water solubility brings along a high polarity and the hydroxyl groups are nucleophiles potentially interfering during coupling, we developed an optimised strategy for simple coupling hydrodabcyI to amino groups in amino acids and peptides, facilitating also the synthesis of the labelled lysine fragment [P2]. Additionally, further characterisation of the novel compound was carried out by measuring and comparing the pH dependences of the absorbance spectra of hydrodabcyI, its isopropylamide and dabcyI [P2].

In order to assess the contribution of the artificial modifications of the substrate by the chromophores, a way to observe the cleavage of natural GSH became necessary. The difference between intact and cleaved GSH is clearly visible by ¹H-NMR spectroscopy in D₂O⁸⁵. The activity of the enzyme is optimal at pH8, but under such basic conditions, the oxidation of GSH to GSSG occurs very fast. To follow the cleavage kinetic quantitatively, a robust NMR assay under anoxic conditions was developed in publication [P3].

To proceed with the mechanistic investigations of NsPCS *via* fluorescence, the double labelled GSH analogue was synthesized, in which the hydrodabcyI is used in the place of dabcyI [P4(b)]

and carried out the quantitative fluorescence-based kinetic experiment with this substrate. In order to obtain a complete and quick conversion, a lower excess of substrate over enzyme was used. The reaction was monitored with a stopped-flow setup and the results indicate, that the double labelled GSH analogue can be cleaved completely with the studied enzyme [P4(d)].

Publication [P1]

Hydrodabcyl: a Superior Hydrophilic Alternative to the Dark Fluorescence Quencher Dabcyl.

Dabcyl is a widely used dark quencher employed in fluorogenic-based probes experiments, but its hydrophobicity leads to limited water solubility. This property can cause problems in biochemical assays with biomolecules which are carried out in aqueous solutions. In absence of well-characterized commercial options, the need for a water-soluble alternative became obvious. Inspired by nature (for example water soluble polyphenols), a new hydrophilic dark quencher hydrodabcyl was developed with the same synthetic strategy as for dabcyl. Instead of using p-anthranilic acid and dimethylaniline, the standard azo coupling was carried out with their hydroxylated congeners p-amino salicylic acid and 5-dimethylamino-resorcinol carrying one and two phenolic hydroxyl groups, respectively. An important aspect of the synthesis was the improved double purification of the 5-dimethylamino-resorcinol by crystallization of the fraction pre-purified over silica gel yielding white crystals. When the purification had been carried out by recrystallization as reported in literature by Petrzilka and Lusuardi⁸⁶, pink crystals were obtained. During synthesis, we discovered that the colour can be attributed to the presence of a degradation product, since the white crystals also turn pink upon storage after several weeks in the refrigerator. When the pink crystals were used, the hydrodabcyl product contained a fluorescent by-product which could not even be separated by HPLC. As expected, hydrodabcyl synthesized from white crystals is completely non-fluorescent. Moreover, in contrast to the parent compound, it is exquisitely water-soluble. The solubility was measured by absorbance spectroscopy, since the precipitate does not contribute to the colouration of the solution. The new chromophore was spectroscopically characterised in DMSO and in aqueous solution revealing that the useful absorption characteristics of dabcyl were conserved in hydrodabcyl. Its application as quencher in a FRET-based experiment was tested with an exemplary peptidase assay. From the dipeptide Serine-Phenylalanine, a fluorogenic probe was synthesized with EDANS as fluorescence donor and hydrodabcyl as a quencher (Hydrodabcyl-Ser-Phe-EDANS). In this small substrate, the solubility of the labels is even more crucial since there are less charges in the molecule being able to compensate hydrophobic labels. The

enzymatic cleavage with thermolysin and papain was monitored by fluorescence spectroscopy and TLC. Even though the reaction proceeded slower with papain, essentially the entire amount of substrate was converted. This result confirmed the superiority of hydrodabcyl, since in a previous report, the same fluorogenic probe containing dabcyI had been shown to be cleaved only in a small amount⁸⁷ by papain. The presented spectral characteristics as well as the proof-of-concept study commend the new hydrodabcyl as an improved alternative for the commonly used dark quencher dabcyI.

Publication [P2]

Chemoselective Attachment of the Water-soluble Dark Quencher Hydrodabcyl to Amino Groups in Peptides and Preservation of its Spectroscopic Properties over a wide pH Range.

The high polarity of hydrodabcyl resulting from the desired water solubility and the low carbonyl reactivity due to the electron donating substituents on the aromatic system can represent a problem during the coupling to amino groups in organic solvents. In fact, standard one-pot amidations with DCC catalysed by HONSu or HOBT failed completely. In publication [P1], the coupling of hydrodabcyl to the amino group was achieved using DMAP as catalyst to form a stronger activated positively charged electrophilic intermediate commonly employed in the Steglich esterification (see paragraph 3.2). Since hydroxyl groups also compete as nucleophiles in the reaction with this strongly electrophilic intermediate, acetyl protection of the three phenolic groups became necessary. However, this turned out not to be a general strategy, since less sterically demanding amines simply reacted with the acetyl groups rather than the active ester leading to N-acetamide derivatives instead of the hydrodabcyl coupling products. In order to facilitate coupling, we converted hydrodabcyl into its N-succinimidyl active ester (hydrodabcyl-ONSu). In publication [P2] we describe the isolation and purification of hydrodabcyl-ONSu to overcome the above discussed issues and to identify a simpler coupling strategy. Hydrodabcyl-ONSu was shown to react selectively with primary and secondary amines even in the presence of other nucleophilic functional groups. To prove the application of the active ester in aqueous solution, natural glutathione was labelled with bimeane and hydrodabcyl in a one pot procedure. This double-labelled derivative is even a fluorogenic probe which might find an application to study the cleavage of the gamma bond in glutathione.

In order to further characterise the novel chromophore, the absorbance spectra of hydrodabcyl, its isopropylamide and dabcyI have been measured depending on the pH value. The isopropylamide was used to mimic the chromophore when linked to a target molecule *via*

amidation. These data show that the absorption spectra of dabcyI change strongly depending on the pH value. In contrast, hydrodabcyI and its amide exhibit only small pH-dependent changes of their absorption spectra which is an advantage for the use as quencher. The pH-dependent preservation of the absorption characteristic of hydrodabcyI and its amide were attributed to the presence of intramolecular hydrogen bonds facilitating charge delocalization and thus allowing a smooth adaptation to pH changes. The same effects including intramolecular keto-enol tautomerism along the hydrogen bonds were shown to explain the observed chemical reactivity of hydrodabcyI on two examples. Firstly, two of the three phenolic hydroxyl groups take part in intramolecular preventing them from being deprotonated. The third one is reacting as its phenolate and was thus selectively protected with a Boc group. Secondly, the presence of hydrodabcyI in the form of different tautomers was proved by a proton-deuteron exchange of aromatic protons in an $^1\text{H-NMR}$ experiment. This exchange in neutral D_2O is astonishing, since it usually does not occur under such mild conditions. In our case, we rationalized this phenomenon by the presence of the keto tautomer in vicinity of the dimethylammonium group generating a CH- acidic CH_2 group. Deprotonation of this CH_2 group enables re-aromatization and thus explains the loss of a formally aromatic proton, which in fact takes place at a CH_2 group of a non-aromatic tautomer.

In conclusion, this publication combines the optimization of the chemical coupling strategy of the novel chromophore hydrodabcyI as well as detailed physical investigations on its pH dependent absorption properties. Both the chemical reactivity and the spectroscopical characteristics of hydrodabcyI can be explained by the presence of intramolecular hydrogen bonds which are mainly responsible for the peculiar properties of this polyphenolic azo dye.

Publication [P3]

Structural and biophysical Analysis of the Phytochelatins-Synthase-like Enzyme from *Nostoc* sp. shows that its Protease Activity is sensitive to the Redox State of the Substrate.

PCS synthesize oligomeric phytochelatin from GSH, which play very important role in heavy metal detoxification and metal homeostasis. NsPCS is the most studied representative of prokaryotic PCS-like proteins, which are characterized by their sequence similarity to eukaryotic PCS enzymes, but the formation of phytochelatin was observed only with a minimal rate. If the synthesis of phytochelatin does not seem to be the main function of PCS-like proteins responsible for, which is then their purpose in prokaryotes? In order to address this question, detailed characterizations of NsPCS are discussed in publication [P3], where three

crystal structures capturing different states of the enzyme along the catalytic cycle are presented. The crystal structure of the wild-type enzyme without substrate (wt-NsPCS) has been resolved with an optimized orientation of the side chains. This analysis allowed displaying a loop, which had not been resolved in the structures reported by Vivares et al.³⁵ The crystal structure of the wild-type enzyme with substrate captures the acyl-enzyme intermediate (acyl-NsPCS) without acidification of the solution as previously used to stabilize the acyl-enzyme intermediate³⁵. In this case, the enzyme-bound γ EC dipeptide formed a disulphide with another GSH molecule as a result of GSSG acting as inhibitor. Contrarily to the structures presented by Vivares et al.³⁵, the catalytically active water molecules necessary for hydrolysing the acyl-enzyme intermediate were visible in both subunits of the homodimeric enzyme. The third structure of the catalytically inactive serine mutant (C70S-NsPCS) lacking the catalytically active thiol contained a reduced GSH molecule in the active site. Since no GSH was added for crystallization, the GSH must have entered the enzyme already during heterologous expression. The conservation of GSH in the enzyme throughout the purification procedure was unexpected, because a soluble small molecule would only remain in the enzyme, if the affinity was extraordinarily high. This completely new crystal structure allowed displaying the orientation of the intact substrate GSH in the active site of NsPCS including the hydrogen bond network.

In addition to the crystal structures, a combination of biophysical techniques (fluorescence and NMR spectroscopy, circular dichroism and calorimetry) and theoretical calculations allowed providing the first quantitative analysis of the enzymatic mechanism of a PS-like protein. A quantitative NMR- based experiment allowed to follow the cleavage kinetics of the natural substrate GSH. This experiment revealed that reduced GSH was processed by NsPCS, whereas its oxidized form GSSG acted as a suicide inhibitor. In other words, only one glycine was cleaved off and the resulting acyl-enzyme intermediate remained stable. In conclusion, the presented studies shed new light on NsPCS as a relatively slow enzyme characterized by an enhanced stability of the acyl-enzyme intermediate. Theoretical calculations even suggest that hydrolysis of the acyl-enzyme intermediate, i.e, the de-acylation, is the rate limiting step of the catalytic cycle. The combined results presented in the third publication enabled to propose a potential role of NsPCS as redox sensor. Moreover, this function allowed us to suggest a theory about the emergence of phytochelatins during evolution. The stability of the acyl-enzyme intermediate forming a disulphide with another GSH molecule automatically increases its lifetime and thus enhances the probability of an *intramolecular* S-N-acyl shift. Due to the reactivity of the thioester, the terminal amino group of the intact GSH molecule can attack the carbonyl of the thioester to form a stable amide. This process is very likely to proceed

spontaneously, since it converts a reactive to a stable compound in an intramolecular reaction. In fact, this acyl shift can be seen as an intramolecular transpeptidation reaction. The spontaneous nature of this process can thus explain the potential birth of a first phytochelatin, which was present in its oxidized form, i.e., containing a disulphide.

Publication [P4]

Modular Synthesis of Glutathione Analogues to study Peptidase Reactions in *vitro* and in *vivo*.

Fluorescence-based kinetic measurements present significant benefits compared to other techniques such as high sensitivity, simple experimental setup and high time resolution. To study the peptidase reaction of NsPCS by fluorescence spectroscopy, a fluorogenic probe is required. Even though attachment of a proper chromophore pair seemed to be simple in theory, the organic synthesis of appropriately labelled GSH as substrate analogues turned out to be challenging. In response to the issues, a modular and adaptable strategy for the synthesis of glutathione analogues from selectively protected amino acids building blocks has been developed and is presented in publication [P4].

A fluorogenic probe for monitoring the enzymatic hydrolysis of a peptide is usually prepared by functionalization of the two amino acids adjacent to the cleavage site with a fluorophore and a quencher, respectively. It was reported that S-alkyl GSH derivatives, the bimane conjugate in particular, can be cleaved by PCS⁸⁸, which infers the opportunity of attaching chromophores on the thiol. For observation of the peptidase activity, a second chromophore needs to be attached to the glycine moiety. Since the negative charge is important for the correct substrate recognition, the carboxyl group is not available for attachment. In nature, some plants synthesize GSH isoforms containing alanine, serine or glutamic acid instead of glycine and also generate the respective PC-isoforms during heavy metal exposure⁸⁹. Consequently, a strategy was designed, where glycine was exchanged by lysine (Lys), which contains an additional functionality (i.e., a primary amino group) in the side chain to attach a chromophore. As can be seen in Figure 23., each of the three amino acids Glu, Cys and Lys contains three differently reactive functional groups, which requires a selective protecting group strategy during organic synthesis.

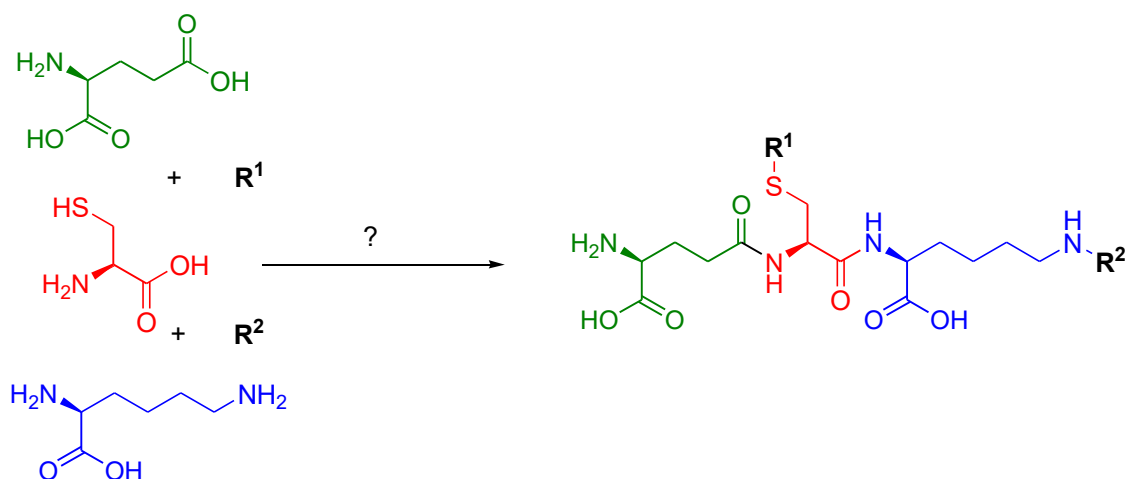


Figure 23. Schematic representation of the task to synthesize a double chromophore-labelled GSH analogue from the amino acids L-glutamic acid, L-cysteine and L-lysine; R^1 and R^2 are chromophores.

A previous GSH synthesis for several derivatives including lysine⁹⁰ relied on benzyl protecting groups. Since catalytic hydrogenolysis is not possible in the presence of sulphur atoms, the global deprotection was carried out with sodium dissolved in liquid ammonia. This procedure is time consuming, dangerous and inconvenient, in fact the strongly basic conditions can lead to racemisation or degradation, as described by Adang et al.⁹⁰. Consequently, most GSH syntheses rely on acid labile *tert*-butyl protecting groups⁹¹. The preparation of *tert*-butyl ester or thioether, however, requires the handling with gaseous isobutene, which is also inconvenient. The trityl group in contrast, offers simple protection and selective deprotection⁹². However, this strategy has so far been applied only for natural GSH, but not for other GSH derivatives. Therefore, it was necessary to invest efforts in the development of the synthesis of appropriate GSH analogues.

Two types of chemical derivatization of GSH are discussed in publication [P4], namely chromophore-labelling and exchange of a peptide bond by a non-cleavable isoster. The main derivative is a double labelled fluorogenic GSH probe with bimane as fluorophore hydrodabcyll as quencher. The ϵ -amino group of lysine was used to attach hydrodabcyll *via* amide bond. This fluorogenic probe was employed in a quantitative fluorescence-based kinetic experiment. In order to obtain a complete and quick conversion, a stopped-flow setup was used with a relatively high amount of enzyme per substrate (i.e., transient kinetics) and the results indicate that this substrate can be cleaved completely. Additionally, the same substrate was injected together with NsPCS into living *Xenopus* embryos yielding four interesting conclusions. Firstly, the embryos grew even better after administration of the double-labelled construct, so it is not cytotoxic and therefore ideal also for *in vivo* investigations. Secondly, the presence of numerous proteases *in vivo*, which did not convert the presented substrate, shows its

remarkable specificity towards PCS. Thirdly, cleavage was observed in presence of various natural peptides proving the selectivity of PCS for our substrate. Finally, this result had shown that the double labelled artificial substrate being converted even in the presence of natural GSH.

Non-cleavable substrate analogues can be useful in two respects. Firstly, they are important for studying enzyme kinetics. In order to determine the affinity of the substrate to an enzyme, the binding process needs to be disconnected from the catalytic turnover. Secondly, non-cleavable substrate analogues often act as inhibitor and may thus find pharmaceutical applications. Since PCS is not present in human, but in the parasitic worm *Schistosoma*⁷⁶, inhibitors for PCS might act as co-drugs against Schistosomiasis. Another pharmaceutical application concerns inhibitors against GSH synthetase being relevant against Malaria⁹³. Furthermore, peptide drugs like GSH derivatives readily undergo enzymatic degradation in gastrointestinal fluids, lowering bioavailability⁹⁴. A decrease in endogenous GSH levels is associated with the onset and progression of many degenerative diseases including but not limited to Parkinson's, dementia and cataracts⁹⁵. Consequently, more stable GSH analogues could allow for oral application as antioxidant against degenerative diseases.

The structure of non-cleavable peptide bond isoster can differ depending on the desired purpose⁹⁶. The option with the highest sterical similarity to the proteinogenic peptide bond is the N-methylated derivative, which is known to be resistant to proteolysis in some cases⁹⁷. For this reason, we applied our general strategy to synthesize an N-methylated GSH with the modified amide bond between cysteine and glycine. Even though it was meant to be a non-cleavable analogue, the crystal structure obtained with this derivative showed again the stalled acyl-enzyme forming a disulphide with a second intact glutathione molecule. Alternative non-cleavable derivative can either lack the carbonyl group representing the reduced form of amide bond CH₂ - amine⁹⁸ ("reduced" derivative) or have the nitrogen replaced by a CH₂ group resulting in a ketone derivative. In publication [P4], strategies and the key steps for the synthesis of both "reduced" and ketone derivatives have been developed. The key intermediate is a cysteine aldehyde, from which both functional groups are available. The aldehyde was synthesized from its Weinreb amide and transformed into the reduced "dipeptide analogue" with amino esters *via* reductive amination. Alternatively, the aldehyde was converted with allyl Grignard and subsequent hydroboration into a hydroxypropyl-cysteiny ketone without racemization.

In conclusion all these examples underline the importance of synthesizing chemically modified GSH analogues. At the same time, the synthetic strategies towards modified GSH analogues

available in literature are limited, which justifies our detailed investigation on methodology. Moreover, due to the various and fundamental roles of GSH in the metabolism of basically all the organisms, a versatile strategy to synthesize and manipulate glutathione is of general interest.

4.3. Description of the own Contribution

The entire work was performed at the University of Bayreuth. The chemical synthesis was performed at the Department of Organic Chemistry I (collaboration with Prof. Dr. Rainer Schobert). The experiments of optic spectroscopy were performed at the Department of Experimental Physics IV and at the Department of Biochemistry. Computational work was performed at the department of Theoretical Biochemistry (collaboration with Prof. Dr. Matthias Ullmann). Expression and purification of the enzyme NsPCS and the determination of the crystal structures were done at the Department of Biochemistry, (collaboration with Prof. Dr. Wulf Blankenfeld). The *in vivo* experiment with the *Xenopus* oocytes was carried out at the Department of genetics (Collaboration with Prof. Dr. Olaf Stemmann).

The contribution of all co-authors to each specific publication is detailed below.

P1: Kempf O., Kempf K., Schobert R., Bombarda* E. – HydrodabcyI: A Superior Hydrophilic Alternative to the Dark Fluorescence Quencher DabcyI. *Anal. Chem.*, **2017**, *89*, 11893-11897

<p>Oxana Kempf (Own contribution):</p>	<p>Synthesis, purification and characterisation of all substances, HPLC, NMR.</p> <p>Biophysical experiments: absorbance and fluorescence spectroscopy, Thin Layer Chromatography.</p> <p>Analysis of the results and contribution to the interpretation.</p> <p>Contribution to the writing of the manuscript.</p> <p>Graphic representation and processing of the images.</p>
<p>Karl Kempf:</p>	<p>Discussions concerning the chemical synthesis.</p>
<p>Rainer Schobert:</p>	<p>Discussion and correction of the manuscript.</p>
<p>Elisa Bombarda:</p>	<p>Design of the project, supervision of the experiments, interpretation of the results, writing the manuscript.</p>

P2: O. Kempf, G.M. Ullmann, R. Schobert, K. Kempf*, E. Bombarda*. – Chemoselective attachment of the water-soluble dark quencher hydrodabecyl to amino groups in peptides and preservation of its spectroscopic properties over a wide pH range. *ACS Omega*, **2021**, *6*, 32896-32903.

<u>Own contribution:</u>	Synthesis, purification and characterisation of all substances, HPLC, NMR, Thin Layer Chromotography. Biophysical experiments: absorbance spectroscopy, pH titration, Analysis of the results and contribution to the interpretation. Contribution to the writing of the manuscript. Graphic representation and processing of the images.
G. Matthias Ullmann:	Discussion and correction of the manuscript.
Rainer Schobert:	Discussion and correction of the manuscript.
Karl Kempf:	Supervision of the chemical synthesis, discussion and writing of the manuscript.
Elisa Bombarda:	Design of the project, supervision of the experiments, interpretation of the results, writing the manuscript.

P3: F. J. Gisdon, C. G. Feiler, O. Kempf, J. M. Förster, J. Haiss, Wulf Blankenfeldt, G. Matthias Ullmann, Elisa Bombarda*. – Structural and biophysical analysis of the phytochelatase-synthase-like enzyme from *Nostoc* sp. shows that its protease activity is sensitive to the redox state of the substrate. *ACS Chemical Biology*, **2022**, *17*, 883-897.

<u>Own contribution:</u>	Implementation of the NMR experiments, contribution to their interpretation and preparation of corresponding figures. Contribution to the correction of the manuscript.
Florian J. Gisdon:	Calculations on the reaction mechanism, analysis of the crystal structures, analysis of the calorimetric experiments. Contribution to the writing of the manuscript and figures preparation.
Christian Feiler:	Protein expression and purification, crystal structure preparation, solution and refinement.
Johannes M. Förster:	Implementation of the NMR experiments and contribution to their interpretation
Jonathan Haiss:	Folding/refolding procedure, thermophoresis and calorimetric experiments.
Wulf Blankenfeld:	Supervision of the crystallographic study, discussion and correction of the manuscript.
G. Matthias Ullmann:	Supervision of the computational study, discussion and correction of the manuscript.
Elisa Bombarda:	Design of the project and coordination of the extended collaboration network. Supervision of the experiments and interpretation of the results. Writing the manuscript.

P4: O. Kempf, O. Stemmann, R. Schobert, K. Kempf*, E. Bombarda*. – Modular Synthesis of Glutathione analogues to study peptidase reactions *in vitro* and *in vivo*. Manuscript close to submission.

<u>Own contribution:</u>	Synthesis, purification and characterisation of all compounds; HPLC, NMR, Thin Layer Chromotography, IR. Biophysical experiments: absorbance and fluorescence spectroscopy, stopped flow experiments. Analysis of the results and contribution to the interpretation. Contribution to the writing of the manuscript. Graphic representation and processing of the images.
G. Matthias Ullmann:	Discussion and correction of the manuscript.
Olaf Stemmann:	Supervision and discussion concerning the <i>in vivo</i> experiments
Rainer Schobert:	Discussion and correction of the manuscript.
Karl Kempf:	Supervision of the chemical synthesis, discussion and writing of the manuscript.
Elisa Bombarda:	Design of the project, supervision of the experiments, interpretation of the results, writing the manuscript.

5. Outlook

In the present work, a novel water-soluble fluorescence quencher was invented and established, the enzymatic mechanism of NsPCS was examined in detail and a synthesis strategy for GSH analogues was developed. We showed in a proof of concept, that our fluorogenic probe enabled monitoring the peptidase activity of NsPCS with fluorescence spectroscopy. The same synthesis strategy can be used to synthesize other derivatives. A potential application is shown in the following section. Even though NsPCS had previously been reported to mainly catalyze the peptidase reaction, formation of phytochelatins (PC₂) by transpeptidase activity was detected³⁷. At this point, NMR spectroscopy limits further studies, since the sensitivity is rather low and thus small amounts of phytochelatins cannot be detected. When the quantification of enzymatic reactions involving very low substrate or product concentrations is desired, fluorescence spectroscopy is the method of choice because of the low detection limit. The next interesting step in this project would thus be the development of a similar strategy for monitoring the transpeptidase activity of NsPCS or eukaryotic PCS enzymes. Ideally, a signal could be generated corresponding to the reaction of peptide transfer. In order to obtain such a signal with fluorescence spectroscopy, one GSH molecule might be labelled with a fluorescence donor and another one with a fluorescence acceptor (Figure 24). If a transpeptidation would combine both chromophores in one phytochelatin molecule, FRET can occur enabling detection of the specific fluorescence of the acceptor upon excitation at the specific wavelength of the donor. In order to limit the number of differently labelled products, the second GSH molecule carrying the donor chromophore should contain a non-cleavable peptide bond.

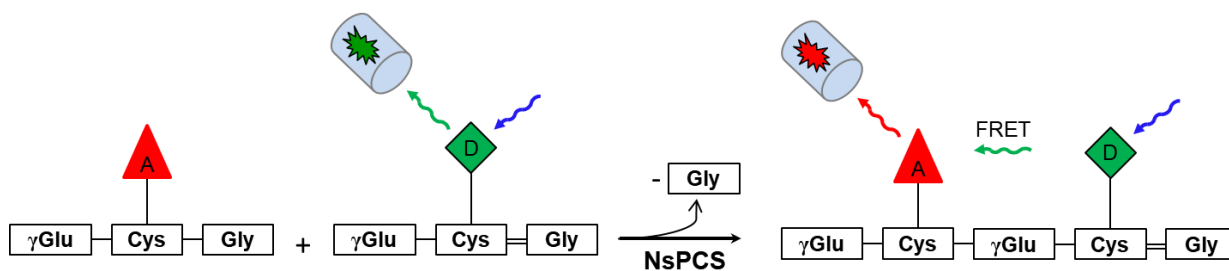


Figure 24. Schematic view of the FRET-based experiment to monitor the transpeptidase activity of NsPCS with GSH⁸⁰. The molecule labelled with the donor contains a non-cleavable bond (=) between cysteine and glycine.

The modular synthesis developed in this work can also be adapted to synthesize a double-labelled phytochelatin (PC₂) as a reference substance for the expected product in the enzymatic reaction. To this purpose, the synthesis of an acridine orange derivative, i.e., a suitable fluorescence acceptor for bimeane has already been started.

The synthetic strategy and the novel fluorescence quencher developed in this work could also be used to study other peptidases or might be implemented in other fields of research. Several recent examples have been motivated by the pandemic outbreak of SARS-CoV-2, which constitutes a big challenge not only for medicine, but also for natural scientists. In fact, the viral life cycle is dependent on several enzymes, among them three proteases: 3C-like protease (3C_lpro), Angiotensin-converting enzyme 2 (ACE2) and a papain-like protease (PLpro). ACE2 is a surface cell receptor to which the virus attaches to enter the host cell. Its protease activity was recently measured with the fluorogenic tripeptide Mca-APK(Dnp)⁹⁹ as a substrate. In this tripeptide, Alanine was functionalized with the fluorophore Mca (7-methoxycoumarin-4-acetic acid) and Lysine with the quencher Dnp (2,4-dinitrophenyl).

In another recent study the activity of SARS-CoV-2 papain-like protease PLpro, the essential coronavirus enzyme responsible for spreading, was studied with the help of a fluorogenic substrate¹⁰⁰.

Taken altogether, the examples mentioned above underline the current importance of the results described in the present thesis and their value for a number of ongoing and future research topics. The main results concern chemical synthesis of glutathione analogues and the use of fluorogenic substrates as a convenient tool to investigate the enzymatic mechanism of proteases and other GSH dependent enzymes by FRET- based experiments.

6. Conference Contribution as a Part of this Dissertation

Participation at conference, meetings etc.:

10-11.11.2011, Thurnau, Workshopmodul: “Fundamental processes in multichromophoric systems I” with talk: “Synthesis of glutathione analogues to study the enzymatic mechanism of phytochelatin synthase by fluorescence spectroscopy”;

23-26.09.2012, Göttingen - Conference: “Annual Meeting of the German Biophysical Society”, with Poster: “Synthesis and characterization of fluorescent GSH-analogues to study the enzymatic mechanism of PCS, an enzyme able to cleave and form peptide bond”;

7-11.04.2013, Banz, Conference: Light Harvesting Processes 2013, with Poster: “New glutathione analogues to study the enzymatic mechanism of phytochelatin synthase”.

23-25.09.2013, Untertiefengrün, Team Building Seminar: „Fundamental processes in multichromophoric systems II“, with talk: “New glutathione analogues to study the enzymatic mechanism of phytochelatin synthase”.

16-20.09.2015, Poster presentation at 250th ACS National Meeting and Exposition (ACS) in Boston, Massachusetts, USA: “Synthesis of glutathione analogues to investigate the mechanism of glutathione-dependent enzymes”.

Participation at events of Graduiertenkollegs:

WS 2011/12, Course: „Introduction to Modelling techniques”.

WS 2011/12, Teaching module: “Fundamental of fluorescence spectroscopy. Applications to the study of bio-molecules”, Dr. Elisa Bombarda.

WS 2012/13, Workshop: “Write it right”.

WS 2012/13, Teaching module: “Bio-molecular kinetics: from binding to catalysis”, Dr. Elisa Bombarda.

WS 2012/13, Bayreuth - Workshop: “Practical course on advanced light microscopy-Monitoring nonlinear dynamics in living matter”, Prof. Dr. Matthias Weiss.

SS 2013, Modul: “Organic solar cells”, Prof. Dr. Mukundan Thelakkat.

WS 2013/14, Teaching module: “The interplay of geometry and electronic structure in the life science”, Prof. Dr. Jürgen Köhler.

7. Other Publications and Research Contribution outside this Dissertation

Kempf K., Kempf O., M. Orozco, U. Bilitewski, Schobert R. Synthesis and Structural Revision of the Fungal Tetramic Acid Metabolite Spiroscytalin. *J. Org. Chem.*, **2017**, *82*, 7791.

Montgomery J. R. D., Kempf K., Miles-Barrett D. M., Kempf O., Lebl T. and Westwood N. J. Preparation and Reactivity of Biomass-Derived Dihydro-Dioxins. *Chem. Sus. Chem.*, **2019**, *12*, 190.

G. Xiao, M.S. Alphey, F. Tran, L. Pirrie, P. Milbeo, Y. Zhou, J. Bickel, O. Kempf, K. Kempf, J.H. Naismith, N.J. Westwood, Next generation Glucose-1-phosphate thymidyltransferase (RmlA) inhibitors: An extended SAR study to direct future design. *Bioorg. and Med. Chem.*, **2021**, *50*, 116477.

K. Kempf, Y. Capello, R. Melhem, C. Lescoat, O. Kempf, S. Chaignepain, A. Groppi, M. Nikolski, D. Deffieux, E. Génot, S. Quideau, About Multi-Target Plant Polyphenols – Affinity-Based Protein Profiling of Bone Cell Proteomes Using C-Glucosidic Vesical(ag)in-Bearing Chemoproteomic Probes. Manuscript submitted to *Angewandte Chemie* **2022**.

Participation at the International Polyphenol Congress Turku (Finland), July **2021**.

1.02.2017-10.09.2017, Stay at the University of St. Andrews as visiting researcher, (Scotland) UK, School of Chemistry, group of Prof. N. J. Westwood. Colorimetric test of different inhibitors in enzymatic activity of Thymidyltransferase RmlA1. Synthesis of phenolic derivatives, reactiv depolymerisation product of Lignin. Extraction of organosolv-Lignin.

1.01.2019-14.06.2021, Stay at the Université de Bordeaux as visiting researcher, France, group OrgaSQ of Prof. S. Quideau. Synthesis of polyphenolic (Quercetin and Kaempferol) derivatives. Implementation of the pull-down methode for identification of target proteins of bioactive polyphenolic compounds.

Acknowledgment

The first person is my supervisor Dr. Elisa Bombarda, who gave me the opportunity to realise this project and finally complete this thesis. I am very thankful for her friendly support from the beginning on. The next person to thank is Prof. Rainer Schobert who allowed me to perform organic synthesis at his department. I also thank Prof. Jürgen Köhler and Prof. Birte Höcker for having accommodated us at their departments including the opportunity to perform spectroscopic experiments. Of course, big thanks to Prof. Matthias Ullmann for friendly and fruitful discussions during whole my thesis.

I thank Graduiertenkolleg 1640, Deutschen Forschungsgemeinschaft and Bayreuther Graduiertenschule for financial support.

I also want to thank Dr. Ulrike Lacher and Kerstin Hannemann from the analytics centre of the University of Bayreuth for providing me all the required data. In general, thanks to all the people from the Schobert lab. From all those I want to thank especially Sebastian Loscher, Matthias Göhl and Marcus Winterer (my very good friend) for chemical discussions. Many thanks to Dr. Claus Hölzel for his huge IT support. I also thank Werner Kern, André Wetzel and Sooruban Shanmugaratnam for friendly technical support in OC I/ Biochemistry. I also want to thank my Bachelor students Carmen and Laura, as well as my Master student Lisa for the teaching experience and fruitful work together. Many thanks to my colleagues Johannes Förster, Florian Gisdon, Christian Feiler, Silke Weninger, Galya Kudryasheva and Regina Müller for discussions and nice working atmosphere. I am very thankful to Violaine Zigan, Claudia Geier and Silvia Kastner for making all bureaucratic stuff easy and very friendly. Thanks to Werner Reichstein and Waltraud Joy for technical support and friendly conditions in EP IV and thanks to Dr. Marti Pärst† for helping with data analysis in the Origin program.

I also want to thank again all the people who I met on my career way. From every single one of you I learned a lot of important things. Special thanks to my first scientific supervisors Dr. Vitaly V. Pozdeev and Dr. Ninel M. Baranova and Sergey V. Gusenkov, without him I never would have thought to start my PhD in Germany.

I want to thank my whole family in Russia and my German family. There have been hard times and I felt always greatly supported by all of you. Thank you so much for everything you did.

The V.I.P. is my husband and the best ever colleague Dr. Karl Kempf. I thank you for incredible time in the lab, great support mentally and physically, especially for long day and night discussion and proofreading the final version of this thesis.

References

- ¹ B. A. Goodman (1994). – Molecular spectroscopy: introduction and general principles. In: M. J. Wilson. (eds) Clay Mineralogy: Spectroscopic and Chemical Determinative Methods. Verlag Springer. Dordrecht.
- ² C. N. Banwell (1983). – Fundamentals of Molecular Spectroscopy. Verlag, New York; McGraw-Hill, 3rd ed.
- ³ D. A. Skoog, D. M. West, F. J. Holler, S. R. Crouch (2014). -Fundamentals of Analytical Chemistry. Verlag Brooks/Cole, Cengage Learning, 9th edition.
- ⁴ S. R. Crouch, D. A. Skoog (2007). – Principles of instrumental analysis. Verlag Thomson Brooks/Cole, Australia.
- ⁵ B. Valeur (2001). – Molecular Fluorescence: Principles and Applications. Verlag Wiley-VCH.
- ⁶ J. R. Lakowicz (2010). – Principles of Fluorescence Spectroscopy. Verlag Springer, 3rd edition.
- ⁷ <https://www.chem.uci.edu/~dmitryf/Library/Themes/fluorescence.html> (pdf, Excitation and emission spectroscopy fundamentals (by B. Herman, J.R. Lakowicz, D.B. Murphy, T.J.Fellers and M.W. Davidson for Olympus).
- ⁸ Image used from <https://www.photometrics.com/learn/physics-and-biophysics/fret>, originally from Alex M Mooney, CC BY-SA 3.0.
- ⁹ File: Conditions_du_FRET.png licensed with Cc-by-sa 3.0,2.5,2.0,1.0, GFDL 2008-03-24T21:27:11Z Maurel Damien.
- ¹⁰ T. Förster. – Zwischenmolekulare Energiewanderung und Fluoreszenz. *Ann. Physik.* **1948**, *2*, 55–75.
- ¹¹ P. Held. <http://www.biotek.com/resources/white-papers/an-introduction-tofluorescence-resonance-energy-transfer-fret-technology-and-ist-application-in-bioscience/> June 20, 2005.
- ¹² H. Yu. – Extending the size limit of protein nuclear magnetic resonance. *Proc. Natl. Acad. Sci. USA*, **1999**, *96*, 332–334.
- ¹³ A. Mazumder and D. K. Dubey (2013). – Nuclear Magnetic Resonance (NMR) Spectroscopy. Verlag Elsevier. <http://dx.doi.org/10.1016/B978-0-12-409547-2.05891-1>

-
- ¹⁴ https://www.reddit.com/r/OrganicChemistry/comments/f5a7xb/nmr_spectroscopy_an_easy_introduction_chemistry/
- ¹⁵ C.-Y. Lee. – Kinetics of Enzyme-Coenzyme Interactions by NMR Spectroscopy. *Biochimica et Biophysica Acta*, **1978**, 527, 289–300.
- ¹⁶ C. Her, A. P. Alonzo, J. Y. Vang, E. Torres, and V. V. Krishnan. – Real-Time Enzyme Kinetics by Quantitative NMR Spectroscopy and Determination of the Michaelis–Menten Constant Using the Lambert-W Function. *J. Chem. Educ.*, **2015**, 92, 1943–1948.
- ¹⁷ N. D. Romanyuk, D. J. Rigden, O. K. Vatamaniuk, A. Lang, R. E. Cahoon, J. M. Jez and P. A. Rea. – Mutagenic Definition of a Papain-Like Catalytic Triad, Sufficiency of the N-Terminal Domain for Single-Site Core Catalytic Enzyme Acylation, and C-Terminal Domain for Augmentative Metal Activation of a Eukaryotic Phytochelatin Synthase. *Plant Physiol.*, **2006**, 141, 858–869.
- ¹⁸ W. Gekeler, E. Grill, E. L. Winnacker, M. H. Zenk. – Survey of the Plant Kingdom for the Ability to Bind Heavy Metals through Phytochelatins. *Zeitschrift Fur Naturforsch. - Sect. C J. Biosci.*, **1989**, 44, 361–369.
- ¹⁹ O.K. Vatamaniuk, E.A. Bucher, J.T. Ward, P.A. Rea. – Worms take the “phyto” out of “phytochelatins”. *Trends Biotechnol.* **2002**, 20, 61–64.
- ²⁰ a) Howden R, Goldsbrough PB, Andersen CR, Cobbett CS. – Cadmiumsensitive, *cad1* mutants of *Arabidopsis thaliana* are phytochelatin deficient. *Plant Physiol.*, **1995**, 107, 1059–1066.
- b) J. M. Gong, D. A. Lee, J. I. Schroeder. – Long-distance root-to-shoot transport of phytochelatins and cadmium in *Arabidopsis*. *Proc Natl Acad Sci USA.*, **2003**, 100, 10118–10123.
- ²¹ N. Estrella-Gómez, D. Mendoza-Cózatl, R. Moreno-Sánchez, D. González-Mendoza, O. Zapata-Pérez, A. Martínez-Hernández, et al. – The Pb-hyperaccumulator aquatic fern *Salvinia minima* Baker, responds to Pb²⁺ by increasing phytochelatins via changes in *SmPCS* expression and in phytochelatin synthase activity. *Aquat Toxicol.*, **2009**, 91, 320–328.
- ²² a) P. Tennstedt, D. Peisker, C. Böttcher, A. Tramczynska, S. Clemens. – Phytochelatin synthesis is essential for the detoxification of excess zinc and contributes significantly to the accumulation of zinc. *Plant Physiol.*, **2009**, 149, 938–948.

-
- a) L. Wie, J. R. Donat, G. Fones and B. A. Ahner. – Interactions between Cd, Cu and Zn. Influence Particulate Phytochelatin Concentrations in Marine Phytoplankton: Laboratory Results and Preliminary Field Data. *Environ. Sci. Technol.*, **2003**, *37*, 3609–3618.
- ²³ C. Cobbett and P. Goldsbrough. – Phytochelatins and metallothioneins: roles in heavy metal detoxification and homeostasis. *Annu. Rev. Plant Biol.*, **2002**, *53*, 159–182.
- ²⁴ S. Verma, R. Dixit and K. C. Pandey. – Cysteine Proteases: Modes of Activation and Future Prospects as Pharmacological Targets. *Frontiers in Pharmacology*, **2016**, *7*, 107.
- ²⁵ Q. Yuan, M. Bomma and Z. Xiao. – Enhanced Extracellular Synthesis of Gold Nanoparticles by Soluble Extracts from *Escherichia coli* Transformed with *Rhizobium tropici* Phytochelatin Synthase Gene. *Metals*, **2021**, *11*, 472.
- ²⁶ S. Klapheck, W. Fliegner, I. Zimmer. – Hydroxymethyl-Phytochelatins [[γ -Glutamylcysteine]_n-Serine] Are Metal-Induced Peptides of the Poaceae. *Plant Physiol.*, **1994**, *104*, 1325–1332.
- ²⁷ P. Meuwly, P. Thibault, A. L. Schwan, W. E. Rauser. – Three families of thiol peptides are induced by cadmium in maize. *Plant J.*, **1995**, *7*, 391–400.
- ²⁸ H. Kubota, K. Sato, T. Yamada, T. Maitani. Phytochelatin homologs induced in hairy roots of horseradish. *Phytochemistry*, **2000**, *53*, 239–245.
- ²⁹ a) E. Grill, W. Gekeler, E. L. Winnacker, M. H. Zenk. – Homophytochelatins are heavy metal-binding peptides of homo-glutathione containing Fabales. *FEBS Lett.*, **1986**, *205*, 47–50.
- b) S. B. Ha, A. P. Smith, R. Howden, W. M. Dietrich, S. Bugg, M. J. O'Connell, P. B. Goldsbrough, C. S. Cobbett. – Phytochelatin synthase genes from *Arabidopsis* and the yeast *Schizosaccharomyces pombe*. *Plant Cell*, **1999**, *11*, 1153–1164.
- ³⁰ P.A. Rea. – Phytochelatin synthase, papain's cousin, in stereo. *Proc. Natl. Acad. Sci. U. S. A.*, **2006**, *103*, 507–508.
- ³¹ O.K. Vatamaniuk, S. Mari, A. Lang, et al. – Phytochelatin synthase, a dipeptidyl transferase that undergoes multisite acylation with γ -glutamylcysteine during catalysis. Stoichiometry and site-directed mutagenic analysis of AtPCS1-catalyzed phytochelatin synthesis. *Journal of Biological Chemistry*, **2004**, *279*, 22449–22460.
- ³² E. Bellini, C. Varotto, M. Borsò, L. Rugnini, L. Bruno and L. S. di Toppi. – Eukaryotic and Prokaryotic Phytochelatin Synthases differ less in Functional Terms than previously thought: A

Comparative Analysis of *Marchantia polymorpha* and *Geitlerinema* sp. PCC 7407. *Plants*, **2020**, *9*, 914.

³³ P.A. Rea. – Phytochelatin synthase: Of a protease a peptide polymerase made. *Physiol. Plant.*, **2012**, *145*, 154–164.

³⁴ S. Clemens, D. Peršoh. – Multi-tasking phytochelatin synthases. *Plant Sci.*, **2009**, *177*, 266–271.

³⁵ D. Vivares, P. Arnoux, D. Pignol. – A papain-like enzyme at work: Native and acyl–enzyme intermediate structures in phytochelatin synthesis. *PNAS*, **2005**, *102*, 18848–18853.

³⁶ E. Harada, E. von Roepenack-Lahaye, S. Clemens. – A cyanobacterial protein with similarity to phytochelatin synthases catalyzes the conversion of glutathione to gamma-glutamylcysteine and lacks phytochelatin synthase activity. *Phytochemistry*, **2004**, *65*, 3179–3185.

³⁷ N. Tsuji, S. Nishikori, O. Iwabe, K. Shiraki, H. Miyasaka, M. Takagi, K. Hirata, K. Miyamoto. – Characterization of phytochelatin synthase-like protein encoded by *alr0975* from a prokaryote, *Nostoc* sp. PCC 7120. *Biochem. Biophys. Res. Commun.*, **2004**, *315*, 751–755.

³⁸ N. Tsuji, S. Nishikori, O. Iwabe, S. Matsumoto, K. Shiraki, H. Miyasaka, M. Takagi, K. Miyamoto, K. Hirata. – Comparative analysis of the two-step reaction catalyzed by prokaryotic and eukaryotic phytochelatin synthase by an ion-pair liquid chromatography assay. *Planta*, **2005**, *222*, 181–191.

³⁹ A. K. Bachhawat, A. Kaur. – Glutathione Degradation. *Antioxidants and Redox Signaling*, **2017**, *27*, 1200–1216.

⁴⁰ W. B. Jakoby (Eds.), I.M. Arias (1976). – Glutathione: Metabolism and Function. Raven Press, New York.

⁴¹ K. Aquilano, S. Baldelli and M. R. Ciriolo. – Glutathione: new roles in redox signalling for an old antioxidant. *Frontiers in Pharmacology Experimental Pharmacology and Drug Discovery*, **2014**, *5*, Article 196.

⁴² M. Deponte. – The Incomplete Glutathione Puzzle: Just Guessing at Numbers and Figures? *Antioxidants and Redox Signaling*, **2017**, *27*, 1130–1161.

⁴³ I. G. Sipes, D. A. Wiersma, D. J. Armstrong (1986). The Role of Glutathione in the Toxicity of Xenobiotic Compounds: Metabolic Activation of 1,2-Dibromoethane by Glutathione.

Biological Reactive Intermediates III. *Advances in Experimental Medicine and Biology*, vol. 197. Verlag Springer, Boston, MA.

⁴⁴ V. I. Lushchak. – Glutathione Homeostasis and Functions: Potential Targets for Medical Interventions. *J. of Amino Acids*, **2012**, vol. 2012, Article ID 736837.

⁴⁵ G. Bjørklund, A. A. Tinkov, B. Hosnedlová, R. Kizek, O. P. Ajsuvakova, S. Chirumbolo, M. G. Skalnaya, M. Peana, M. Dadar, A. El-Ansary, H. Qasem, J. B. Adams, J. Aaseth, A. V. Skalny. – The role of glutathione redox imbalance in autism spectrum disorder: A review. *Free Radical Biology and Medicine*, **2020**, 160, 149–162.

⁴⁶ S. Baldelli, F. Ciccarone, D. Limongi, P. Checconi, A. T. Palamara, M. R. Ciriolo. – Glutathione and Nitric Oxide: Key Team Players in Use and Disuse of Skeletal Muscle. *Nutrients*, **2019**, 11, 2318.

⁴⁷ J. R. Grunwell, S. E. Gillespie, J. M. Ward, A. M. Fitzpatrick, L. A. Brown, T. W. Gauthier, K. B. Hebbar. – Comparison of Glutathione, Cysteine, and Their Redox Potentials in the Plasma of Critically Ill and Healthy Children. *Frontiers in pediatrics*, **2015**, 3, 46.

⁴⁸ W. Wang and N. Ballatori. – Endogenous glutathione conjugates: occurrence and biological functions. *Pharmacological Reviews*, **1998**, 50, 335–355.

⁴⁹ M. K. Johansson and R. M. Cook. – Intramolecular Dimers: A New Design Strategy for Fluorescence-Quenched Probes. *Chem. Eur. J.*, **2003**, 9, 3466–3471.

⁵⁰ O. Kempf, K. Kempf, R. Schobert, E. Bombarda. – HydrodabcyI: A Superior Hydrophilic Alternative to the Dark Fluorescence Quencher DabcyI. *Anal. Chem.*, **2017**, 89, 11893–11897.

⁵¹ G. Blum, R. M. Weimer, L. E. Edgington, W. Adams, M. Bogyo. – Comparative Assessment of Substrates and Activity Based Probes as Tools for Non-Invasive Optical Imaging of Cysteine Protease Activity. *PLoS ONE*, **2009**, 4, e6374.

⁵² a) A. Hantzsch, Ber. Dtsch. Chem. Ges., **1908**, 41, 1187–1195.

b) R. W. Linton, L. D. Smith, *J. Franklin Inst.*, **1942**, 234, 286–288.

⁵³ C. D. F. Martins, M. M. M. Raposo and S. P. G. Costa. – Intermolecular Quenching of Edans/DabcyI Donor – Acceptor FRET Pair. *Proceedings*, **2019**, 41, 34.

⁵⁴ M. Moustafa "Design and Synthesis of Novel Quenchers for Fluorescent Hybridization Probes" (**2011**). Electronic Thesis and Dissertation Repository. 259. The University of Western Ontario.

-
- ⁵⁵ A. Chevalier, P.-Y. Renard, A. Romieu. – Azo-Based Fluorogenic Probes for Biosensing and Bioimaging: Recent Advances and Upcoming Challenges. *Chem. Asian J.*, **2017**, *12*, 2008–2028.
- ⁵⁶ H. M. Bandara, S. C. Burdette. – Photoisomerization in different classes of azobenzene. *Chem. Soc. Rev.*, **2012**, *41*, 1809–1825.
- ⁵⁷ C. M. Ettles "Progress Toward Synthesis of Molecular Beacons Incorporating DABCYL Analog Quenchers" (**2013**). Electronic Thesis and Dissertation Repository. 1790. The University of Western Ontario.
- ⁵⁸ T. Schultz, J. Quenneville, B. Levine, A. Toniolo, S. L. Martínez, M. Schmitt, J. P. Shaffer, M. Z. Zgierski, A. Stolow. – Mechanism and Dynamics of Azobenzene Photoisomerization. *J. Am. Chem. Soc.*, **2003**, *125*, 8098–8099.
- ⁵⁹ G. Gabor and E. Fischer. – Spectra and Cis-Trans Isomerism in Highly Bipolar Derivatives of Azobenzene. *J. Phys. Chem.*, **1971**, *75*, 581–583.
- ⁶⁰ D. M. Shin and D. G. Whitten. – Solvent-Induced Mechanism Change in Charge-Transfer Molecules. Inversion versus Rotation Paths for the *Z* → *E* Isomerization of Donor-Acceptor Substituted Azobenzenes. *J. Am. Chem. Soc.*, **1988**, *110*, 5206–5208.
- ⁶¹ M. E. Sanborn, B. K. Connolly, K. Gurunathan, M. Levitus. – Fluorescence Properties and Photophysics of the Sulfoindocyanine Cy3 Linked Covalently to DNA. *J. Phys. Chem. B.*, **2007**, *111*, 11064–11074.
- ⁶² S. E. Wheeler, J. W. G. Bloom. – Toward a More Complete Understanding of Noncovalent Interactions Involving Aromatic Rings. *J. Phys. Chem. A*, **2014**, *118*, 32, 6133–6147.
- ⁶³ P. Felderbauer, J. Schnekenburger, R. Lebert, K. Bulut, M. Parry, T. Meister, V. Schick, F. Schmitz, W. Domschke, E. W. Schmidt. – A novel A121T mutation in human cationic trypsinogen associated with hereditary pancreatitis: functional data indicating a loss-of-function mutation influencing the R122 trypsin cleavage site. *J. Med. Genet.*, **2008**, *45*, 507–512.
- ⁶⁴ K.-A. Kreuzer, A. Bohn, J. Lupberger, J. Solassol, P. le Coutre and C. A. Schmidt. – Simultaneous Absolute Quantification of Target and Control Templates by Real-Time Fluorescence Reverse Transcription-PCR Using 4-(4'-Dimethylaminophenylazo)benzoic Acid as a Dark Quencher Dye. *Clinical Chemistry*, **2001**, *47*, 486–490.

-
- ⁶⁵ X. Zhang, V. Kotikam¹, E. Rozners, B. P. Callahan. – Enzymatic Beacons for Specific Sensing of Dilute Nucleic Acid and Potential Utility for SARS-CoV-2 Detection. *bioRxiv*, **2021** doi.org/10.1101/2021.08.30.458287.
- ⁶⁶ F. Guzmán, S. Barberis, A. Illanes. – Peptide synthesis: chemical or enzymatic. *Electronic Journal of Biotechnology*, **2007**, *10*, 279–314.
- ⁶⁷ Da’san M. M. Jaradat. – Thirteen decades of peptide synthesis: key developments in solid phase peptide synthesis and amide bond formation utilized in peptide ligation. *Amino Acids*, **2018**, *50*, 39-69.
- ⁶⁸ A. Isidro-Llobet, M. Álvarez and F. Albericio. – Amino Acid-Protecting Groups. *Chem Rev.*, **2009**, *109*, 2455-2504.
- ⁶⁹ S. B. H. Kent. – Chemical synthesis of peptides and proteins. *Ann. Rev. Biochem.*, **1988**, *57*, 957-989.
- ⁷⁰ A. B. Lutjen, M. A. Quirk, A. M. Barbera, E. M. Kolonko. – Synthesis of (E)-cinnamyl ester derivatives via greener Steglich esterification. *Bioorganic & Medicinal Chemistry*, **2018**, *26*, 5291–5298.
- ⁷¹ H. Wissman, H.-J. Kleiner. – Neue Peptidsynthese. *Angew. Chem.*, **1980**, *92*, 129–130.
- ⁷² S. Clemens, E. J. Kim, D. Neumann, J. I. Schroeder. – Tolerance to toxic metals by a gene family of phytochelatins from plants and yeast. *EMBO J.*, **1999**, *18*, 3325–3333.
- ⁷³ S. Yamazaki, Y. Ueda, A. Mukai, K. Ochiai, T. Matoh. – Rice phytochelatins OsPCS1 and OsPCS2 make different contributions to cadmium and arsenic tolerance. *Plant Direct.*, **2018**, *2*, 1–15.
- ⁷⁴ E. Filiz, I. A. Saracoglu, I. I. Ozyigit, B. Yalcin. – Comparative analyses of phytochelatins synthase (PCS) genes in higher plants. *Biotechnology & Biotechnological Equipment*, **2019**, *33*, 178–194.
- ⁷⁵ K. Hématy, M. Lim, C. Cherk, M. Pislewska-Bednarek, C. Sanchez-Rodriguez, M. Stein, R. Fuchs, C. Klapprodt, V. Lipka, A. Molina, E. Grill, P. Schulze-Lefert, P. Bednarek and S. Somerville. – Moonlighting Function of Phytochelatins Synthase1 in Extracellular Defense against Fungal Pathogens. *Plant Physiol.*, **2020**, *182*, 1920–1932.

-
- ⁷⁶ C. Rigouin, E. Nylin, A. A. Cogswell, D. Schaumlöffel, D. Dobritsch, D. L. Williams. – Towards an Understanding of the Function of the Phytochelatin Synthase of *Schistosoma mansoni*. *PLOS Neglected Tropical Diseases*, **2013**, *7*, e2037.
- ⁷⁷ a) J. G. Bundy, P. Kille. – Metabolites and metals in Metazoa – what role do phytochelatin play in animals? *Metallomics*, **2014**, *6*, 1576–1582.
- b) M. Li, E. Barbaro, E. Bellini, A. Saba, L. Sanità di Toppi, C. Varotto. – Ancestral function of the phytochelatin synthase C-terminal domain in inhibition of heavy metal-mediated enzyme overactivation. *Journal of Experimental Botany*, **2020**, *71*, 6655–6669.
- ⁷⁸ A. Polonikov. – Endogenous Deficiency of Glutathione as the Most Likely Cause of Serious Manifestations and Death in COVID-19 Patients. *ACS Infect. Dis.*, **2020**, *6*, 1558–1562.
- ⁷⁹ O. Kempf, E. Bombarda, K. Kempf, G.M. Ullmann, R. Schobert. – Patent: Hydrodabcyll. International patent WO 2016/083611 A1 (EP 3031797 A1; US 2017/0327460 A1).
- ⁸⁰ Picture is from Elisa Bombarda
- ⁸¹ F. J. Gisdon, C. G. Feiler, O. Kempf, J. M. Förster, J. Haiss, W. Blankenfeldt, G. M. Ullmann, E. Bombarda. – Structural and biophysical analysis of the phytochelatin-synthase-like enzyme from *Nostoc* sp. shows that its protease activity is sensitive to the redox state of the substrate. *ACS Chem. Biol.*, **2022**, *17*, 883-897.
- ⁸² A. Grzam, P. Tennstedt, S. Clemens, R. Hell, A. J. Meyer. – Vacuolar sequestration of glutathione *S*-conjugates outcompetes a possible degradation of the glutathione moiety by phytochelatin synthase. *FEBS Lett.*, **2006**, *580*, 6384–6390.
- ⁸³ E. Sato, H. Hatori and Y. Kanaoka. – Fluorogenic bimane substrate with Dabsyl group for endopeptidases: chymotrypsin, collagenase and thermolysin. *J. Pharmacobiodyn.*, **1991**, *14*, 599–604.
- ⁸⁴ P. Crisalli and E. T. Kool. – Multi-Path Quenchers: Efficient Quenching of Common Fluorophores. *Bioconjugate Chem.*, **2011**, *22*, 2345–2354.
- ⁸⁵ R. J. Hopkinson, P. S. Barlow, C. J. Schofield and T. D. W. Claridge. – Studies on the reaction of glutathione and formaldehyde using NMR. *Org. Biomol. Chem.*, **2010**, *8*, 4915–4920.
- ⁸⁶ T. Petrzilka, W. G. Lusuardi. – Synthese von Haschisch-Inhaltsstoffen. *Helv. Chim. Acta*, **1973**, *56*, 510.

-
- ⁸⁷ S. Weimer, K. Oertel, H. L. Fuchsbauer. – A quenched fluorescent dipeptide for assaying dispase- and thermolysin-like proteases. *Anal. Biochem.*, **2006**, *352*, 110–119.
- ⁸⁸ R. Blum, A. Beck, A. Korte, A. Stengel, T. Letzel, K. Lenzian, E. Grill. – Function of phytochelatin synthase in catabolism of glutathione-conjugates. *Plant J.*, **2007**, *49*, 740–749.
- ⁸⁹ M. H. Zenk. – Heavy metal detoxification in higher plants-a review. *Gene*, **1996**, *179*, 21–30.
- ⁹⁰ A. E. P. Adang, A. J. G. Duindam, J. Brussee, G. J. Mulder, A. van der Gen. – Synthesis and nucleophilic reactivity of a series of glutathione analogues, modified at the gamma-glutamyl moiety. *Biochem. J.*, **1988**, *255*, 715–720.
- ⁹¹ a) J. J. Pastuszak, A. Chimiak. – Glutathion Synthesis as Test of the t-Butyl Thiol Protection. *J. für Prakt. Chem.*, **1980**, *Bd. 322*, H. 3, 495–498.
- b) S. Minchev, N. V. Sofroniev. – The Use of S-Acetamidomethyl-L-cysteine in the Synthesis of Glutathione, Glutathione Fragments, and Their Amides. *Liebigs Ann. Chem.*, **1987**, 69–71.
- c) W. Zeng, B. Hemmasi. – Solution synthesis of phytochelatins, isopeptides from the plant kingdom. *Liebigs Ann. Chem.*, **1992**, 311–315.
- ⁹² a) G. Amiard, N. le Sec, R. Heyrnes, and L. Velluz. – Patent: Method of making glutathione. United States Patent Office 2,900,375, 1959.
- b) M. Maltese. – Patent: Tritylation reactions based on metallic catalysts. International Patent WO 2007/009944 A1.
- ⁹³ Y. N. Kumar, G. Jeyakodi, R. Thulasibabu, K. Gunasekaran, P. Jambulingam. – Screening and Identification of Inhibitors against Glutathione Synthetase, A Potential Drug Target of Plasmodium falciparum. *Combinatorial Chemistry & High Throughput Screening*, **2015**, *18*, 492–504.
- ⁹⁴ M. Liu, M. Sharma, G.-L. Lu, N. Yin, M. Al Gailani, S. Sreebhavan, J. Wen. – Preformulation studies of l-glutathione: physicochemical properties, degradation kinetics, and *in vitro* cytotoxicity investigations. *Drug Development and Industrial Pharmacy*, **2020**, *46*, 717–731.
- ⁹⁵ a) E. W. Flagg, R. J. Coates, D. P. Jones, T. E. Byers, R. S. Greenberg, G. Gridley, J. K. McLaughlin, W. J. Blot, M. Haber, S. Preston-Martin, J. B. Schoenberg, D. F. Austin, J. F. Jr. Fraumeni. – Dietary glutathione intake and the risk of oral and pharyngeal cancer. *Am. J. Epidemiol.*, **1994**, *139*, 453–465.

b) F. J. Giblin. – Glutathione: a vital lens antioxidant. *Journal of Ocular Pharmacology and Therapeutics*, **2000**, 121–135.

⁹⁶ A. Choudhary and R. T. Raines. – An Evaluation of Peptide-Bond Isosteres. *ChemBiochem.*, **2011**, *12*, 1801–1807.

⁹⁷ S. M. Miller, R. J. Simon, S. Ng, R. N. Zuckermann, J. M. Kerr, W. H. Moos. – Comparison of the Proteolytic Susceptibilities of Homologous L-Amino Acid, D-Amino Acid, and N-Substituted Glycine Peptide and Peptoid Oligomers. *Drug Development Research*, **1995**, *35*, 20–32.

⁹⁸ B. M. Haffar, S. J. Hocart, D. H. Coy, S. Mantey, H. C. Chiang, R. T. Jensen. – Reduced Peptide Bond Pseudopeptide Analogues of Secretin. *J. Biol. Chem.*, **1991**, *266*, 316–322.

⁹⁹ X. Liu, R. Raghuvanshi, F. D. Ceylan and B. W. Bolling. – Quercetin and Its Metabolites Inhibit Recombinant Human Angiotensin-Converting Enzyme 2 (ACE2) Activity. *J. Agric. Food Chem.*, **2020**, *68*, 13982–13989.

¹⁰⁰ W. Rut, Z. Lv, M. Zmudzinski, S. Patchett, D. Nayak, J. Snipas, F. El Oualid, T. T. Huang, M. Bekes, M. Drag, S. K. Olsen. – Activity profiling and crystal structures of inhibitorbound SARS-CoV-2 papain-like protease: A framework for anti-COVID-19 drug design. *Sci. Adv.* **2020**, *6*, eabd4596.

Appendix: Publications I-IV

Publication I

Hydrodabcyl: a superior hydrophilic alternative to the dark fluorescence quencher dabcyll

Oxana Kempf,[†] Karl Kempf, [‡] Rainer Schobert[‡] and Elisa Bombarda*,[†]

[†]Department of Biochemistry and [‡]Organic Chemistry Laboratory, University of Bayreuth, Universitaetsstr. 30, 95440, Bayreuth, Germany

E-mail: elisa.bombarda@uni-bayreuth.de

Anal. Chem. 2017, 89, 11893-11897.

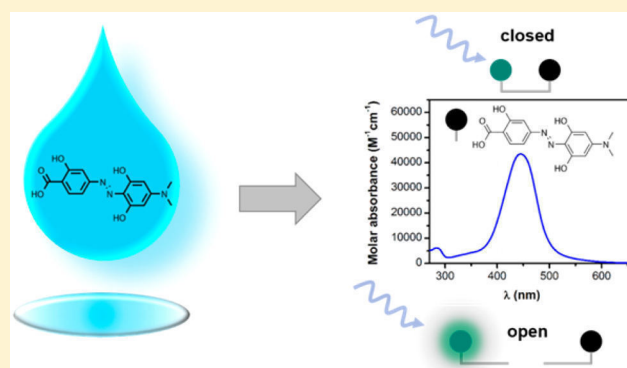
Reprinted with permission from [Hydrodabcyl: A Superior Hydrophilic Alternative to the Dark Fluorescence Quencher Dabcyll. Oxana Kempf, Karl Kempf, Rainer Schobert, and Elisa Bombarda, Anal. Chem. 2017, 89, 11893-11897, DOI: 10.1021/acs.analchem.7b03488]. Copyright 2017 American Chemical Society

HydrodabcyI: A Superior Hydrophilic Alternative to the Dark Fluorescence Quencher DabcyI

Oxana Kempf,[†] Karl Kempf,[‡] Rainer Schobert,[‡] and Elisa Bombarda^{*,†}[†]Department of Biochemistry and [‡]Organic Chemistry Laboratory, University of Bayreuth, Universitaetsstrasse 30, 95440, Bayreuth, Germany

Supporting Information

ABSTRACT: Dark fluorescence quenchers are nonfluorescent dyes that can modulate the fluorescence signal of an appropriate fluorophore donor in a distance-dependent manner. Dark quenchers are extensively used in many biomolecular analytical applications, such as studies with fluorogenic protease substrates or nucleic acids probes. A very popular dark fluorescence quencher is dabcyI, which is a hydrophobic azobenzene derivative. However, its insolubility in water may constitute a major drawback, especially during the investigation of biochemical systems whose natural solvent is water. We designed and synthesized a new azobenzene-based dark quencher with excellent solubility in aqueous media, which represents a superior alternative to the much-used dabcyI. The advantage of hydrodabcyI over dabcyI is exemplarily demonstrated for the cleavage of the fluorogenic substrate hydrodabcyI-Ser-Phe-EDANS by the proteases thermolysin and papain.



Biomolecular processes are extensively studied by employing fluorescence dyes.¹ There is a broad range of fluorescent dyes, the spectroscopic characteristics of which depend on several physicochemical parameters such as their hydrophobicity and oxidation state or the pH value and ionic strength of the medium.² The strategy of using such single-labeled probes was refined by the development of dual-labeled probes which combine a reporter dye with a quencher moiety.³ Typically, these probes may exist in two conformations differing in their fluorescence properties: a “closed” form in which the reporter and the quencher are in close proximity and an “open” form in which these groups are spatially separated. If the quencher is a fluorescence dye itself, both the increase in the fluorescence of the quencher and the decrease in the fluorescence of the reporter can be followed. However, an overlap of quencher and reporter fluorescence spectra may cause background noise necessitating a meticulous instrumental setup and data analysis. Dark quenchers (e.g., nonfluorescent dyes) offer a solution to this problem because they do not occupy any crucial emission bandwidth. Dual-labeled probes comprising a reporter and a dark quencher are also called fluorogenic probes since the biochemical event to be observed causes their transition from a nonfluorescent to a (typically strongly) fluorescent form.

DabcyI (4-(4'-dimethylaminophenylazo)benzoic acid (1), Figure 1) is a dark quencher in dual-labeled probes widely used for a variety of biomolecular applications such as enzymatic catalysis and nucleic acid probes.^{4–7} The absorption band of dabcyI (1) in the range of 350–550 nm overlaps with the emission band of many common fluorescent dyes such as 5-

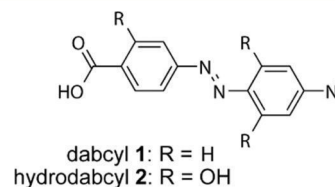


Figure 1. Chemical structures of 4-(4'-dimethylaminophenylazo)benzoic acid (dabcyI (1)) and 4-(2',6'-dihydroxy-4'-dimethylamino-phenylazo)-2-hydroxybenzoic acid (hydrodabcyI (2)).

((2'-aminoethyl)amino)naphthalene-1-sulfonic acid (EDANS) ($\lambda_{em, Max} = 490$ nm), bimane ($\lambda_{em, Max} = 480$ nm) and many fluorescein, coumarin, and rhodamine derivatives. DabcyI (1) is an azobenzene push–pull functionalized at the para-positions of the phenyl rings. Its conjugated π -system and its lack of polar substituents render it a hydrophobic compound, virtually insoluble in aqueous media. In fact, stock solutions of dabcyI (1) need to be prepared in DMSO. Although dabcyI (1) is one of the most popular acceptors for developing FRET-based probes, its insolubility in water severely limits its use in biological systems where the natural solvent is water. Even when this hydrophobicity can be partly compensated for by the hydrophilicity of the substrate to which dabcyI (1) is linked (e.g., long DNA segments or peptide chains), it poses a real problem in the case of comparatively small substrates. Such

Received: August 26, 2017

Accepted: October 26, 2017

Published: October 26, 2017

solubility problems were reported for various dabcyI-labeled substrates.^{5,8} In particular, any incomplete dissolution leads to inaccurate estimations of the concentrations and consequently to erroneous calculations of stability and rate constants. Most attempts to overcome the problems stemming from the insolubility of dabcyI (**1**) such as performing the enzymatic assays in mixtures of water and DMSO⁵ can be a source of new problems due to the modification of the polar environment of the reaction. Instead of adjusting the polarity of the solvent, we designed and synthesized a new azobenzene derivative, hydrodabcyI (**2**), that is spectroscopically dabcyI-like yet far more hydrophilic when compared to dabcyI (**1**).

EXPERIMENTAL SECTION

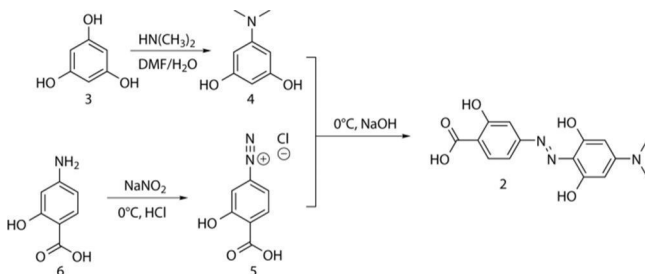
All procedural information can be found in the [Supporting Information](#).

RESULTS AND DISCUSSION

Technically, hydrodabcyI (**2**) (4-(2',6'-dihydroxy-4'-dimethylaminophenylazo)-2-hydroxybenzoic acid, [Figure 1](#)) is a trihydroxy derivative of the parent dabcyI (**1**). Since phenolic OH groups were known to affect the emitting properties of a molecule, which is apparent for instance from the intensity increase and red-shift of the fluorescence when going from phenylalanine to tyrosine, it took some deliberation to ensure the darkness of the new chromophore. We found that the addition of three hydroxy groups to the azobenzene of **1** led to a nonfluorescent molecule. This finding is in line with previous work on the coumarin chromophore that showed that the addition of an OH group at C-7 of coumarin gives rise to a distinctly fluorescent molecule while attachment of three OH groups affords nonfluorescent coumarin derivatives.⁹ Accordingly, trihydroxydabcyI derivatives were not fluorescent either. Moreover, the three hydroxy groups had to be positioned in a way that precludes the formation of catechol chelate complexes with biologically relevant metal ions (e.g., Fe(III)¹⁰) which would possibly interfere with the system under investigation. This aspect is particularly important for the investigation of enzymatic reactions in which metals are essential cofactors and for possible applications *in vivo*.

HydrodabcyI (**2**) was synthesized in two steps ([Scheme 1](#), for details see the [Supporting Information](#)). Phloroglucinol (**3**) was

Scheme 1. Synthesis of HydrodabcyI (**2**)



converted with dimethylamine to 5-dimethylamino-resorcinol (**4**), which in turn was reacted with 4-diazosalicylic acid (**5**) to give hydrodabcyI (**2**). The intermediate **4** was prepared according to a protocol by Petržilka and Lusuardi¹¹ and obtained as pink crystals as described ([Figure S1](#) in the [Supporting Information](#)). However, when used as such for the azo coupling reaction with **5**, it afforded a fluorescent product that proved unsuitable as a dark quencher. A careful

examination of every single step of the procedure pointed to an impurity as the cause of the pink coloration and possibly of the fluorescence of the final product (cf. [Supporting Information](#)). In fact, when the unspecified impurity was removed by a preceding column chromatography, **4** was obtained as colorless crystals ([Figure S1](#) in the [Supporting Information](#)). Its reaction with **5** afforded **2** as a nonfluorescent compound in 58% yield over both steps. Though seemingly marginal, this modification to the original protocol is crucial for obtaining **2** in a quality that allows its use as a dark quencher.

HydrodabcyI (**2**) is soluble in water, up to a concentration of 5.7×10^{-4} M at 20 °C. In contrast, it was not possible to prepare an aqueous solution of dabcyI (**1**) due to precipitation even at low concentration ([Figure 2a](#)). The attachment of

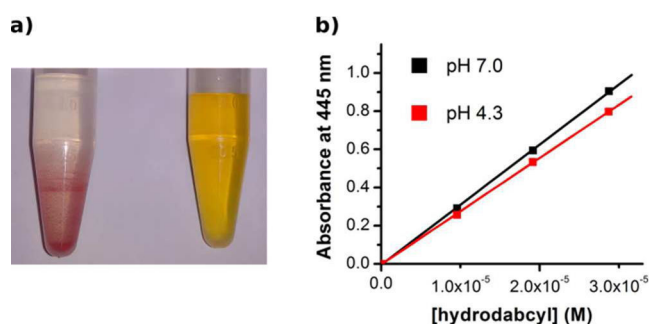


Figure 2. (a) Solubility in water: on the left, evident precipitation of dabcyI (**1**) (intended concentration $\sim 7 \mu\text{M}$); on the right, a clear solution of hydrodabcyI (**2**) ($7 \mu\text{M}$). (b) Concentration dependence of the absorbance at 445 nm of hydrodabcyI (**2**) in a buffered solution at pH 7.0 (black) and at pH 4.3 (red). The solution at pH 4.3 was obtained by gradual acidification of the solution at pH 7.0 ([Supporting Information](#) for details). The temperature was set at 20 °C.

hydroxy groups to the dabcyI core imparts water solubility without adding electric charges as would have the addition of ionic solubilizers such as sulfonate groups.¹² Consequently, hydrodabcyI (**2**) will not significantly modify the electrostatic profile of the molecule to which it is linked and thus the binding properties of the labeled molecule are expected not to be altered much. This aspect has important implications for investigations of biological systems in which molecular interactions are frequently driven by electrostatics (e.g., enzymatic reactions). Additionally, the carboxyl group of hydrodabcyI (**2**) remains available for the coupling to an amino group in the substrate through a standard amide bond formation. Practical advantages of the good solubility of hydrodabcyI (**2**) are the ease of preparing solutions and of cleansing used glassware.

Saturated solutions of hydrodabcyI (**2**) in water show a pH of 4.5, which is significantly lower than the pH of pure water. In fact, both dabcyI (**1**) and hydrodabcyI (**2**) bear a carboxyl group and have therefore an acidic character. The acidic environment favors the protonation of the carboxyl group, thus increasing the hydrophobic character of the molecule. While the hydroxy groups of hydrodabcyI (**2**) compensate for this effect, dabcyI (**1**) turns even less soluble in water as the pH drops. Nevertheless, experiments are normally carried out at controlled pH; therefore, we performed the same test in a buffered aqueous solution at pH 8.0 where the carboxyl group is supposed to be deprotonated and thus charged. Expectedly, in an aqueous buffer of pH 8.0 the solubility of both dabcyI (**1**) and hydrodabcyI (**2**) is increased, distinctly so in the case of

hydrodabcyll (2) (25 mM) but still unsufficiently so in the case of dabcyll (1) (cf. Table S1 in the Supporting Information), confirming the superiority of hydrodabcyll.

In the majority of their applications, quenchers such a dabcyll (1) or hydrodabcyll (2) are linked to the actual molecules of interest, e.g., to peptide substrates in order to monitor protease activities. Both dabcyll (1) and hydrodabcyll (2) can be readily coupled to an amino group of a peptide via a standard amide bond formation. However, this linkage eliminates the free carboxylic acid on the quenchers and so the option to improve their solubility, or that of their peptide conjugates, by elevating the pH. To investigate this aspect, we linked the two dark quenchers to the amino group of a lysine to obtain the compounds Lys-dabcyll and Lys-hydrodabcyll. Interestingly, in a buffered aqueous solution at pH 8.0, the concentration of Lys-dabcyll was only 7.6×10^{-6} M whereas we could prepare a 6.6 mM solution of Lys-hydrodabcyll without reaching saturation. Accordingly, the solubility of Lys-hydrodabcyll is presumably much higher than 6.6 mM and therefore close to that of L-Lys which is about 40 mM or 5.8 g kg^{-1} of water.¹³ In other words, amide conjugation of hydrodabcyll (2) to peptides does not significantly alter the solubility of the latter, whereas conjugation to dabcyll (1) is expected to lower their solubility in aqueous media. The modification of the solubility of a reactant in a biochemical process may hamper and distort its experimental study considerably. For instance, a distinctly reduced solubility of the product of an enzymatic reaction may hinder its release from the active site, resulting in an artifactual inhibiting effect. The solubility of hydrodabcyll was accurately measured spectroscopically at different pH by certifying the linear dependence between absorbance and concentration (Figure 2b and Supporting Information for more details). From basic pH values down to pH 6.0, solutions with concentrations in the millimolar range can be prepared directly at the desired pH. At pH < 6.0 the solubility is lower, however, solutions with millimolar concentrations can still be prepared by gradual acidification of an alkaline solution down to a pH value of 4.3. The excellent solubility of hydrodabcyll (2) and its conjugates with biomolecules makes it the quencher of choice in most biochemical applications.

The absorption spectra of dabcyll (1) and hydrodabcyll (2) in DMSO are quite similar to the latter showing a slight bathochromic shift of the main absorption band and a greater molar absorbance (Figure 3). Both effects enhance the

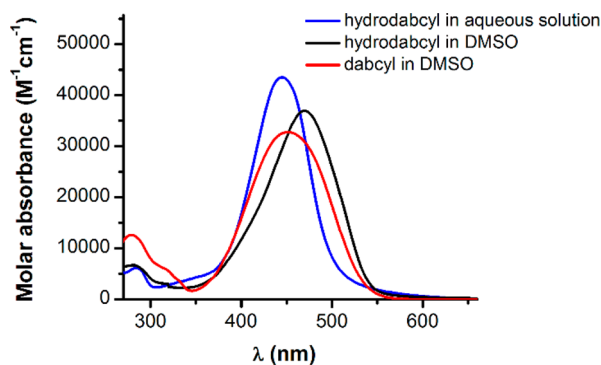


Figure 3. Comparison of molar absorbances of dabcyll (1) in DMSO (red curve, $\lambda_{\text{Max}} = 451 \text{ nm}$, $\epsilon_{451} = 32000 \text{ M}^{-1} \text{ cm}^{-1}$), hydrodabcyll (2) in DMSO (black curve, $\lambda_{\text{Max}} = 470 \text{ nm}$, $\epsilon_{470} = 37000 \text{ M}^{-1} \text{ cm}^{-1}$) and 2 in buffered aqueous solution pH 8.0 (blue curve $\lambda_{\text{Max}} = 445 \text{ nm}$, $\epsilon_{445} = 43000 \text{ M}^{-1} \text{ cm}^{-1}$); all at 20 °C.

quenching power of hydrodabcyll (2) at larger wavelengths and advocate its preferential use, even in applications where dabcyll (1) has been customarily employed, so far. On the other hand, in aqueous solution, the absorption maximum of hydrodabcyll (2) ($\lambda_{\text{Max}} = 445 \text{ nm}$, $\epsilon_{445} = 43000 \text{ M}^{-1} \text{ cm}^{-1}$) is shifted toward smaller wavelength (hypsochromic shift) in comparison to its spectrum in DMSO ($\lambda_{\text{Max}} = 470 \text{ nm}$, $\epsilon_{470} = 37000 \text{ M}^{-1} \text{ cm}^{-1}$) as shown in Figure 3. However, this hypsochromic shift is partly compensated by its greater molar absorbance in aqueous solution, thus rendering hydrodabcyll (2) an effective quencher at wavelengths up to 500 nm also in aqueous solution.

Hydrodabcyll (2) has the requisite properties for serving as a useful dark quencher in fluorogenic probes. In order to observe hydrodabcyll (2) in action we synthesized a peptidic substrate featuring only two amino acids: serine labeled with hydrodabcyll (2) as quencher-acceptor and phenylalanine labeled with EDANS as fluorophore donor (Figure 4 and Supporting

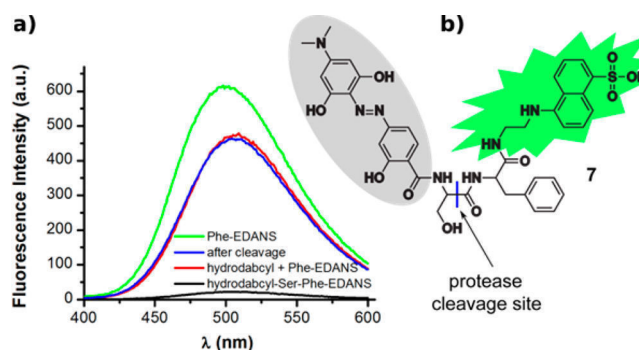


Figure 4. (a) Fluorescence spectra of 20 μM hydrodabcyll-Ser-Phe-EDANS (7) alone (black) and after 5 h incubation with thermolysin (blue). For comparison, the fluorescence spectra of 20 μM Phe-EDANS alone (green) and an equimolar amount of hydrodabcyll (2) + Phe-EDANS (red). The spectra were recorded in 100 mM Tris-HCl (pH 7.5) containing 2 mM CaCl_2 at 37 °C; $\lambda_{\text{Ex}} = 336 \text{ nm}$. (b) Chemical structure of hydrodabcyll-Ser-Phe-EDANS (7). The quencher hydrodabcyll (2) and the fluorophore EDANS are marked in gray and green, respectively. The protease cleavage site is indicated by a blue bar.

Information for details of the synthesis procedure). A dipeptide is the minimal substrate for protease reactions, ideal to prove the applicability or even superiority of hydrodabcyll (2) in labeling small molecules. The dipeptide Ser-Phe was chosen because it is a preferential cleavage site of the P1' protease thermolysin, an enzyme that is commercially available. Furthermore, the same dipeptide labeled with EDANS and dabcyll (1) had already been tested with several proteases,¹⁴ therefore allowing a comparison of dabcyll (1) and hydrodabcyll (2) during a typical biochemical application. It should be noted that in this case hydrodabcyll (2), due to its high polarity, needs to have its hydroxy groups protected by acetylation prior to the amide bond formation in order to increase yields and reactivity. Subsequent deprotection under mild conditions then restores the advantageous polarity and solubility of the conjugate (cf. Supporting Information).

In the double-labeled substrate, the fluorescence of EDANS linked to the Phe moiety is largely quenched by hydrodabcyll (2) linked to the Ser moiety (black curve in Figure 4). The fluorescence of EDANS decreases also when an equimolar amount of hydrodabcyll (2) is added to Phe-EDANS (green and

red curves in Figure 4). However, when the fluorophore and the quencher are not kept close together, as in the double labeled dipeptide, the quenching efficiency is lower in line with the distance-dependence of energy-transfer-based processes. Interestingly, the fluorescence intensity curve detected when the labeled dipeptide was incubated with the enzyme thermolysin (blue curve in Figure 4) coincided with the curve of Phe-EDANS in the presence of an equimolar amount of hydrodabcyll (2) (red curve in Figure 4) and not with the fluorescence intensity curve of Phe-EDANS alone (green curve in Figure 4). This finding indicates that the hydrodabcyll moiety has a certain quenching ability even when not covalently linked to the fluorophore and that this ability is roughly the same for hydrodabcyll (2) and its amide with serine. This fact has to be taken into account during the procedure to determine the reference points for calibrating the signal accurately. Several types of physical quantities can be estimated provided the appropriate calibration of the signal is made.

Figure 5a shows the restoration of the fluorescence of EDANS as a function of time upon adding different

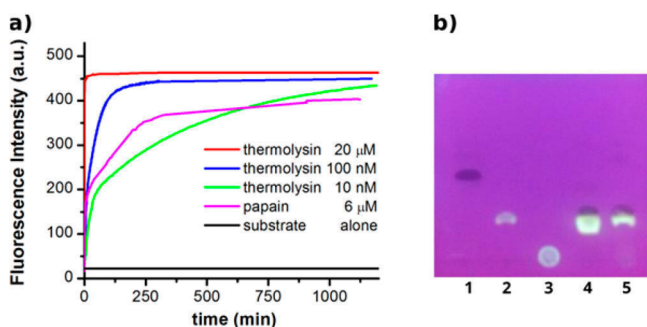


Figure 5. (a) Time traces of the hydrolysis of 20 μM of hydrodabcyll-Ser-Phe-EDANS (7) at 37 $^{\circ}\text{C}$, ($\lambda_{\text{Ex}} = 336 \text{ nm}$, $\lambda_{\text{Em}} = 515 \text{ nm}$) by thermolysin (different concentrations) and papain (6 μM). Thermolysin was added in different enzyme to substrate concentration ratios: 1:2000 (green), 1:200 (blue), 1:1 (red). The magenta curve describes the hydrolytic reaction by papain. The black line corresponds to the fluorescence level of the substrate alone, before adding the enzyme. (b) Products of hydrodabcyll-Ser-Phe-EDANS (7) after proteolytic cleavage indicated by TLC: hydrodabcyll-Ser-Phe-EDANS (7) (lane 1, $R_f = 0.5$), Phe-EDANS (lane 2, $R_f = 0.3$), EDANS (lane 3, $R_f = 0-0.1$), reaction mixture after proteolytic cleavage with thermolysin (lane 4, bright spot $R_f = 0.3$ and dark spot $R_f = 0.33$) and with papain (lane 5, bright spot $R_f = 0.3$ and dark spot $R_f = 0.33$).

concentrations of thermolysin to a solution of the labeled dipeptide. As expected, the larger the excess of the substrate with respect to the enzyme, the slower the reaction. Interestingly, despite the different concentration ratio between labeled substrate and enzyme, the same fluorescence level is eventually reached, indicating that the same amount of substrate molecules has been cleaved. When the enzyme is added in stoichiometric amount (1:1) to the labeled substrate the reaction is so fast that it cannot be observed on the chosen time scale. Under these conditions, the initial amount of substrate is expected to be fully cleaved, defining the maximum fluorescence level corresponding to a complete cleavage of the substrate. Consequently, since all the time traces reached the same fluorescence level, we conclude that the cleavage reaction proceeded to completion, independently of the amount of enzyme added. In order to confirm the exhaustive cleavage of the substrate, fresh enzyme was added to the mixture of

substrate and enzyme after reaching signal saturation. Since no appreciable fluorescence increase was observed, we excluded the presence of noncleaved substrate and concluded that the fluorescence level truly corresponds to the fluorescence signal of the fully processed substrate.

Additional evidence for the cleavage of the substrate was provided by the determination of the degradation product with thin-layer chromatography (TLC) (Figure 5b). Hydrodabcyll (2) confers an orange-red color to the substrate to which it is attached making it visible under UV light as a dark spot. Accordingly, the double-labeled substrate hydrodabcyll-Ser-Phe-EDANS (7) appeared as a dark spot with a retention factor (R_f) of 0.5 (Figure 5b, lane 1). The references of the potential products EDANS and Phe-EDANS are shown as white spots in lanes 2 and 3 of Figure 5b. In agreement with the work of Weimar et al.,¹⁴ EDANS remained close to the starting line ($R_f = 0-0.1$), whereas Phe-EDANS had an R_f value of 0.3. The mixture resulting from the reaction of thermolysin with an excess of double-labeled substrate (ratio 1:200) was applied in lane 4. The presence of a bright spot with the same R_f as Phe-EDANS together with the absence of a dark spot with the same R_f as the intact double-labeled substrate indicates that thermolysin cleaved the Ser-Phe peptide bond in the double-labeled substrate. The dark spot with an R_f of 0.33 overlapping with the bright spot of Phe-EDANS most likely corresponds to hydrodabcyll-Ser, the other product of the cleavage. Interestingly, the R_f of the putative spot of hydrodabcyll-Ser is lower than 0.53, the R_f of the putative spot of dabcyll-Ser, as reported in the literature.¹⁴ The same trend can be recognized when observing that the double-labeled substrate including hydrodabcyll (2) has a lower retention factor ($R_f = 0.5$) than the one including dabcyll (1) ($R_f = 0.72$).¹⁴ As a lower retention factor R_f is an indication of higher polarity, this result is in keeping with the higher polarity conferred by hydrodabcyll (2) as compared to dabcyll (1). Taken together our results demonstrate the retention of the activity of thermolysin in cleaving the peptide bond between serine and phenylalanine in the hydrodabcyll-Ser-Phe-EDANS (7) despite the presence of the chromophores. They also corroborate the usefulness and the advantages of hydrodabcyll (2) in fluorogenic probes.

Furthermore, we tested the proteolysis of hydrodabcyll-Ser-Phe-EDANS (7) by another enzyme, the cysteine protease papain (Figure 5). In the work of Weimar et al.,¹⁴ where the fluorogenic substrate was dabcyll-Ser-Phe-EDANS, only a small portion of the dipeptide was processed after an incubation of several hours with papain. In our experiment, we incubated the same amount of hydrodabcyll-Ser-Phe-EDANS (7) (20 μM) with 6 μM of papain. This relatively high concentration of papain was necessary to allow the detection of the reaction in a comparable time range. This shows that papain is much slower than thermolysin in cleaving the dipeptide, in agreement with the findings of Weimar et al.¹⁴ However, in contrast to them, papain was able to cleave the entire amount of the fluorogenic substrate, when dabcyll (1) was substituted with hydrodabcyll (2), as evidenced both by the evolution of the fluorescence signal and the analysis of the degradation products by TLC (Figure 5). This result is noteworthy, as it shows that the hydrophobicity of dabcyll (1) may indeed represent a handicap for fluorogenic probes when used in the biochemical system (e.g., interfering with proteolysis) and points out the higher applicability of hydrodabcyll (2).

CONCLUSION

HydrodabcyI (2) is a new dark fluorescence quencher with an optimal solubility-stability-absorption profile. Its small dimension, the absence of charged groups, and its absorption range make hydrodabcyI (2) the dark quencher of choice in tandem with many commercially available fluorescence donors. HydrodabcyI (2) overcomes the problem of insolubility in aqueous media, doing away with the need of organic cosolvents, and it lends itself ideally to high-throughput enzymatic tests. Thus, hydrodabcyI (2) represents a vastly improved and superior alternative to the very popular dabcyI (1) in the design of fluorogenic probes.

ASSOCIATED CONTENT

Supporting Information

The Supporting Information is available free of charge on the ACS Publications website at DOI: [10.1021/acs.analchem.7b03488](https://doi.org/10.1021/acs.analchem.7b03488).

Supporting data, chemical synthesis, and characterization (PDF)

AUTHOR INFORMATION

Corresponding Author

*E-mail: elisa.bombarda@uni-bayreuth.de.

ORCID

Rainer Schobert: [0000-0002-8413-4342](https://orcid.org/0000-0002-8413-4342)

Elisa Bombarda: [0000-0002-1385-3710](https://orcid.org/0000-0002-1385-3710)

Notes

The authors declare no competing financial interest. A patent for hydrodabcyI is pending (WO 2016/083611 A1, issued June 2, 2016).

ACKNOWLEDGMENTS

The present work was supported by the DFG Grant BO 3578/1 and by the RTG Grant 1640 (Photophysics of Synthetic and Biological Multichromophoric Systems). We thank Prof. Dr. G. Matthias Ullmann for fruitful discussions and Markus Petermichl for help in acquiring NMR spectra.

REFERENCES

- (1) Lakowicz, J. R. *Principles of Fluorescence Spectroscopy*, 3rd ed.; Springer: New York, 2006.
- (2) Hauglang, R. P. *Handbook of Fluorescence Probes and Research Products*, 9th ed.; Molecular Probes, Inc.: Eugene, OR, 2002.
- (3) Johansson, M. K.; Cook, R. M. *Chem. - Eur. J.* **2003**, *9*, 3466–3471.
- (4) Bernacchi, S.; Mely, Y. *Nucleic Acids Res.* **2001**, *29*, e62.
- (5) Matayoshi, E. D.; Wang, G. T.; Krafft, G. A.; Erickson, J. *Science* **1990**, *247*, 954–958.
- (6) Tyagi, S. *Nat. Biotechnol.* **1996**, *14*, 947–948.
- (7) Tyagi, S.; Marras, S. A.; Kramer, F. R. *Nat. Biotechnol.* **2000**, *18*, 1191–1196.
- (8) Holskin, B. P.; Bukhtiyarova, M.; Dunn, B. M.; Baur, P.; de Chastonay, J.; Pennington, M. W. *Anal. Biochem.* **1995**, *227*, 148–155.
- (9) Balaiah, V.; Seshadri, T. R.; Venkateswarlu, V. *Proc. Indian. Acad. Sci. (Math. Sci.)* **1942**, *16*, 68–82.
- (10) Avdeef, A.; Sofen, S. R.; Bregante, T. L.; Raymond, K. N. *J. Am. Chem. Soc.* **1978**, *100*, 5362–5370.
- (11) Petrzilka, T.; Lusuardi, W. G. *Helv. Chim. Acta* **1973**, *56*, 510–518.
- (12) Loudwig, S.; Bayley, H. J. *Am. Chem. Soc.* **2006**, *128*, 12404–12405.

(13) Lide, D. R. *CRC Handbook of Chemistry and Physics*, 85th ed.; CRC Press: Boca Raton, FL, 2004.

(14) Weimer, S.; Oertel, K.; Fuchsbaauer, H. L. *Anal. Biochem.* **2006**, *352*, 110–119.

Supporting Information

Hydrodabcyl: a superior hydrophilic alternative to the dark fluorescence quencher dabcyI

Oxana Kempf,[†] Karl Kempf,[‡] Rainer Schobert[‡] and Elisa Bombarda^{*,†}

[†]Department of Biochemistry and [‡]Organic Chemistry Laboratory, University of Bayreuth,
Universitaetsstr. 30, 95440, Bayreuth, Germany

E-mail: elisa.bombarda@uni-bayreuth.de

Table of contents

Chemicals and instrumentation	S-2 – S-3
Chemical synthesis	S-4 – S-8
Solubility tests	S-9 – S-11
Fluorimetric and TLC assays	S-12
NMR spectra	S-13 – S-16
Mass analysis	S-17 – S-18
References	S-19

Chemicals and instrumentation

Chemicals

EDANS (*N*-(2-aminoethyl)-5-naphthylamine-1-sulfonic acid) and *N*-*tert*-butoxycarbonyl-L-phenylalanine (Boc-Phe) were purchased from Anaspec, *N*-*tert*-butoxycarbonyl-*O*-*tert*-butyl-L-serine (Boc-Ser(*t*Bu)-OH) was obtained from Bachem (Bubendorf, Switzerland). T₃P-coupling reagent (propanephosphonic acid anhydride, 2,4,6-tripropyl-1,3,5,2,4,6-trioxatriphosphorinane-2,4,6-trioxide, 50 % in THF) was a free sample from Euticals SpA, Italy. Thermolysin from *Geobacillus stearo*, papain from *Papaya latex*, DMAP (4-(dimethylamino)-pyridine) and all other chemicals were purchased from Sigma-Aldrich and used without further purification, unless indicated otherwise. The aqueous solution used in this work was a 50 mM sodium phosphate buffer (NaP) pH 8.0.

NMR spectroscopy

The ¹H and ¹³C NMR spectra were taken on a Bruker Avance 300 MHz spectrometer. Chemical shifts are reported in parts per million (ppm) referenced with respect to residual solvent (CHCl₃ = 7.26/77.16 ppm, DMSO = 2.50/39.52 ppm)¹.

Melting point

Melting points were measured with a Melting Point B-565 (Buchi) in melting point tubes.

Mass spectrometry

High resolution mass spectra were obtained with a UPLC/Orbitrap MS system in ESI mode.

IR spectroscopy

IR spectra were recorded with a FT-IR spectrometer PerkinElmer S100 equipped with an Attenuated Total Reflection (ATR) unit.

Chromatography stationary phases

For column chromatography silica gel (Macherey-Nagel 60, particle size 0.040 - 0.063 mm) was used. The retention factor (R_f) values were determined by thin layer chromatography on pre-coated silica plates (Merck TLC Silica gel 60 F254) and spots were visualized by UV light and stained with ceric ammonium molybdate (CAM) solution, followed by treatment with a heat gun.

HPLC

HPLC was performed on Phenomenex RP Kinetex 5 μ C18 100 Å, 250 \times 4.6 mm (analytical) and 250 \times 21.2 mm (preparative) column. 0.1 % HCOOH/H₂O and methanol (MeOH) were used as eluents for HPLC experiments with flow rate of 0.7 mL/min (analytical) and 14.9 mL/min (preparative).

UV/Vis spectroscopy

A double beam Perkin Elmer Lambda 750 UV/Vis spectrophotometer equipped with a thermostated cuvette holder was used to record the absorption spectra over a wavelength range of 270 - 650 nm at 20 °C in quartz cuvettes with 1 cm light path (Hellma). Fluorescence was measured with a Cary Eclipse fluorimeter (VARIAN) equipped with a thermostated cuvette holder. Origin 8 (Microcal) was used for data analysis.

pH measurements

The pH was measured with the Mettler-Toledo SevenMulti pH-meter equipped with a micro-electrode (InLab Micro, Mettler-Toledo).

Ultrasound bath

When required, solutions were degassed in an ultrasonic bath Bandelin SONODEX Super RX 106 (240 W) *in vacuo*.

Chemical Synthesis

Hydrodabcyl (2)

The compound 4-(2',6'-dihydroxy-4'-dimethylaminophenylazo)-2-hydroxybenzoic acid (hydrodabcyl (2)) was synthesized in two steps as shown in Scheme 1 in the main text.

In the first step 5-dimethylamino-resorcinol (4) was prepared by an optimized variant of a protocol published by Petrzilka and Lusuardi². The optimization implies the addition of a purification over silica gel yielding colorless crystals, rather than pink ones as described in the literature². We attributed the reported pink color to a contamination by a degradation product. This assumption is supported by the observation that the product turns pink when it is stored for several weeks in the refrigerator. If not removed, this contamination leads to a fluorescent by-product in the following step, which cannot be separated even by HPLC. Our optimized method avoids the formation of this by-product. We did not identify the impurity. However, our results suggest that the compound that was responsible of the pink discoloration was also responsible for the fluorescence of the final product. Although minimal, this modification of the protocol is requisite for obtaining 5-dimethylamino-resorcinol (4) in a pure form, and it also proves that the reaction between 4 and 4-diazosalicylic acid (5) does not lead to a fluorescent product, hence opening the way to obtain a water soluble dark quencher.

a)



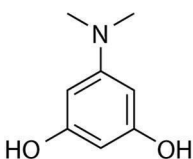
b)



Figure S1. Crystals of 5-dimethylamino-resorcinol (4). The pink crystals in a) were obtained following the protocol of Petrzilka and Lusuardi² and the colorless crystals in b) were obtained following our improved protocol.

5-Dimethylamino-resorcinol² (4)

Phloroglucinol (**3**, 9.23 g, 73.2 mmol) was dissolved in a degassed mixture of DMF (128 mL) and water (95 mL) under argon. Dimethylamine hydrochloride (8 g, 91.5 mmol) was added and then pellets of solid sodium hydroxide (3.66 g, 91.5 mmol) were added one by one during 5 h. The resulting mixture was stirred overnight at room temperature. Over the next 48 h, the addition of dimethylamine hydrochloride and sodium hydroxide was repeated three times (3×9.15 mmol each). The resulting solution was concentrated *in vacuo* and the residue was purified by column chromatography (cyclohexane / ethyl acetate 1/1, R_f 0.38). The product was crystallized from dichloromethane to obtain colorless crystals (8.2 g, 73 %) which were used immediately for the next step.



Melting point: 151 °C (142 - 143 °C)²

¹H-NMR (300 MHz; DMSO-*d*₆; Me₄Si): δ = 8.81 (s, 2 H), 5.60 (s, 3 H), 2.78 (s, 6 H) ppm.

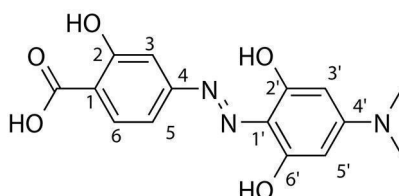
¹³C-NMR (75 MHz; DMSO-*d*₆; Me₄Si): δ = 158.8 (\times 2), 152.3, 92.0 (\times 2), 91.5, 40.1 (\times 2) ppm.

IR (ATR): $\tilde{\nu}$ = 3276, 2972, 2884, 2512, 1604, 1512, 1462, 1435, 1377, 1347, 1312, 1276, 1247, 1128, 1042, 1005, 987, 853, 831, 809, 686, 634, 576 cm⁻¹.

4-(2',6'-Dihydroxy-4'-dimethylaminophenylazo)-2-hydroxybenzoic acid (**2**) from azo-coupling³ of **4** with 4-diazosalicylic acid (**5**)

An ice-cold freshly prepared aqueous 2.5 M solution of sodium nitrite (9 mL, 22.5 mmol) was added dropwise to a solution of 4-aminosalicylic acid (**6**, 3.46 g, 22.5 mmol) in 6 M solution of hydrochloric acid (6 mL) at 0 - 5 °C. The resulting suspension was then stirred for another 15 min and added dropwise to a mixture of **4** (3.45 g, 22.5 mmol) and 1 M aqueous sodium hydroxide solution (23.5 mL) at 0 - 5 °C. The mixture was heated at 70 °C for 15 min and then stirred for 1 h at room temperature. Methanol was added to the resulting red suspension. This mixture was then put in an ultrasonic bath for some minutes. The impurities were filtered and the filtrate was evaporated. The remainder was diluted with 0.1 M sodium hydroxide solution, filtered, and the filtrate was treated with formic acid and ethanol adjusting a pH < 4.0. This mixture was placed in the fridge for about 15 h, and then centrifuged for 10 min at 4 °C (Heraeus Multifuge X3 FR Thermo Scientific Centrifuge operating at 4283 rpm). The pellet obtained was suspended in 0.1 % formic acid and again centrifuged

as before; this procedure was repeated three times. Then the residue was re-suspended in double-distilled water and centrifuged. This procedure was repeated twice. Finally, the product was dispersed in double-distilled water by means of an ultrasonic bath and then frozen in liquid nitrogen and dried by lyophilisation. Pure final product **2** was obtained as a red powder (5.7 g, 80 %), which was stored in a dark fridge at 4 - 8 °C. HPLC: T = 16.5 min (0.1 % HCOOH/H₂O, 55 - 45 v/v in MeOH, λ_{max} = 455 nm);



Melting point: 253 °C

¹H-NMR (300 MHz; DMSO-*d*₆; Me₄Si): δ = 7.80 (d, *J* = 8.5 Hz, 1 H, 6-H), 7.40 (d, *J* = 1.6 Hz, 1 H, 3-H), 7.18 (dd, *J* = 8.5, 1.6 Hz, 1 H, 5-H), 5.71 (s, 2 H, 3'-H, 5'-H), 3.08 (s, 6 H, NMe), ppm.

¹³C-NMR (75 MHz; DMSO-*d*₆; Me₄Si): δ = 171.6 (COOH), 162.9 (C2', C6'), 157.7 (C2, C4), 151.6 (C4'), 131.2 (C6), 124.4 (arC^q), 110.1 (arC^q), 109.7 (C5), 105.1 (C3), 91.4 (C3', C5'), 40.0 (N(CH₃)₂) ppm.

IR (ATR): $\tilde{\nu}$ = 3352, 3083, 2908, 2737, 2475, 1874, 1656, 1620, 1502, 1473, 1426, 1387, 1337, 1291, 1226, 1191, 1133, 1087, 1018, 983, 965, 886, 847, 811, 776, 729, 675 cm⁻¹.

HRMS-ESI: calcd for [M + H]⁺ C₁₅H₁₆N₃O₅ 318.1085, found 318.1081.

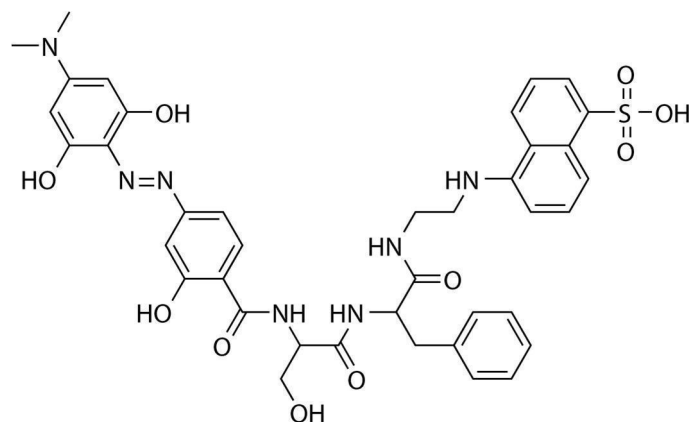
Synthesis of hydrodabcyyl-Ser-Phe-EDANS (7)

The synthesis of the substrate hydrodabcyyl-Ser-Phe-EDANS was performed according to the method described by S. Weimer *et al.*⁴, with the difference that in the last step triacetylated hydrodabcyyl **8** was employed instead of dabcyyl (**1**). For the synthesis of **8** see the dedicated paragraph below.

2-*N*-(4-((4-(*N,N*-dimethylamino)-2,6-dihydroxyphenyl)azo)-2-hydroxybenzoyl-L-serinyl-L-phenylalanylamido)-*N*-ethylaminonaphthalene-5-sulfonic acid (7)

A stirred solution of **8** (0.151 g, 0.34 mmol) in 10 mL anhydrous THF was cooled to 0 °C and treated with triethylamine (0.155 mL, 1.113 mmol). A solution of T₃P, 50 % in THF (0.32 mL, 0.534 mmol), was added dropwise. Ser-Phe-EDANS⁴ (0.17 g, 0.34 mmol) was dissolved in 6 mL anhydrous DMF and added to the reaction mixture. The resulting mixture was stirred for 1.5 h at 0 °C and then concentrated *in vacuo*. The crude product was deacetylated by addition of a solution of

piperidine (1 mL) in methanol (30 mL). The reaction mixture was stirred for 1 h at room temperature and the product was purified by HPLC after acidification with formic acid (0.1 % HCOOH/H₂O, 55 - 45 v/v in MeOH).



¹H-NMR (300 MHz; DMSO-*d*₆; Me₄Si): δ = 8.79 (d, J = 7.1 Hz, 1 H), 7.80 - 8.39 (m, 7 H), 7.25 - 7.37 (m, 3 H), 7.10 - 7.22 (m, 5 H), 6.55 (dd, J = 14.0, 7.4 Hz, 1 H), 5.75 (s, 2 H), 4.76 (dd, J = 12.3, 7.4 Hz, 1 H), 4.45 - 4.59 (m, 2 H), 4.39 (br s, 1 H), 3.75 - 3.64 (m, 2 H), 3.15 - 3.21 (m, 2 H), 3.06 - 3.13 (m, 8 H), 2.82 - 2.95 (m, 2 H), 1.89 (s, 1 H) ppm.

¹³C-NMR (75 MHz; DMSO-*d*₆; Me₄Si): δ = 171.2, 169.6, 167.5, 160.1, 158.6, 158.0, 154.2, 150.6, 146.2, 143.4, 137.7, 130.2, 130.1, 129.1 (\times 2), 128.0 (\times 2), 126.1 (\times 2), 124.4, 123.7, 122.7, 122.5, 116.3, 116.2, 113.8, 110.0, 105.8, 104.9, 103.2, 91.6 (\times 2), 61.5, 55.5, 54.9, 54.3, 45.8, 43.3, 40.2 (\times 2), 37.8 ppm.

IR (ATR): $\tilde{\nu}$ = 3264, 2934, 1635, 1528, 1489, 1418, 1228, 1162, 1049, 1021, 1003, 887, 820, 779, 699 cm⁻¹.

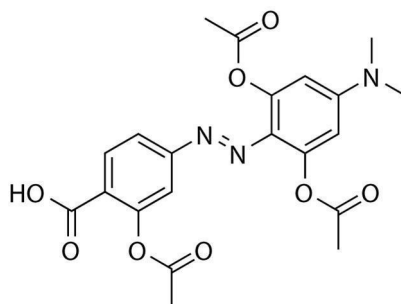
HRMS-ESI: calcd for [M + H]⁺ C₃₉H₄₂N₇O₁₀S 800.2708, found 800.2697.

Synthesis of triacetylated hydrodabcyl

Acetylation of hydrodabcyl was performed based on a literature protocol⁵.

4-(2',6'-Diacetoxy-4'-dimethylaminophenylazo)-2-acetoxybenzoic acid (8)

A mixture of **2** (3.5 g, 11 mmol), dry DMSO (10 mL), and THF (50 mL) was treated with triethylamine (9.2 mL, 66 mmol), DMAP (0.123 mg, 1.1 mmol) and acetic anhydride (4.4 mL, 46.2 mmol), and the resulting mixture was stirred at room temperature overnight. The solvent was evaporated and the remainder was partitioned between ethyl acetate and a 1 M aqueous solution of sodium hydrogen sulfate. The phases were separated and the water layer was extracted with ethyl acetate three times. The combined organic phases were dried over anhydrous sodium sulfate and evaporated *in vacuo*. The residue was purified by column chromatography (ethyl acetate + 0.1 % HCOOH, R_f 0.1) and then recrystallized from cyclohexane / diethyl ether, 1:1 to obtain dark red crystals (3.9 g, 80 %).



Melting point: 130 - 131 °C

¹H-NMR (300 MHz; DMSO-*d*₆; Me₄Si): δ = 8.06 (d, J = 8.3 Hz, 1 H), 7.56 (dd, J = 8.3, 1.8 Hz, 1 H), 7.29 (d, J = 1.8 Hz, 1 H), 6.53 (s, 2 H), 3.09 (s, 6 H), 2.30 (s, 6 H), 2.28 (s, 3 H) ppm.

The unprocessed residual peaks in the aromatic region may be sign of partial de-acetylation of the compound after long storage in DMSO and do not represent a major problem. In fact, **8** is an analogue of hydrodabcyl (**2**) that was designed only to make the benzoic acid more susceptible to nucleophilic attack and thus facilitating the coupling of **2** through amide bond formation, as mentioned in the main text. After coupling, the acetyl groups have to be removed, preferably with mild condition. Therefore lability of these groups, as indicated by the partial de-acetylation, is not only tolerated but also solicited.

¹³C-NMR (75 MHz; DMSO-*d*₆; Me₄Si): δ = 169.4, 169.0 (\times 3), 165.4, 156.7, 163.4, 151.4, 147.9, 132.9, 125.6, 124.4, 119.2, 116.0, 104.0 (\times 2), 40.1 (\times 2), 21.1, 20.9 (\times 2) ppm.

IR (ATR): $\tilde{\nu}$ = 2925, 2849, 2644, 2536, 1772, 1758, 1684, 1617, 1603, 1538, 1484, 1419, 1355, 1281, 1201, 1184, 1117, 1085, 1044, 1020, 979, 921, 892, 881, 845, 819, 785, 744, 690, 670 cm⁻¹.

HRMS-ESI: calcd for [M + H]⁺ C₂₁H₂₂N₃O₈ 444.1401, found 444.1394.

Solubility tests

To measure the solubility, saturated solutions of the studied compounds were prepared in pure water (resistivity 18 M Ω cm, Milli Q system, Millipore) and buffered aqueous solution pH 8.0 (50 mM sodium phosphate). The solutions were centrifuged at 5000 rpm for one hour (HERAEUS SEPA TECH Labofuge A). The concentration of the supernatant was determined by absorption spectroscopy at 20 °C after appropriate dilution to avoid instrumental saturation.

To test the solubility of hydrodabcyll at different pH in a practical range of concentrations, buffered solutions (50 mM sodium phosphate) have been prepared at four different pH: 8.0, 7.0, 6.0 and 5.5, respectively. The amount of hydrodabcyll required to reach a concentration of 5 mM was immersed in each buffer-solution. Since we observed that keeping the solution 1 h at 30 °C in an ultrasonic bath was unnecessary for obtaining the solubility, this additional procedure was abandoned for the preparation reported here.

The solubility of hydrodabcyll was confirmed by monitoring the absorbance in function of its concentration (Figure 2 in the main text and Figure S2). Since the stock solution was too concentrated to be measured directly, three diluted solutions with different concentrations (10 μ M, 20 μ M and 30 μ M) were prepared from the stock solution. The aliquots were taken from different parts of the volume of the stock solution to test the homogeneity. The linear increase of the absorbance with the concentration of the solute according to the Lambert-Beer law indicates that the stock solution is homogeneous (Figure 2b in the main text, black line). The same experiment was successfully repeated at pH 6 to confirm the solubility also at this slightly acidic pH (Figure S2). Instead, to reach complete solubility at pH < 6.0, the pH of the stock solution (5 mM range) at pH 7.0 was decreased at the desired value with few drops of 5 M HCl solution. Following gradual acidification of the medium the mM solution of hydrodabcyll remained clear till pH 4.3. With the same procedure described above, we could prove the solubility of hydrodabcyll till pH 4.3 (Figure 2 in the main text, red line). At pH < 4.3 hydrodabcyll precipitates, therefore pH 4.3 has to be considered the lowest pH at which the solubility of hydrodabcyll in the mM range can be warranted.

The experimental data in Figure 2 in the main text and Figure S2 were analyzed according to Beer–Lambert law with the equation:

$$A_{445} = \epsilon_{445} \cdot c \cdot l \quad (1)$$

where A_{445} is the absorbance at 445 nm, l is the path length of the light beam through the sample (in our case 1 cm), c is the molar concentration of the sample, ϵ_{445} is the molar extinction coefficient of the sample at 445 nm. The slope of the straight line is $\epsilon_{445} \cdot l$. Since the path length l is known, this

procedure allows also to determine the extinction coefficient or molar absorbance of the dye at the indicated wavelength

Table S1. Summary of the results of the solubility-tests (NaP buffer = Sodium-phosphate buffer)

Solvent	Substance	Solubility	Comments
Water, 20 °C	hydrodabcyl	5.71×10^{-4} M	pH = 4.5
	dabcyl	n.d.	not determined due to precipitation
50 mM NaP buffer, pH = 8.0	hydrodabcyl	2.54×10^{-2} M	
	dabcyl	5.41×10^{-4} M	
50 mM NaP buffer, pH = 8.0	Lys-hydrodabcyl	$> 6.61 \times 10^{-3}$ M	The solution was not saturated ^a
	Lys-dabcyl	7.62×10^{-6} M	

^a In the preparation of the solution of Lys-hydrodabcyl we were limited by the product availability and not by its solubility.

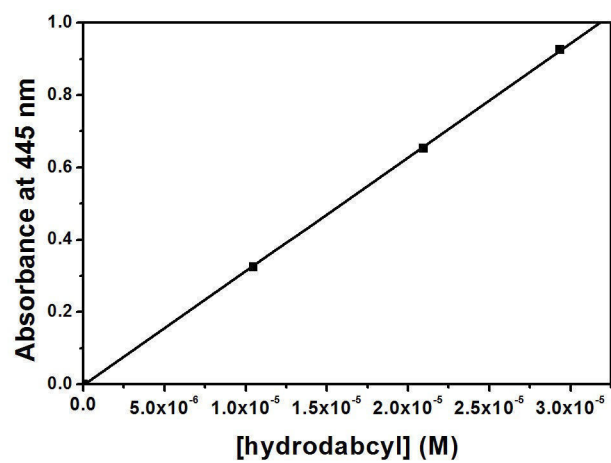


Figure S2. Concentration dependence of the absorbance at 445 nm of hydrodabcyll in buffered solution pH 6.0 at T = 20 °C.

Fluorimetric and TLC assays

Fluorimetric assay

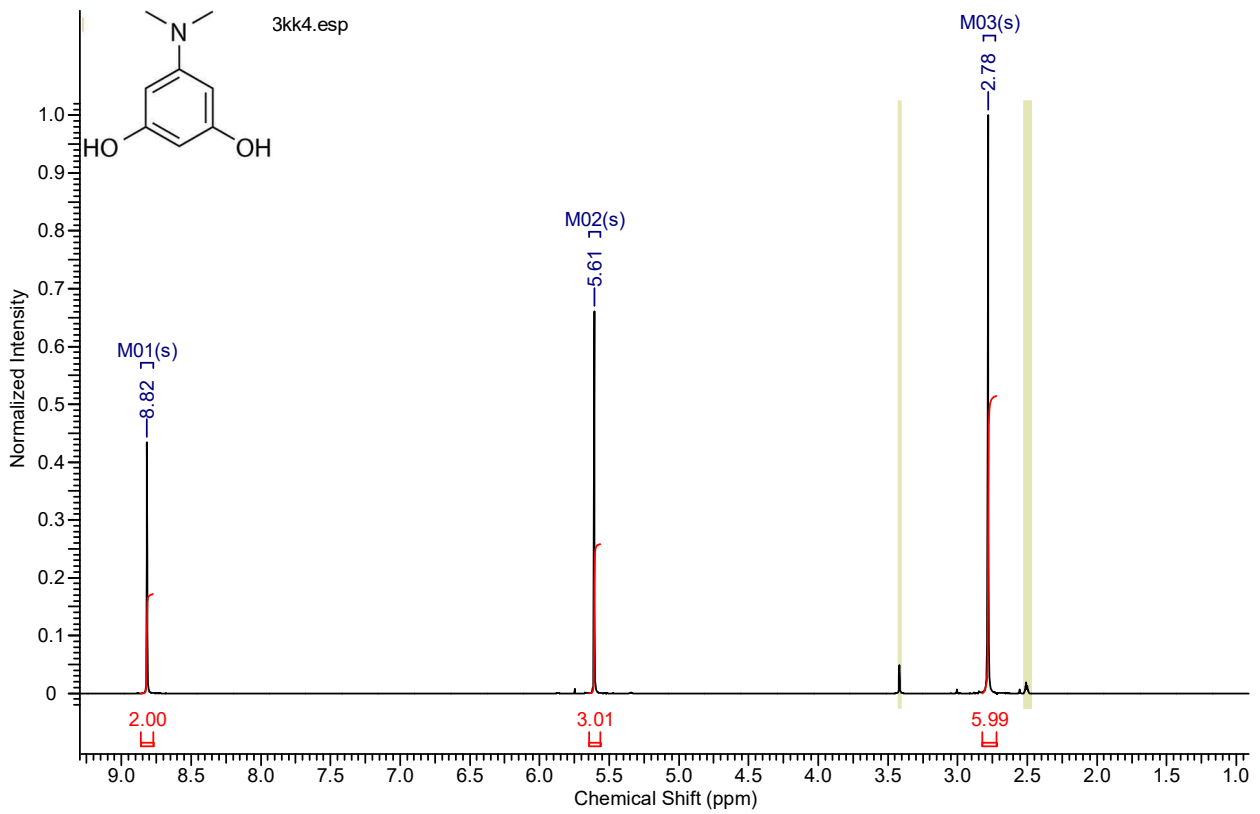
The fluorimetric assay with hydrodabcyI-Ser-Phe-EDANS was performed according to the literature⁴. Stock solutions of the substrate with a concentration of 1 mM were made in 100 mM Tris-HCl (pH 7.5) containing 2 mM CaCl₂ (thermolysin) or in 100 mM citrate pH 6.5 (papain). The concentration of the stock solutions was 6.6 mg/mL for thermolysin 4 mg/ml for papain. In typical experiments, 20 μM of the double-labelled dipeptide was incubated in 100 mM Tris-HCl/2 mM CaCl₂ (pH 7.5) or 100 mM citrate (pH 6.5) at 37 °C for 10min before hydrolysis was initiated by adding an aliquot of the protease stock solution (final concentrations of 20 μM, 100 nM and 10 nM for thermolysin and 6.0 μM for papain). Emission (λ_{ex} 336 nm, λ_{em} 515 nm) was monitored using 1-cm-pathlength cuvettes. All data given in the figures represent the means of at least three measurements. In all the experiments, the same amount (20 μM) of hydrodabcyI-Ser-Phe-EDANS (7) was used to allow the quantitative comparison of the fluorescence levels.

Thin-layer chromatography experiment

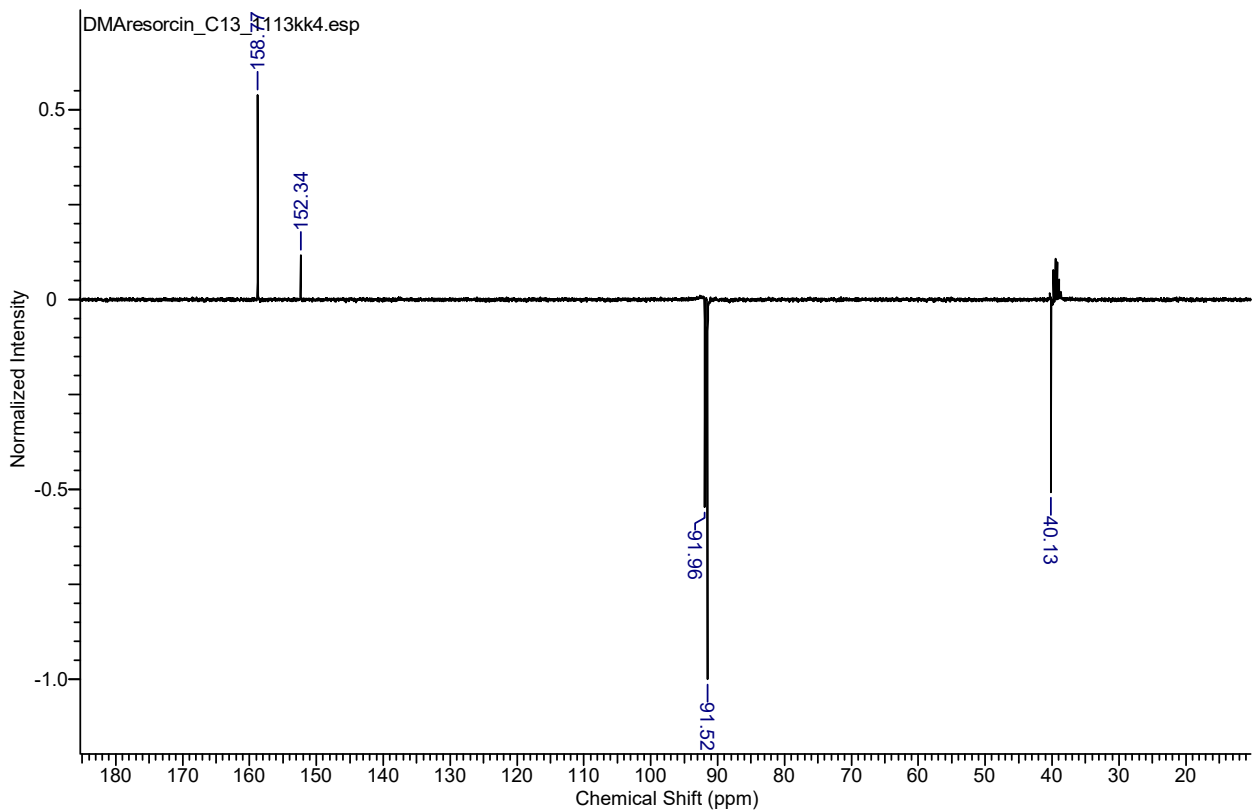
Thin-layer chromatography (TLC) was used to determine the degradation products of the proteolytic cleavage of hydrodabcyI-Ser-Phe-EDANS (7, Figure 5b in the main text). The analyzed reaction mixtures were incubated overnight, applied onto silica 60 aluminum sheets, separated by trichloromethane/methanol/water (65:25:4), and irradiated with an UV lamp at 340 nm

NMR spectra

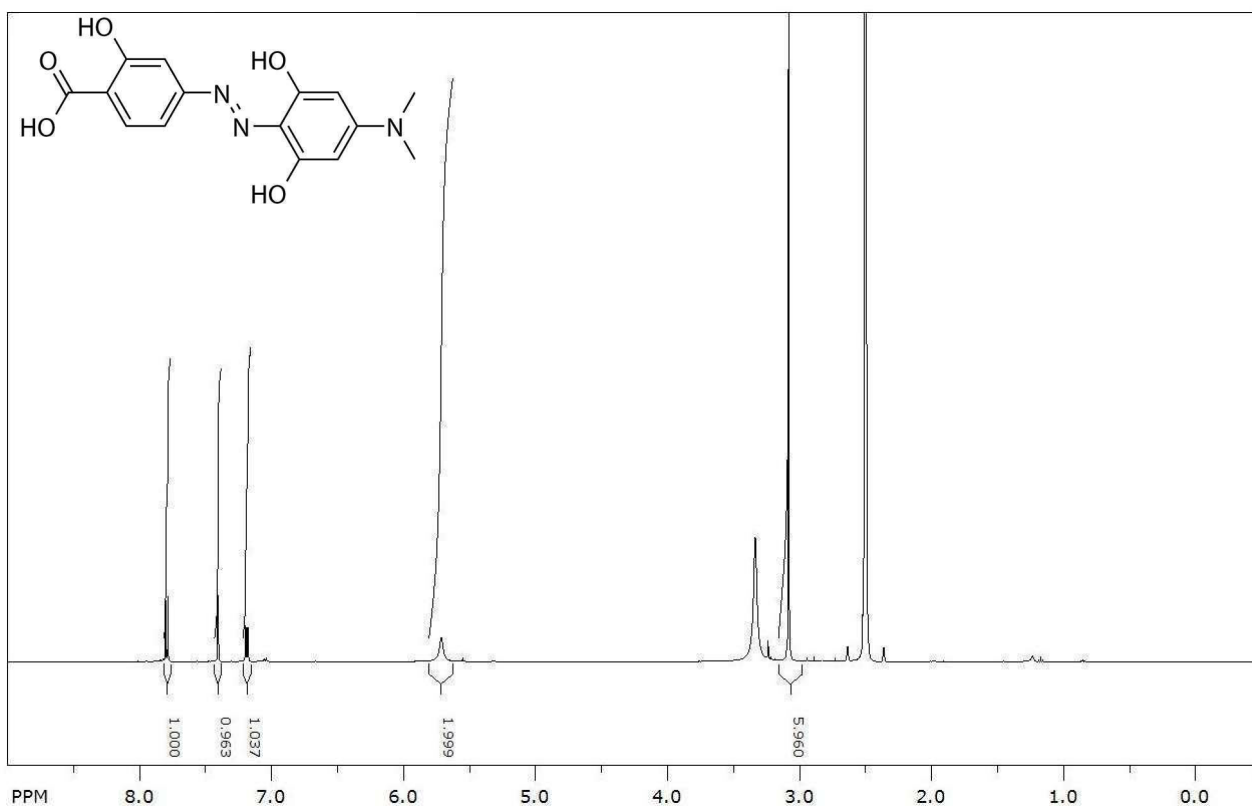
^1H NMR of compound **4** in $\text{DMSO-}d_6$



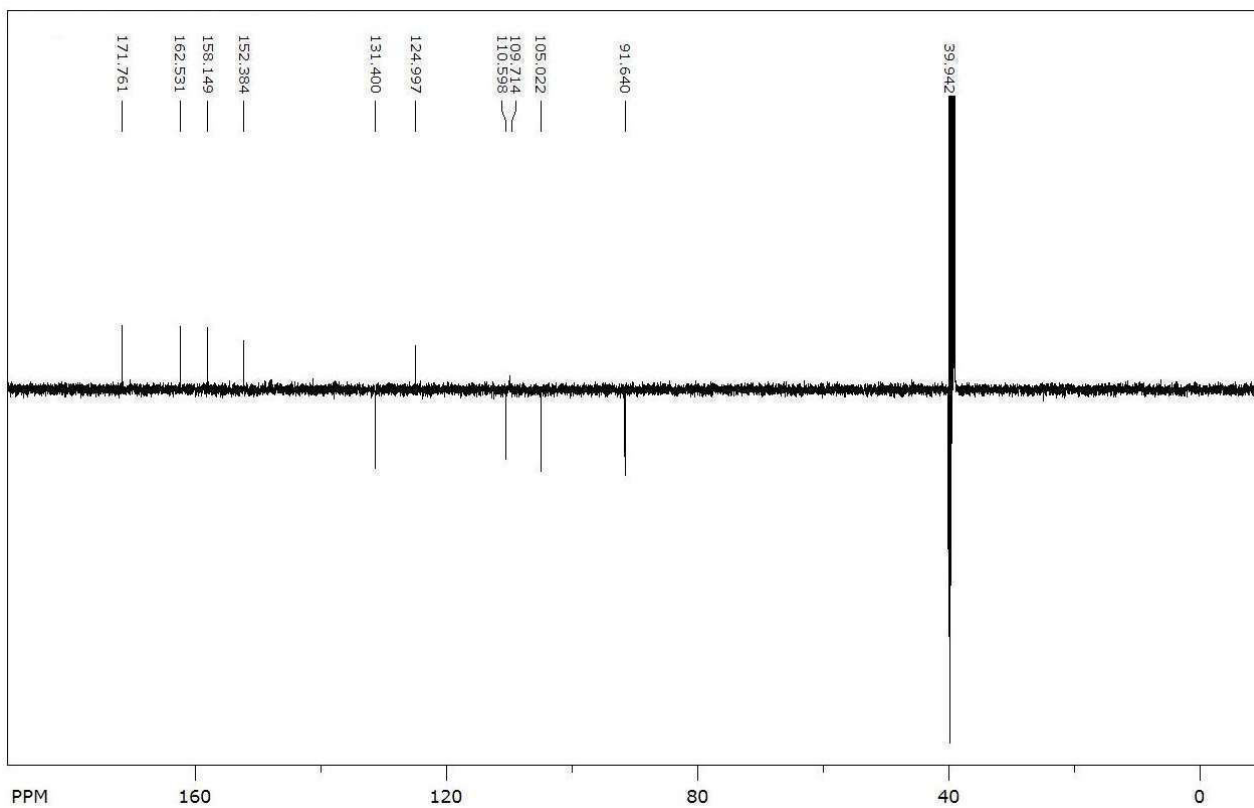
^{13}C NMR of compound **4** in $\text{DMSO-}d_6$



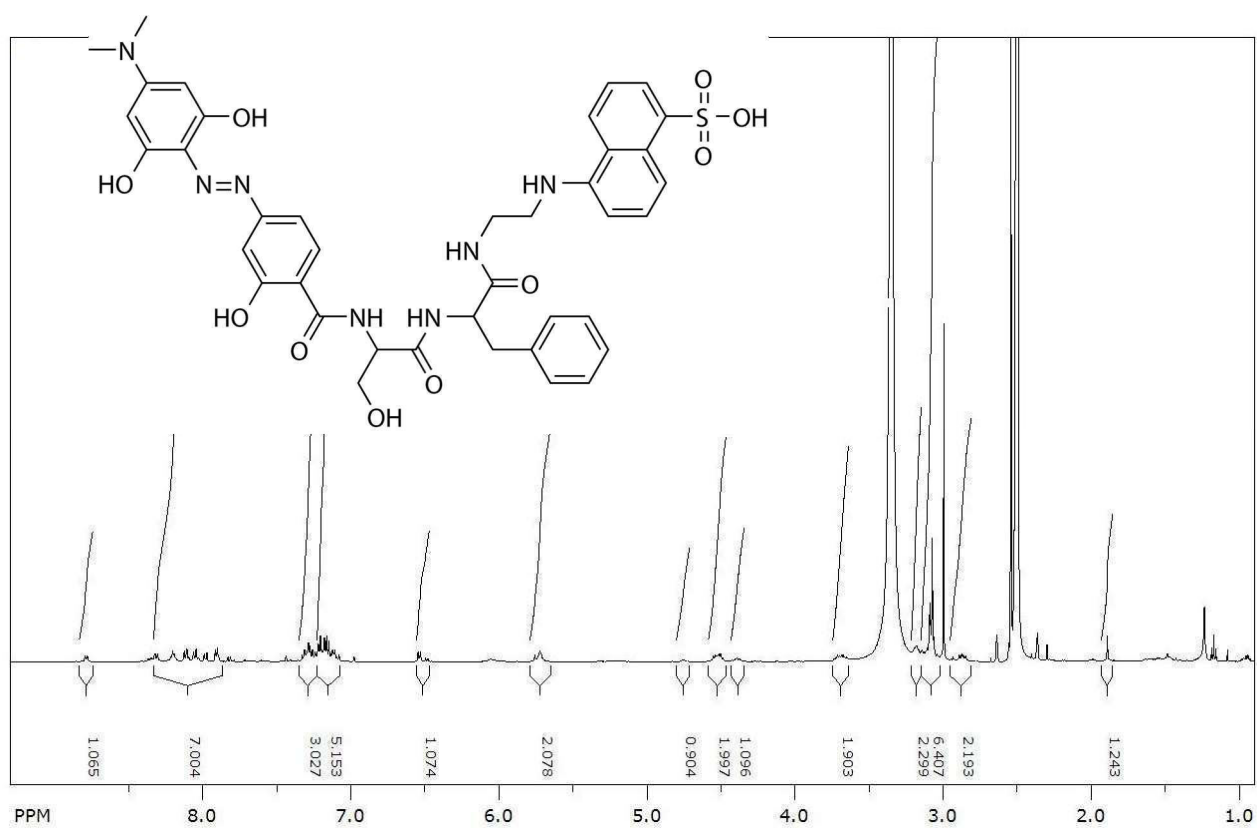
^1H NMR of compound **2** in $\text{DMSO-}d_6$



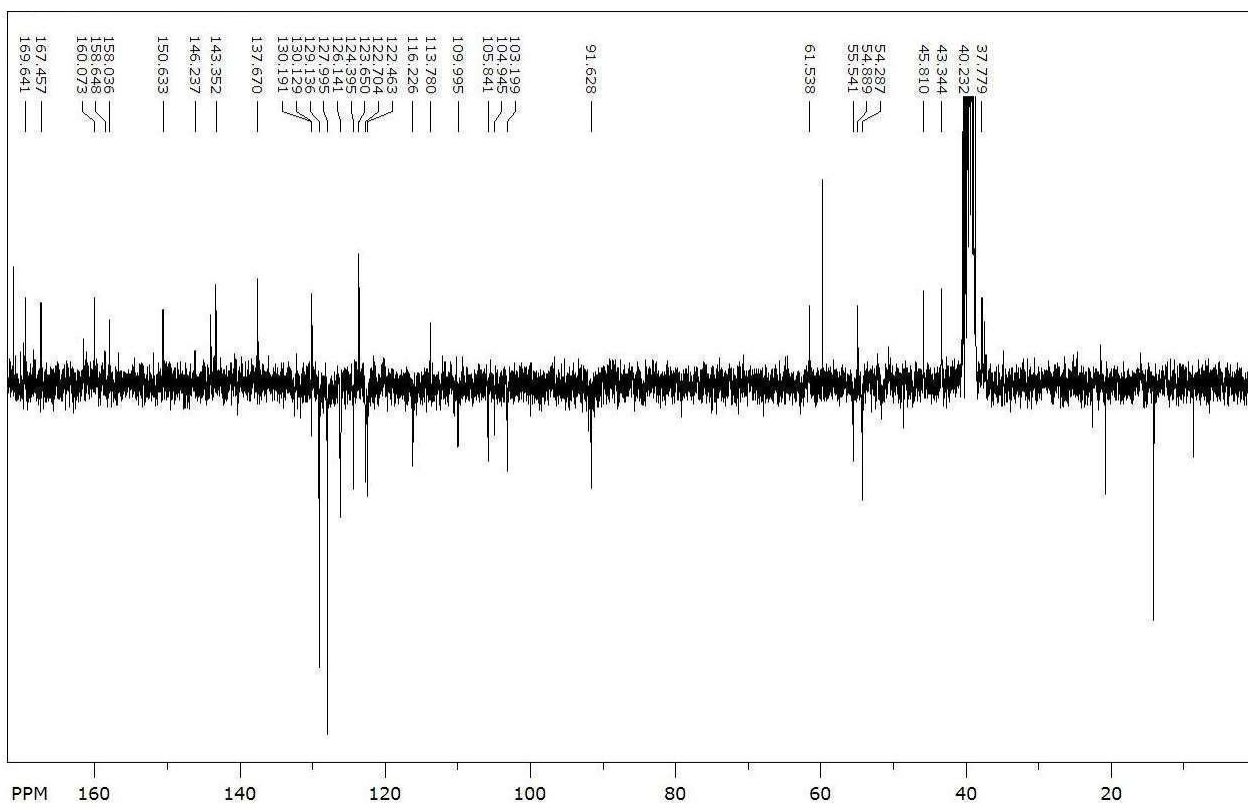
^{13}C NMR of compound **2** in $\text{DMSO-}d_6$



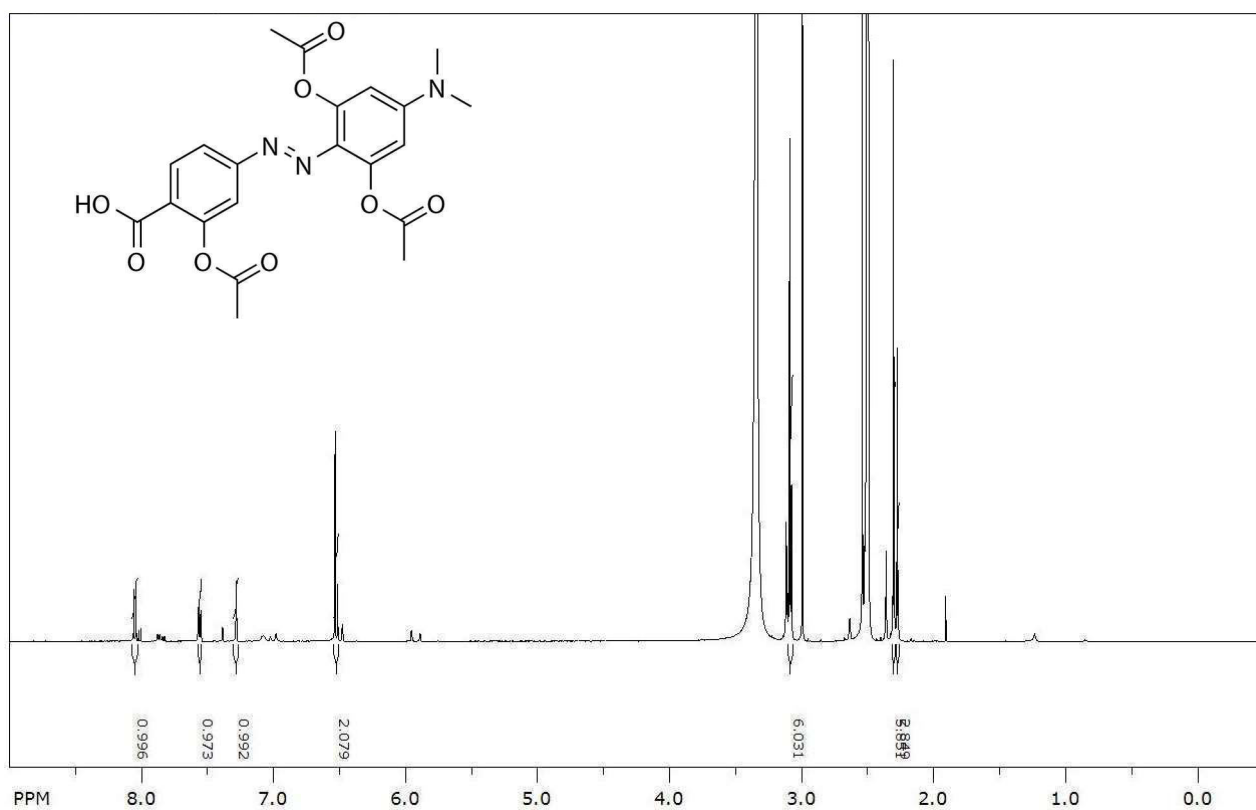
¹H NMR spectrum of compound 7



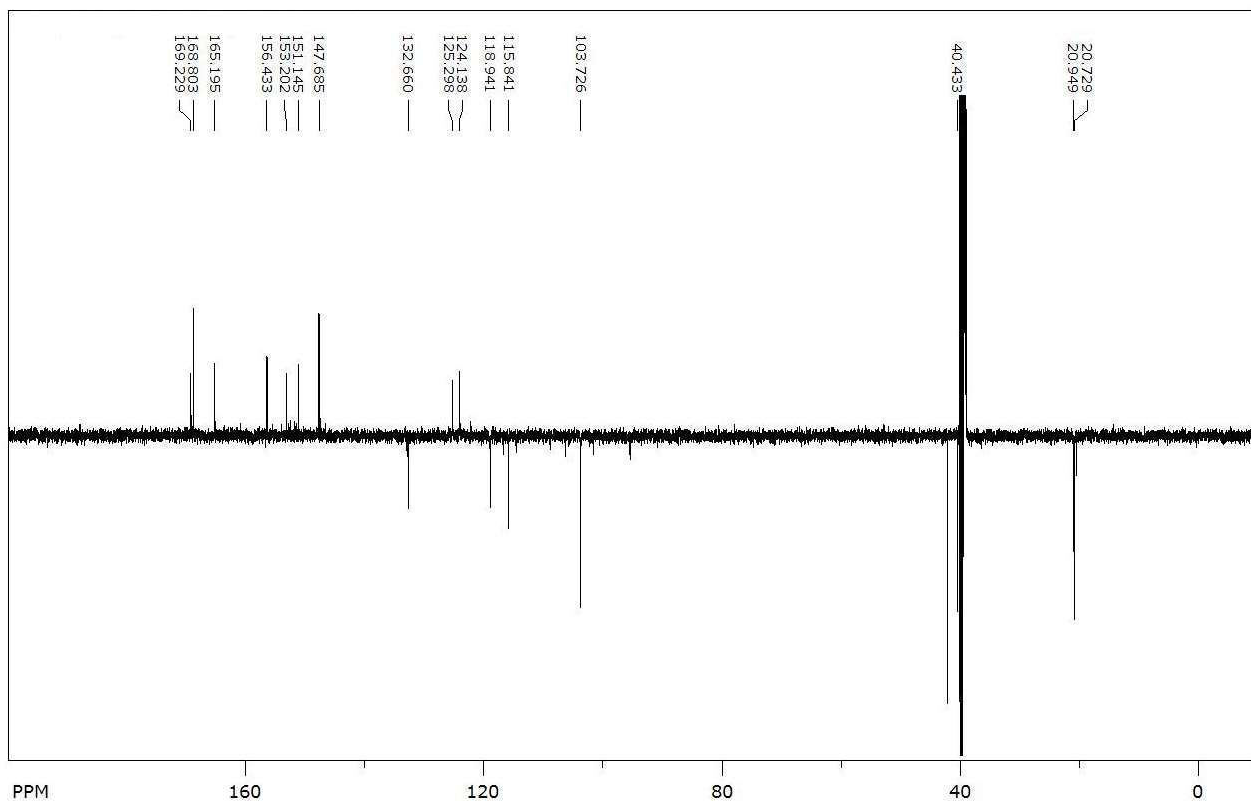
¹³C NMR spectrum of compound 7



¹H NMR spectrum of compound **8**



¹³C NMR spectrum of compound **8**



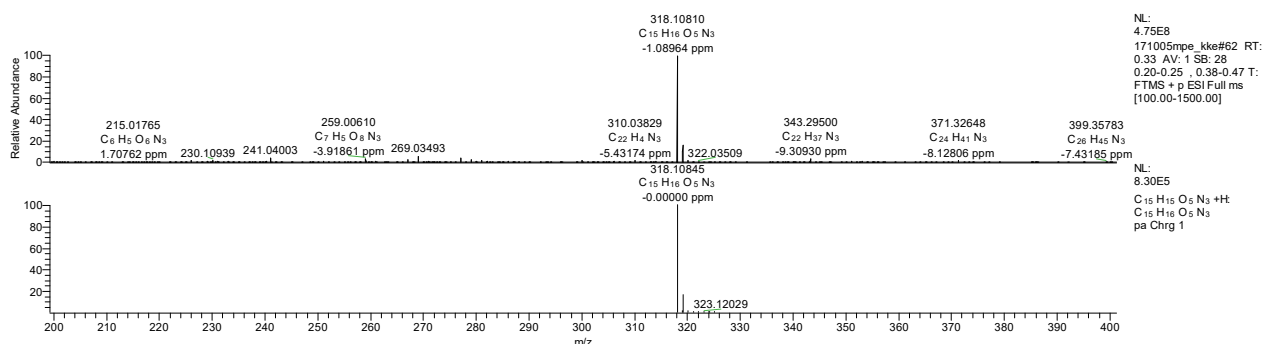
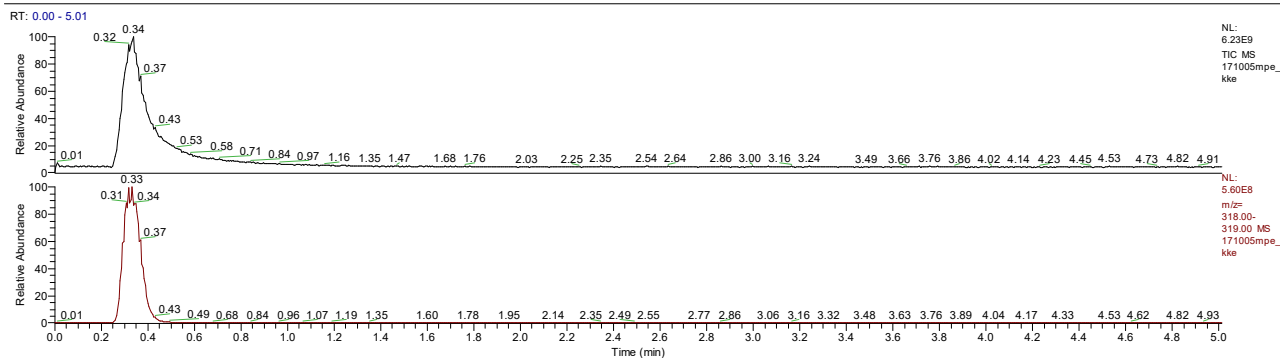
Mass Analysis

Hydrodabeyl (2)

C:\Xcalibur\data\171005mpe_kke

10/05/17 11:26:22

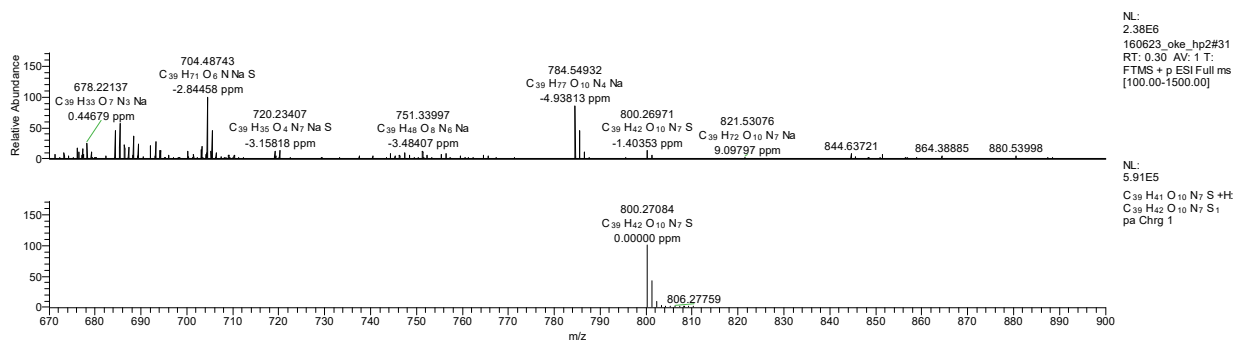
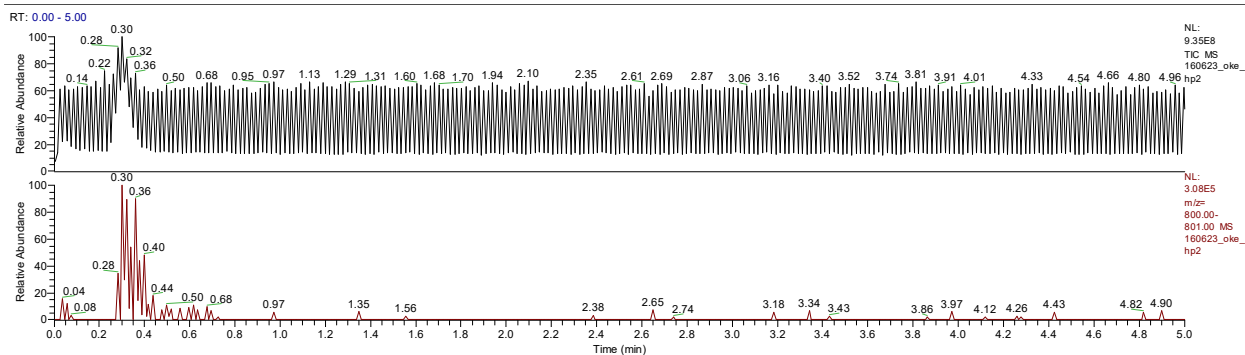
DAB(OH)3 KKe MPe in DMSO



Hydrodabeyl-Ser-Phe-EDANS (7)

C:\Xcalibur\data\160623_oke_hp2

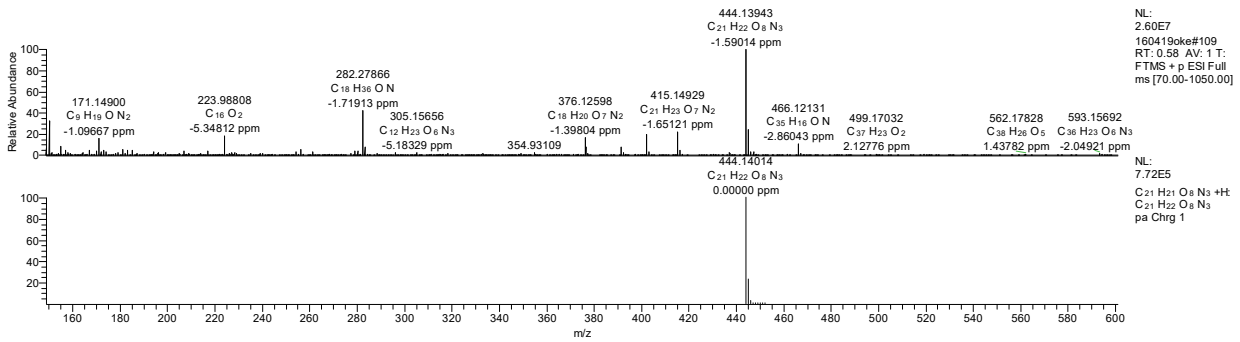
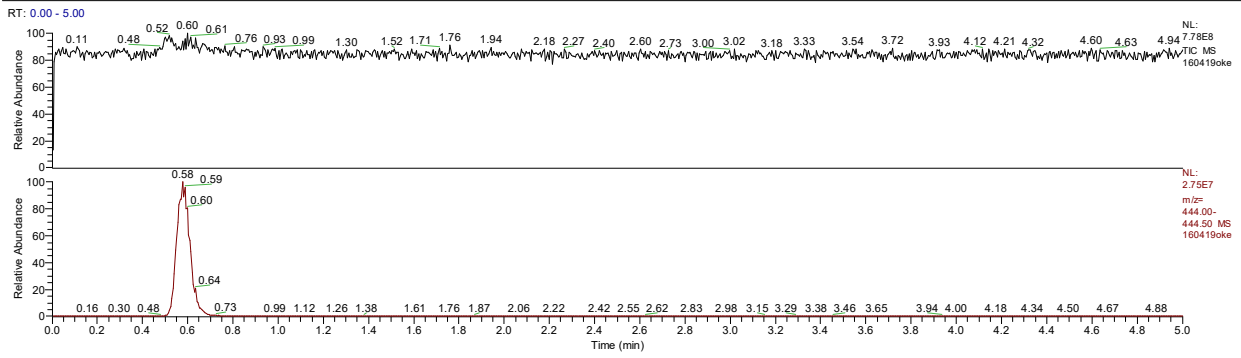
06/24/16 11:15:00



Hydrodabcyyl-triacetylated (8)

C:\Xcalibur\data\160419oke

04/19/16 09:27:58



References

- (1) Gottlieb, H. E.; Kotlyar, V.; Nudelman, A. *J. Org. Chem.* **1997**, *62* (21), 7512.
- (2) Petrzilka, T.; Lusuardi, W. G. *Helv. Chim. Acta* **1973**, *56* (1), 510.
- (3) Christie, R. M. *Colour Chemistry*; RSC Publishing: Cambridge, 2001.
- (4) Weimer, S.; Oertel, K.; Fuchsbauer, H. L. *Anal Biochem* **2006**, *352* (1), 110.
- (5) Smith, A. B.; Kanoh, N.; Ishiyama, H.; Minakawa, N.; Rainier, J. D.; Hartz, R. A.; Cho, Y. S.; Cui, H.; Moser, W. H. *J. Am. Chem. Soc.* **2003**, *125* (27), 8228.

Publication II

Chemoselective attachment of the water-soluble dark quencher hydrodabcyl to amino groups in peptides and preservation of its spectroscopic properties over a wide pH range

Oxana Kempf,^{†,∞} G. Matthias Ullmann,[~] Rainer Schobert,[‡] Karl Kempf,^{* ,∞} and Elisa Bombarda^{*,†}

[†]Department of Biochemistry, [~]Computational Biochemistry and [‡]Organic Chemistry Laboratory, University of Bayreuth, Universitätsstr. 30, 95440, Bayreuth, Germany.

[∞]ISM, University of Bordeaux, 351 Cours de la Libération, 33405, Talence, France.

ACS Omega. 2021, 6, 32896-3290

Reprinted with permission from [Chemoselective attachment of the water-soluble dark quencher hydrodabcyl to amino groups in peptides and preservation of its spectroscopic properties over a wide pH range. Oxana Kempf, G. Matthias Ullmann, Rainer Schobert, Karl Kempf and Elisa Bombarda, ACS Omega. 2021, 6, 32896-32903.21, DOI: DOI:10.1021/acsomega.1c04891]. Copyright 2021 American Chemical Society

Chemoselective Attachment of the Water-Soluble Dark Quencher HydrodabcyI to Amino Groups in Peptides and Preservation of Its Spectroscopic Properties over a Wide pH Range

Oxana Kempf, G. Matthias Ullmann, Rainer Schobert, Karl Kempf,* and Elisa Bombarda*

Cite This: *ACS Omega* 2021, 6, 32896–32903

Read Online

ACCESS |



Metrics & More

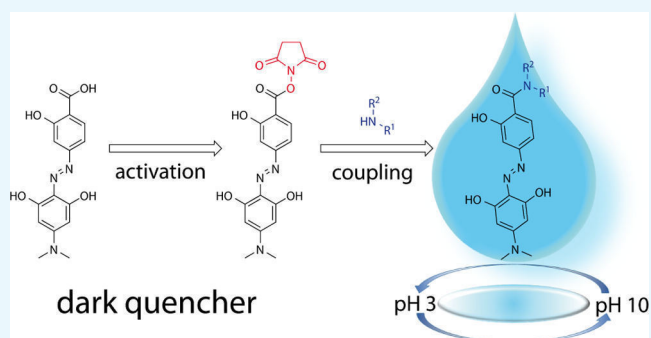


Article Recommendations



Supporting Information

ABSTRACT: The water-soluble quencher hydrodabcyI can be activated as an *N*-succinimidyl ester that is readily accessible from crude hydrodabcyI and storable for a long time. With primary and secondary amines, it reacts swiftly and chemoselectively, even in the presence of other competing nucleophiles such as those typically present in natural peptides. One of the three phenolic OH groups of hydrodabcyI is amenable to selective mono-Boc protection resulting in reduced polarity, advantageous to its further use in organic synthesis. The advantages of hydrodabcyI over dabcyI in spectrometric applications are exemplified by the pH dependence of its absorbance spectra.



INTRODUCTION

In the investigation of biomolecular reactions, molecules containing a fluorophore and a neighboring dark quencher are often used for spectroscopic quantifications.¹ Because of the presence of these two chromophores, the molecule is not fluorescent. If in the course of the reaction the fluorophore gets separated from the quencher, the appearing fluorescence can be measured with high sensitivity and temporal resolution. DabcyI [4-(4'-dimethylaminophenylazo)-benzoic acid, **1**] is a widely used dark quencher^{2–5} that exhibits no fluorescence and is appropriate for quenching many common fluorophores such as bimeans, dansyl, coumarin, and fluorescein derivatives. Although its hydrophobicity is beneficial for organic synthesis, its poor water solubility hampers biological applications, which are usually carried out in aqueous solution. Moreover, random interactions with hydrophobic regions of biomacromolecules, membranes, and test tubes may lead to unwanted side effects. The use of water-soluble derivatives of dabcyI can help to overcome these issues. In a previous publication,⁶ we reported the synthesis of the water-soluble derivative hydrodabcyI [4-(2',6'-dihydroxy-4'-dimethylaminophenylazo)-2-hydroxybenzoic acid, **2**] and its purification by sequential cycles of precipitation and centrifugation to achieve purity, enabling its direct use in spectroscopic applications. For most purposes, however, hydrodabcyI has to be linked to target molecules. During organic synthesis, the water solubility and high polarity of hydrodabcyI turned out to be a major challenge. The encountered problems include laborious purification, low yields, or the necessity of specific protecting groups.

In this work, we describe a general strategy to activate hydrodabcyI (**2**) and to chemically link it to amino groups

without the protection of its phenolic hydroxyl groups. This new strategy is based on the synthesis and isolation of the hydrodabcyI *N*-succinimidyl active ester [hydrodabcyI-ONSu (**3**), **Scheme 1**] from crude hydrodabcyI. This active ester is sufficiently reactive to afford significantly increased yields of amides when coupling it to amino groups. Moreover, active ester **3** is stable enough to allow convenient isolation, purification by column chromatography on silica gel with standard solvent systems, and long-term storage. In addition, we studied the pH-dependence of the UV/vis absorbance of hydrodabcyI (**2**) in order to understand the influence of the hydroxyl groups on its electrostatic properties and to characterize its spectroscopic properties in the pH range of potential applications.

EXPERIMENTAL SECTION

Chemicals and Analytical Methods. All reactions were carried out under a nitrogen or argon atmosphere using dry solvents under anhydrous conditions unless otherwise noted. DMF, carbonyldiimidazole (CDI), and all other chemicals were purchased from Sigma-Aldrich and used without further purification unless indicated otherwise. The ¹H and ¹³C NMR spectra were recorded on a Bruker Avance 300 MHz

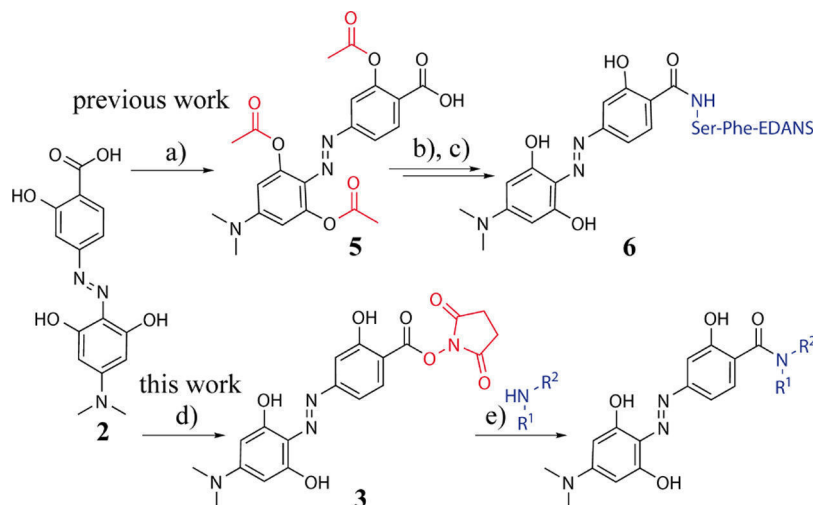
Received: September 5, 2021

Accepted: November 4, 2021

Published: November 22, 2021



Scheme 1. Strategies for the Coupling of HydrodabcyI (2) to Amines Either via Acetyl Protection of the Phenolic OH Groups (Marked in Red) in 5 and *In Situ* Activation of the Carboxylic Acid to Obtain 6 [Previous Work (a–c)] or via Isolation of *N*-Succinimidyl (Marked in Red) Active Ester 3 to Obtain a Labeled Compound [This Work (d,e)]^a



^aPrevious work: (a) 4.2 equiv. Ac₂O, 6 equiv. NEt₃, 0.1 equiv. DMAP, THF/DMSO; 80%. (b) Ser-Phe-EDANS, dipeptide labeled on the Phe-carboxy group as amide with 5-(2-aminoethylamino)-1-naphthalenesulfonic acid (EDANS), 1.6 equiv. propylphosphonic anhydride (T3P), 50% in THF, 3.3 equiv. NEt₃, THF/DMF, 0 °C, 1.5 h. (c) piperidine/MeOH, r.t., 1 h; 30% yield over the two steps. This work: (d) 1 equiv. NHS, 1 equiv. CDI, DMF, r.t., overnight; 44%. (e) 1–2 equiv. amine (primary or secondary, HNR¹R²), 2 equiv. NEt₃, DMF, r.t., overnight; 70–100%. More details are provided in the [Supporting Information](#).

spectrometer. Chemical shifts are reported in parts per million (ppm) referenced with respect to residual solvent (DMSO = 2.50/39.52 ppm). The following abbreviations were used to indicate multiplicities: s = singlet, d = doublet, dd = double doublet, t = triplet, m = multiplet, br s = broad singlet, and qdd = double doublet of quartet. High-resolution mass spectra (HRMS) were obtained by electrospray ionization and performed on a Q Exactive Orbitrap MS system, Thermo Fisher Scientific. For column chromatography, silica gel (40–63 μm, Merck) was used. The retention factors (*R_f*) were determined by thin layer chromatography on pre-coated silica plates (Merck TLC Silica gel 60 F254). The spots were visualized by UV light and stained with ceric ammonium molybdate solution, followed by treatment with a heat gun.

Synthesis of the HydrodabcyI-ONSu Ester (3). A mixture of hydrodabcyI (50 mg, 0.158 mmol) and *N*-hydroxysuccinimide (NHS) (18 mg, 0.158 mmol) in DMF (5 mL) was treated with CDI (26 mg, 0.158 mmol) and stirred overnight at room temperature under argon. The resulting mixture was dissolved in ethyl acetate (100 mL) and washed with aqueous citric acid (5% w/w, 2 × 50 mL) and brine (2 × 50 mL). The aqueous phases were extracted with ethyl acetate (2 × 100 mL). The organic layers were dried over anhydrous Na₂SO₄ and evaporated *in vacuo*. The crude product was purified by column chromatography on silica gel (dry package, elution with cyclohexane/ethyl acetate 1:2) to afford ester 3 (29 mg, 44%) as a dark red solid (*R_f* = 0.4, EtOAc); HRMS (–ESI) solution in methanol *m/z*: [MOMe – H][–] calculated for C₁₆H₁₆N₃O₅[–], 330.10954; found, 330.10951. ¹H NMR (300 MHz, DMSO-*d*₆): δ ppm 2.88 (s, 4 H), 3.09 (s, 6 H), 5.72 (s, 2 H), 7.27 (d, *J* = 1.7 Hz, 1 H), 7.32 (dd, *J* = 8.8, 1.7 Hz, 1 H), 7.89 (d, *J* = 8.8 Hz, 1 H), 10.62 (br s, 1 H). ¹³C NMR (75 MHz, DMSO-*d*₆): δ 170.6, 170.6, 170.6, 161.3, 161.3, 160.9, 158.4, 152.9, 132.6, 125.9, 110.0, 106.8, 105.8, 91.8, 91.8, 40.1, 40.1, 25.5, 25.5. (For more details, see the [Supporting Information](#)).

General Procedure for Coupling of HydrodabcyI to Amines (Compounds 4–11). The amino compound (1 to 2 equiv.) was added to a stirred solution of hydrodabcyI-ONSu ester (3) (1 equiv.) in DMF (5 mL) at room temperature. The reaction mixture was stirred overnight at room temperature. Thereafter, it was diluted with ethyl acetate (100 mL) and washed with aqueous citric acid (5% w/w, 2 × 25 mL) and brine (2 × 25 mL). The aqueous phases were extracted with ethyl acetate (2 × 100 mL). The organic layers were dried over anhydrous Na₂SO₄ and evaporated *in vacuo*. The crude product was purified by column chromatography on silica gel.

Procedure for Coupling of HydrodabcyI to a Peptide in Aqueous Solution: One-Pot Double-Functionalization of Glutathione (Compound 12). A solution of monobromo-bimane (16.4 mg, 0.06 mmol) in acetonitrile (1.5 mL) was added to a stirred solution of glutathione (18.4 mg, 0.06 mmol) and NaHCO₃ (15 mg, 0.18 mmol) in degassed water (6 mL) under argon atmosphere according to Radkowsky and Kosower.⁷ After 30 min, a solution of 3 (25 mg, 0.06 mmol) in DMF (2 mL) was added and the reaction was allowed to stir for another 4 h at room temperature under argon. The crude mixture was diluted with water containing 0.1% HCOOH and purified by semipreparative Amersham Äkta—900 HPLC (column Kinetex 5 μm C18 100 Å, 250 × 21.2 mm, 10 mL/min, 30% CH₃CN/70% H₂O + 0.1% HCOOH) to afford double-labeled glutathione (12, 5 mg, at least 20% yield after semipreparative HPLC) as a dark red solid. No other coupling products were detected. HPLC analysis showed complete consumption of 3. However, some glutathione singly labeled with bimane and free hydrodabcyI acid due to partial hydrolysis of the active ester was detected. To minimize incomplete labeling, the reaction could be optimized, for example, by adding a higher excess of 3. ¹H NMR (500 MHz, DMSO-*d*₆/D₂O 9:1): δ ppm 1.64 (s, 3 H), 1.68–1.77 (m, 3 H), 1.89–2.01 (m, 1 H), 2.04–2.16 (m, 1 H), 2.26 (t, *J* = 6.4 Hz, 2 H), 2.30 (s, 3 H), 2.69 (dd, *J* = 13.5, 9.4

Hz, 1 H), 2.97 (dd, $J = 13.5, 4.5$ Hz, 1 H), 3.03 (s, 6 H), 3.55–3.66 (m, 2 H), 3.77 (d, $J = 14.8$ Hz, 1 H), 3.81 (d, $J = 14.8$ Hz, 1 H), 4.32 (t, $J = 5.2$ Hz, 1 H), 4.45 (dd, $J = 9.4, 4.5$ Hz, 1 H), 7.11 (dd, $J = 8.5, 1.5$ Hz, 1 H), 7.15 (d, $J = 1.5$ Hz, 1 H), 7.88 (d, $J = 8.5$ Hz, 1 H). ^{13}C NMR (125.76 MHz, DMSO- d_6 /D $_2$ O 9:1): δ 174.5, 173.5, 172.2, 170.9, 168.1, 160.8, 160.8, 159.2, 150.1, 148.6, 147.6, 147.6, 130.8, 126.1, 113.7, 113.7, 113.5, 113.5, 111.6, 109.9, 105.3, 92.3, 92.3, 53.4, 52.6, 42.5, 40.8, 40.8, 34.4, 32.2, 27.8, 25.3, 11.8, 7.3, 7.0. HRMS (+ESI) m/z : $[M + H]^+$ calcd for $\text{C}_{35}\text{H}_{41}\text{N}_8\text{O}_{12}\text{S}^+$, 797.25592; found, 797.25302. Analytical HPLC Shimadzu (column Halo 90 Å, C18, 2.7 μm , 2.1 mm \times 150 mm, 0.3 mL/min, $\text{CH}_3\text{CN}/\text{H}_2\text{O} + 0.1\%$ HCOOH). Method: 30% CH_3CN till 7 min, from 7.5 min 40% CH_3CN , $t_{\text{R}} = 6.9$ min.

Titration and Absorbance Measurements. The pH was measured with a Mettler Toledo SevenMulti pH meter equipped with a microelectrode (InLab Micro, Mettler Toledo). A double beam PerkinElmer LAMBDA 750 UV/vis spectrophotometer equipped with a thermostated cuvette holder was used to record absorption spectra over a wavelength range of 250–700 nm at 20 °C in 2 mL quartz cuvettes from Hellma with a 1 cm light path. The absorbance behavior of hydrodabcyI (2) and its isopropyl amide derivative (4) has been investigated in aqueous solution over a wide range of pH values: for hydrodabcyI, from pH = 3.2 to pH = 10.5 and for its isopropyl amide derivative, from pH = 2.4 to pH = 10.5. DabcyI (1) was investigated in aqueous solution from pH = 3.5 to pH = 10.5 and in DMSO/aqueous solution 50:50%, from pH = 2.2 to pH = 7.3.

In order to control the pH along the entire investigated pH range, the aqueous solution contained a mixture of buffers: *N*-cyclohexyl-3-aminopropanesulfonic acid (CAPS, useful pH range: 9.7–11.1), *N*-cyclohexyl-2-aminoethanesulfonic acid (CHES, useful pH range: 8.6–10), 4-(2-hydroxyethyl)-1-piperazine ethanesulfonic acid (HEPES, useful pH range: 2.5–3.5 or 6.8–8.2), 2-(*N*-morpholino)ethanesulfonic acid (MES, useful pH range: 5.8–6.5), and ammonium acetate (useful pH range: 3.7–5.7). The concentration of each compound in the mixture was 15 mM. In all the experiments, the pH of the solution was adjusted to 10.5 with drops of NaOH (19 M) and then gradually reduced by the dropwise addition of 5 M HCl. The concentration of dabcyI, hydrodabcyI, and hydrodabcyI-isopropyl amide was 12.7 μM in all experiments.

RESULTS AND DISCUSSION

Shortcomings of the One-Pot Coupling of HydrodabcyI (2) to Amines in the Presence of Transacylation Reagents. HydrodabcyI (2) is to be linked to its target via an amide bond between its carboxyl group and an amino group. In the standard one-pot amidation protocol for amino acids, the carboxylic acid is activated by dicyclohexylcarbodiimide (DCC),⁸ followed by the formation of an active ester with hydroxybenzotriazole or NHS and eventually acylation of the amine. However, such a formation of an active ester *in situ*, that is, in the presence of amino derivatives, failed with hydrodabcyI (2) because of the low reactivity of its carboxyl group, which is attached to an electron-rich phenyl ring. Reactions with the stronger acylation catalyst *N,N*-dimethylaminopyridine (DMAP) worked but gave a high yield of 85% only in the case of the isopropyl amide of 2. The one-pot amidation of hydrodabcyI with functionalized primary amines proceeded with poor yields throughout, for example, with only 10% for

the primary amide of the *N*^αBoc-lysine ethyl ester. The coupling to peptides containing unprotected competing *O*-nucleophiles such as serine esters failed completely. Although we had previously reported the use of protected tris(acetyl)-hydrodabcyI (5) for the labeling of a serine-containing peptide (6) in ca. 30% yield (Scheme 1), this strategy is not generally applicable due to the electrophilic nature and migration tendency of the acetyl groups. For instance, the reaction of tris(acetyl)hydrodabcyI (5) with the primary amine of the *N*^αBoc-lysine ethyl ester exclusively afforded the primary acetamide of the *N*^α(Boc)-*N*^ε(acetyl)-lysine ethyl ester. These findings led us to the conclusion that the isolation of the active ester intermediate might be required to achieve efficient coupling between hydrodabcyI (2) and structurally diverse amines.

Separation of Activation and Coupling Steps by Isolation of the Active Ester of HydrodabcyI. For efficient labeling of amino derivatives with hydrodabcyI (2), we decided to disconnect activation and coupling by isolating the hydrodabcyI-ONSu active ester, (3 in Scheme 1). We tried out three condensation reagents for the synthesis of 3: DCC, ethyl-dimethylaminopropyl carbodiimide (EDC), and CDI. With DCC, ester 3 was obtained in less than 30% yield. Moreover, the byproduct dicyclohexylurea led to problems during purification because it is of similar polarity as 3 and cannot be removed completely from the product. The water-soluble EDC failed to produce substantial amounts of condensation products and led to the formation of emulsions upon extraction. With CDI, the desired active ester 3 was obtained in a pure form and 44% yield.

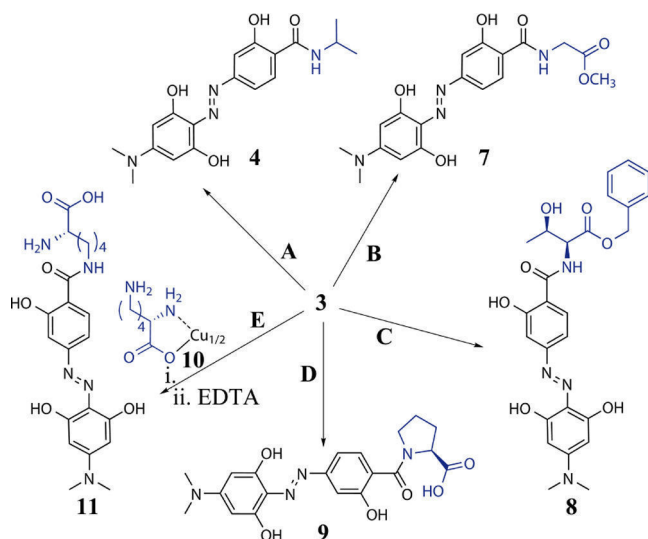
The active ester 3 is surprisingly stable and allows easy handling during aqueous workup, standard column chromatography, and long-term storage in the dark. As a solid, 3 is completely stable for at least one week at room temperature and for at least eight months in the fridge at 4 °C or freezer at –20 °C (see NMR spectra in Figure S1 in the Supporting Information). Solutions of 3 in DMSO were found to be stable for at least three months at room temperature.

Coupling of the HydrodabcyI Active Ester to Amino Derivatives. In order to evaluate the applicability of 3 in peptide chemistry and biology, we assessed its reactivity toward different commercially available amino acid derivatives in five exemplary test reactions A–E (Scheme 2).

In test reaction A, isopropylamide 4 of hydrodabcyI could be obtained quantitatively when employing active ester 3 instead of hydrodabcyI. In test reaction B, glycine methyl ester hydrochloride reacted quantitatively with 3 to give the desired hydrodabcyI amide 7. In test reaction C, the threonine benzyl ester with the unprotected hydroxy group afforded amide 8 in 70% yield. In test reaction D, the secondary amino group of proline in the presence of the unprotected carboxy group was *N*-acylated to give amide 9 in over 90% yield. Test reaction E showed that lysine can be regioselectively functionalized on the ϵ -amino group by employing its copper chelate complex⁹ 10, which is soluble only in water. This reaction highlights the advantage of active ester 3 being applicable in aqueous solutions. Direct decomplexation with EDTA in a non-optimized one-pot procedure gave ϵ -(hydrodabcyIamido)-lysine 11 in 30% yield.

The selectivity for primary and secondary amino groups that were observed in the presence of oxygen nucleophiles such as alcohol and carboxyl groups (test reactions C and D, respectively, in Scheme 2) was also confirmed in the presence

Scheme 2. Test Reactions of HydrodabcyI Active Ester 3 with Primary and Secondary Amines (in Blue)^a



^a(A) 1.2 equiv. Isopropylamine, DMF; 99%; (B) 1.1 equiv. Glycine Methyl Ester Hydrochloride, 1.1 equiv. NEt₃, DMF, r.t., Overnight; 99%; (C) L-threonine Benzylester Oxalate, 2 equiv. NEt₃, DMF, r.t., Overnight; 70%; (D) 2 equiv. L-proline, 2 equiv. NEt₃, DMF, r.t., Overnight; 92%; and (E) Two-Step Reaction: i. 2 equiv. L-lysine Copper(II) Complex **10**, Water/DMF and ii. 25 mL of 0.1% Na₂EDTA Solution; 30%. More details are provided in the [Supporting Information](#).

of aromatic azacycles such as indole and imidazole (data not shown). To verify the possibility of selectively functionalizing the *N*-terminus of an unprotected peptide in aqueous solution, we carried out one-pot double-functionalization of glutathione with hydrodabcyI and bimane. Bimane is a fluorescent azacycle that is widely used for labeling glutathione due to the straightforward linking procedure. Moreover, the emission spectrum of bimane overlaps with the absorption spectrum of hydrodabcyI. Because a dark quencher is often used in combination with a fluorophore to create FRET-based fluorogenic probes,¹ this test proves the real-world applicability of the new hydrodabcyI-ONSu active ester (**3**) in aqueous

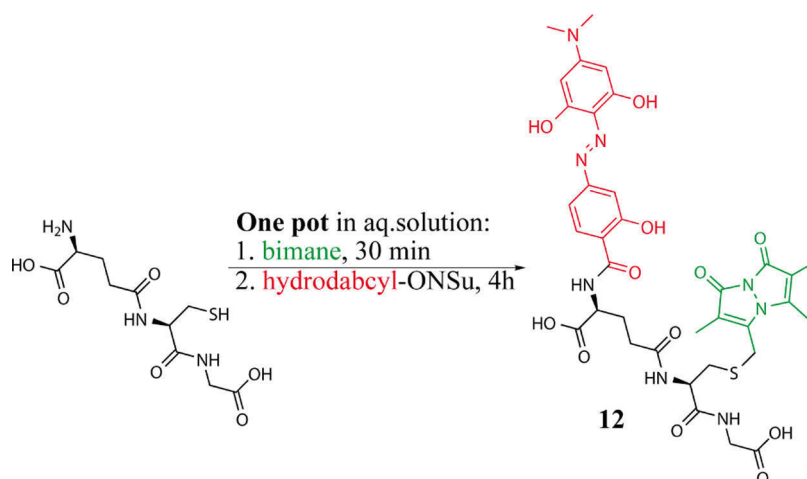
media. The reaction conditions were based on the standard procedure for functionalizing glutathione with bimane,⁷ followed by simply adding **3** to the same mixture (details in the [Experimental Section](#)). Double-labeled glutathione (**12**, [Scheme 3](#)) and no other coupling products were detected by HPLC, indicating that the reaction proceeded with high selectivity.

Importance of Intramolecular Hydrogen Bonds for the Reactivity of the Phenol Groups. HydrodabcyI (**2**) contains three phenolic hydroxyl groups, which do not require protection for activation and coupling under the mildly basic conditions described above. We explain their reduced nucleophilicity by their engagement in *intramolecular* H bonds. As shown in [Scheme 4](#), two of these hydroxyl groups can be involved in pericyclic keto–enol tautomerism.¹⁰ Even though the enol-form **2a** is probably dominant, the molecule can also exist in another tautomer (structure **2b**), resulting from proton transfer within hydrogen bonds.

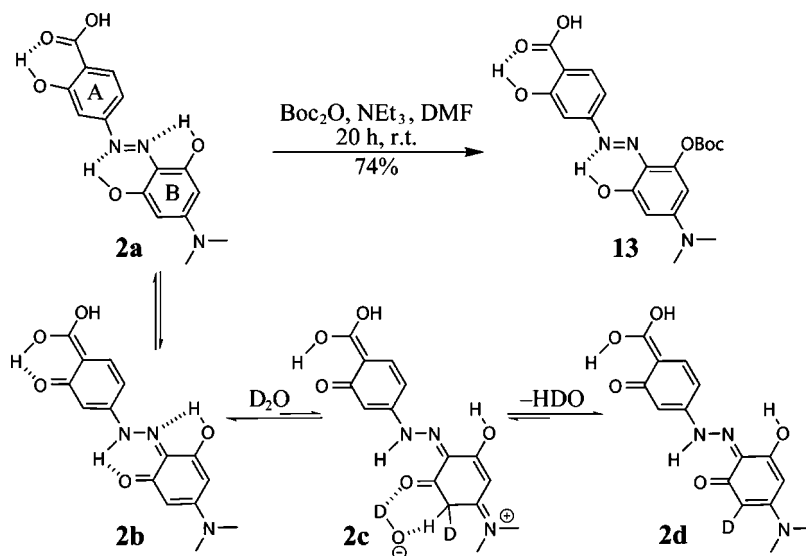
Moreover, the *intramolecular* hydrogen bonds between the diazo-*ortho*-phenol groups and the neighboring nitrogen atoms differ in the size of the rings that they generate, a five- versus a six-membered ring ([Scheme 4](#)). Quantum chemical calculations show that the H–N distance is 1.7 Å in the six-membered ring and 2.3 Å in the five-membered ring, suggesting that the six-membered ring is more stable due to steric restraints.

The reduced stability of the hydrogen bond in the five-membered ring may lead to a slightly higher acidity of the involved hydroxyl group compared to the two other hydroxyl groups of hydrodabcyI (**2**). This effect becomes obvious in the reaction of hydrodabcyI (**2**) with an excess of Boc₂O, resulting in the selective monoprotection of one OH group of the B ring, most likely because of its engagement in the less stable five-membered ring of **2** ([Scheme 4](#)). A similar selectivity has also been described for flavonoids, where the β-ketone protects the adjacent phenol from alkylation under basic conditions.^{11,12} Surprisingly, proton–deuteron exchange in DMSO-*d*₆-D₂O (9:1) solution showed the complete disappearance of the signal corresponding to the aromatic protons in the B ring after one night at room temperature. Because the exchange of aromatic protons is unlikely in aqueous solutions,

Scheme 3. Test Reaction of HydrodabcyI Active Ester 3 with an Unprotected Peptide; Glutathione in Black Doubly Labeled with Bimane in Green and HydrodabcyI in Red (**12**) is Obtained by a One-Pot Synthesis in Aqueous Solution (See Details in the [Experimental Section](#))



Scheme 4. Regioselective Mono-Boc-Protection of HydrodabcyI (2) due to Engagement of Two of the Three Hydroxyl Groups in Intramolecular H Bonds Leading to Stable Six-Membered Rings^a



^aThe reaction sequence 2a–2d is the suggested mechanism for the observed proton–deuteron exchange in ring B. It is drawn only once to avoid overflow; however, it concerns both aromatic protons of ring B. The exchange of the second aromatic proton occurs *via* the same mechanism after rotation of the ring in 2d.

the transition between 2b and 2d can be explained by postulating the presence of the nonaromatic tautomer 2c (NMR spectra in the Supporting Information).

Originally, we synthesized the mono-Boc derivative 13 in order to protect 2 before its activation as the active ester 3. However, we found that the activation eventually proceeded well also without protection. Nevertheless, the Boc protection can be used when 2 needs to be purified because the precipitation of crude 2 is time consuming and does not always lead to high purity. Even though in the present work, we did not use 13 for further applications, its selective synthesis highlights the importance of intramolecular H bonds for the decreased reactivity of the phenolic hydroxyl groups in 2. Derivative 13 may also be used when hydrodabcyI needs to be introduced at an early stage of a longer synthesis, and it facilitates isolation and purification steps due to its reduced polarity. In contrast to unprotected hydrodabcyI (2), derivative 13 can be extracted from the water phase with ethyl acetate and purified by normal phase column chromatography. It is also soluble in methanol, whereas 2 is only soluble in DMSO or water. From these observations, we conclude that the intramolecular hydrogen bonds in the six-membered rings reduce the acidity and, therefore, also the nucleophilicity of the involved hydroxyl groups enabling isolation and coupling of the hydrodabcyI-ONSu ester without the need of protective groups.

pH Dependence of the UV/Vis Absorption Spectra as an Example of the Superiority of HydrodabcyI (2) over DabcyI (1). As hydrodabcyI (2) was designed to be employed in spectroscopic investigations, a meticulous characterization of its spectroscopic properties is appropriate. One major aspect for applications in aqueous solution is the pH dependence of its absorbance. In addition to the protonation sites shared with dabcyI (carboxyl and diazo groups), hydrodabcyI bears three hydroxyl groups, the influence of which on its absorbance properties needs to be explored (Figures 1 and 2). Both hydrodabcyI 2 and dabcyI 1 comprise push–pull systems

linking an electron-donating dimethylamino group and an electron-withdrawing acyl group. This push–pull system generates an intramolecular charge transfer, which is responsible for the main absorption band around 450 nm. We first analyzed the pH dependence of the absorbance of dabcyI in 50% DMSO where it is well soluble. The acidification of the solution (gray arrow in Figure 1a) induced a bathochromic shift of the major absorption band (blue arrow) accompanied by a hyperchromic effect. The dashed lines indicate the pH range (Figure 1a) where the carboxylate (red line) and the diazo groups (blue line) are expected to get protonated. In aqueous solution above pH = 6, the absorbance spectrum of 1a showed a similar maximum at 450 nm. Upon acidification (gray arrow in Figure 1b), a decrease of the major band was observed in the pH range where the carboxylate starts to get protonated.^{13–15} However, the resulting uncharged molecule 1b is poorly soluble and prone to precipitation in aqueous media.¹⁶ Therefore, the significant drop in absorbance at 450 nm below pH = 6 (red arrow in Figure 1b) was mainly due to the precipitation of 1b. The formation of visible aggregates⁸ due to precipitation results in spectral deformation. Not only is the absorbance at 450 nm drastically diminished, but the gain in absorbance at 580 nm is attenuated as well, due to fewer absorbing molecules in the illuminated volume (blue arrow).

In contrast to dabcyI (1), the acidification of an aqueous solution of hydrodabcyI (2) (Figure 2a) neither led to a sudden decrease of the major band of the spectrum nor to the appearance of an additional band at a large wavelength. Consequently, the quenching ability of hydrodabcyI remained constant over a broader pH range, which is a significant advantage when it is used in dual probes for quantitative fluorimetric assays.

In the applied pH range, hydrodabcyI (2) can exist at least in four different protonation states, namely dianion 2e, monoanion 2f, neutral 2a, and cation 2g (Figure 2b). The isosbestic point at 467 nm in the pH range 10–6 is due to a

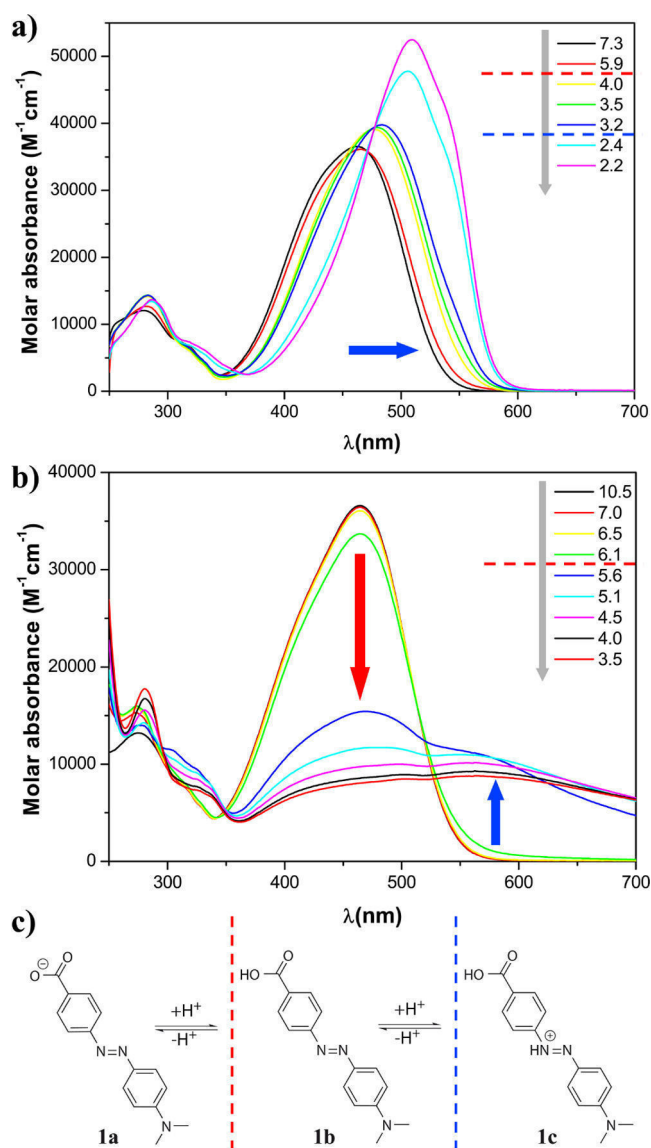


Figure 1. pH dependence of the molar absorbance of dabcyI (**1**) at 20 °C. The pH was controlled with an aqueous mixture of buffers CAPS, CHES, HEPES, MES, and ammonium acetate, each present at 15 mM. (a) 50% DMSO and 50% buffer mix; (b) 100% aqueous mixture of buffers; and (c) protonation states of **1**. The dashed lines indicate the qualitative estimation of the transition between the protonation states. The gray arrows represent the experimental acidification of the solution.

small red shift of the main band, which could be attributed to the protonation of one phenolate of ring B in **2e** (red asterisk in Figure 2a). At pH lower than 6, we observe only a decrease without a shift of the main absorption band. The formation of neutral **2a** and cation **2g** occurs in a similar pH range and cannot be distinguished by qualitative inspection of the spectra. The presence of cation **2g** below pH 3.7 can be associated with the appearance of a small band at about 350 nm (blue arrow).

In most practical applications, hydrodabcyI (**2**) will be linked to a biomolecule through its carboxyl group. To mimic the spectroscopic behavior of hydrodabcyI in its function as an amide label, we used its isopropylamide **4** as a surrogate for the chromophore resulting from the functionalization of a peptide. The protonation states of **4** are different from those of **2**,

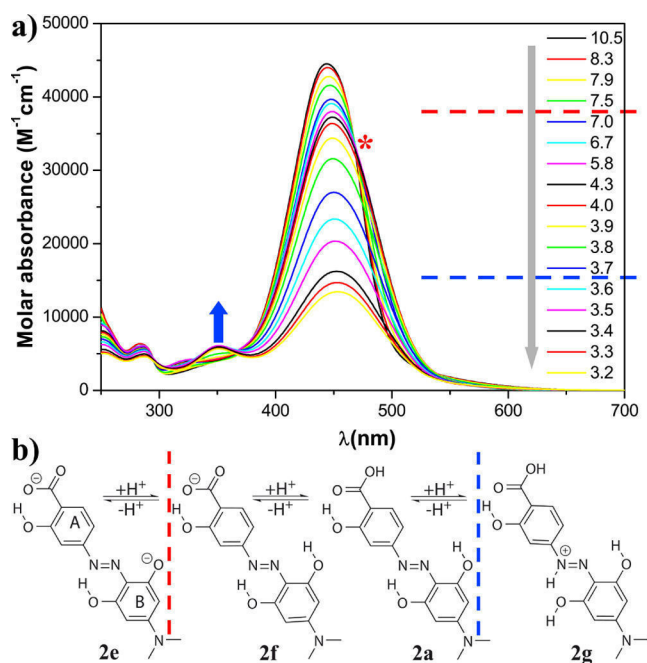


Figure 2. (a) pH dependence of the molar absorbance at 20 °C of hydrodabcyI (**2**) in an aqueous mixture of buffers CAPS, CHES, HEPES, MES, and ammonium acetate, each one present at 15 mM and (b) protonation states. The gray arrow represents the experimental acidification of the solution. The red dashed line indicates the putative pH range of the protonation of the phenolate, and the red asterisk indicates the corresponding spectral effect, that is, the isosbestic point. The blue dashed line indicates the putative pH range of the protonation of the diazo group, and the blue arrow indicates the corresponding spectral effect, that is, the appearance of the local maximum at 350 nm.

namely the monophenolate **4a**, the neutral compound **4b**, and the mono cation **4c** (Figure 3b). However, similar arguments to rationalize the pH dependence of their UV/vis absorbance can be raised. The main absorption maximum shows similar pH dependence as in hydrodabcyI with an isosbestic point at 463 nm between pH 8 and 3.3 (red asterisk in Figure 3a), showing the equilibrium between **4a** and **4b**. Additionally, below pH = 2.6, we observe the appearance of a small band at 350 nm and of a shoulder at about 500 nm associated with the protonation of the diazo group in **4c** (blue arrow and asterisk in Figure 3a). In contrast to hydrodabcyI (**2**), the latter changes in the absorbance of **4** occur at significantly lower pH values due to the absence of the negatively charged carboxylate. Additionally, in order to compare the spectroscopic behavior of dabcyI and hydrodabcyI as amide labels, which is the relevant form in most of their applications, we synthesized dabcyI-isopropylamide (**14**) (protocol in the Supporting Information), a nonhydroxylated congener of **4**. However, **14** was completely insoluble in aqueous solution, and its absorption spectra could not be recorded. This result indicates that dabcyI may reduce the solubility of the peptide to which it is linked, underlining once more its inferiority to hydrodabcyI in aqueous solutions. A detailed quantitative analysis of the pH behavior of the compounds presented in this work is ongoing and will be the object of a future publication.

In order to provide a quick overview of the pH dependence of the absorption band that is most relevant for the potential applications, we plotted the absorbance at the maximum wavelength as a function of pH for the three compounds under

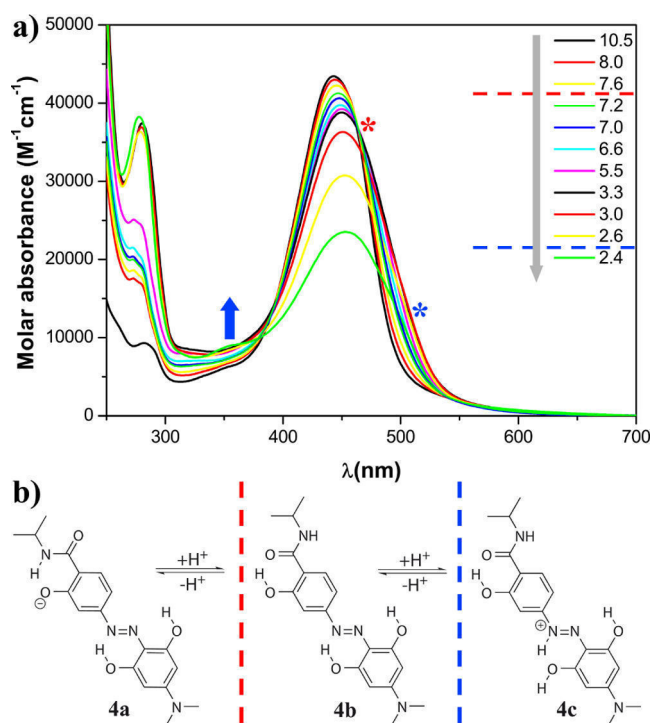


Figure 3. (a) pH dependence of the molar absorbance at 20 °C of hydrodabcylyl isopropylamide (4) in an aqueous mixture of buffers CAPS, CHES, HEPES, MES, and ammonium acetate, each present at 15 mM and (b) protonation states. The gray arrow represents the experimental acidification of the solution. The red dashed line indicates the putative pH range of the protonation of the phenolate, and the red asterisk indicates the corresponding spectral effect, that is, the isosbestic point. The blue dashed line indicates the putative pH range of the protonation of the diazo group, and the corresponding spectral effects are indicated by the blue arrow showing the appearance of the local maximum at 350 nm and the blue asterisk showing the shoulder at around 500 nm visible below pH 2.6.

investigation. For all of them, the decreasing pH induced a moderate bathochromic shift (6–8 nm). Hypochromism, however, was by far the most pronounced effect. Therefore, we monitored the absorbance at the wavelength for which we had initially measured the maximum at basic pH and which we deemed most meaningful for a description of the overall tendency. The molar absorbance (Figure 4a) showed a steep drop at pH = 5.5 for the parent compound dabcylyl (1, green curve) but only at pH = 3.5 for hydrodabcylyl (2, red curve) and at an even lower pH value for its isopropylamide (4, black curve). This effect has already been discussed in detail above (Figures 1–3). Nonetheless, Figure 4a shows a clear and concise roundup of the cardinal features. In the case of hydrodabcylyl (2), the decrease in absorbance is attributed to the protonation in a similar pH range of the carboxylate and of the diazo group. In the case of hydrodabcylyl isopropylamide (4), the decrease in absorbance at low pH can only be attributed to the protonation of the diazo group because it does not contain a carboxyl group. The abrupt decrease in absorption observed for dabcylyl (1) is mainly due to aggregation, followed by precipitation in concomitance with the protonation of the carboxylate. In contrast, the precipitation of hydrodabcylyl (2) is negligible and occurs at a much lower pH value due to the higher solubility of the compound. Likewise, no precipitation of 4 was detected in the investigated pH range. The fact that the protonation of the

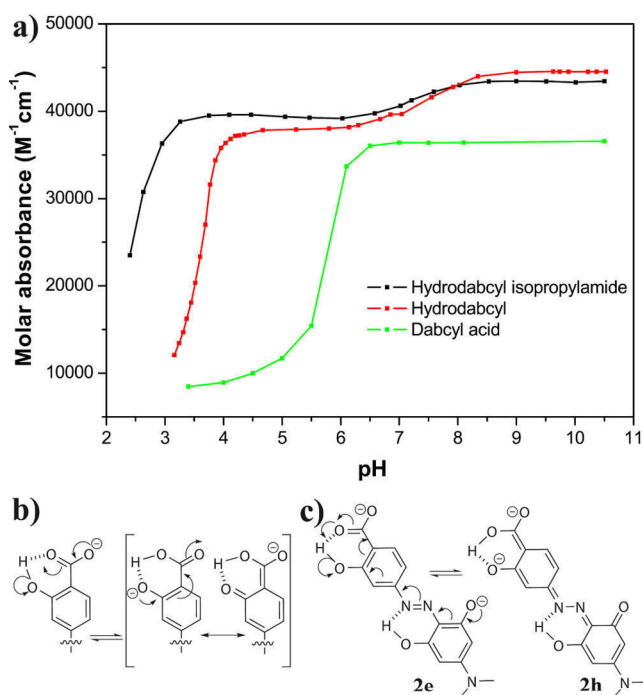


Figure 4. pH dependence of the molar absorbance of hydrodabcylyl (2, red), hydrodabcylyl isopropylamide (4, black), and dabcylyl (1, green). (a) Evolution of the signal detected at the wavelength of maximal absorbance (445 nm for hydrodabcylyl and its isopropylamide and 463 nm for dabcylyl). Each compound was dissolved in a buffer mix at 20 °C (15 mM each of CAPS, CHES, HEPES, MES, and acetate buffer). The line connecting the experimental points is only a visual guide. (b) Three-center delocalization of the carboxylate anion leading to higher acidity of the hydroxylated compound. (c) Delocalization of the phenolates leading to comparably high acidity of the phenolic OH groups.

carboxylate of 2 occurs at a much lower pH value than that of 1 is due to two different effects. On the one hand, the intramolecular H bond at the carboxylate group in 2 (Figure 4b) allows for the delocalization of its negative charge to the phenolate. This delocalization over three oxygen atoms results in the stabilization of the negative charge and thus in a decrease of the acidity when compared to 1. On the other hand, the precipitation of 1 withdraws the protonated form constantly from the equilibrium in solution and leads to an apparent shift of the protonation equilibrium to higher pH values.

The absorbance change of small amplitude for both hydroxylated compounds 2 and 4 (red and black curves in Figure 4a) in the pH range between 6 and 9 can be attributed to the deprotonation of a phenol group. This deprotonation occurs at a lower pH value than expected for a standard phenol group and can be explained with the mesomeric stabilization by the carbonyl group forming a vinylogous carboxylate 2e (Figure 4c). In addition, the two negative charges can be delocalized over tautomer 2h.

The obvious advantage of hydrodabcylyl (2) and its isopropylamide (4) in comparison with dabcylyl (1) is their ability to retain the absorption properties over a broader pH range because of their enhanced solubility and the charge delocalization mediated by intramolecular H bonds.

CONCLUSIONS

The dark quencher hydrodabcyI (2) can be conveniently activated for amide bond formation in the form of its *N*-succinimidyl ester (3), which is stable in the solid state and may be stored for months in the fridge or as DMSO solution at room temperature. HydrodabcyI *N*-succinimidyl ester (3) reacts selectively and swiftly at room temperature with primary and secondary amines in good to quantitative yields. This selective amide bond formation also takes place in the presence of other protein-typical nucleophilic functional groups such as hydroxyl, carboxyl, and the aromatic imino groups of imidazole and indole. HydrodabcyI *N*-succinimidyl ester (3) can even be used in water. In fact, we showed that an unprotected peptide (glutathione) can be successfully labeled with bimeane and hydrodabcyI *N*-succinimidyl ester (3) by a one-pot synthesis in aqueous solution. Furthermore, mono-Boc protection of hydrodabcyI (2) proceeds regioselectively affording a derivative with properties convenient for organic synthesis of other derivatives. The observed chemical and physical behavior of hydrodabcyI can be rationalized by the presence of intramolecular hydrogen bonds. Two of the three hydroxyl groups are engaged in pericyclic keto–enol tautomerism, which explains their decreased nucleophilicity. Due to the charge delocalization mediated by intramolecular H bonds and their increased solubility, hydrodabcyI (2) and its isopropylamide 4 retained their UV/vis absorption properties over a wider pH range in comparison to the parent compound dabcyI (1). The pH dependence characteristics presented in this paper emphasize the superiority of hydrodabcyI over dabcyI for applications in aqueous solution.

ASSOCIATED CONTENT

Supporting Information

The Supporting Information is available free of charge at <https://pubs.acs.org/doi/10.1021/acsomega.1c04891>.

Synthetic protocols and NMR spectra of new compounds (PDF)

AUTHOR INFORMATION

Corresponding Authors

Karl Kempf – ISM, University of Bordeaux, 33405 Talence, France; Email: karl.kempf@u-bordeaux.fr

Elisa Bombarda – Department of Biochemistry, University of Bayreuth, 95440 Bayreuth, Germany; orcid.org/0000-0002-1385-3710; Email: elisa.bombarda@uni-bayreuth.de

Authors

Oxana Kempf – Department of Biochemistry, University of Bayreuth, 95440 Bayreuth, Germany

G. Matthias Ullmann – Computational Biochemistry, University of Bayreuth, 95440 Bayreuth, Germany; orcid.org/0000-0002-6350-798X

Rainer Schobert – Organic Chemistry Laboratory, University of Bayreuth, 95440 Bayreuth, Germany; orcid.org/0000-0002-8413-4342

Complete contact information is available at: <https://pubs.acs.org/doi/10.1021/acsomega.1c04891>

Notes

The authors declare no competing financial interest.

ACKNOWLEDGMENTS

We are indebted to Prof. Stéphane Quideau who gave us the opportunity to use the facilities of his lab at the University of Bordeaux. We are very thankful to Dr. Philippe Peixoto for fruitful discussions and very helpful ideas. The present work was supported by the DFG grant BO 3578/1 and by the SFB 1357 (project C03). This publication was funded by the University of Bayreuth Open Access Publishing Fund.

REFERENCES

- (1) Johansson, M. K.; Cook, R. M. Intramolecular Dimers: A New Design Strategy for Fluorescence-Quenched Probes. *Chem.—Eur. J.* **2003**, *9*, 3466–3471.
- (2) Bernacchi, S.; Mély, Y. Exciton Interaction in Molecular Beacons: A Sensitive Sensor for Short Range Modifications of the Nucleic Acid Structure. *Nucleic Acids Res.* **2001**, *29*, No. e62.
- (3) Matayoshi, E. D.; Wang, G. T.; Krafft, G. A.; Erickson, J. Novel Fluorogenic Substrates for Assaying Retroviral Proteases by Resonance Energy Transfer. *Science* **1990**, *247*, 954–958.
- (4) Tyagi, S. Taking DNA Probes into a Protein World. *Nat. Biotechnol.* **1996**, *14*, 947–948.
- (5) Tyagi, S.; Marras, S. A. E.; Kramer, F. R. Wavelength-Shifting Molecular Beacons. *Nat. Biotechnol.* **2000**, *18*, 1191–1196.
- (6) Kempf, O.; Kempf, K.; Schobert, R.; Bombarda, E. HydrodabcyI: A Superior Hydrophilic Alternative to the Dark Fluorescence Quencher DabcyI. *Anal. Chem.* **2017**, *89*, 11893–11897.
- (7) Radkowsky, A. E.; Kosower, E. M. Bimanes. 17. (Haloalkyl)-1,5-Diazabicyclo[3.3.0]octadienediones (Halo-9,LO-Dioxabimanes): Reactivity toward the Tripeptide Thiol, Glutathione. *J. Am. Chem. Soc.* **1986**, *108*, 4527–4531.
- (8) Hayne, J. D.; White, J. M.; McLean, C. A.; Villemagne, V. L.; Barnham, K. J.; Donnelly, P. S. Synthesis of Oxorhenium(V) and Oxotechnetium(V) Complexes That Bind to Amyloid- β Plaques. *Inorg. Chem.* **2016**, *55*, 7944–7953.
- (9) Wiejak, S.; Masiukiewicz, E.; Rzeszutarska, B. A Large Scale Synthesis of Mono- and Di-Urethane Derivatives of Lysine. *Chem. Pharm. Bull.* **1999**, *47*, 1489–1490.
- (10) Sıdır, İ.; Gülseven Sıdır, Y.; Berber, H.; Taşal, E. A Study on Solvatochromism of Some Monoazo Dye Derivatives. *J. Mol. Liq.* **2013**, *178*, 127–136.
- (11) Karimova, E. R.; Spirikhin, L. V.; Baltina, L. A.; Abdullin, M. I. Synthesis and Identification of Quercetin Benzyl Ethers. *Russ. J. Gen. Chem.* **2014**, *84*, 1711–1715.
- (12) Lu, K.; Chu, J.; Wang, H.; Fu, X.; Quan, D.; Ding, H.; Yao, Q.; Yu, P. Regioselective Iodination of Flavonoids by *N*-Iodosuccinimide under Neutral Conditions. *Tetrahedron Lett.* **2013**, *54*, 6345–6348.
- (13) Tobey, S. W. The Acid Dissociation Constant of Methyl Red. A Spectrophotometric Measurement. *J. Chem. Educ.* **1958**, *35*, 514–515.
- (14) Daniels, F.; Alberty, R. A.; Williams, J. W.; Cornwell, C. D.; Bender, P.; Harriman, J. E. *Experimental Physical Chemistry*; McGraw-Hill, 1970.
- (15) Khouri, S. J.; Abdel-Rahim, I. A.; Alshamaileh, E. M.; Altwaiq, A. M. Equilibrium and Structural Study of *M*-Methyl Red in Aqueous Solutions: Distribution Diagram Construction. *J. Solut. Chem.* **2013**, *42*, 1844–1853.
- (16) Tawarah, K. M.; Khouri, S. J. The Tautomeric and Acid-Base Equilibria of *p*-Methyl Red in Aqueous Solutions. *Dyes Pigments* **1992**, *20*, 261–270.

Chemoselective attachment of the water-soluble dark quencher hydrodabcyI to amino groups in peptides and preservation of its spectroscopic properties over a wide pH range

Oxana Kempf,[†] G. Matthias Ullmann,[~] Rainer Schobert,[‡] Karl Kempf,^{*,∞} and Elisa Bombarda^{*,†}

[†]Department of Biochemistry, [~]Computational Biochemistry and [‡]Organic Chemistry Laboratory, University of Bayreuth, Universitätsstr. 30, 95440, Bayreuth, Germany.

[∞]ISM, University of Bordeaux, 351 Cours de la Libération, 33405, Talence, France.

Supporting Information

List of abbreviations

CH – cyclohexane

DMF – dimethylformamide

DMSO – dimethylsulfoxide

EDTA – ethylenediaminetetraacetic acid

EtOAc – ethyl acetate

EtOH – ethanol

NEt₃ – triethylamine

r.t. – room temperature

–ESI – electron spray ionisation in negative mode

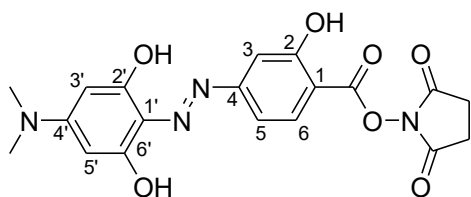
+ESI – electron spray ionisation in positive mode

Chemicals and analytical methods

All reactions were carried out under a nitrogen or argon atmosphere using dry solvents under anhydrous conditions, unless otherwise noted. N,N'-dimethylformamide (DMF), carbonyldiimidazole (CDI) and all other chemicals were purchased from Sigma-Aldrich and used without further purification, unless indicated otherwise. The ¹H and ¹³C NMR spectra were recorded on a Bruker Avance 300 MHz spectrometer. Chemical shifts are reported in parts per million (ppm) referenced with respect to residual solvent (DMSO = 2.50/39.52 ppm). The following abbreviations were used to indicate multiplicities: s = singlet, d = doublet, dd = double doublet, t = triplet, m = multiplet, br. s = broad singlet and qdd = double doublet of quartet. High resolution (HRMS) mass spectra were obtained by electrospray ionization and performed on a Q-exactive Orbitrap MS system, Thermo Fischer Scientific. For column chromatography, silica gel (40-63 μm, Merck) was used. The retention factors (R_f) were determined by thin layer chromatography on pre-coated silica plates (Merck TLC Silica gel 60 F254). The spots were visualized by UV light and stained with ceric ammonium molybdate (CAM) solution, followed by treatment with a heat gun.

Chemical Synthesis

Hydrodabcyl-ONSu ester (**3**)

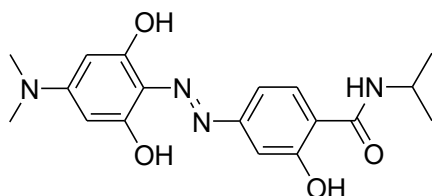


$^1\text{H-NMR}$ (300 MHz, DMSO-d_6) δ ppm 2.88 (s, 4 H, CH_2 NSu), 3.09 (s, 6 H, $\text{N}(\text{CH}_3)_2$), 5.72 (s, 2 H, 2'-H, 6'-H), 7.27 (d, $J = 1.7$ Hz, 1 H, 3-H), 7.32 (dd, $J = 8.8, 1.7$ Hz, 1 H, 5-H), 7.89 (d, $J = 8.8$ Hz, 1 H, 6-H), 10.62 (br. s., 1 H, OH).

$^{13}\text{C-NMR}$ (75 MHz, DMSO-d_6) δ 170.6 ($2 \times \text{CO NSu}$), 170.6 (COON), 161.3 ($\text{C}2'$, $\text{C}6'$), 160.9 ($\text{C}2$), 158.4 ($\text{C}4'$), 152.9 ($\text{C}4$), 132.6 ($\text{C}6$), 125.9 ($\text{C}1'$), 110.0 ($\text{C}5$), 106.8 ($\text{C}1$), 105.8 ($\text{C}3$), 91.8 ($\text{C}3'$, $\text{C}5'$), 40.1 ($\text{N}(\text{CH}_3)_2$), 25.5 ($2 \times \text{CH}_2$ NSu).

HRMS (+ESI) m/z : [MOMe-H] $^-$ calculated for $\text{C}_{16}\text{H}_{16}\text{N}_3\text{O}_5^-$ 330.10954; found 330.10951.

Hydrodabcyl-isopropylamide (**4**)



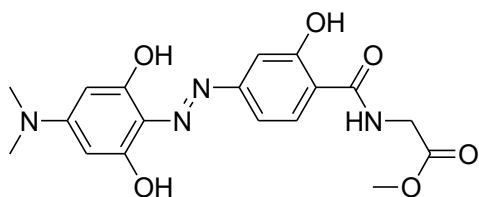
Isopropylamine (50 μL , 0.58 mmol) is added to a stirred solution of **3** (20 mg, 0.05 mmol) in DMF (5 mL) at room temperature. The reaction mixture was stirred overnight at room temperature. Thereafter, it was diluted with ethyl acetate (50 mL) and washed with aqueous citric acid (5 % w/w, 2 x 25 mL) and brine (2 x 25 mL). The organic layer was dried over anhydrous Na_2SO_4 and evaporated *in vacuo*. The crude product was purified by column chromatography on silica (dry package, elution: CH/EtOAc 1:1) to afford a new compound **4** (18 mg, 99 % yield) as a dark red solid ($R_f = 0.32$, CH/EtOAc 1:1).

$^1\text{H-NMR}$ (300 MHz, DMSO-d_6) δ ppm 1.17 - 1.22 (d, 6 H), 3.07 (s, 6 H), 4.16 (s, 1 H), 5.72 (s, 2 H), 7.20 (dd, $J = 8.5, 2.0$ Hz, 1 H), 7.33 (d, $J = 2.0$ Hz, 1 H), 7.94 (d, $J = 8.5$ Hz, 1 H), 8.53 (d, $J = 7.8$ Hz, 1 H), 12.90 - 13.22 (m, 1 H).

$^{13}\text{C NMR}$ (75 MHz, DMSO-d_6) δ 168.2, 161.8, 157.7, 157.6, 151.2, 128.6, 128.6, 124.2, 112.5, 110.1, 105.8, 91.4, 91.4, 41.0, 40.0, 40.0, 22.1, 22.1.

HRMS (+ESI) m/z : $[M + H]^+$ calculated for $C_{18}H_{23}N_4O_4^+$ 359.17138; found 359.17065.

Hydrodabcyl-L-glycine methyl ester (7)



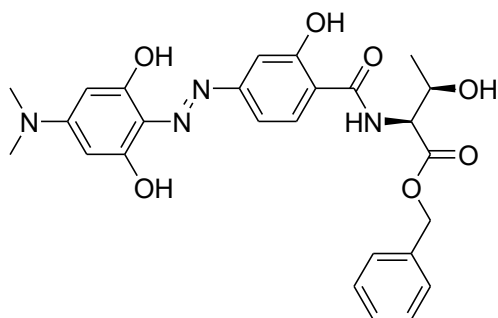
L-glycine methyl ester hydrochloride (7 mg, 0.055 mmol) and NEt_3 (8 μ L, 0.055 mmol) were added to a stirred solution of **3** (19 mg, 0.05 mmol) in DMF (5 mL) at room temperature. The reaction mixture was stirred overnight at room temperature. Thereafter, it was diluted with ethyl acetate (100 mL) and washed with aqueous citric acid (5 % w/w, 2 x 50 mL) and brine (2 x 50 mL). The organic layer was dried over anhydrous Na_2SO_4 and evaporated *in vacuo*. The crude product was purified by column chromatography on silica (dry package, elution: ethyl acetate) to afford a new compound **7** (19 mg, 99 % yield) as a dark red solid (R_f = 0.5, EtOAc).

1H NMR (300 MHz, $DMSO-d_6$) δ ppm 3.07 (s, 6 H), 3.68 (s, 3 H), 4.07 (d, J =5.7 Hz, 2 H), 5.72 (s, 2 H), 7.27 (dd, J =8.6, 1.9 Hz, 1 H), 7.32 (d, J =1.9 Hz, 1 H), 7.91 (d, J =8.6 Hz, 1 H), 9.20 (t, J =5.7 Hz, 1 H), 12.42 - 12.51 (m, 1 H).

^{13}C NMR (75 MHz, $DMSO-d_6$) δ 170.1, 168.9, 161.1, 161.1, 157.8, 151.5, 129.2, 124.4, 112.4, 110.3, 106.0, 91.5, 91.5, 51.9, 41.0, 40.0, 40.0.

HRMS (-ESI) m/z : $[M - H]^-$ calculated for $C_{18}H_{19}N_4O_6^-$ 387.13101; found 387.13111.

Hydrodabcyl-L-threonine benzyl ester (8)



L-threonine benzyl ester hemioxalate (21 mg, 0.07 mmol) and NEt_3 (20 μ L, 0.14 mmol) were added to a stirred solution of **3** (29 mg, 0.07 mmol) in DMF (5 mL) at room temperature. The reaction mixture was stirred overnight at room temperature. Thereafter, it was diluted with ethyl acetate (100 mL) and washed with aqueous citric acid (5 % w/w, 2 x 50 mL) and brine (2 x 50 mL). The organic layer was dried over anhydrous Na_2SO_4 and evaporated *in vacuo*. The crude

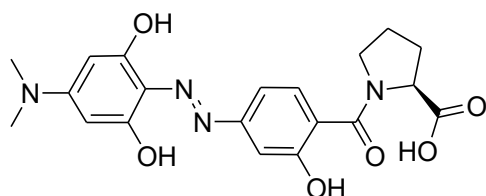
product was purified by column chromatography on silica (dry package, elution: ethyl acetate) to afford a new compound **8** (25 mg, 70 % yield) as a dark red solid ($R_f = 0.4$, EtOAc).

$^1\text{H-NMR}$ (300 MHz, $\text{DMSO-}d_6$) δ ppm 1.16 (d, $J=6.5$ Hz, 3 H), 3.07 (s, 6 H), 4.27 (qdd, $J=6.5$, 6.5, 6.5, 5.6, 3.4 Hz, 1 H), 4.57 (dd, $J=8.0$, 3.4 Hz, 1 H), 5.18 (s, 2 H), 5.22 (d, $J=5.6$ Hz, 1 H), 5.73 (s, 2 H), 7.23 - 7.41 (m, 7 H), 8.00 (d, $J=8.5$ Hz, 1 H), 8.84 (d, $J=7.9$ Hz, 1 H), 11.75 - 11.97 (m, 1 H).

$^{13}\text{C NMR}$ (75 MHz, $\text{DMSO-}d_6$) δ 170.5, 166.8, 159.0, 157.6, 151.2, 136.0, 130.9, 128.4, 128.4, 128.0, 127.6, 127.6, 124.3, 114.6, 110.3, 106.1, 91.4, 91.4, 66.2, 66.0, 58.5, 40.0, 40.0, 20.5

HRMS (-ESI) m/z : $[\text{M} - \text{H}]^-$ calculated for $\text{C}_{26}\text{H}_{27}\text{N}_4\text{O}_7^-$ 507.18743; found 507.18806.

Hydrodabcyl-L-proline (**9**)



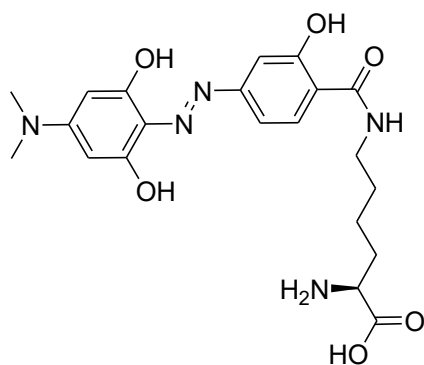
L-proline (23 mg, 0.2 mmol) and NEt_3 (28 μL , 0.2 mmol) were added to a stirred solution of **3** (42 mg, 0.1 mmol) in DMF (5 mL) at room temperature. The reaction mixture was stirred overnight at room temperature. Thereafter, it was diluted with ethyl acetate (100 mL) and washed with aqueous citric acid (5 % w/w, 2 x 50 mL) and brine (2 x 50 mL). The organic layer was dried over anhydrous Na_2SO_4 and evaporated *in vacuo*. The crude product was purified by column chromatography on silica (dry package, elution: EtOAc / 0.1% HCOOH) to afford a new compound **9** (38 mg, 92 % yield) as a dark red solid ($R_f = 0.14$, EtOAc / 0.1% HCOOH).

$^1\text{H-NMR}$ (300 MHz, $\text{DMSO-}d_6$) δ ppm 1.71 - 1.97 (m, 3 H), 2.16 - 2.34 (m, 1 H), 3.01 - 3.11 (m, 6 H), 3.44 - 3.61 (m, 2 H), 4.30 - 4.45 (m, 1 H), 5.75 (s, 2 H), 7.04 - 7.38 (m, 3 H), 10.02 - 10.86 (m, 1 H), 12.26 - 12.81 (m, 1 H).

$^{13}\text{C NMR}$ (75 MHz, $\text{DMSO-}d_6$) δ 173.2, 167.5, 160.4, 160.2, 157.1, 156.4, 150.2, 129.2, 123.4, 120.7, 110.7, 106.2, 91.1, 91.1, 59.0, 48.4, 39.9, 39.9, 29.0, 24.7.

HRMS (+ESI) m/z : $[\text{M} + \text{H}]^+$ calculated for $\text{C}_{20}\text{H}_{23}\text{N}_4\text{O}_6^+$ 415.16121; found 415.16078.

Hydrodabcyll- ϵ -L-lysine (**11**)

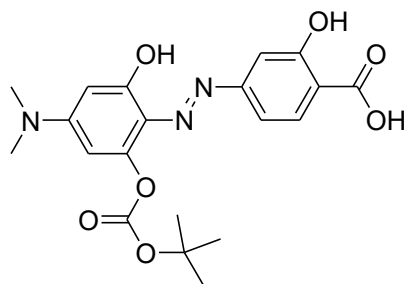


L-lysine copper (II) complex freshly prepared¹ (50 μ L, 0.58 mmol) was added to a stirred solution of **3** (20 mg, 0.05 mmol) in DMSO (5 mL) at room temperature. The reaction mixture was stirred overnight at room temperature. 0.1 M EDTA disodium salt (25 mL) was poured into the residue and stirred for 1 h at room temperature. The crude mixture was purified by puriFlash Interchim (column PF-30C18AQ-F0025, 15mL/min, 40% CH₃CN/60 % H₂O + 0.1% HCOOH isocratic) to afford a new compound **11** (5 mg, 30 % yield) as a dark red solid.

¹H NMR (300 MHz, methanol-*d*₄) δ ppm 1.45 - 1.60 (m, 2 H), 1.62 - 1.75 (m, 2 H), 1.93 - 2.09 (m, 2 H), 3.24 (s, 6 H), 3.38 (t, *J*=6.1 Hz, 2 H), 4.04 (t, *J*=6.6 Hz, 1 H), 4.93 - 5.05 under water signal (m, 2 H), 6.90 - 7.08 (m, 2 H), 7.73 (d, *J*=8.4 Hz, 1 H).

HRMS (+ESI) *m/z*: [M + H]⁺ calculated for C₂₁H₂₈N₅O₆⁺ 446.20341; found 446.20282.

Hydrodabcyll-mono-tert-butylcarbonate (**13**)



NEt₃ (44 μ L, 0.315 mmol) was added to a mixture of hydrodabcyll **2** (50 mg, 0.158 mmol) and di-tert-butylidicarbonate (69 mg, 0.315 mmol) in DMF (5 mL) at room temperature. The reaction mixture was stirred overnight at room temperature. Thereafter, it was diluted with ethyl acetate (100 mL) and washed with brine (3 x 50 mL). The organic layer was dried over anhydrous Na₂SO₄ and evaporated *in vacuo*. The crude product was purified by column chromatography on silica (dry package, elution: ethyl acetate / 10% EtOH) to afford a new

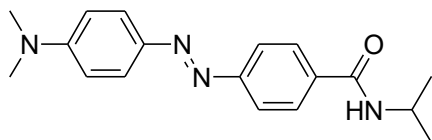
compound **13** (49 mg, 74 % yield) as a dark red solid ($R_f = 0.35$, EtOAc : isopropanol : water 4 : 1 : 0.5).

^1H NMR (300 MHz, DMSO- d_6) δ ppm 1.49 (s, 9 H), 3.10 (s, 6 H), 5.90 (d, $J=2.5$ Hz, 1 H), 6.53 (d, $J=2.5$ Hz, 1 H), 7.01 - 7.07 (m, 2 H), 7.82 (d, $J=8.8$ Hz, 1 H), 14.81 (br. s., 2 H).

^{13}C NMR (75 MHz, DMSO- d_6) δ 171.4, 163.0, 161.5, 155.2, 152.0, 151.3, 150.9, 131.2, 123.6, 115.9, 110.1, 105.8, 100.9, 95.5, 83.3, 40.1, 40.1, 27.3, 27.3, 27.3.

HRMS (-ESI) m/z : $[\text{M} - \text{H}]^-$ calculated for $\text{C}_{20}\text{H}_{22}\text{N}_3\text{O}_7^-$ 416.14632; found 416.14629.

Dabcyl-isopropylamide (**14**)



1 (269 mg, 1 mmol) was dissolved in DMF (5mL) and filled with dichloromethane (45 mL). To this reaction mixture isopropyl amide (172 μL , 2 mmol), NEt_3 (348 μL , 2.5 mmol) and T3P (1.15 mmol) were added. The reaction mixture was stirred overnight at room temperature. Thereafter, it was diluted with ethyl acetate (50 mL) and washed with brine (50 mL). The aqueous phase was extracted with dichloromethane (2 x 50 mL) The organic layer were combined and dried over anhydrous Na_2SO_4 and evaporated *in vacuo*. The crude product was purified by column chromatography on silica (dry package, elution: CH/EtOAc 2:1 + 0.5 % NEt_3) to afford a new compound **14** (249 mg, 80 % yield) as an orange solid ($R_f = 0.55$, CH/EtOAc 1:1 + 0.5 % NEt_3).

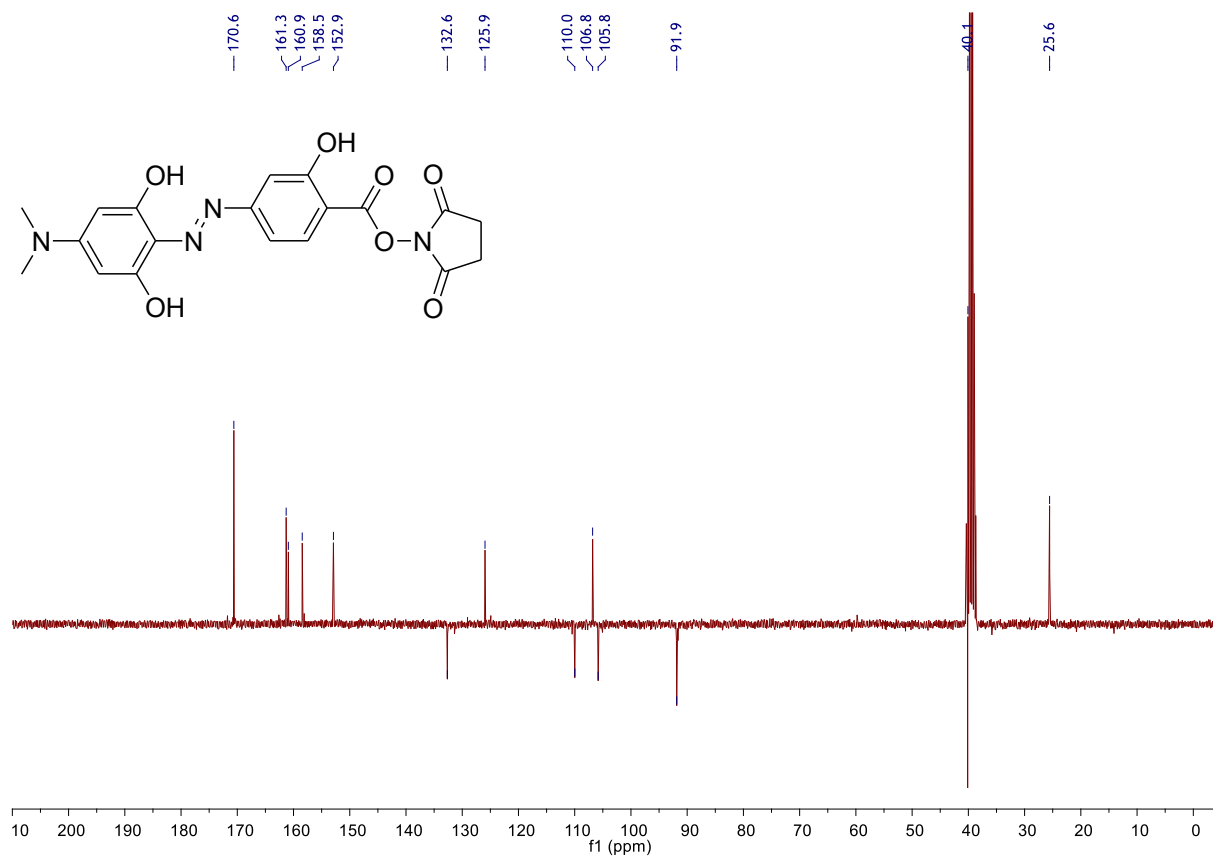
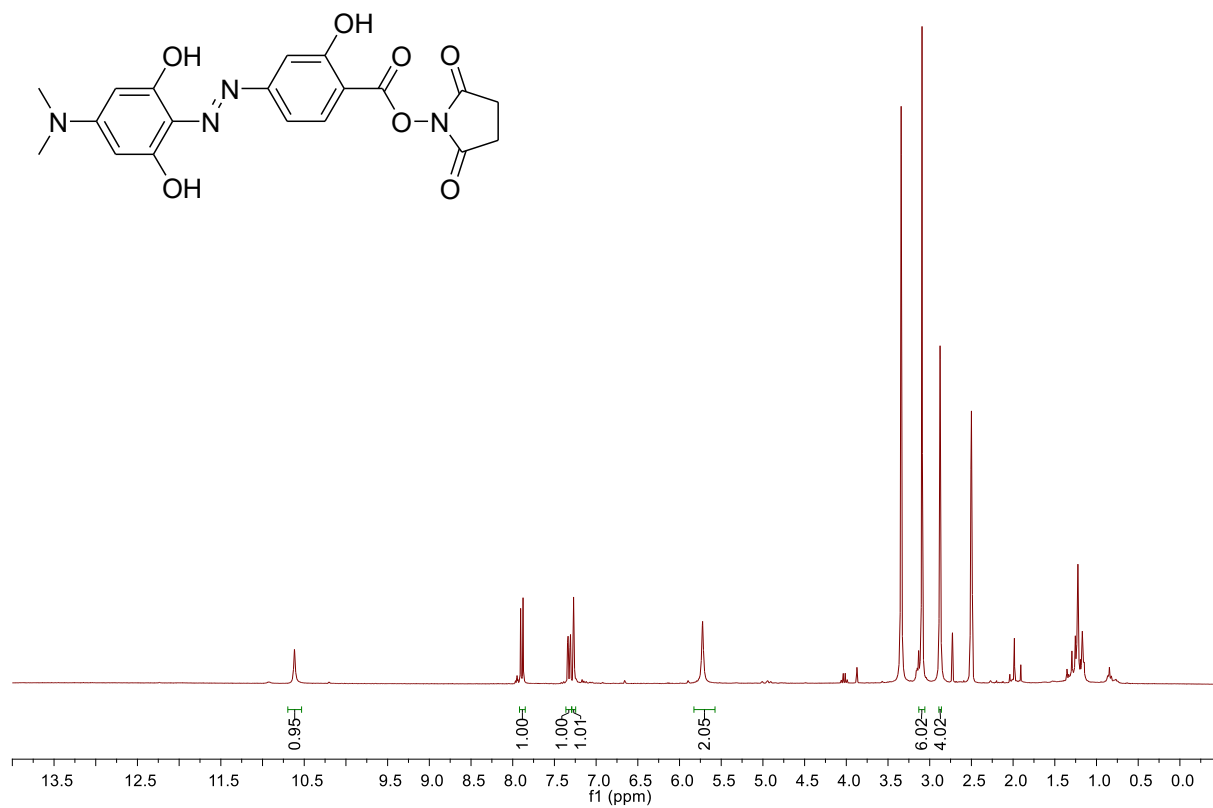
^1H NMR (300 MHz, DMSO- d_6) δ ppm 1.17 (br. s., 3 H), 1.19 - 1.22 (m, 3 H), 3.08 (s, 6 H), 4.12 (dq, $J=13.4, 6.6$ Hz, 1 H), 6.85 (d, $J=8.8$ Hz, 2 H), 7.81 (dd, $J=8.4, 4.5$ Hz, 4 H), 7.99 (d, $J=8.2$ Hz, 2 H), 8.32 (d, $J=7.7$ Hz, 2 H).

^{13}C NMR (75 MHz, DMSO- d_6) δ 164.7, 153.8, 152.8, 142.6, 135.1, 128.4, 128.4, 125.1, 125.1, 121.4, 121.4, 111.6, 111.6, 41.1, 39.8, 39.8, 22.3, 22.3.

HRMS (+ESI) m/z : $[\text{M} + \text{H}]^+$ calculated for $\text{C}_{18}\text{H}_{23}\text{N}_4\text{O}^+$ 311.18664; found 311.18534.

NMR spectra

Hydrodabicyl-ONSu ester (3)



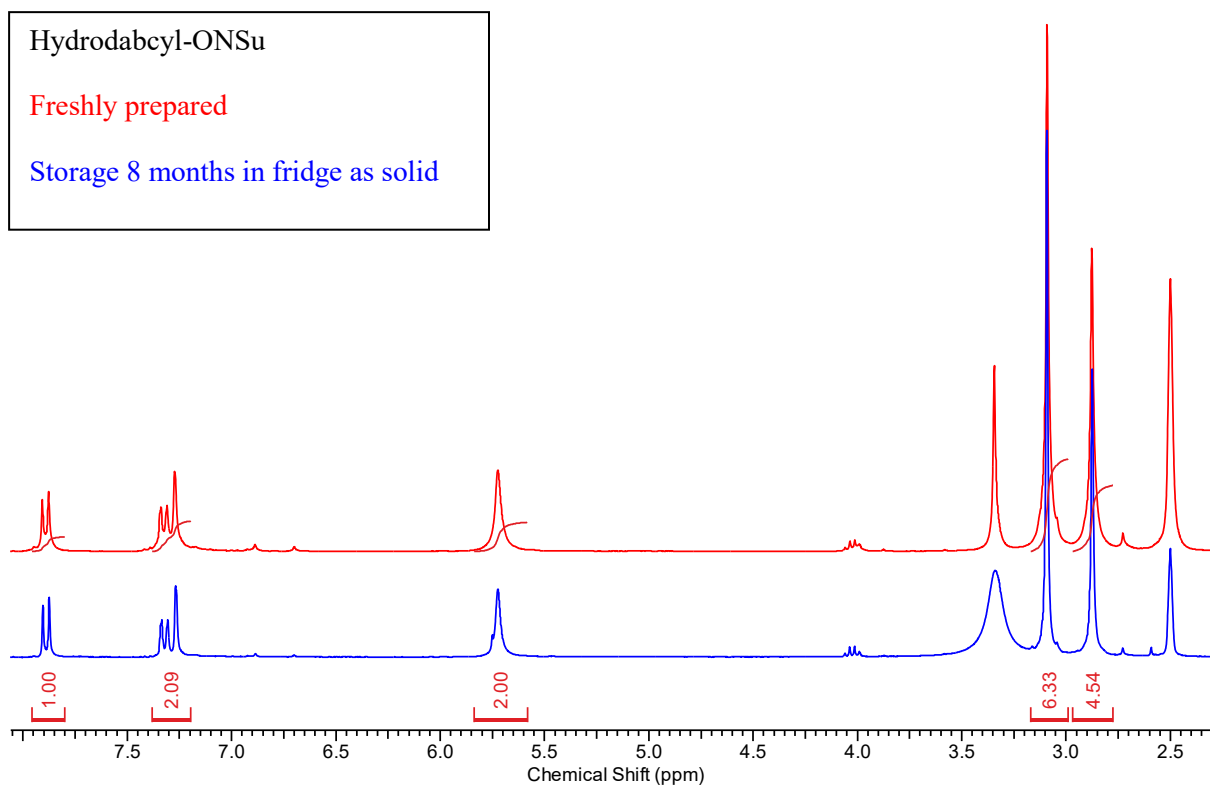


Figure S1. Stability test of hydrodabcyyl-ONSu (**3**). $^1\text{H-NMR}$ spectra in $\text{DMSO-}d_6$ of **3** freshly prepared (in red) and after 8 months of storage at $4\text{ }^\circ\text{C}$ as solid (in blue).

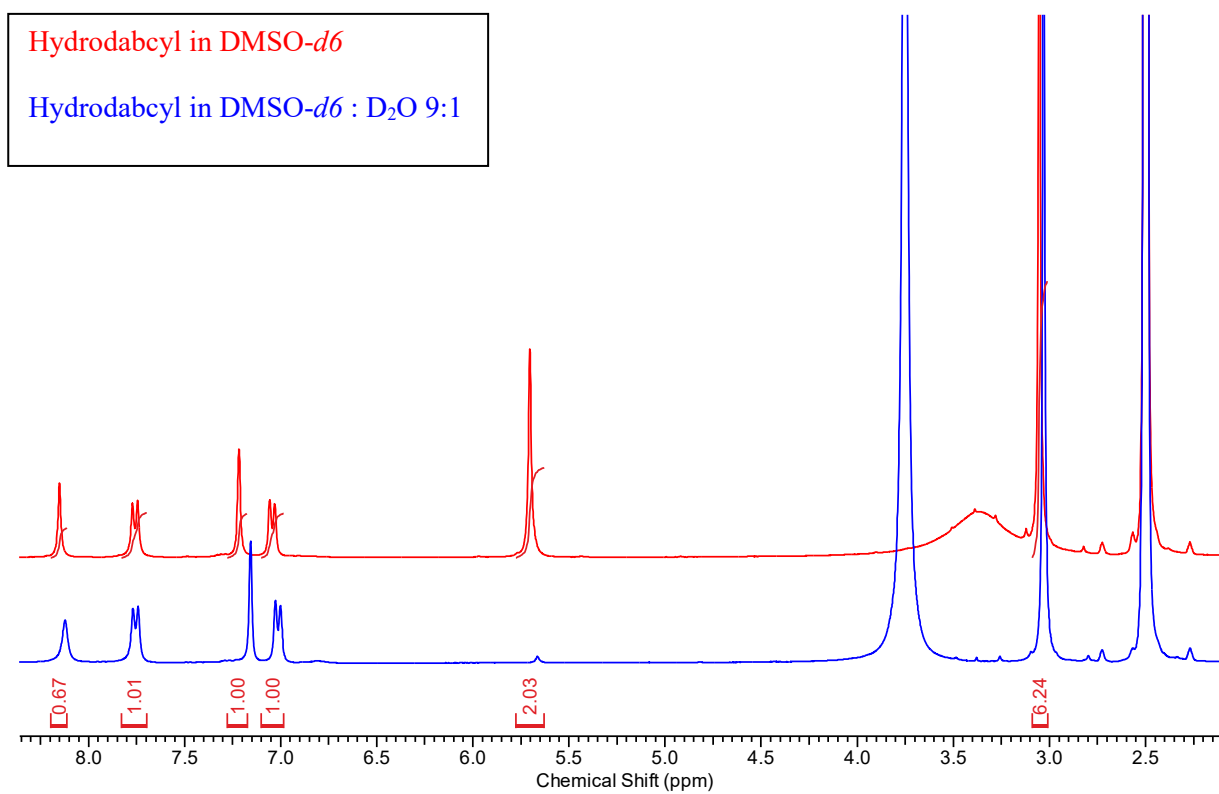
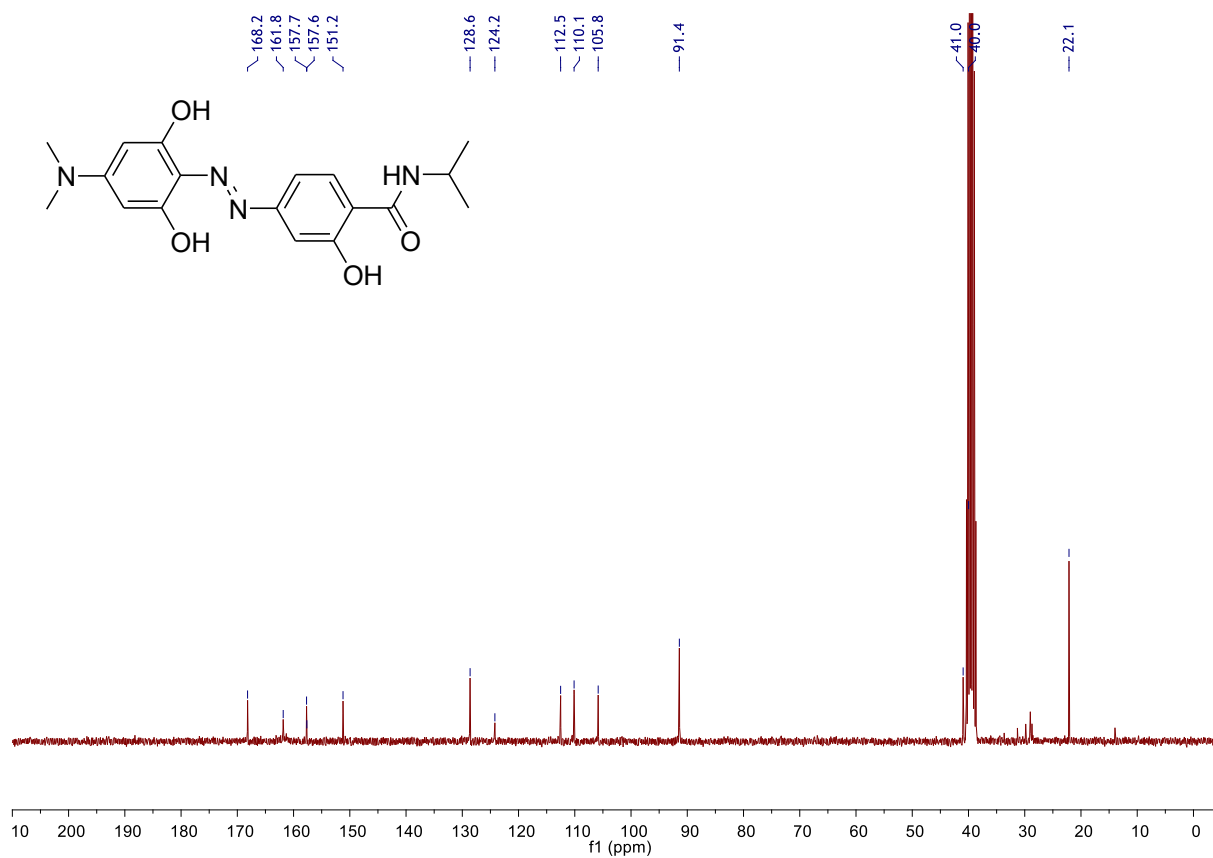
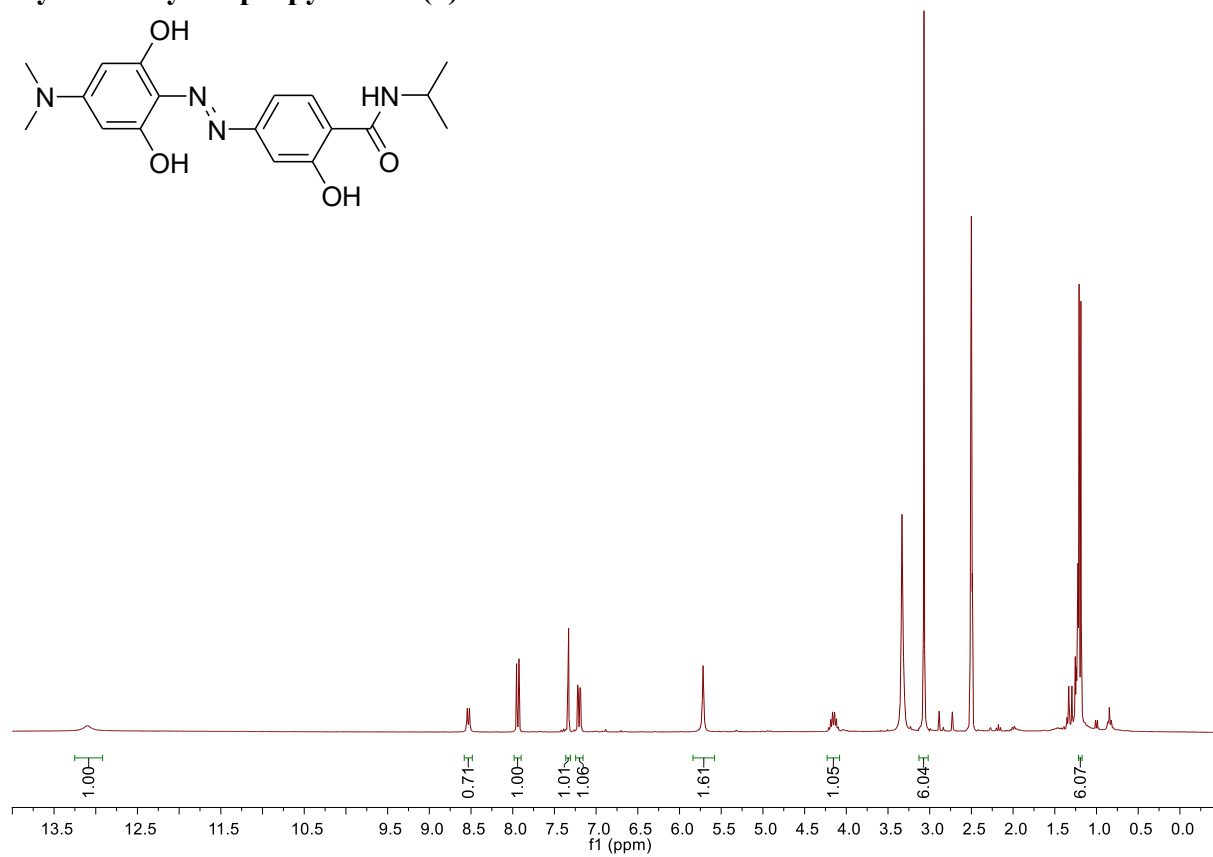
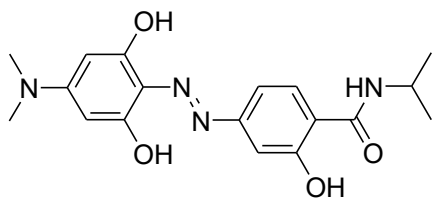
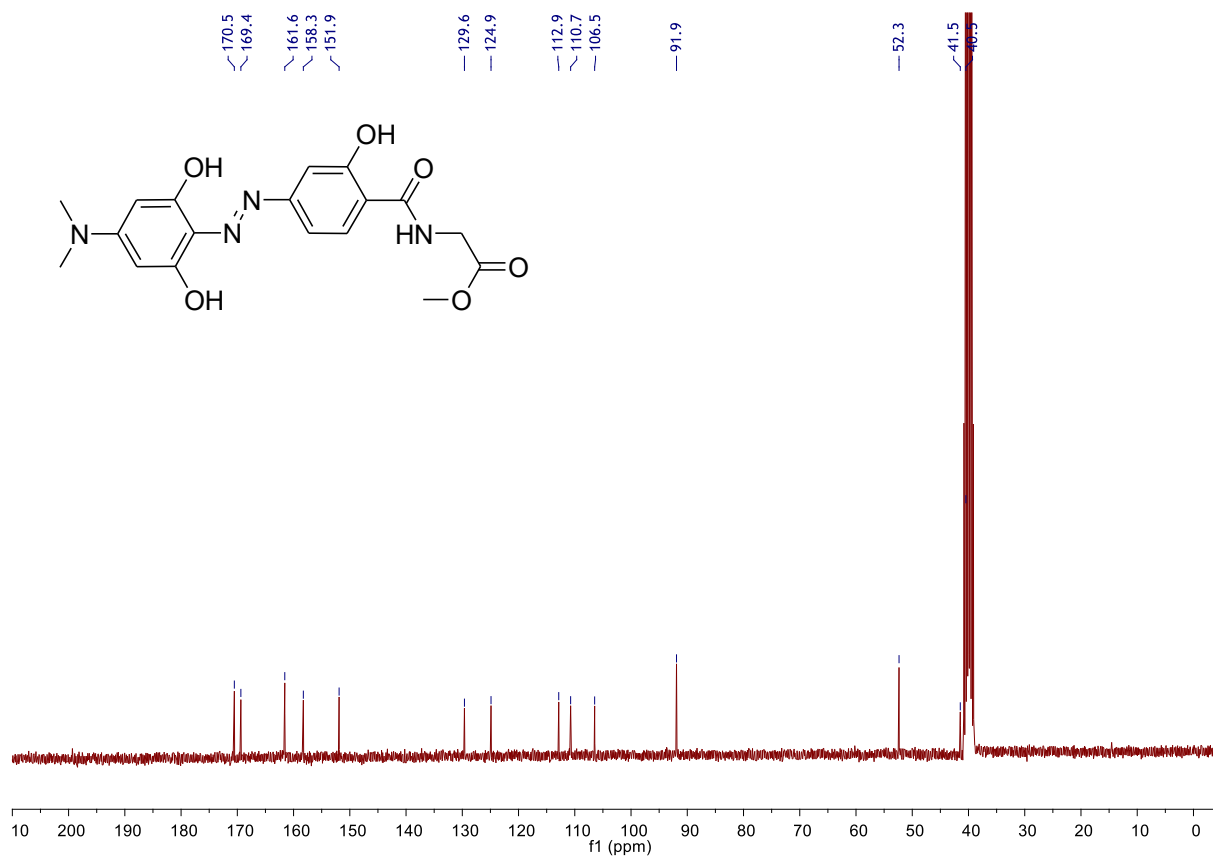
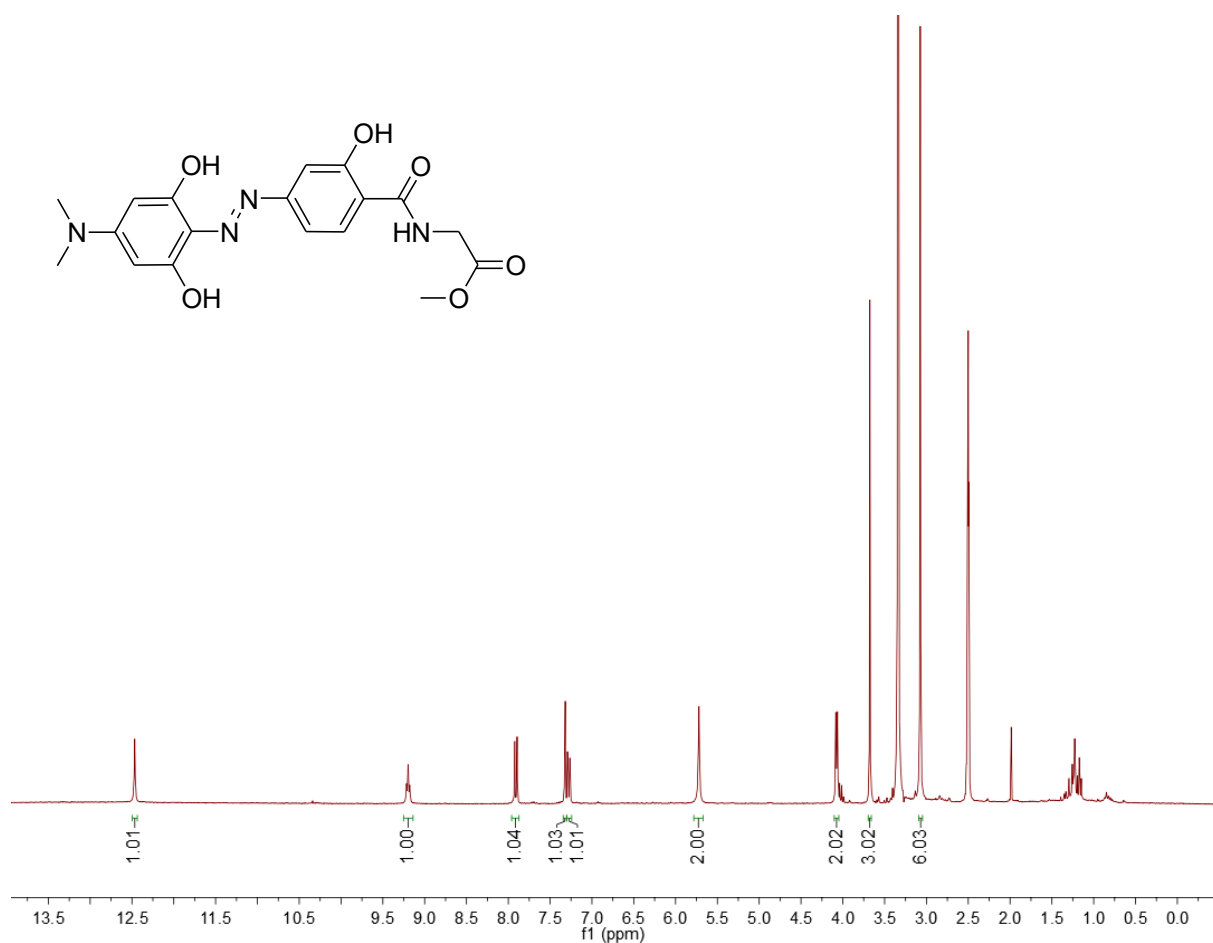
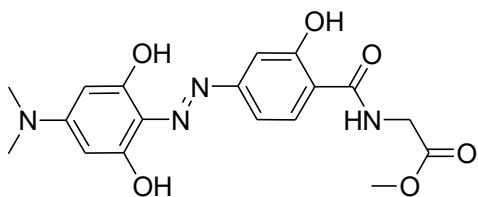


Figure S2. Exchange of the aromatic proton of hydrodabcyyl (**2**) by deuterium from D_2O (in blue)

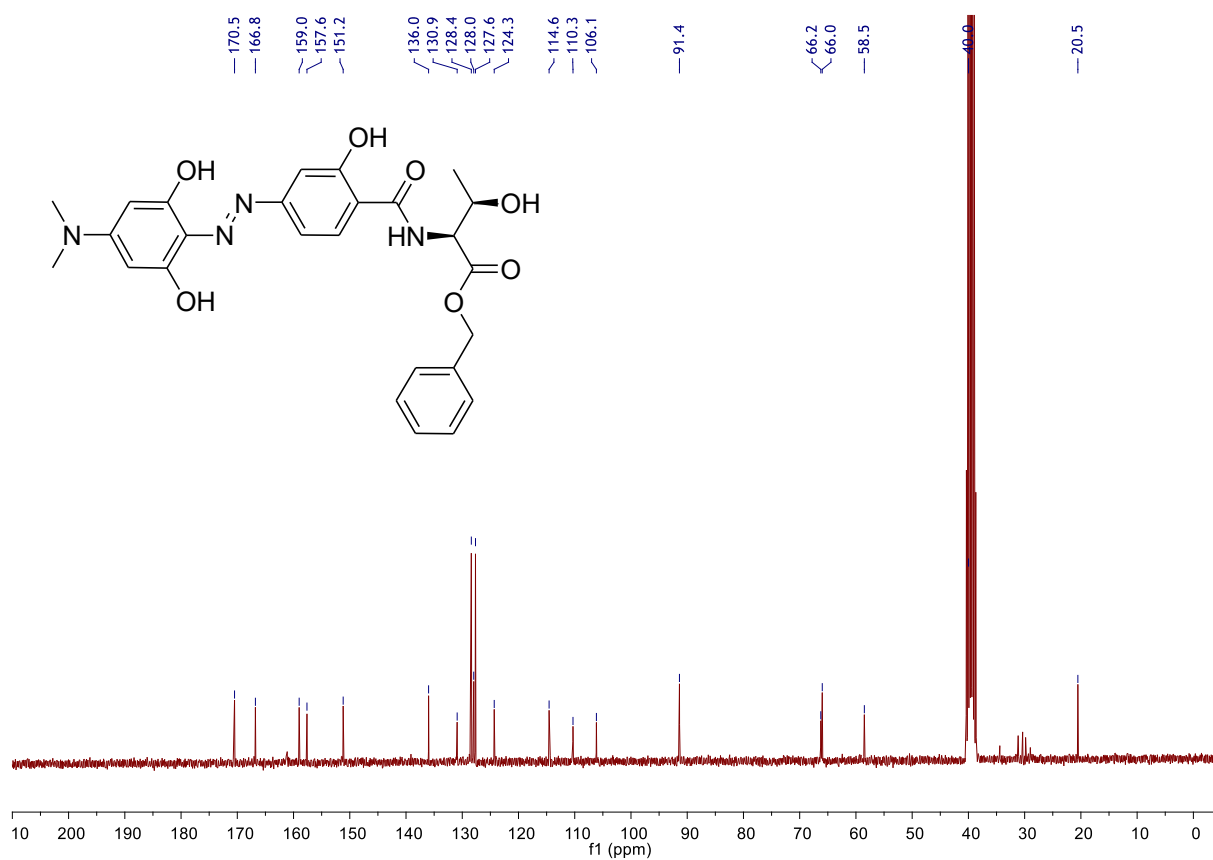
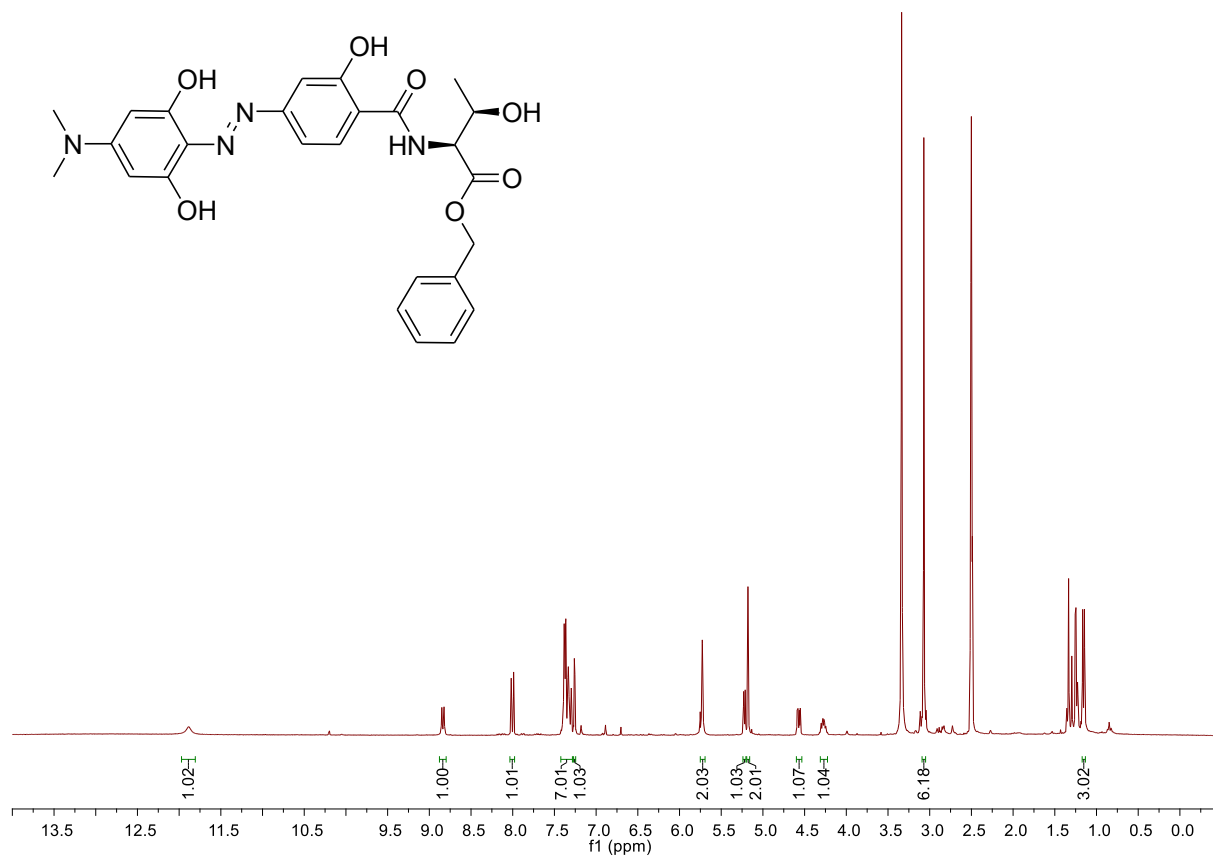
HydrodabcyI-isopropylamide (4)



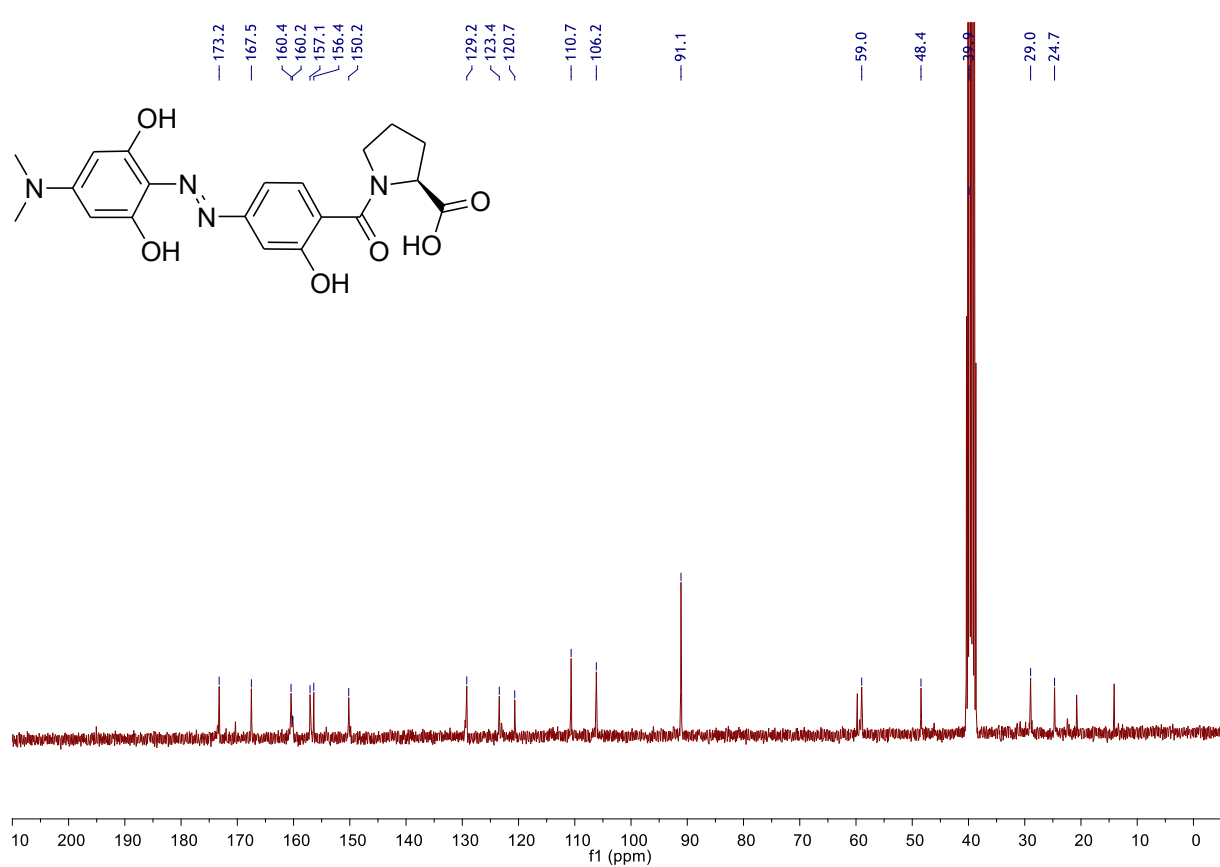
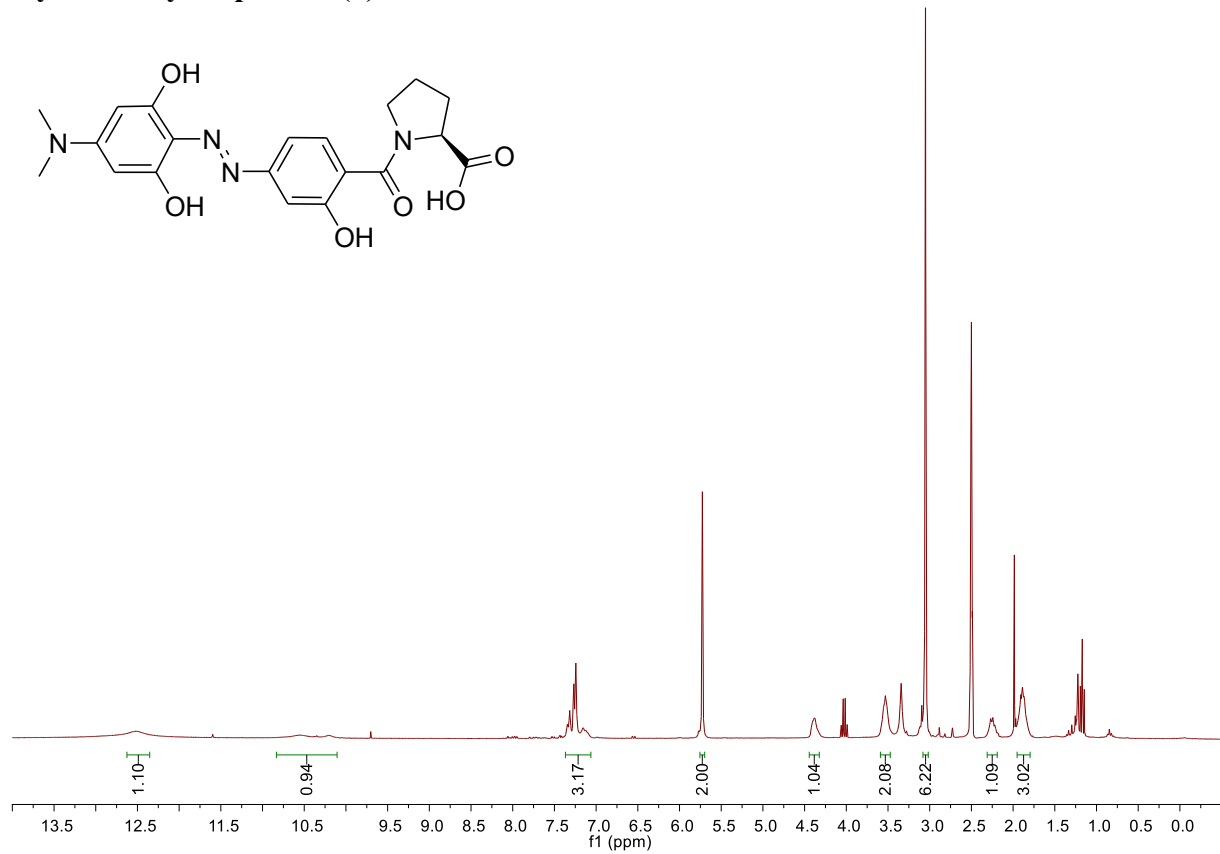
HydrodabcyL-L-glycine methyl ester (7)



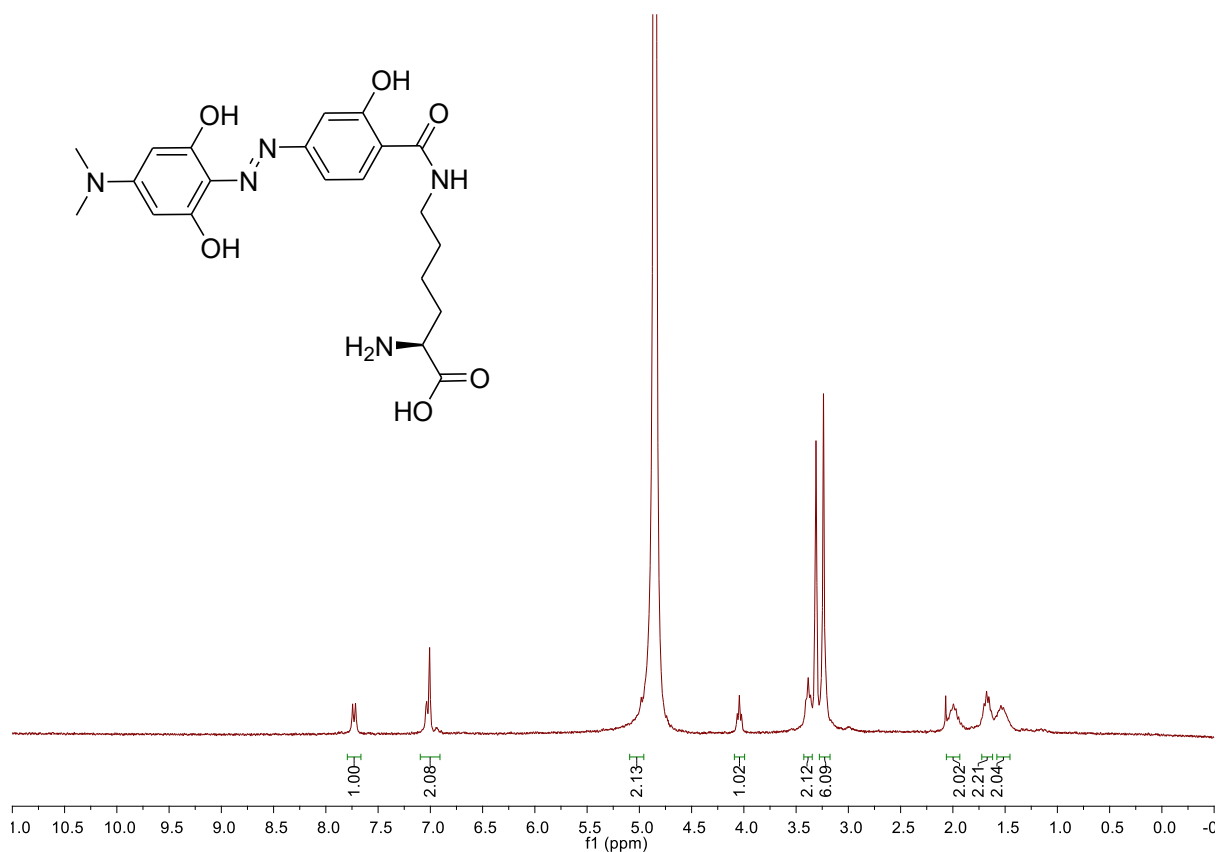
HydrodabcyL-L-threonine benzyl ester (8)



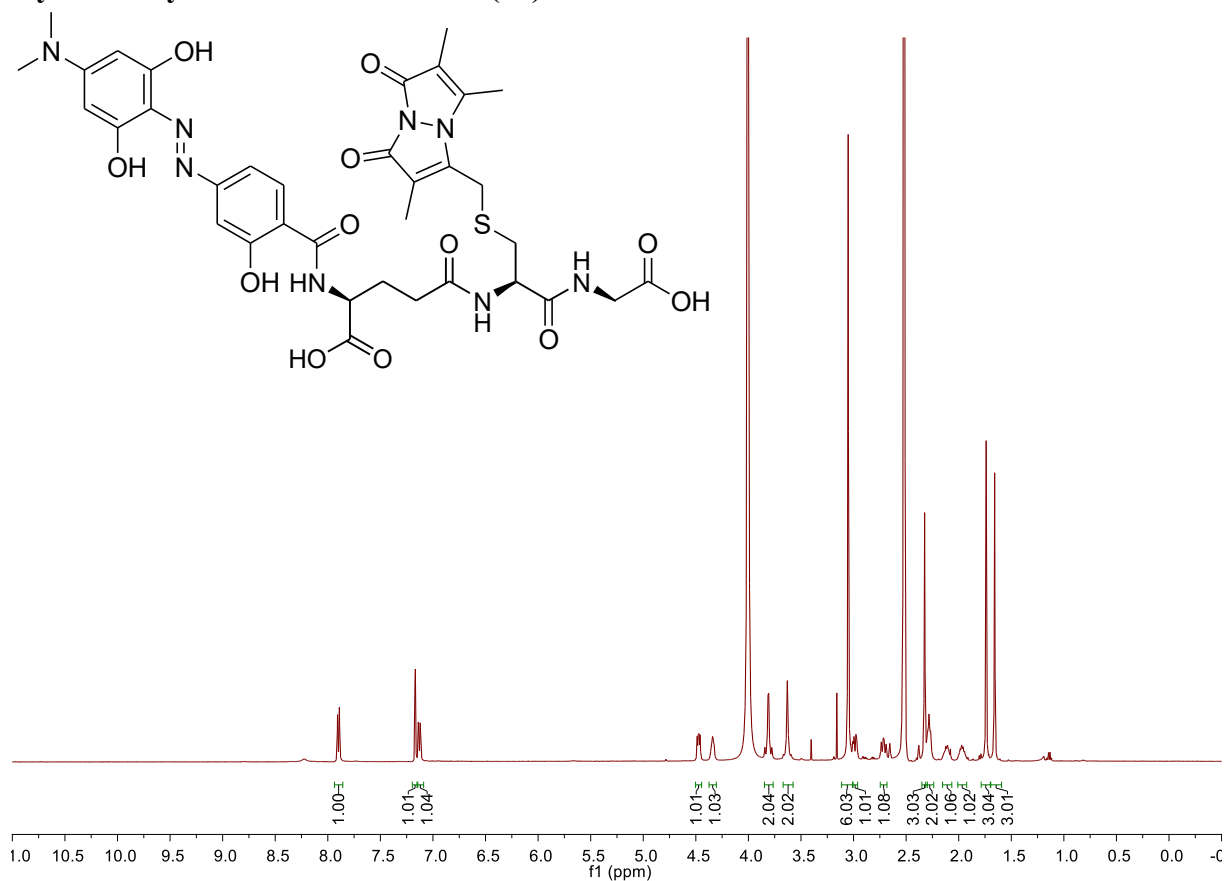
HydrodabcyL-L-proline (9)



HydrodabcyL-ε-L-lysine (11)



HydrodabcyL-Glutathione-Bimane (12)



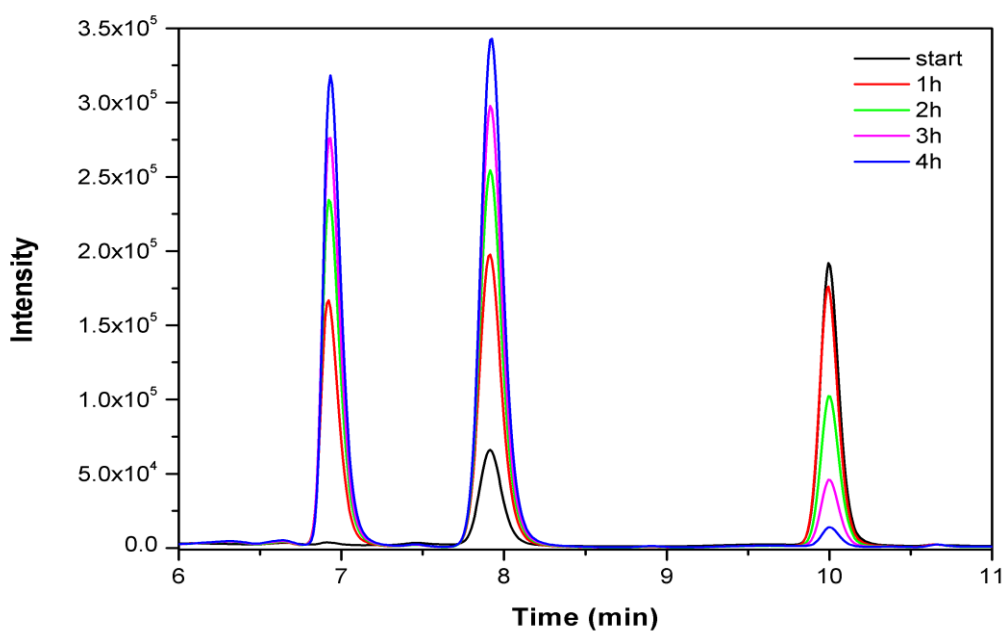
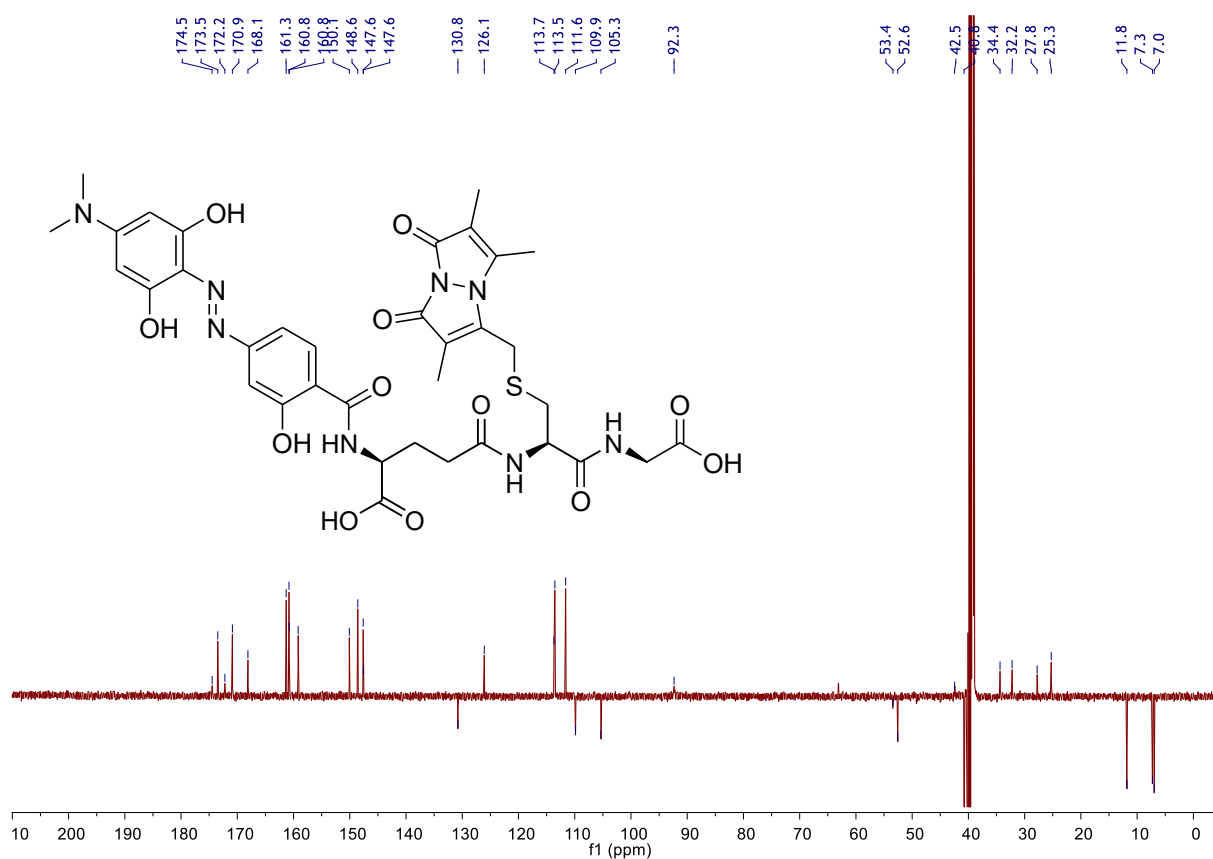


Figure S3. HPLC chromatogram of reaction monitoring of the one-pot double-functionalization of glutathione with hydrodabcygl-ONSu (**3**) and-bimane at 450 nm: start addition of **3** (in black), after 1h reaction (in red), 2h (in green), 3h (in magenta) and 4 h (in blue). The retention time: at 7 min is hydrodabcygl-glutathione-bimane (**12**), at 8 min is hydrolysed hydrodabcylic acid (**2**), at 10 min is hydrodabcygl-ONSu (**3**).

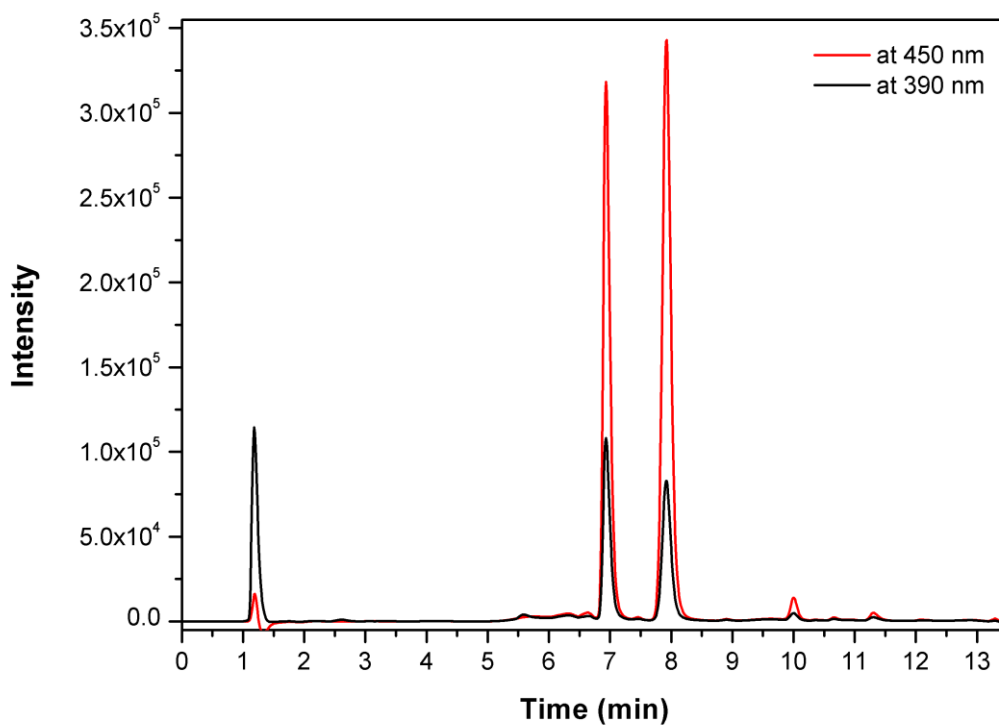
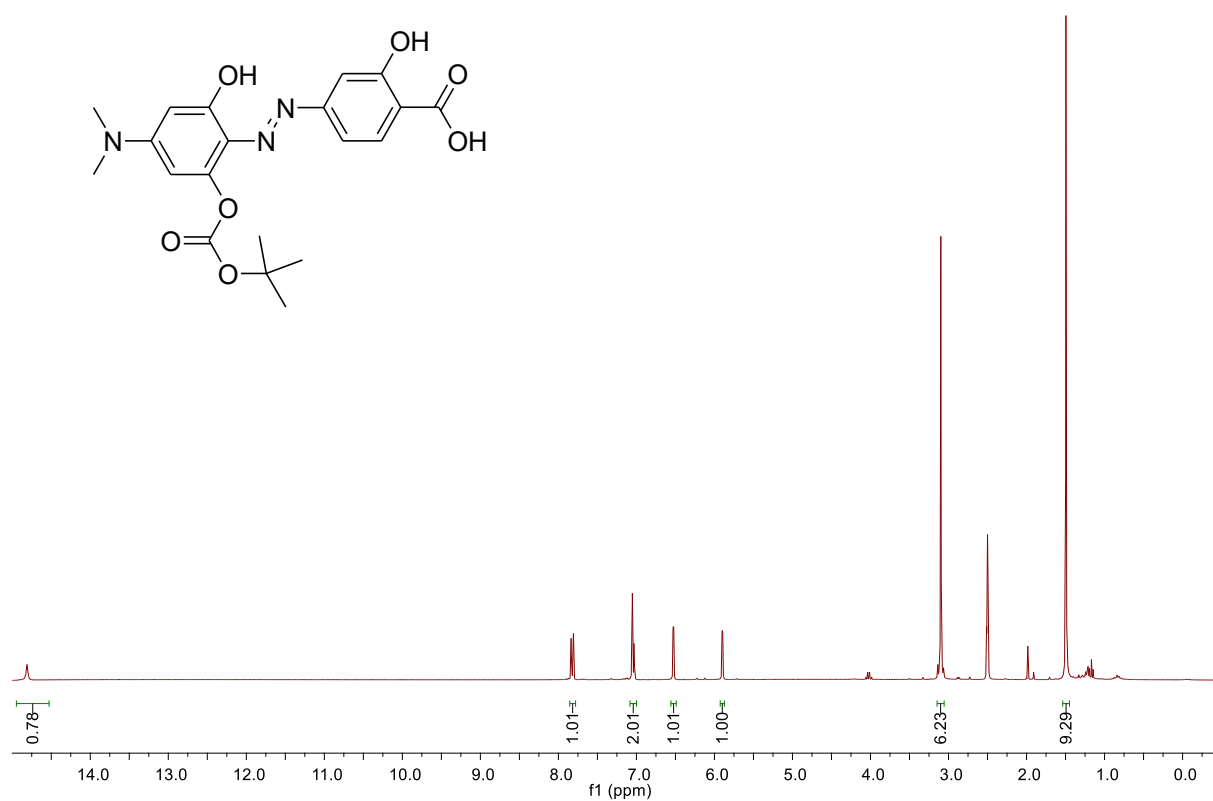
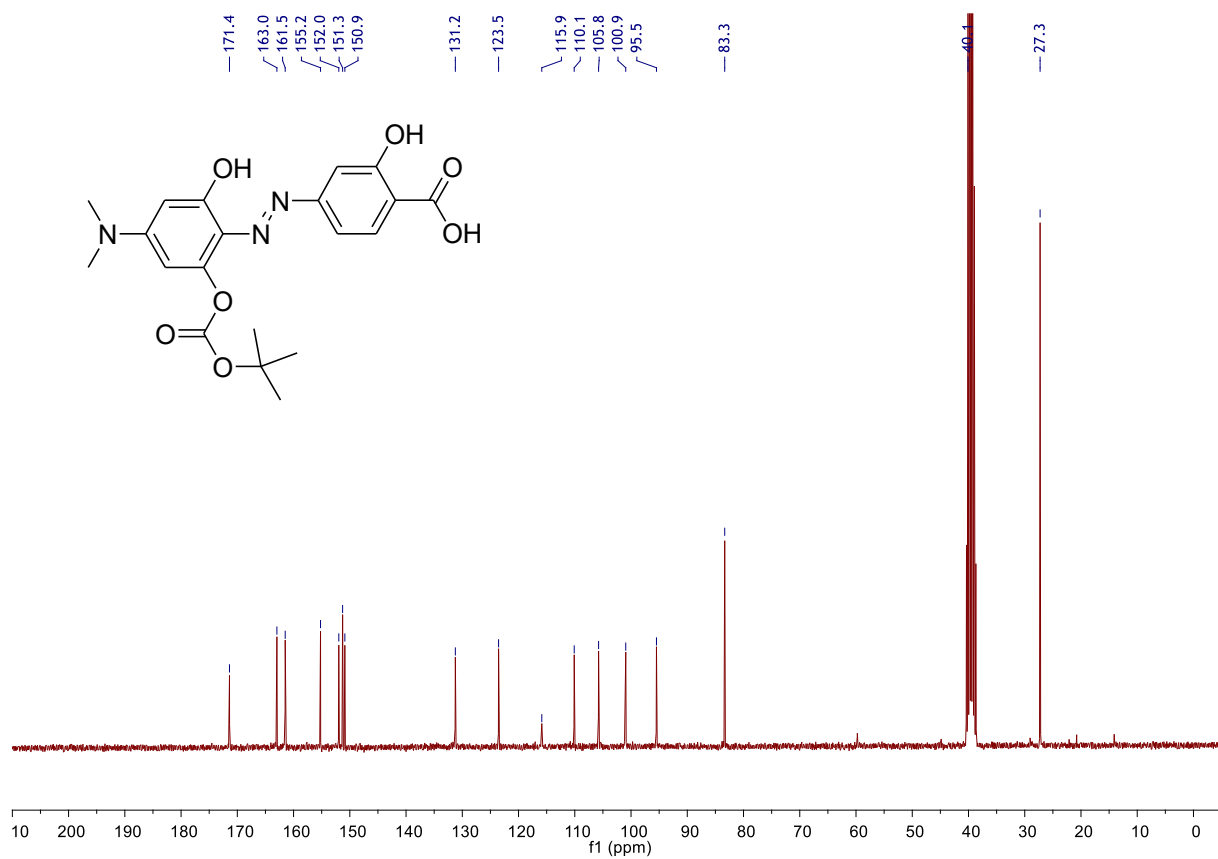


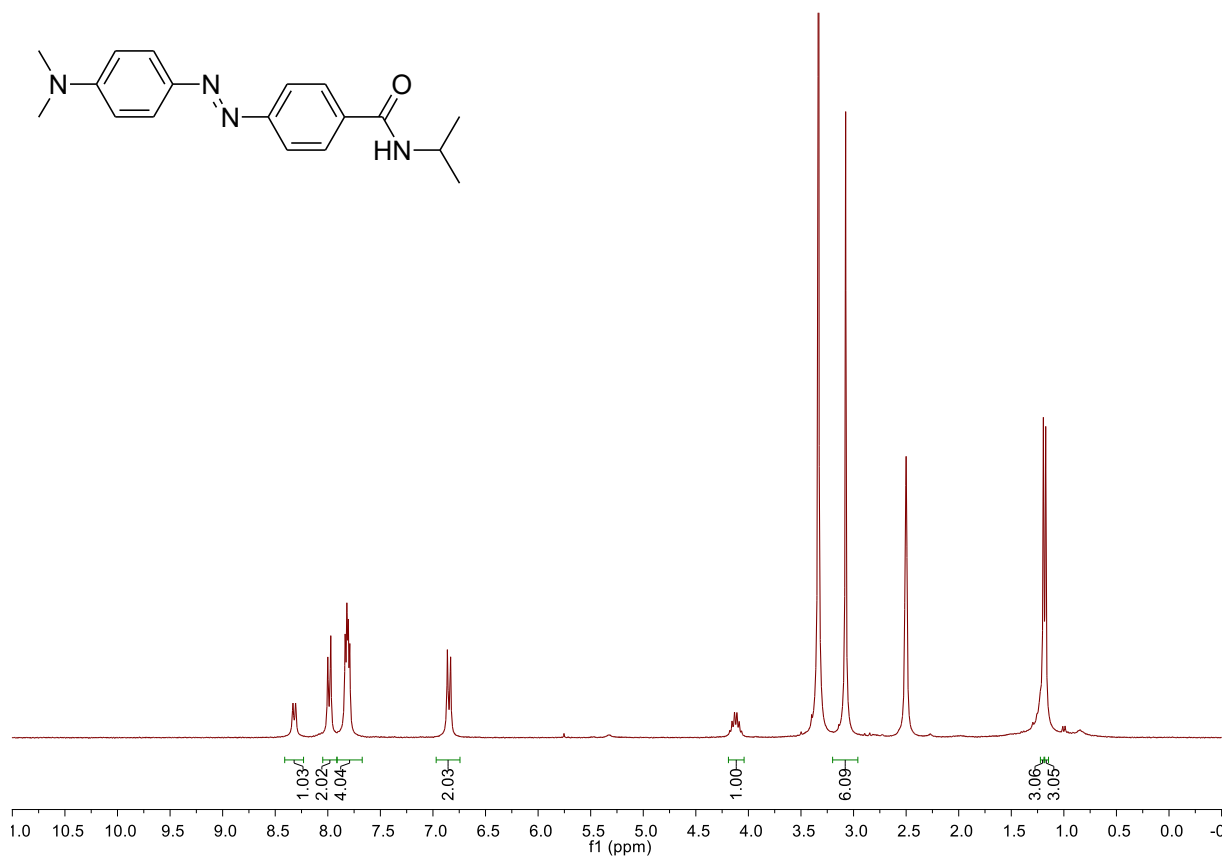
Figure S4. HPLC chromatogram of reaction monitoring after 4 h at 450 nm (in red) and at 390 nm (in black).

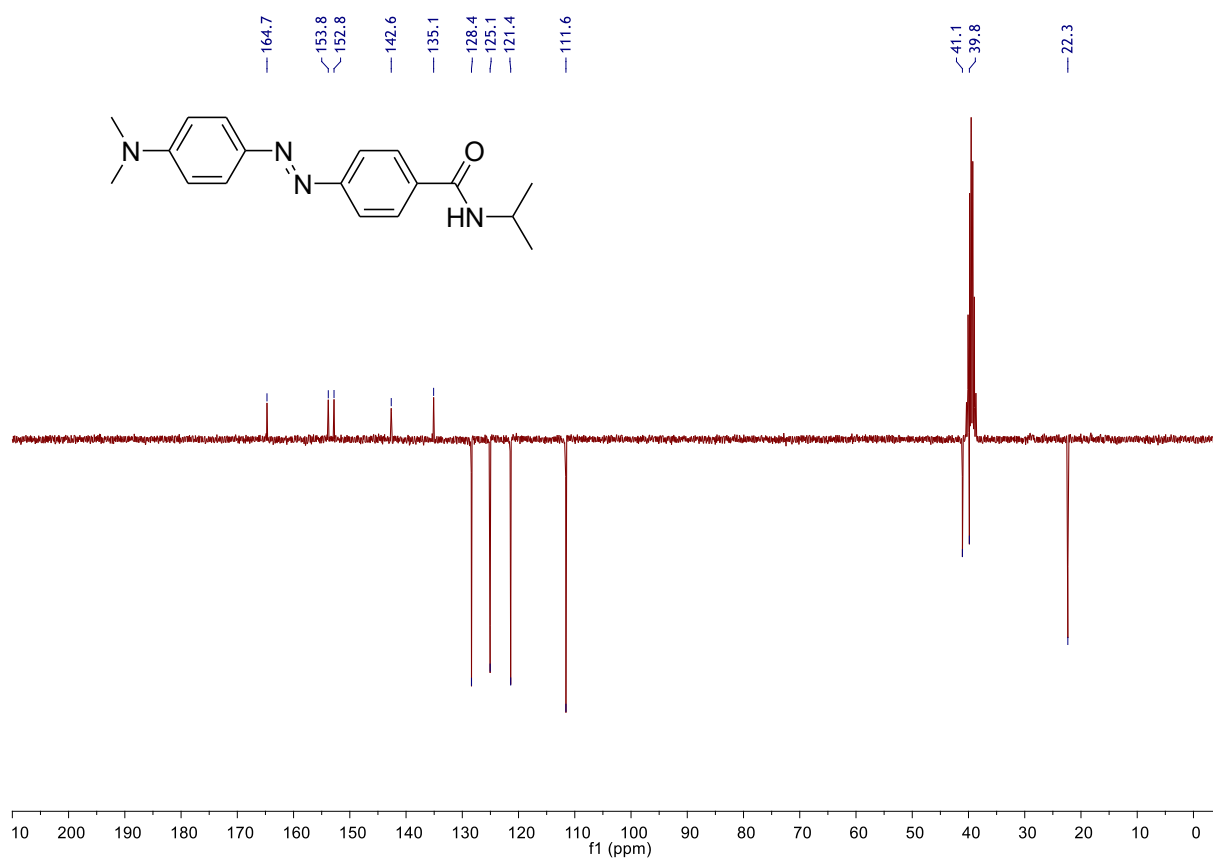
Hydrodabcyyl-mono-tert-butylcarbonate (13)





DabcyI-isopropylamide (14)





¹ Wiejak, S; Masiukiewicz, E; Rzeszutarska, B. A Large Scale Synthesis of Mono- and Di-urethane Derivatives of Lysine. *Chem. Pharm. Bull.* **1999**, *47*, 1489–1490.

Publication III

Structural and biophysical analysis of the phytochelatin-synthase-like enzyme from *Nostoc* sp. shows that its protease activity is sensitive to the redox state of the substrate

Florian J. Gisdon^{1,2}, Christian G. Feiler³, Oxana Kempf¹, Johannes M. Förster², Jonathan Haiss¹, Wulf Blankenfeldt^{3,4}, G. Matthias Ullmann², Elisa Bombarda^{1*}

¹ Department of Biochemistry and ² Computational Biochemistry, University of Bayreuth, Universitätsstr. 30, 95440, Bayreuth, Germany.

³ Department Structure and Function of Proteins, Helmholtz Centre for Infection Research, Inhoffenstr. 7, 38124 Braunschweig, Germany

⁴ Institute for Biochemistry, Biotechnology and Bioinformatics, Technische Universität Braunschweig, Spielmannstr. 7, 38106 Braunschweig, Germany

ACS Chemical Biology, 2022, 17, 883-897.

Reprinted with permission from [Structural and biophysical analysis of the phytochelatin-synthase-like enzyme from *Nostoc* sp. shows that its protease activity is sensitive to the redox state of the substrate. Florian J. Gisdon, Christian G. Feiler, Oxana Kempf, Johannes M. Förster, Jonathan Haiss, Wulf Blankenfeldt, G. Matthias Ullmann, Elisa Bombarda. ACS Chem. Biology, 2022, 17, 883-897. <https://doi.org/10.1021/acscembio.1c00941>]. Copyright 2022 American Chemical Society

Structural and Biophysical Analysis of the Phytochelatin-Synthase-Like Enzyme from *Nostoc* sp. Shows That Its Protease Activity is Sensitive to the Redox State of the Substrate

Florian J. Gidon, Christian G. Feiler, Oxana Kempf, Johannes M. Foerster, Jonathan Haiss, Wulf Blankenfeldt, G. Matthias Ullmann, and Elisa Bombarda*



Cite This: *ACS Chem. Biol.* 2022, 17, 883–897



Read Online

ACCESS |



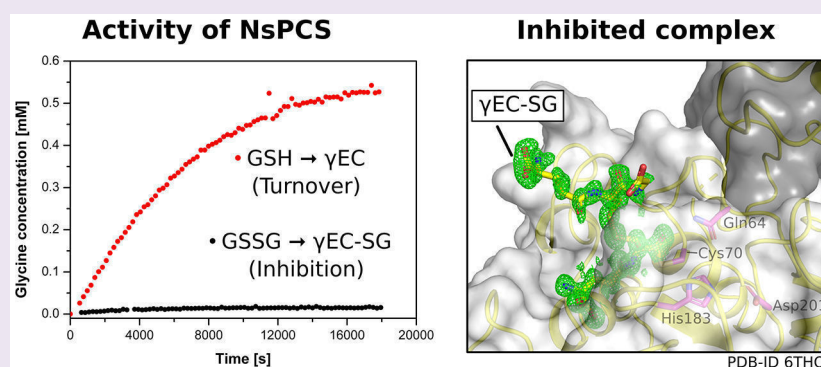
Metrics & More



Article Recommendations



Supporting Information



ABSTRACT: Phytochelatins (PCs) are nonribosomal thiol-rich oligopeptides synthesized from glutathione (GSH) in a γ -glutamylcysteinyl transpeptidation reaction catalyzed by PC synthases (PCSs). Ubiquitous in plant and present in some invertebrates, PCSs are involved in metal detoxification and homeostasis. The PCS-like enzyme from the cyanobacterium *Nostoc* sp. (NsPCS) is considered to be an evolutionary precursor enzyme of genuine PCSs because it shows sufficient sequence similarity for homology to the catalytic domain of the eukaryotic PCSs and shares the peptidase activity consisting in the deglycination of GSH. In this work, we investigate the catalytic mechanism of NsPCS by combining structural, spectroscopic, thermodynamic, and theoretical techniques. We report several crystal structures of NsPCS capturing different states of the catalyzed chemical reaction: (i) the structure of the wild-type enzyme (wt-NsPCS); (ii) the high-resolution structure of the γ -glutamyl-cysteine acyl-enzyme intermediate (acyl-NsPCS); and (iii) the structure of an inactive variant of NsPCS, with the catalytic cysteine mutated into serine (C70S-NsPCS). We characterize NsPCS as a relatively slow enzyme whose activity is sensitive to the redox state of the substrate. Namely, NsPCS is active with reduced glutathione (GSH), but is inhibited by oxidized glutathione (GSSG) because the cleavage product is not released from the enzyme. Our biophysical analysis led us to suggest that the biological function of NsPCS is being a part of a redox sensing system. In addition, we propose a mechanism how PCS-like enzymes may have evolved toward genuine PCS enzymes.

INTRODUCTION

Phytochelatins (PCs) are cysteine-rich nonribosomal peptides involved in metal homeostasis and detoxification with the typical structure $(\gamma\text{-GluCys})_n\text{Gly}$ (n between 2 and 4).¹ PCs are synthesized by the enzyme PC synthase (PCS) by linking glutathione under the release of glycine. At the first glance, this enzyme shows high resemblance to cysteine proteases. However, the catalytic repertoire of PCS goes beyond the hydrolytic cleavage of peptides because it can also work as a transpeptidase under physiological conditions and thus forms peptide bonds without the use of ATP. In eukaryotes, PCS appears to be ubiquitous in the plant kingdom.^{2,3} It is also present in many invertebrates such as protozoa and nematodes,^{4–6} but it has not been found in vertebrates. This

peculiar distribution makes PCS an interesting drug target against parasitic representatives of these animal groups.⁷ In prokaryotes, a number of cyanobacteria and proteobacteria⁸ possess genes that encode for proteins that show approximately 30% similarity to the PCS consensus Pfam domain 05023⁹ but no significant similarity to any other group of proteins. Thus, these bacterial proteins have been assigned as

Received: November 30, 2021

Accepted: March 14, 2022

Published: April 4, 2022



being PCS-like. Similar to PCS, PCS-like proteins use GSH as the substrate. However, while they are able to cleave off the glycine residue to form γ -Glu-Cys (γ EC), the formation of PC in PCS-like proteins was detected only in low amounts and thus the transpeptidase activity of these proteins is still debated.^{10–13}

Several features allow us to assign PCS and its prokaryotic homologue to clan CA of cysteine peptidases, whose archetype is papain according to the peptidase database MEROPS (<https://www.ebi.ac.uk/merops/>, release 12.4).^{14,15} The striking feature of clan CA is the presence of a catalytic triad with a catalytic cysteine assisted by a histidine and an asparagine (as in papain) or an aspartic acid (as in PCS), which seems to be a permissible substitution from a catalytic viewpoint.¹⁶ Moreover, these key residues in clan CA peptidases are not only the same but they also follow the same order in the sequence, as would be expected for divergent evolution from a common ancestor rather than convergent evolution from unrelated progenitors.^{17,18} The catalytic triad of the PC synthase of *Nostoc* sp. (NsPCS) is Cys70-His183-Asp201, as confirmed by crystal structures¹⁹ and is in line with the catalytic triad Cys25-His162-Asn175 in papain.^{20,21} The catalytic cysteine (Cys70 in NsPCS) is conserved with no exception within all eukaryotic and prokaryotic PCS enzymes, supporting its essential role in catalysis. The substitution of only one of the residues of the catalytic triad abolishes the enzymatic activity.²² In particular, the mutation of Cys70 to Ser in NsPCS was shown to inactivate the enzyme.²³

The eukaryotic PCS consists of two domains: the N-terminal conserved catalytic domain and the more variable C-terminal domain.²⁴ Prokaryotic PCSs are homologous to the N-terminal domain but miss the C-terminal domain. A sequence alignment shows that NsPCS possesses 34.5% identity and 53.0% similarity with the N-terminal domain of PCS from *Arabidopsis thaliana* (AtPCS1). Notably, the truncated N-terminal domain of AtPCS1 is sufficient for catalysis, that is, it cleaves GSH into γ -Glu-Cys and Gly, and it is even able to synthesize PCs from GSH in media containing Cd²⁺.²⁵ It is therefore not surprising that the ability to cleave GSH is shared by the prokaryotic PCS.

Although extensively studied, the spectrum of functions of PCS is still a matter of debate.^{13,17,26} The sole role in heavy metal detoxification seems not sufficient to explain the ubiquity of this protein in the plant kingdom as well as in yeast and nematodes. Amounting evidence supports the hypothesis that PCS serves functions besides cadmium and arsenic detoxification, for example, through roles in essential metal homeostasis³ and in innate immunity.²⁷ The role of the PCS-like proteins is even less clear because they are seemingly not able to produce larger amounts of PC. In order to better identify the tasks of PCS-like proteins, their detailed mechanistic characterization is a priority.

In this work, we focus on the alr0975 protein from *Nostoc* sp. strain PCC 7120 (*syn. Anabaena* sp. strain PCC 7120),²⁸ which is a PCS-like protein¹⁰ that we name NsPCS. We report several crystal structures of the NsPCS: (i) the structure of wild-type enzyme (wt-NsPCS); (ii) the high-resolution structure of the γ -glutamyl-cysteine acyl-enzyme intermediate (acyl-NsPCS); and (iii) the structure of an inactive variant of NsPCS, with the catalytic cysteine mutated into serine (C70S-NsPCS). Furthermore, we analyze the affinity of the enzyme for the substrate and the catalytic activity experimentally and support this work by theoretical calculations. This investigation

provides the first quantitative analysis of the enzymatic mechanism of a PCS-like protein, with some implications for possible roles of such enzymes in prokaryotes.

RESULTS

Our goal is to dissect the mechanism of the peptidase reaction catalyzed by NsPCS and to identify its biological implications. To reach a deep understanding of the enzymatic mechanism, it is necessary to relate the thermodynamic and kinetic data to the structural features of the enzyme. In order to merge all these different aspects, it is important to approach the enzymatic mechanism also from a theoretical point of view. With electrostatic and quantum chemical calculations, it is possible to gain insights into enzymatic mechanisms.²⁹ To this purpose, the knowledge of the 3D structure of the enzyme capturing different states of the chemical reaction is a prerequisite.

Crystal Structure of NsPCS with and without the Substrate. We cloned the gene of alr0975 from *Nostoc* sp. strain PCC 7120 excluding the previously predicted signal sequence responsible for the periplasmic secretion of the protein,¹⁰ see the [Supporting Information](#). Additionally, we introduced the mutation Cys70 to Ser (C70S-NsPCS) in order to analyze the reasons of its inactivity²³ at the atomic level and to investigate binding independent from catalysis. The structure of both variants, wt-NsPCS and C70S-NsPCS have been determined by X-ray crystallography. In addition, we crystallized an acyl-form of NsPCS (acyl-NsPCS), which has the γ EC moiety covalently bound. At variance to previous work,¹⁹ in which the acyl-enzyme was crystallized at an extremely acidic pH (pH 2.6–3.4), we obtained these crystals at a significantly higher pH (pH 5.5). Moreover, the higher resolution of our acyl-enzyme structure allows us to obtain more details about the bound ligand. We could not only confirm the oxidation at the sulfur atom of the cysteine of the covalently bound γ EC moiety that was previously reported¹⁹ but we could also resolve a second glutathione bound via a disulfide bond to the acylated γ EC moiety. The most relevant features of the reported crystal structures are represented in [Figure 1](#).

The structure of the native protein (PDB ID: 6TH5) has a resolution of 1.99 Å with $R_{\text{work}} = 19.9\%$ and $R_{\text{free}} = 23.8\%$ and is very similar to the one previously resolved (PDB ID: 2BTW).¹⁹ The structure of the acyl-form (PDB ID: 6THO) has a higher resolution, 1.09 Å ($R_{\text{work}} = 11.8\%$; $R_{\text{free}} = 14.8\%$) than the one previously resolved (PDB ID: 2BU3).¹⁹ The structure of the serine mutant C70S-NsPCS (PDB ID: 6TJL) was refined to a resolution of 1.87 Å ($R_{\text{work}} = 20.5\%$, $R_{\text{free}} = 26.8\%$). Data collection statistics are summarized in [Table 1](#).

All the three NsPCS structures are homodimers, displaying root-mean-square deviations (RMSDs) lower than 0.25 Å between the two chains [$\text{RMSD}(\text{C70S-NsPCS}) = 0.19$ Å, $\text{RMSD}(\text{wt-NsPCS}) = 0.19$ Å, $\text{RMSD}(\text{acyl-NsPCS}) = 0.23$ Å].

The structure of the mutated protein C70S-NsPCS is nearly identical to that of the native enzyme, indicating that rather than structural changes, the substitution of the sulfur atom of the cysteine by the oxygen of a serine is the key point for the loss of the activity.

Unexpectedly, we observed electron density for one molecule of glutathione (GSH) in the active site of C70S-NsPCS, even if GSH was not added during crystallization. The ligand therefore seems to have been co-purified after

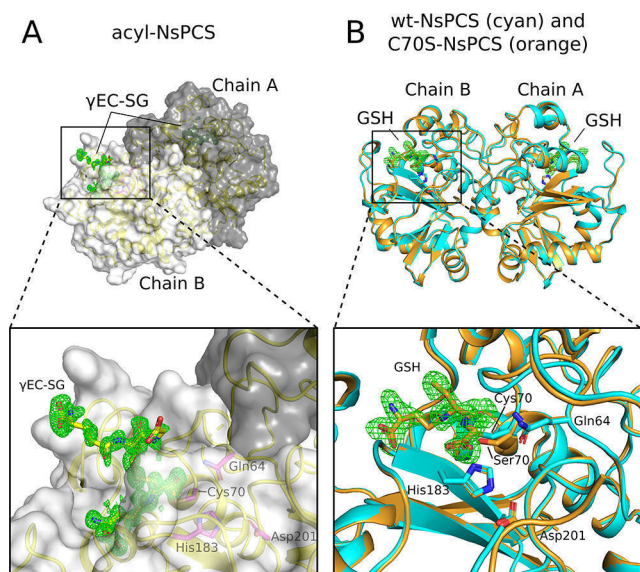


Figure 1. (A) Binding pocket of acyl-NsPCS (PDB ID: 6THO). Active site residues are shown as magenta sticks. The electron density of the mono-deglycinated oxidized form of glutathione (γ EC-SG) is shown. (B) Superimposition of wt-NsPCS (PDB ID: 6TH5) and C70S-NsPCS (PDB ID: 6TJL). The ligand GSH is present in the mutant structure C70S-NsPCS and is represented with its electron density. For all structures, the $F_o - F_c$ electron density before incorporation of the substrate (omit map) is represented as a mesh with a sigma-level of 3.

overexpression in *E. coli* and remained tightly bound during purification and crystallization of the protein.

Investigation of Binding of GSH and GSSG to the Active Site. In order to measure the affinity of an enzyme for its substrate, the catalytic activity has to be separated from binding. Therefore, in our case, C70S-NsPCS represents the variant of choice to focus on the binding process. The fact that the uncleaved substrate is stably captured by C70S-NsPCS confirms that this mutation abolishes the activity of the enzyme without precluding binding. On the other hand, the presence of GSH in the binding pocket of the recombinant protein hampers binding studies, and removal of the ligand is an unavoidable prerequisite for such experiments.

In order to eliminate the substrate from the binding pocket, the protein was unfolded, and then dialyzed to remove the substrate from the solution and finally refolded. To check if the native fold is reached, a spectroscopic analysis of the non-refolded (i.e., before unfolding) and refolded proteins was performed.

We recorded the CD spectrum of the C70S-NsPCS during the unfolding/refolding process. As shown in Figure 2, the evolution of the CD signature indicates the loss of the secondary structure during unfolding and its restoration after refolding. An additional confirmation of the occurrence of the unfolding and refolding process was provided by the analysis of the fluorescence signal. Due to the presence of eight tyrosines, an excitation wavelength of 295 nm was chosen in order to selectively excite the tryptophan residues. The emission spectrum of the non-refolded C70S-NsPCS presents a maximum at 336 nm, which indicates a clear hypsochromic shift when compared to the emission of a tryptophan residue in aqueous solution whose maximum is at 350 nm (Figure 2B). Emission at a lower wavelength is typical of nonsolvent

Table 1. Data Collection and Refinement Statistics

	wt-NsPCS	acyl-NsPCS	C70S-NsPCS
PDB ID	6TH5	6THO	6TJL
Data Collection			
Space group	$P2_1$	$P2_12_12_1$	$P2_1$
a, b, c (Å)	61.36, 46.67, 68.58	49.28, 57.96, 139.47	61.39, 47.83, 67.9
α, β, γ (deg)	90.00, 92.26, 90.00	90.00, 90.00, 90.00	90.00, 91.80, 90.00
resolution (Å)	34.26–1.99 (2.07–1.99) ^a	29.21–1.09 (1.10–1.09) ^a	46.25–1.87 (1.92–1.87) ^a
R_{merge} (%)	11.5 (66.5) ^a	5.6 (42.7) ^a	8.4 (84.1) ^a
R_{pim} (%)	9.8 (57.0) ^a	3.4 (26.2) ^a	5.3 (53.3) ^a
$I/\sigma(I)$	6.6 (1.3) ^a	12.1 (2.7) ^a	10.2 (1.34) ^a
completeness (%)	97.4 (98.5) ^a	98.6 (99.3) ^a	99.3 (99.5) ^a
redundancy	2.2 (1.9) ^a	3.6 (3.4) ^a	3.3 (3.3) ^a
$CC_{1/2}$	0.987 (0.845) ^a	0.998 (0.815) ^a	0.997 (0.621) ^a
Refinement			
number of reflections	26210 (2924) ^a	164587 (5490) ^a	32749 (2683) ^a
$R_{\text{work}}/R_{\text{free}}$	0.199 (0.282) ^a /0.238 (0.313) ^a	0.118 (0.200) ^a /0.148 (0.205) ^a	0.205 (0.311) ^a /0.268 (0.323) ^a
Number of Atoms			
protein	6790	8451	7027
ligand/ion	5	124	74
water	318	768	118
B-Factors (Å ²)			
protein	26.8	14.3	48.5
ligand/ion	27.8	28.4	43.9
water	28.8	32.0	33.1
RMSD			
bond length (Å)	0.006	0.007	0.016
bond angles (deg)	0.554	1.042	1.413

^aValues in parentheses are for the highest-resolution shell.

exposed tryptophan residues in line with the buried location of both tryptophan residues in NsPCS. During the unfolding process we observe the shift of the emission band toward higher wavelengths until reaching the profile of the typical spectrum of fully water-exposed tryptophan residues. This hyperchromic shift reports the loss of structural features leading to the disruption of the hydrophobic core and the consequent exposure of the tryptophan residues to the aqueous solution (Figure 2B). The shift of the emission band was reversed during the refolding process until the emission spectrum regained the original profile, indicating the restoration of the original structure.

The spectroscopic analysis of the refolded protein made us confident that the protein refolds to the native conformation. Nevertheless, we desired to test if the refolded protein is also functional. Because the C70S mutant is inactive, we unfolded and refolded the wild-type enzyme following the same protocol and checked the quality of the procedure with CD and fluorescence spectroscopy, obtaining the confirmation of the restoration of the original structure as for C70S-NsPCS. We performed a real-time ¹H NMR experiment to monitor the time course of the production of free glycine at pH 8. The activity of the refolded wt-NsPCS was compared to the activity of the non-refolded wt-NsPCS from the same batch.

The activity assay shows that the refolded protein is active. However, although the refolded protein is able to cleave the

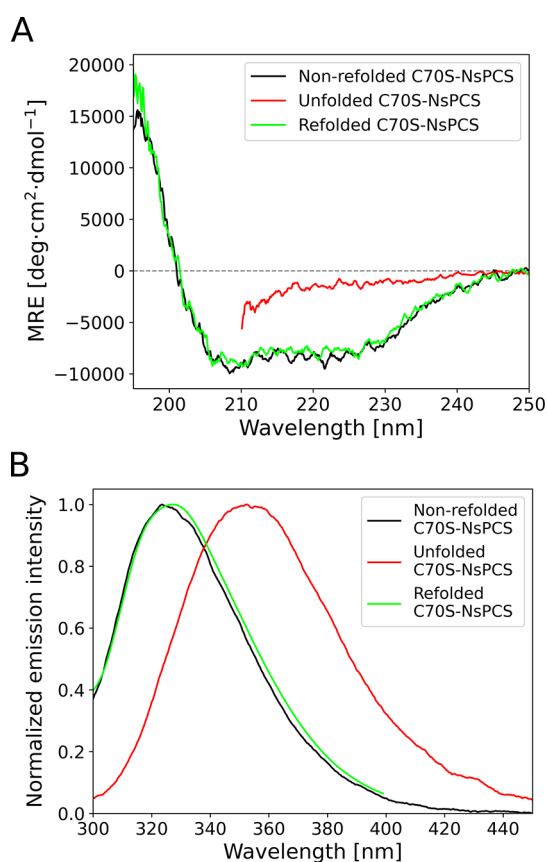


Figure 2. (A) CD spectra of C70S-NsPCS: non-refolded (black), unfolded in 3 M GdmCl (red), and refolded by elimination of GdmCl (green). The spectrum in 3 M GdmCl was cut at $\lambda = 210$ nm because the high salt concentration causes a high noise at shorter wavelengths. (B) Normalized fluorescence spectra ($\lambda_{\text{ex.}} = 295$ nm) of non-refolded (black), unfolded (red), and refolded (green) C70S-NsPCS. Temperature was set at 25 °C.

entire amount of the substrate, it appears to work much more slowly than the non-refolded protein. The time dependence of free glycine release (Figure 3) indicates that in the time during which the non-refolded enzyme has processed all the substrate (after about 1600 s), the refolded enzyme processed only about 10% of it. However, both the refolded and the non-refolded enzymes are able to process the entire amount of the substrate.

To characterize the binding pocket, we analyzed the hydrogen bond network (Figure 4). The experimental binding study was performed with isothermal titration calorimetry (ITC). First of all, we measured the binding of GSH to the purified recombinant non-refolded C70S-NsPCS, that is, the protein that retained the substrate in the binding site. The thermogram shows only the effect of dilution, confirming that the mutated enzyme is saturated with GSH. Because GSH is often oxidized to GSSG, we decided to determine the affinity of the C70S-NsPCS to both molecules, GSH and GSSG. The binding experiments have been performed under an argon atmosphere to prevent the oxidation of the thiol groups. Because the protein is a homodimer, we initially fitted the experimental data to a two-site model. No significant interaction between the two binding sites has been detected in line with the fact that the two binding pockets are far apart from each other. Therefore, the data have been further analyzed with a one-site model (Table 2).

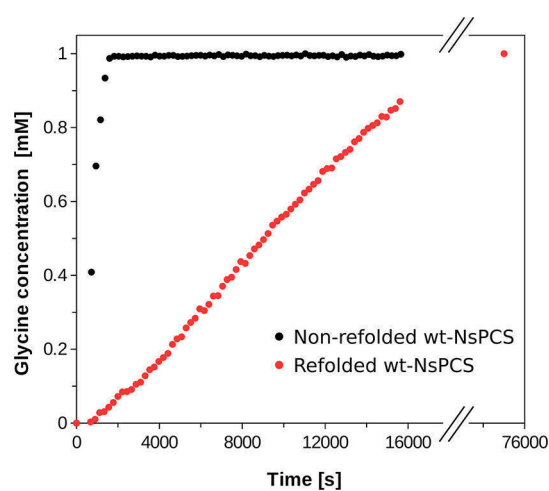


Figure 3. Time-dependent production of free glycine resulting from GSH cleavage mediated by NsPCS. The concentration of free glycine was measured by ^1H NMR and quantified by comparison with sodium trimethylsilylpropanesulfonate (DSS) as the internal NMR standard. Because the used GSH concentration has been 1 mM, the final concentration of detected glycine was normalized to 1 mM.

The affinities of C70S-NsPCS for GSH ($5 \times 10^5 \text{ M}^{-1}$) and GSSG ($1 \times 10^5 \text{ M}^{-1}$) are similar. The fit of the experimental data indicates that only 10 to 20% of the protein is able to bind the substrate (see parameter p in Table 2). Notably, also the activity assay by NMR showed that a similar small amount of refolded protein retained activity. This similarity between the percentages of active and binding protein was replicated with different batches of protein indicating the significance of this finding.

In order to consolidate the result of ITC we measured the affinity of the refolded C70S-NsPCS for GSH with microscale thermophoresis. First of all, we tested the binding of GSH to the purified recombinant non-refolded C70S-NsPCS which is expected to retain the substrate in the binding pocket. As expected, no binding could be detected because the binding pocket is occupied. Afterward, we measured the binding of GSH to the refolded C70S-NsPCS and obtained a binding constant of $K_a = (8 \pm 4) \times 10^5 \text{ M}^{-1}$. Noticeably, the binding constant measured by microscale thermophoresis is fully in line with the binding constant measured by ITC (Table 2).

The affinity of the enzyme for the reduced (GSH) and oxidized (GSSG) forms of glutathione is similar within 1 order of magnitude, suggesting that the oxidation of glutathione does not substantially affect binding. This observation prompted us to test if GSSG can be a substrate for the enzyme. We performed a real-time ^1H NMR experiment to monitor and compare the time course of the production of free glycine at pH 8 using GSSG and GSH as substrates, respectively. Only a very small amount of free glycine was detected when GSSG was added in the reaction tube containing the enzyme (Figure 5), indicating that GSSG is not an optimal substrate for NsPCS. Additionally, the quantification of the free glycine which is present when the reaction is terminated (plateau of the time trace) reveals that the concentration of the free glycine is similar to the concentration of active sites of the enzyme present in the reaction tube. This result indicates that the free glycine was produced in a stoichiometric amount and leads us to suggest that each monomer of the enzyme interacts with one molecule of GSSG and is able to cleave one of its two

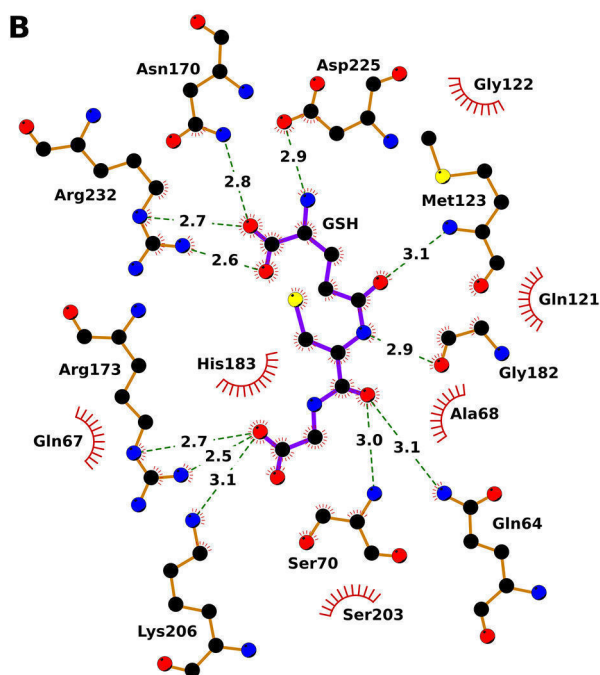
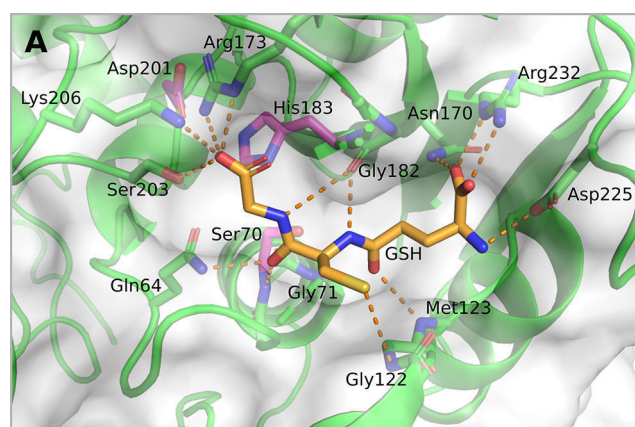


Figure 4. Hydrogen bond network of GSH in the binding pocket of NsPCS. (A) Possible hydrogen bond interactions of GSH with NsPCS in the structure C70S-NsPCS (PDB ID: 6TJL), subunit A. Interaction possibilities were obtained with the in-house program Hbond. (B) Binding site representation of GSH in the binding pocket of NsPCS, subunit A calculated with LigPlot+ (<https://www.ebi.ac.uk/thornton-srv/software/LigPlus/>, Version 1.4).³⁰

Table 2. Thermodynamic Quantities Obtained from ITC^a

	C70S-NsPCS + GSH	C70S-NsPCS + GSSG
ΔH [kcal mol ⁻¹]	-12 ± 1	-11.6 ± 0.4
K_a [M ⁻¹]	$(5 \pm 3) \times 10^5$	$(1.0 \pm 0.2) \times 10^5$
ΔS [kcal mol ⁻¹ K ⁻¹]	-0.014	-0.016
ΔG [kcal mol ⁻¹]	-7.9	-6.9
R^2	0.935	0.990
p	0.20 ± 0.01	0.118 ± 0.003

^aThe correction parameter p corresponds to the fraction of binding protein (see **Material and Methods**). ΔH and K_a are experimentally determined. ΔS and ΔG are calculated from $\Delta G = -RT \ln K_a$ and $\Delta G = \Delta H - T\Delta S$.

glycine residues, without the subsequent release of the γ EC-SG moiety. This hypothesis is supported by the crystal structure of

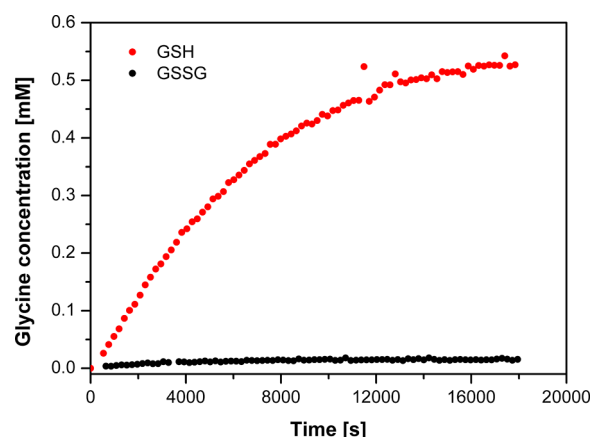


Figure 5. Time-dependence of the production of free glycine resulting from the substrate cleavage, GSH (red dots), and its oxidized form GSSG (black dots). The concentration of free glycine was measured under the anoxic condition by ¹H NMR and quantified by comparison with DSS as an internal NMR standard.

acyl-NsPCS which reveals that γ EC-SG and not γ EC is bound in the acyl-enzyme.

Electrostatic Analysis of the Substrate Binding. Our experimental observations indicate that NsPCS catalyzes the cleavage of GSH but is trapped in the acylated state when GSSG is used as the substrate. In order to understand the different reactivities of the enzyme, we performed electrostatic calculations. These calculations are particularly suited to this purpose because, due to the charges present on both GSH and GSSG, the binding of both molecules to the enzyme has an exquisite electrostatic character. For our calculations, we used the crystal structures C70S-NsPCS and acyl-NsPCS to create models of the complexes with GSH, GSSG, and their cleaved forms γ EC and γ EC-SG, respectively. All the molecules have been modeled as noncovalently bound in the binding pocket of the enzyme (see **Material and Methods** for a detailed description of the procedure).

We calculated the electrostatic interaction energies between the enzyme and the analyzed ligands using the Poisson–Boltzmann equation (see **Table 3**). The so-calculated energies contribute mainly to the enthalpic part of the binding energy.

The electrostatic interactions stabilize the binding of GSSG and γ EC-SG by more than 20 kcal mol⁻¹, whereas only -16.5 and -14.1 kcal mol⁻¹ are the electrostatic energies for the binding of the reduced forms GSH and γ EC, respectively. The complex NsPCS + γ EC was modeled in two ways and slightly different electrostatic interaction energies have been obtained:

Table 3. Electrostatic Contribution to the Interaction Energy between NsPCS and Different Variants of Its Substrate

crystal structure	structural model	electrostatic contribution (kcal mol ⁻¹)
C70S-NsPCS (GSH bound)	NsPCS + GSH	-16.5
	NsPCS + γ EC	-14.1
	NsPCS + GSSG	-22.4
	C70S-NsPCS + GSH	-16.3
acyl-NsPCS (γ EC bound)	NsPCS + γ EC	-18.2
	NsPCS + γ EC-SG	-22.2

−14.1 kcal mol^{−1} for the complex based on the crystal structure of C70S-NsPCS and −18.2 kcal mol^{−1} for the complex based on the crystal structure of the acyl-NsPCS (Table 3). The difference between the interaction energy calculated for the complex NsPCS + GSH (−16.5 kcal mol^{−1}) and the one calculated for the complex NsPCS + γ EC (−14.1 kcal mol^{−1}) can be considered as the interaction of the glycine moiety of GSH with PCS showing that γ EC when hydrolytically cleaved from C70 interacts less strongly with the enzyme than GSH.

In addition, we have simulated the encounter of GSH with NsPCS using a Monte Carlo technique.³¹ We considered three forms of NsPCS differing in the occupancy of the binding pocket: (i) NsPCS bearing empty binding pockets, (ii) NsPCS with bound GSH in the binding pockets, and (iii) NsPCS with one acylated binding pocket and GSH bound in the other (see Figure 6). In NsPCS with empty binding pockets, we could observe the formation of the encounter complex in the area around the active site (Figure 6A). In contrast, NsPCS with GSH bound in both binding pockets shows no specific encounter complex formation (Figure 6B), indicating that the binding of GSH prevents another GSH molecule from approaching the active site region. Finally, Figure 6C shows the results of the calculation in which γ EC is covalently bound in one pocket of the homodimer and GSH is noncovalently bound in the other pocket. In line with the finding for NsPCS with GSH bound to both binding pockets, at the pocket with bound GSH, no encounter complex formation is observed. Instead the pocket with bound γ EC, representing the acyl-enzyme state, shows an encounter complex formation.

Michaelis–Menten Analysis of the Catalytic Reaction.

In order to measure the catalytic activity, we used the wild-type enzyme. We focused on the peptidase activity that is the only activity that is doubtlessly recognized to be performed by NsPCS. The reaction consists in the cleavage of glycine from the substrate (GSH) concomitant to the formation of the acyl-enzyme intermediate, followed by the hydrolysis of the acyl-adduct.

We designed a new test to quantify the peptidase activity of NsPCS based on real-time ¹H NMR under anoxic conditions. Due to the fast oxidation of the substrate GSH, the catalytic activity of NsPCS at pH 8 was highly sensitive to oxygen exposure. Therefore, we elaborated a protocol to eliminate the presence of oxygen in the reaction mixture (see Materials and Methods for details).

The deglycination of GSH was monitored and a Michaelis–Menten analysis was performed. For comparison, the reference spectra of the substrate GSH, its oxidized form GSSG, and the expected products γ EC and free glycine have been measured. During the reaction, the newly appearing resonances can be attributed to free glycine and γ EC and the disappearing resonance corresponds to GSH. No resonance indicating oxidation of GSH was detectable during the 4 h of the experiment, indicating that the protocol to maintain the anoxic condition was successful. The time-dependence of the accumulation of free glycine is used to estimate the initial velocities of the reaction. A plot of the initial velocity versus the substrate concentration displays the typical Michaelis–Menten behavior (Figure 7), with a Michaelis–Menten constant K_M of 0.2 mM and a turnover number k_{cat} of 3.5 s^{−1}.

QM/MM Analysis of the Reaction Mechanism. NsPCS belongs to the superfamily of papain-like cysteine peptidases. Hence, it is expected to cleave its natural substrate GSH

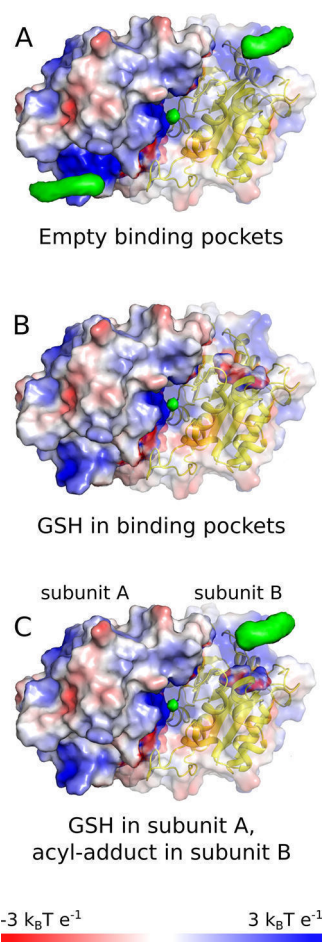


Figure 6. Comparative representation of encounter complex densities (shown in green) of GSH around NsPCS. NsPCS is shown in the surface representation, colored by electrostatic potential on the solvent accessible surface. One subunit of each homodimer is opaque, and the other is transparent, with a translucent cartoon representation of the protein. The electrostatic potential was calculated with 0.1 M ionic strength. (A) NsPCS with empty binding pockets. Encounter complexes form at both binding pockets. (B) GSH bound to both binding pockets. No encounter complexes form near the binding pockets indicating that a second GSH molecule is not able to approach the active site when a GSH is already bound in the binding pocket. (C) GSH bound to subunit A and γ EC bound covalently to subunit B. The simulation shows that after deglycination, a second GSH molecule can approach the active pocket in subunit B. All the simulations were performed with 100,000 runs and 1,000,000 Monte Carlo steps each. The isovalue is set to 5500 and describes the minimal number of encounters which occurred as a visible green surface.

according to a mechanism similar to the one of papain. To test this assumption, we performed quantum mechanics/molecular mechanics (QM/MM) calculations on both enzymes, NsPCS and papain. In the case of papain, we chose the substrate Phe-Ser-Ile with an acetylated N-terminus and N-methylated C-terminus based on previous mechanistic studies and experimental binding data.³²

The peptidase reaction performed by both enzymes can be divided into two steps: the acylation reaction and the hydrolytic cleavage. In NsPCS, the acylation reaction consists in the cleavage of the substrate resulting in glycine and γ EC. The latter remains covalently linked to the enzyme as so-called acyl-adduct. In papain, the investigated acylation reaction

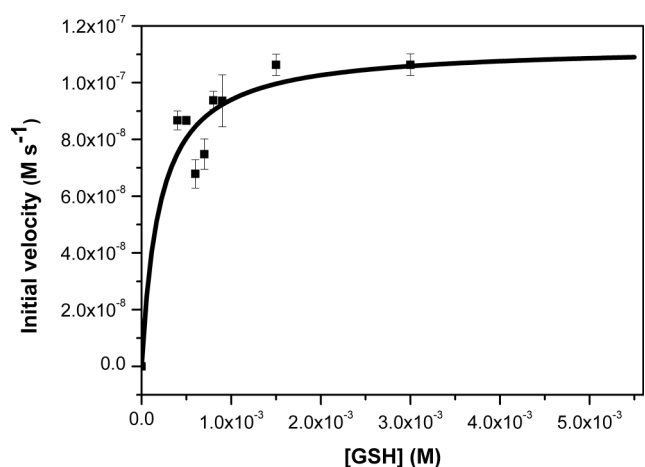


Figure 7. Plot of the initial velocities of the peptidase reaction catalyzed by NsPCS as a function of the concentration of the substrate GSH. For each substrate concentration, the accumulation of free glycine is monitored and the initial velocity of the reaction is determined and plotted against the concentration of the substrate. The solid line represents the fit of the experimental data according to the Michaelis–Menten equation.

consists in the cleavage of the substrate between serine and isoleucine. Similarly, the latter remains covalently linked to the enzyme. In both enzymes, a subsequent hydrolytic reaction leads to the cleavage of the acyl-adduct. The calculations for the acylation reaction are performed on the crystal structure of C70S-NsPCS, which has the full substrate GSH bound to its

active site and therefore represents the ideal starting point to study the cleavage reaction. In order to simulate the enzymatic activity, the serine was converted computationally into the native cysteine. The calculations for the deacylation have been performed on the crystal structure of the acyl-enzyme. We compared the obtained energy profiles with the energy profile of the corresponding reaction steps in papain (Figure 8).

The acylation reaction can be divided into two steps: (i) the activation of the nucleophile by proton transfer from cysteine to the catalytic histidine resulting in the ion-pair state (Figure 8, reaction coordinates 1–3) and (ii) the nucleophilic attack and cleavage of the substrate via a tetrahedral state (Figure 8, reaction coordinates 3–7). The comparison of the reaction profiles of the two enzymes shows that the energy barrier for the activation of the nucleophile in NsPCS ($6.1 \text{ kcal mol}^{-1}$) is higher than in papain ($0.9 \text{ kcal mol}^{-1}$). Additionally, the ion-pair state is less stable in NsPCS than in papain, as the less pronounced minimum in the energy profile of NsPCS indicates (reaction coordinate 3). In papain, the catalysis proceeds via the formation of a stable tetrahedral intermediate state (reaction coordinate 5). The values of the classical potential energy suggest that also the reaction path for NsPCS displays a tetrahedral intermediate, which reacts further to form the acyl-enzyme state; nevertheless, the occurrence of a stable tetrahedral intermediate for NsPCS is not observed after zero-point-energy correction. The zero point energy of a quantum mechanical system accounts for the ground-state fluctuations according to the Heisenberg uncertainty principle; therefore, after the zero-point-energy correction, the energy of

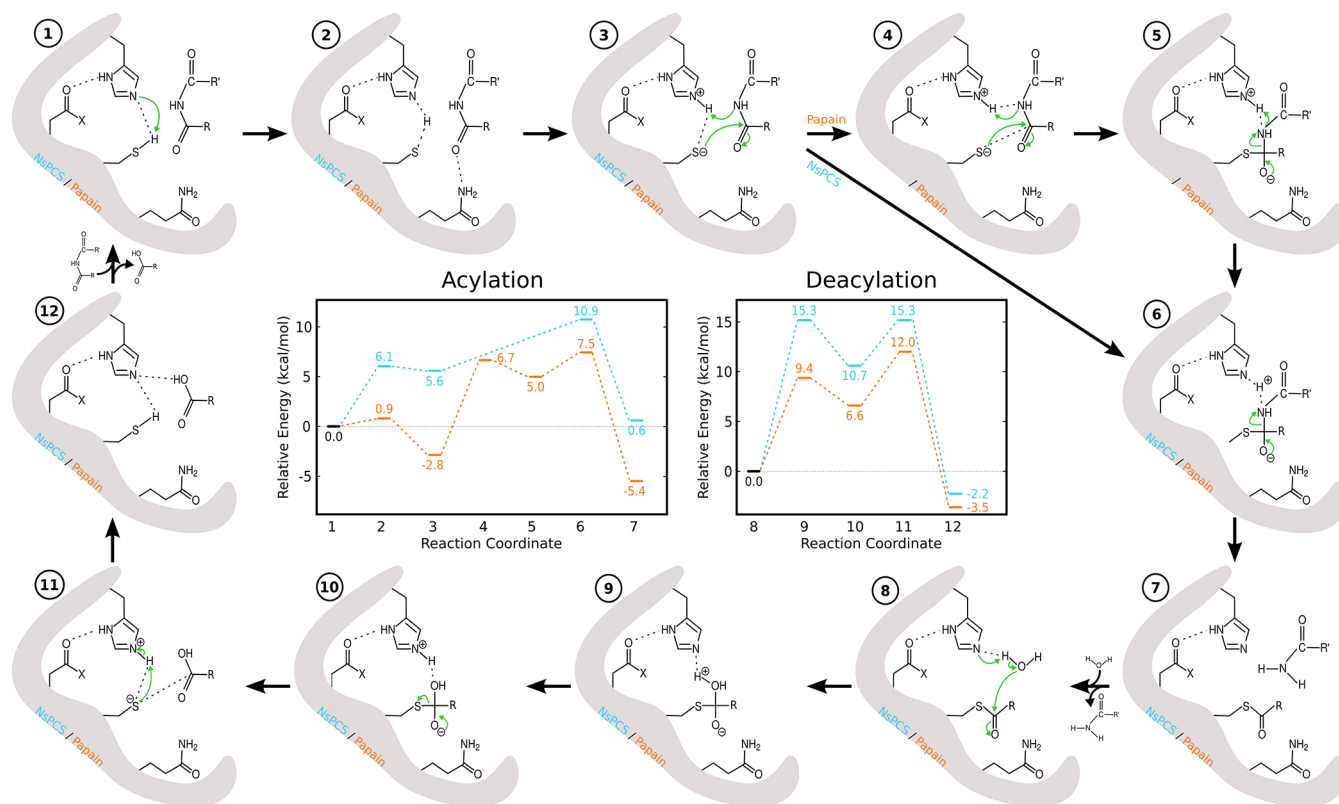


Figure 8. Comparison of the enzymatic mechanism of NsPCS (cyan) and papain (orange). Comparable states along the reaction coordinate are shown in the energy diagrams and structurally represented with the corresponding numbers. States 4 and 5 have been identified only for papain and not for NsPCS. The energies were calculated with a QM/MM approach and zero-point energy corrected. The reaction coordinate corresponds to the number of the states.

the system is higher than its energy in the classical limit, which is the mathematical minimum of the potential well. Because different states may have different zero point energies, energetically close states in the reaction path may appear indistinguishable, when zero-point-energy correction is applied. According to the Eyring equation, the rate constants at 303.15 K for the rate-limiting step in the acylation reaction of NsPCS and papain are 9.2×10^4 and $4.6 \times 10^7 \text{ s}^{-1}$, respectively, suggesting a faster process in papain. The calculated rate constants represent the actual cleavage reaction without binding of the substrate GSH and release of the cleaved-off glycine. However, substrate binding and product release contribute to the measured rate constants. Thus, only a qualitative comparison with the experimentally obtained rate constants is meaningful, also because we consider only the enthalpic and not the entropic contribution to the energy barrier.

During the hydrolytic cleavage of the acyl-enzyme, a water molecule in the active site attacks and cleaves the thioester bond of the acyl-enzyme, leading to the release of γ EC in NsPCS and Phe-Ser in papain. The hydrolytic cleavage can be divided into two steps: (i) the formation of a tetrahedral state (Figure 8, reaction coordinates 8–10) and (ii) the cleavage of the covalent enzyme substrate complex and re-protonation of the catalytic nucleophile (Figure 8, reaction coordinates 10–12). The energy profiles of NsPCS and papain look similar. The two identified transition states and the intermediate of the reaction catalyzed by NsPCS are roughly 3–6 kcal mol⁻¹ higher than the corresponding state in the reaction catalyzed by papain. For the hydrolytic cleavage, the rates of NsPCS and papain calculated according to the Eyring equation at 303.15 K are 6.3×10^1 and $1.3 \times 10^4 \text{ s}^{-1}$, respectively.

DISCUSSION

The function of an enzyme is interconnected to its catalytic behavior, which has its rationale in the conformational and chemical features of the enzyme at the atomic level. Therefore, in our attempt to understand the mechanism of NsPCS and to identify its biological functions, we started by determining the crystal structure of three relevant forms of the enzyme: the ligand-free enzyme, the acyl-enzyme, and a mutant enzyme with the substrate bound noncovalently.

New Structural Features in NsPCS and the Acyl-Enzyme. The structure of the native protein (NsPCS) resolved in this study is similar to the one in the literature¹⁹ (RMSD of 0.28 Å). However, a careful optimization of the hydrogen-bond network led to the re-orientation of several sidechains in comparison to the previous work, in particular for amino acids close to the active site, such as Asn170 or Gln67. The structure of the acyl-enzyme is very well superimposable to the structure of the native enzyme. We could resolve all loop regions, including the loop comprising the residues 83–106, which was partly undefined in the previous structure¹⁹ (PDB ID: 2BU3). Because of its vicinity to the active site of the other monomer, this loop was previously called “protruding loop” and its incompleteness was attributed to the flexibility required by the catalytic reaction. However, the lack of unresolved regions in our structure together with the absence of a significant structural difference between the acylated and the ligand-free forms of the enzyme indicates that the catalytic reaction does not require much flexibility in the active site and the active site of NsPCS is rather preshaped to accommodate the substrate. Additionally, because we do not detect

significant structural differences between the protruding loop regions in both monomers, we have no reason to invoke mechanistic differences between the two monomers.

Based on our binding study, we exclude a cooperative behavior between the two monomers at variance to suggestions of Vivares et al.¹⁹ This conclusion is supported by our structural study. In fact, the two binding pockets are far apart from each other and the apparent absence of mechanistic differences between the two monomers pleads for their independence.

We succeeded to crystallize the acyl-enzyme at pH 5.5, which is significantly higher than the pH at which the acyl-enzyme was previously trapped.¹⁹ Therefore, we think that the acidic pH and the consequent protonation of the catalytic histidine is not the reason for the stabilization of the acyl-enzyme, as previously suggested. In fact, the electrostatic calculations indicate that His183 titrates at extremely low pH (see the Supporting Information). Moreover, in our high-resolution structure, we could detect a second molecule of GSH bound via a disulfide bond to the acylated γ EC moiety. Therefore, we suggest that the reason of the stabilization of the acyl-enzyme resides in the larger size of the ligand (γ EC-SG instead of γ EC) and thus in the larger number of interactions. The hydrolytic cleavage reaction occurs through the formation of a tetrahedral complex due to the arrival of a water molecule attacking the thioester bond. In contrast to the structure of Vivares et al.,¹⁹ where a water molecule was found only in one monomer, we see this water molecule ideally placed in both monomers.

The substrate is retained in the binding pocket of the inactive mutant C70S-NsPCS.

Unexpectedly in the crystal structure of the catalytically inactive C70S-NsPCS, the active site is occupied by a molecule of GSH. Considering that GSH was not added during crystallization, we assume that the protein has been exposed to GSH during expression in *E. coli*. Because the mutation impairs activity, the substrate is not processed. Surprisingly, it is also not released during purification. This finding suggests a tight complex between the enzyme and the substrate, in contrast to what was previously insinuated on the basis of the Michaelis–Menten analysis of the catalytic mechanism of PCS from *Silene cucubalus*.³⁵ However, in order to quantify the affinity of an enzyme for its substrate, it is required to separate binding from catalysis. For this purpose, the C70-NsPCS was taken as the variant of choice to focus on binding. However, the ideality of this variant is partly downscaled by the necessity to remove the substrate from the binding pocket through the invasive procedure of unfolding/refolding. Although successful in regaining the original conformation, the unfolding/refolding procedure showed one drawback: when applied to the wild-type, the enzymatic activity slowed down significantly. The hampered catalysis indicates that the features responsible for the enzymatic activity were not properly restored during the refolding process, at least not in all molecules. However, because no difference in the spectroscopic properties of the refolded and non-refolded proteins emerged, these unrestored features are such to be unable to affect the spectroscopic properties. We can explain the reduced velocity of cleavage in two ways: (i) the entire amount of the refolded enzyme is able to process the substrate at a lower speed or (ii) the kinetics of the catalytic reaction is not modified, but only a small amount of the refolded protein is active. We consider the second hypothesis more likely because the percentage of refolded

enzyme able to bind the substrate (as shown by the binding study) correlates well with the amount of refolded enzyme for which activity was restored. We conclude that the refolding protocol is able to generate a small amount of enzyme which is fully functional and suitable for further analysis.

Oxidation of GSH Does Not Substantially Affect Binding but It Drastically Affects Activity. The affinity of GSH to C70S-NsPCS is $5 \times 10^5 \text{ M}^{-1}$ and no cooperative behavior was observed between the two monomers. This finding is not surprising because the two binding pockets are far apart from each other. The binding constant is higher than believed in earlier studies.³³ A relatively high binding constant is important because NsPCS is found in the periplasm where the concentration of GSH is not as high as in the cytoplasm.^{34,35} However, the binding constant is not as high as expected, considering that the substrate GSH remains in the binding pocket during purification.

The enthalpic contribution to the binding interaction is very high ($-12 \text{ kcal mol}^{-1}$ for GSH binding, see Table 2), pleading for a strong interaction. Accordingly, the entropic component of the binding energy is small, which can be explained with a compensation between favorable and unfavorable contributions. On the one hand, the binding pocket is largely solvent exposed which minimizes the favorable entropic contribution due to water release. On the other hand, the binding pocket with the ligand bound in the C70S-NsPCS structure is superimposable to the empty binding pocket in the wild-type structure, indicating that the binding pocket is prepared to accommodate the substrate; hence, the unfavorable entropic contribution due to the loss of conformational degrees of freedom upon binding is also expected to be marginal. However, thermodynamic reasons are not sufficient to justify the persistence of GSH in the binding pocket during purification steps and kinetic arguments have to be evoked. In fact, if the substrate is not released, it means that the dissociation is sufficiently slow not to occur during the time of the purification. Normally, a very low dissociation rate is associated with a high affinity constant. This statement, however, is not exclusive. In fact, reminding that the association equilibrium constant can be expressed as the ratio of the association and dissociation rates as follows, $K = k_{\text{on}}/k_{\text{off}}$, the dissociation process can be slow also with a moderate equilibrium constant, provided the association process is likewise slow. According to the affinity constant of NsPCS for its substrate, the overall dissociation rate, k_{off} will be about 6 orders of magnitude slower than the overall association rate, k_{on} . Therefore, if k_{on} is sufficiently slow, k_{off} can potentially compete with the time of the purification process.

In our case, the purification process lasts about 3 days, that is, $2.6 \times 10^5 \text{ s}$. Therefore, strictly speaking, the dissociation rate has to be lower than about $4 \times 10^{-6} \text{ s}^{-1}$ to ensure the persistence of the substrate in the binding pocket during these 3 days. To allow this happening and according to an affinity constant of $5 \times 10^5 \text{ M}^{-1}$, the association process needs to be in the order of a second.

Such a slow association can be explained with the necessity of releasing the solvation water prior to binding. In general, water molecules solvating the binding pocket act as a significant obstacle to ligand binding.³⁶ In our system, this effect is enhanced by the presence of numerous charges in both the substrate and the binding pocket, which render the surface of contact highly polar and therefore strengthen the interaction

between the molecular surface and the water of solvation. However, in order to accommodate GSH in the binding pocket in view of acylation, both the substrate and the binding pocket have to be fully desolvated. The encounter of solvated molecules is a fast process; in contrast, the release of the water of solvation is a slow process,³⁶ which can be particularly slow when the water molecules are retained in a polar environment, as in NsPCS. The combination of all such processes may result in a very low overall association rate, k_{on} . Additionally, once the molecular partners are desolvated, they will interact strongly, due to their charged profile no more shielded by the solvation shell, reducing the probability of dissociation even more. The strong stabilization of the GSH in the binding pocket is confirmed by the large enthalpy of association measured by ITC (Table 2) and by the interaction energy obtained by the electrostatic calculation (Table 3). These considerations about the kinetic behavior of NsPCS will be tested in further studies.

The affinity of the enzyme for the reduced and oxidized forms of glutathione is similar within 1 order of magnitude. Moreover, the binding of both substrates to the enzyme has a similar enthalpic character, in line with the extended network of hydrogen bonds that is found between protein residues and the substrate (see Figure 4). Our results indicate that the oxidation of GSH does not substantially affect binding, although it drastically affects activity because GSSG acts as suicide inhibitor. We can conclude that γ EC-SG stabilizes the acyl-enzyme and inhibits the catalytic turnover. This hypothesis is confirmed by our success to trap the acyl-enzyme with γ EC-SG, without applying the extreme acidic conditions that had previously been assumed as necessary for the stabilization of the acyl-enzyme.¹⁹

Mechanistic Aspects of the Catalytic Reaction. To our knowledge, the only quantitative analysis of the catalytic reaction of a PCS protein up to date is the study of the catalytic mechanism of PCS from *S. cucubalus*³³ in which the dependence of the rate of PC formation on glutathione concentration yielded a K_{M} value of 6.7 mM and $k_{\text{cat}} = 0.2 \text{ s}^{-1}$ in the presence of 0.1 mM Cd^{2+} . The study of Grill et al.³³ was performed on a eukaryotic PCS and the Michaelis–Menten analysis concerns the production of PC, that is, it is applied to a reaction that includes both peptidase and transpeptidase reactions. Instead, our study is performed on a prokaryotic PCS and concerns the deglycination of GSH, that is, in our case, the reaction consists only in the peptidase activity. Moreover, the effect of oxygen on catalysis was not considered in the study of Grill et al.,³³ and we show here that oxygen plays an important role for the activity of NsPCS.

Despite the catalytic process monitored in this earlier study is different from ours, the Michaelis–Menten parameters are similar. In fact, our analysis of the catalytic reaction of NsPCS leads to a Michaelis–Menten constant K_{M} of 0.2 mM and a turnover number k_{cat} of 3.5 s^{-1} , which are 1 order of magnitude lower and 1 order of magnitude higher than the respective values reported in the study of the catalytic mechanism of PCS from *S. cucubalus*.³³ This similarity can be rationalized by our finding that the rate-limiting step is most likely the deacylation reaction, which is common to both catalytic processes.

We performed QM/MM calculations to dissect the enzymatic mechanism and to identify the transition states. The comparison between the energy barriers obtained for the acylation and the deacylation leads us to conclude that the deacylation is the slowest chemical step. In the literature, the experimental rate measured for the cleavage of peptidic

substrates by papain³⁷ is about $2 \times 10^3 \text{ s}^{-1}$ which is within a factor of six in agreement with our calculated rate $1.3 \times 10^4 \text{ s}^{-1}$. Also in the case of NsPCS, the catalytic rate k_{cat} of 3.5 s^{-1} , resulting from our Michaelis–Menten analysis of the peptidase reaction, is in good agreement with our calculated rate for the deacylation of 6.3 s^{-1} . Because the measured rate reflects the rate-limiting step, the good agreement between the experimental and the calculated rate suggests that deacylation is the rate-limiting step of the peptidase reaction catalyzed by NsPCS.

Our findings indicate that the binding of the substrate to the active site is a high-energy-barrier process, both in association and in dissociation. In fact, the binding of the substrate implies the energy-costly disruption of an extended and well-ordered network of water molecules solvating the binding site. On the other side, the binding of the substrate is stabilized by strong electrostatic interactions as confirmed by the high enthalpy, which implies a high energy barrier also for the complex dissociation. The kinetic consequences of such an energetic profile consist in a slow dissociation rate and a comparatively slow association rate, consistent with the moderate binding constant that was measured.

NsPCS Activity is Sensitive to the Redox State of the Substrate, Suggesting a Potential Function of NsPCS in Cyanobacteria. Our electrostatic calculations contribute to rationalize the catalytic reaction. In fact, on the one hand, we could show that the deglycination of GSH leads to a product (γEC), which binds less strongly than the substrate and therefore can more easily leave the catalytic site to be replaced by a new unprocessed substrate. The cleavage disrupts a covalent bond in the substrate, leading to the destabilization of the complex. Moreover, the cleavage induces an amino group in the cleaved-off glycine which tends to be positively charged, leading to the repulsion of the glycine from the positively charged binding pocket. On the other hand, the tighter complex of NsPCS with GSH compared to the one with the cleaved form γEC appears to be stable enough to allow efficient cleavage also at low concentrations of GSH. A tight complex is in line with the location of NsPCS in the periplasm, where the concentration of GSH is not as high as in the cytoplasm.^{34,35}

Our binding study shows that GSH binds the enzyme also when the catalytic cysteine is mutated into serine, as indicated by the presence of the uncleaved substrate GSH in the binding pocket of C70S-NsPCS, revealed by crystallography. The outcome of the electrostatic calculations further explains this finding. In fact, because no deglycination occurs in the inactive serine mutant, the complex will not be destabilized by the loss of glycine and GSH remains trapped.

Our docking simulations show two interesting features. Particularly inspiring is the simulation in which one active site is occupied by GSH, that is, the intact substrate, and the other with γEC covalently bound to Cys70, that is, the state in which the glycine moiety is cleaved off. At the active site with bound GSH, a second GSH molecule is prevented from approaching the active site and thus oxidation of GSH to GSSG cannot occur. At the active site with γEC bound, a second GSH molecule is able to approach the pocket and thus the disulfide bond formation between the second GSH molecule and the bound γEC to form $\gamma\text{EC-SG}$ may occur. Accordingly, in the crystal structure of acyl-NsPCS, $\gamma\text{EC-SG}$ is found and not γEC . These observations explain also why in the binding site of the crystal structure of C70S-NsPCS, where the substrate cannot

be cleaved and the acyl-enzyme is not formed, the reduced GSH and not the oxidized form GSSG is found. Furthermore, the different reactivity of NsPCS for the reduced and the oxidized forms of glutathione indicates that NsPCS is sensitive to the redox state of the substrate leading to the conclusion that the activity of NsPCS depends on the redox potential of the solution. Namely, under reducing conditions, glutathione is present in its reduced form GSH. GSH can bind to NsPCS and is cleaved into γEC and glycine. Thus, under reducing conditions, free glycine is continuously produced. If the conditions are getting more oxidizing, the oxidized form of glutathione GSSG builds up. GSSG binds to NsPCS and one of its two glycines is cleaved off. The so-generated $\gamma\text{EC-SG}$ remains covalently bound to the enzyme and inhibits the enzyme as we have shown by kinetic NMR experiments (Figure 5). Alternatively, GSH can bind to the acyl-enzyme via a disulfide bond forming $\gamma\text{EC-SG}$. The result would be the same: NsPCS is inhibited by $\gamma\text{EC-SG}$ and no further production of free glycine occurs. Therefore, because NsPCS is not active anymore under oxidizing conditions, GSSG accumulates in the periplasm. In other words, if the redox conditions are sufficiently reducing to maintain glutathione in the reduced form (GSH), the cleavage reaction occurs and glycine is produced by the activity of PCS; instead, in oxidizing conditions, when GSSG is formed, the enzyme is blocked. This scenario suggests that NsPCS may be involved in redox sensing, opening a new hypothesis in the search of the physiological role of the PCS-like enzyme.

These considerations allow further speculation about the physiological role of NsPCS. The analysis of the sequence of NsPCS using SignalP (<https://services.healthtech.dtu.dk/service.php?SignalP-5.0>)³⁸ shows that the enzyme has an N-terminal Sec signal peptide, indicating that the enzyme is secreted into the periplasm. The genome of *Nostoc* sp. PCC 7120 is sequenced and annotated (NCBI Accession code: NC_003272²⁸). The gene for NsPCS is located in an operon together with the genes for a potential ABC transporter and a hypothetical protein, which seems to be a membrane protein with homology to ABC transporters (see analysis in the Supporting Information). Thus, the following scenario seems possible: one ABC transporter exports GSH to the periplasm, and the other ABC transporter imports the glycine that results from the NsPCS activity to the cytoplasm. If the conditions in the periplasm get oxidizing, the flux of glycine into the cell will stop, providing a signal inside the cell, for example, to switch between oxic and anoxic metabolism. Alternatively, the hypothetical protein may function as a receptor sensing the glycine level directly. Another option would be that GSSG would be the signaling molecule, which might be sensed directly in the periplasm or after being imported into the cytoplasm. The idea that NsPCS is a part of a redox signaling chain could be tested experimentally and may solve the mystery of the function of PCS-like enzymes. This hypothesis may also explain why PCS is not found in insects or vertebrates which are strictly aerobic, but can be found in protozoa or nematodes, which are also able to survive under anoxic conditions.

Furthermore, the rationalization of the binding mode of the substrate with NsPCS allows also speculation about the evolution of genuine PCS in higher organisms because the approach of a second GSH molecule and the formation of a $\gamma\text{EC-SG}$ may sporadically lead to transpeptidation and thus to the formation of phytochelatin, which was found as a low-yield

product of NsPCS.^{10,12,23} If this hypothesis is correct, the potential function of PCS-like enzymes as a redox-sensor may have led to a transpeptidase activity in the genuine PCS and the formation of longer PCs during evolution.

CONCLUSIONS

The enzyme PCS in plants is known to synthesize the metal chelating peptide PC and thus is involved in metal homeostasis and detoxification. The bacterial homologues of this enzyme, so-called PCS-like enzymes, can serve as a structural model for PCS. However, the function of these PCS-like enzymes in bacteria is not known. In this work, we combined structural, spectroscopical, thermodynamic, and theoretical techniques to investigate the mechanism of the PCS-like enzyme NsPCS from *Nostoc* sp. We delineated the energetic profile of the catalytic reaction whose rate-limiting step appears to be the deacylation. The high energy barriers are compatible with the low reaction rate. Several interesting features have been uncovered by our study. When the active-site cysteine is mutated into serine, the substrate GSH binds to the protein such that GSH was co-purified with the mutant enzyme and crystallized. Our analysis indicates that the substrate binds tightly and shows a slow exchange. Interestingly, in the crystal, no indication of oxidation of the substrate GSH bound to the mutant enzyme is found (i.e., no GSSG formation), even though the crystal was grown under aerobic conditions. In contrast, in the crystal structure of the acyl-enzyme (an intermediate of the catalytic cycle), γ EC-SG is bound. We explained this behavior by the differences in the electrostatics between GSH and γ EC as corroborated by Monte Carlo simulations. These findings prompted us to test whether GSH and GSSG can both serve as a substrate for NsPCS. Our results were unexpected. In fact, we found that GSH is cleaved into γ EC and glycine under an enzymatic turnover. Instead when GSSG binds to the enzyme, one glycine is cleaved off resulting in γ EC-SG covalently bound to the enzyme and the reaction stops. From this finding, we conclude that NsPCS is active under reducing conditions, but gets inhibited under oxidizing conditions. Our observation together with the analysis of the genetic context of the NsPCS gene and the fact that NsPCS has a signal peptide directing the enzyme to the periplasm lead us to suggest that NsPCS may be a part of a signaling system that senses the redox state of the periplasm.

From an evolutionary point of view, PCS-like enzymes may be considered as precursors of the genuine PCSs found in plants, that is, the enzymes that form PC by transpeptidation. Our finding that γ EC-SG is bound stably to NsPCS and basically inhibits the enzyme is also interesting in this evolutionary context. In fact, one could imagine that the close proximity between the covalently bound γ EC and a second glutathione molecule in γ EC-SG may have sporadically led to transpeptidation, which eventually became a new function.

Taken together, our biophysical analysis allows us to characterize NsPCS as a relatively slow enzyme which may work as a part of a redox sensing system in cyanobacteria. Moreover, we propose a mechanism how PCS-like enzymes may have gained the function of transpeptidation.

MATERIALS AND METHODS

Cloning. Wild-type NsPCS gene (aln0975) lacking the natural signal sequence (Δ ssNsPCS) was amplified using the primer pair NsPCS_for 5'-TTA TTA CAT ATG CAA ACT TTG ACA CTT

TCA CC-3' and NsPCS_rev 5'-TAA TAA CTC GAG CTA ATC TTG TGT TTT ACT TAC-3'. The purified PCR product was ligated with the plasmid p109³⁹ using NdeI and XhoI insertion sites, generating a plasmid coding for an N-terminally His6-lysozyme-tagged fusion protein. The plasmid carrying the wild-type gene served as a template for standard QuikChange (Stratagene) mutagenesis using the complementary primer set C70S_NsPSC_for 5'-GTT AAT CAA GCT TAC TCT GGT GTA GCT AGT ATA ATT ATG-3' and C70S_NsPSC_rev 5'-CAT AAT TAT ACT AGC TAC ACC AGA GTA AGC TTG ATT AAC-3' to generate a variant of NsPCS in which the catalytic Cys is mutated into a Ser. The correct integrity of the gene fragment and the introduction of the mutation were confirmed by DNA sequencing.

Protein Expression and Purification. Proteins were recombinantly expressed in Rosetta 2 (DE3) plyS cells harboring the respective plasmids. Ampicillin-supplemented (100 μ g mL⁻¹) LB broth was inoculated with an overnight culture at an OD₆₀₀ of 0.02. Cells were grown until the mid-log phase at 310 K before the temperature was lowered to 293 K and gene expression was induced with 0.5 mM IPTG overnight. Harvested cells were resuspended in 150 mM phosphate buffer pH 8.0, 300 mM NaCl (buffer A) supplemented with 100 μ M phenylmethylsulfonylfluoride and disrupted with a microfluidizer (Microfluidics). Cleared lysate (100,000 g, 30 min) was passed over a HiTrap chelating column (GE Healthcare) charged with NiSO₄ using an AKTA prime system (GE Healthcare). The column was developed with a gradient to buffer B (buffer A containing 500 mM imidazole), and fractions were analyzed by sodium dodecyl sulfate-polyacrylamide gel electrophoresis. NsPCS-containing fractions were pooled in a dialysis bag to which His-tagged human rhinovirus 3C peptidase (in house production) was added in a ratio of 1:40. Dialysis against 50 mM 4-(2-hydroxyethyl)-1-piperazineethanesulfonic acid (HEPES) pH 8.0, 150 mM NaCl was carried out overnight at 277 K. After the dialysis, the recovered protein was again passed over a Ni-charged HiTrap chelating column to remove uncleaved protein and peptidase. The flow-through was concentrated and applied to size-exclusion chromatography using a Superdex 75 column (GE Healthcare) in the same buffer. Fractions containing pure protein were concentrated to 25 mg mL⁻¹ and either flash frozen in liquid nitrogen prior to storage at -80 °C or used immediately.

Protein Crystallization. Initial crystallization conditions were identified using commercial screens (Qiagen) and a Phoenix robot (Art Robbins Instruments). Initial hits were optimized using a hanging drop vapor diffusion setup with a 500 μ L reservoir and drops consisting of 1 μ L of protein (12 mg mL⁻¹) and 1 μ L of reservoir solution. Large rod-shaped crystals were obtained using 17% PEG 8000, 0.1 M MES pH 5.5, and 0.2 M calcium acetate as mother liquor. The acyl-enzyme was obtained by co-crystallization of wild-type NsPCS protein (12 mg mL⁻¹) preincubated with glutathione at a final concentration of 5 mM using the same mother liquor composition. All crystals grew within 2 days to an approximate size of 150 \times 150 \times 600 μ m. Prior to data collection, crystals were washed briefly with cryoprotectant containing mother liquor supplemented with 20% glycerol before plunging into liquid nitrogen.

Data Collection. Diffraction data have been collected on BL14.1 of the BESSY II electron storage ring (Berlin-Adlershof, Germany) on a Rayonix MX-225 CCD and Pilatus 6M detector.⁴⁰ C70S-NsPCS mutant data were collected in nonoverlapping 1° (Rayonix MX-225 CCD) and the acyl-enzyme in nonoverlapping 0.1° (Pilatus 6M) oscillation images, respectively.

Data were integrated with XDS,⁴¹ scaled with AIMLESS from CCP4 suite.⁴² A value of 0.5 of CC1/2⁴³ in the highest shell was chosen as the cutoff criterion in respect to completeness of data. Data collection statistics are summarized in Table 1.

Structure Determination and Refinement. The crystal structure of C70S-NsPCS was determined by molecular replacement with phenix.phaser⁴⁴ searching with a monomer of NsPCS (PDB ID: 2BTW)¹⁹ as a model. Initial phases for the acyl-enzyme structure were obtained by molecular replacement searching with a monomer of the C70S mutant. Iterative refinement was carried out with phenix-re-

fine⁴⁴ and manual adjustments by hand were done in Coot.⁴⁵ Coordinates and structure factor amplitudes have been deposited in the Protein Data Bank⁴⁶ with access codes indicated in Table 1.

Protein Unfolding and Refolding. NsPCS variants were unfolded at room temperature in buffer containing 6 M guanidinium chloride (GdmCl), 50 mM Na₃PO₄, and 10% glycerol at pH 8. As the final protein concentration, 100 μg mL⁻¹ was obtained. For refolding, the obtained solution was dialyzed at 277 K overnight against a buffer containing 3 M GdmCl and then for at least 4 h against buffers containing 1 M GdmCl and no GdmCl, respectively.

ITC Measurement. ITC measurements were performed using a Nano-ITC instrument (TA instruments). Prior to measurements, the buffer for sample preparation (50 mM Na₃PO₄ at pH 8, and 300 mM NaCl) was degassed in an ultrasonic bath for 5 min and kept under an argon atmosphere. The concentrations of refolded proteins were adjusted to 1 mM (C70S-NsPCS) and 0.1 mM (wt-NsPCS) with respective concentrations for ligand solutions of 1 mM GSSG and 0.5 mM GSH prepared in buffer. Measurements were performed at 303.15 K without stirring to prevent protein aggregation. The time interval between two successive ligand injections was extended to ensure equilibration. Each 500 s 2.01 μL injections were made for C70S-NsPCS and injections with varied volumes were made for wt-NsPCS (injections 1–2: 0.17 μL, injections 3–8: 0.52 μL, injections 9–10: 0.75 μL, injections 11–13: 0.98 μL, and injections 15–16: 2.01 μL). The syringe and the instrument cell were purged with argon to prevent any trace of oxygen. The data were processed using NanoAnalyze (TA instruments) and corrected by subtracting the enthalpy of dilution of the ligand in buffer. The measured differential heat per mole, dH, was analyzed according to the one-site-differential binding model⁴⁷ and fitted to the equation

$$dH = \frac{\Delta H \Delta M_T \cdot \frac{K_a [X]}{1 + K_a [X]} \cdot \left(1 - \frac{K_a [X]}{1 + K_a [X]}\right) + \Delta h_{\text{dil}} \cdot [X]}{[X] + M_T \cdot \left(\frac{K_a [X]}{1 + K_a [X]} - \left(\frac{K_a [X]}{1 + K_a [X]}\right)^2\right)}$$

where ΔH is the enthalpy change upon binding, K_a is the association equilibrium constant, and Δh_{dil} is the enthalpy of dilution of the binding species.

The free ligand concentration [X] is calculated as follows

$$[X] = M_T \cdot \frac{\frac{X_T}{M_T} - \frac{1}{M_T \cdot K_a} - 1 + \left(\left(1 + \frac{1}{M_T \cdot K_a} - \frac{X_T}{M_T}\right)^2 + \frac{4 \cdot \frac{X_T}{M_T}}{M_T \cdot K_a} \right)^{1/2}}{2}$$

where M_T and X_T are the total receptor concentration and the total ligand concentration, respectively, given by

$$M_T = p \cdot M_{t_0} \cdot (e^{\sum dV_{\text{injected}}/V_0})$$

$$X_T = X_{t_0} \cdot (1 - e^{\sum dV_{\text{injected}}/V_0})$$

where M_{t₀} and X_{t₀} are the respective concentrations before injections, dV_{injected} is the injection volume at a time, and V₀ is the initial volume within the measured cell. The model allows the correction of the total receptor concentration M_T to estimate the concentration of the receptor that is truly able to bind the ligand (parameter *p*).

Thermophoresis. The microscale thermophoresis experiments have been performed with the Monolith NT.LabelFree (Nanotemper Technologies). The assay buffer was 50 mM HEPES pH 8 with 100 mM NaCl.

The samples were left to incubate for 5 min being loaded into the standard treated capillaries (Nanotemper Technologies). Data collection was carried out at 25 °C. The solution inside the capillary is locally heated with a focused IR-laser, which is coupled into the path of exciting light using a hot mirror, at 20, 30, and 40% power.

The sample is excited at 270 nm. The resulting fluorescence from the aromatic residues of the protein is detected with a photodiode at 370 nm. The IR-laser is switched on after 5 s from the beginning of the detection and let on for 30 s. The fluorescence intensity detected

at the beginning of the heating procedure is called F_{cold} and the fluorescence detected during the heating procedure is called F_{hot}. The normalized fluorescence F_{norm} = F_{hot}/F_{cold} was plotted against the ligand concentration. Data analysis was carried out using MO.Affinity Analysis v2.3 (Nanotemper Technologies).

NMR Spectroscopy. NMR measurements were carried out on a Bruker AVANCE III 600 MHz spectrometer with a sample volume of 600 μL. Spectra were recorded at 600.2 MHz 1H frequency and a calibrated temperature of 303.15 K. Data processing was performed with NMRPipe.⁴⁸ Buffer conditions were 50 mM phosphate buffer pH 8.0. The NMR buffer was degassed in an ultrasonic bath under vacuum for 5 min. All solutions were prepared and stored under an argon atmosphere, and all experimental steps were performed under an argon atmosphere to prevent the oxidation of glutathione. To compare the activity of NsPCS with different substrates, the concentration of GSH and GSSG was 600 μM. For the Michaelis–Menten kinetics, different samples of GSH were prepared with concentrations of 500 μM, 600 μM, 700 μM, 800 μM, 900 μM, 1 mM, 1.5 mM, and 3 mM of GSH. To compare the activity of wt-NsPCS and refolded wt-NsPCS, the concentration of GSH was 1 mM, and 300 mM NaCl was added to the buffer. All samples contained 0.1 mM sodium trimethylsilylpropanesulfonate (DSS) and 10% D₂O. In all cases, the reaction was started by adding 30 nM enzyme to the substrate solution. Each sample was rapidly collected and poured in a NMR tube purged with argon using a syringe purged with argon as well. An NMR spectrum was taken roughly every 110 s. The progress of the observed reaction was monitored using the increasing glycine signal. The DSS signal was used as reference for the glycine concentration. 1D spectra were normalized by the DSS concentration, number of scans, and length of the 90° proton pulse. To perform the Michaelis–Menten analysis, the time traces describing the accumulation of free glycine have been fitted with one exponential term for each substrate concentration. The initial increase of the exponential curve could be approximated with a straight line whose slope gives the initial velocity of the reaction in the presence of a given concentration of substrate. The initial velocities were then plotted versus the corresponding substrate concentrations.

Computational Preparation of Protein Structures. Protein structures for all simulations were prepared with the program CHARMM⁴⁹ using the CHARMM27⁵⁰ force field. Present disulfide bonds were set. The protein was surrounded by a 6 Å explicit water layer, whereas available water molecules from the crystal structure were included. All hydrogen atoms were added with the HBUILD routine in CHARMM. An optimization of all water molecules was performed to adapt to the protein, followed by an optimization of all hydrogen atoms. Protonation probabilities of prepared structures were calculated using MEAD^{51,52} and GMCT.⁵³ Thereby, a Metropolis Monte Carlo titration algorithm^{54,55} is applied on a Poisson–Boltzmann continuum electrostatic model. Protonation probabilities are dependent on pH and were calculated in steps of 0.25 in the pH range 0–14. 200 equilibration scans and 100,000 production scans were performed at 300 K, with 0.1 M ionic strength and permittivity 4 for protein and 80 for solvent. The protonation states of titratable groups were set according to this calculation (see Table S2 in the Supporting Information). For investigation of NsPCS, the crystal structure of C70S-NsPCS and acyl-NsPCS were used. For the simulations, the active site serine of C70S-NsPCS was mutated to cysteine with PyMOL (The PyMOL Molecular Graphics System, Version 2.4.0a0 Schrödinger, LLC). Simulations for papain were performed on a crystal structure with synthetic inhibitor E-64-c (2.1 Å, PDB ID: 1PE6).⁵⁶ Analogously to other studies, the substrate Phe-Ser-Ile with acetylated N-terminus and N-methylated C-terminus was used.^{32,57} The substrate in the crystal structure 1PE6 is attached covalently to papain. For modeling of the noncleaved substrate, a structure with a substrate analogue (2.8 Å, PDB ID: 1PAD)²⁰ was superimposed. The modeled substrate was optimized with CHARMM.

Ligand Binding Calculations. Docking of the ligand GSH to NsPCS variants was performed with MCMAP,³¹ which applies Monte Carlo sampling of ligand movements within the electrostatic field of a

receptor. For each simulation, 100,000 runs were performed with 1,000,000 Monte Carlo steps at 300 K. The initial center of mass separation of the protein and the ligand was set to 130 Å, the maximum separation was set to 180 Å. The Monte Carlo run was reset after 50 rejected steps in a row. The maximal displacement was set to 3 Å, the maximal rotation was set to 5 rad. Electrostatic potential maps with 2 Å grid spacing for the outer potential grid and with 1 Å for the inner potential grid were used. APBS⁵⁸ was used for electrostatic potential map calculations, with permittivity 4 for protein and 80 for solvent at 300 K. An ion concentration of 0.1 M was adjusted, with a single positive or a single negative charge and radius 2.0 Å. The solvent radius was set to 1.4 Å. For calculating the density of GSH around PCS, the center of mass of GSH was recorded every 100th Monte Carlo step. The interaction energies between PCS and the various ligands were calculated with the program solinprot from the MEAD package. The dielectric constants of the protein and the water were set at 4 and 80, respectively. The ionic strength was set to 0.1 M.

Reaction Path Search Simulation. The reaction path search was performed with a QM/MM model within pDynamo⁵⁹ and the CHARMM27⁵⁰ force field in combination with ORCA^{60,61} on the B3LYP:6-31+G** level.^{62–65}

The protein structures, which were prepared with CHARMM, were treated with MM, whereas a small relevant region for the catalysis was treated with QM. The QM/MM boundary was treated with a link-atom scheme and electrostatic embedding, as implemented in pDynamo. All atoms in the QM region and within an 8 Å MM layer around the QM region were set flexible. Beyond that, a linearly increasing force constant from 0 to 12 kcal mol⁻¹ Å⁻¹ was applied for further 8 Å on the atoms. All other atoms were restraint with 12 kcal mol⁻¹ Å⁻¹. The sidechains included in the QM region were truncated between C α and C β . Exceptions are mentioned explicitly. For NsPCS, the QM region consisted of the catalytic triad residues Cys70, His183 (protonated at position ϵ), and Asp201. Furthermore, Gln64 (truncated between C β and C γ) for the oxyanion hole and Arg173 (truncated between C γ and C δ) were included. The complete residues Gly (only present for the acylation reaction), and Cys of the substrate GSH were included into the QM region, with addition of the atoms C δ , O ϵ , and C γ with both hydrogen atoms of residue γ Glu. For the acylation reaction, an interacting water molecule near the carboxyl group of the substrate was included. For the deacylation reaction two interacting water molecules were included. All remaining parts belong to the MM region.

For papain, the QM region contained the catalytic triad residues Cys25, His159 (protonated on position ϵ), and Asn175. Furthermore, Gln19 (truncated between C β and C γ) for the oxyanion hole was included. The complete residue Ser of the substrate together with backbone atoms O and C of residue Phe (only present for the acylation reaction), and atoms N, H, C α , and H α of residue Ile were included into the QM region. For the deacylation reaction, two interacting water molecules were included.

Reaction path search was performed with PyCPR.^{29,66} Reaction path exploration was performed by adiabatic surface scans with an root-mean-square gradient criterion of 0.002 kcal mol⁻¹ Å⁻¹, and structures of stable states were optimized by a conjugate gradient minimizer with the root-mean-square gradient threshold set to 0.002 kcal mol⁻¹ Å⁻¹. As collective variables for the adiabatic scans, the proton transfer from the cysteine or serine nucleophile to the catalytic histidine and the nucleophilic attack of the cysteine or serine nucleophile on the substrate were used. Initial path estimates between the stable states were obtained by a growing string method,⁶⁷ as implemented in pDynamo. Transition paths were obtained by PyCPR. States were characterized by vibrational frequency calculations.

■ ASSOCIATED CONTENT

SI Supporting Information

The Supporting Information is available free of charge at <https://pubs.acs.org/doi/10.1021/acschembio.1c00941>.

Sequence alignments, sequence analysis of the NsPCS operon, protonation probability of the catalytic histidine, list of models used for the simulations, and protonation states of all the titratable residues (PDF)

■ Accession Codes

PDB IDs: 6TH5—wild-type NsPCS; 6THO—wild-type NsPCS with covalently bound γ EC-SG; 6TJL—mutant C70S-NsPCS with noncovalently bound GSH.

■ AUTHOR INFORMATION

Corresponding Author

Elisa Bombarda — Department of Biochemistry, University of Bayreuth, 95440 Bayreuth, Germany; orcid.org/0000-0002-1385-3710; Email: elisa.bombarda@uni-bayreuth.de

Authors

Florian J. Gisdon — Department of Biochemistry, University of Bayreuth, 95440 Bayreuth, Germany; Computational Biochemistry, University of Bayreuth, 95440 Bayreuth, Germany

Christian G. Feiler — Department Structure and Function of Proteins, Helmholtz Centre for Infection Research, 38124 Braunschweig, Germany

Oxana Kempf — Department of Biochemistry, University of Bayreuth, 95440 Bayreuth, Germany

Johannes M. Foerster — Computational Biochemistry, University of Bayreuth, 95440 Bayreuth, Germany; orcid.org/0000-0003-0442-9413

Jonathan Haiss — Department of Biochemistry, University of Bayreuth, 95440 Bayreuth, Germany

Wulf Blankenfeldt — Department Structure and Function of Proteins, Helmholtz Centre for Infection Research, 38124 Braunschweig, Germany; Institute for Biochemistry, Biotechnology and Bioinformatics, Technische Universität Braunschweig, 38106 Braunschweig, Germany; orcid.org/0000-0001-9886-9668

G. Matthias Ullmann — Computational Biochemistry, University of Bayreuth, 95440 Bayreuth, Germany; orcid.org/0000-0002-6350-798X

Complete contact information is available at:

<https://pubs.acs.org/doi/10.1021/acschembio.1c00941>

■ Notes

The authors declare no competing financial interest.

■ ACKNOWLEDGMENTS

We thank K. Schweimer for the highly competent support during NMR experiments and S. Shanmugaratnam for the great and friendly all-around technical support. We are very thankful to S. Clemens for fruitful discussions at the beginning of this project. Diffraction data have been collected on BL14.1 at the BESSY II electron storage ring operated by the Helmholtz-Zentrum Berlin.⁶⁸ The present work was supported by the DFG grant BO 3578/1 and DFG Priority Program 1927 through grant UL 174/9.

■ REFERENCES

- (1) Cobbett, C.; Goldsbrough, P. Phytochelatins and Metallothioneins: Roles in Heavy Metal Detoxification and Homeostasis. *Annu. Rev. Plant Biol.* **2002**, *53*, 159–182.
- (2) Gekeler, W.; Grill, E.; Winnacker, E.-L.; Zenk, M. H. Survey of the Plant Kingdom for the Ability to Bind Heavy Metals through Phytochelatins. *Z. Naturforsch., C: J. Biosci.* **1989**, *44*, 361–369.

- (3) Filiz, E.; Saracoglu, I. A.; Ozyigit, I. I.; Yalcin, B. Comparative Analyses of Phytochelatin Synthase (PCS) Genes in Higher Plants. *Biotechnol. Equip.* **2019**, *33*, 178–194.
- (4) Clemens, S.; Kim, E. J.; Neumann, D.; Schroeder, J. I. Tolerance to Toxic Metals by a Gene Family of Phytochelatin Synthases from Plants and Yeast. *EMBO J.* **1999**, *18*, 3325–3333.
- (5) Cazalé, A. C.; Clemens, S. Arabidopsis Thaliana Expresses a Second Functional Phytochelatin Synthase. *FEBS Lett.* **2001**, *507*, 215–219.
- (6) Vatamaniuk, O. K.; Bucher, E. A.; Ward, J. T.; Rea, P. A. Worms take the “phyto” out of ‘phytochelatin’. *Trends Biotechnol.* **2002**, *20*, 61–64.
- (7) Ray, D.; Williams, D. L. Characterization of the Phytochelatin Synthase of *Schistosoma mansoni*. *PLoS Neglected Trop. Dis.* **2011**, *5*, No. e1168.
- (8) Clemens, S. Evolution and Function of Phytochelatin Synthases. *J. Plant Physiol.* **2006**, *163*, 319–332.
- (9) Marchler-Bauer, A.; Anderson, J. B.; DeWeese-Scott, C.; Fedorova, N. D.; Geer, L. Y.; He, S.; Hurwitz, D. I.; Jackson, J. D.; Jacobs, A. R.; Lanczycki, C. J.; et al. CDD: A Curated Entrez Database of Conserved Domain Alignments. *Nucleic Acids Res.* **2003**, *31*, 383–387.
- (10) Harada, E.; von Roepenack-Lahaye, E.; Clemens, S. A cyanobacterial protein with similarity to phytochelatin synthases catalyzes the conversion of glutathione to γ -glutamylcysteine and lacks phytochelatin synthase activity. *Phytochemistry* **2004**, *65*, 3179–3185.
- (11) Tsuji, N.; Nishikori, S.; Iwabe, O.; Shiraki, K.; Miyasaka, H.; Takagi, M.; Hirata, K.; Miyamoto, K. Characterization of Phytochelatin Synthase-like Protein Encoded by Alr0975 from a Prokaryote, *Nostoc* Sp. PCC 7120. *Biochem. Biophys. Res. Commun.* **2004**, *315*, 751–755.
- (12) Rea, P. A. Phytochelatin synthase, papain’s cousin, in stereo. *Proc. Natl. Acad. Sci. U.S.A.* **2006**, *103*, 507–508.
- (13) Bellini, E.; Varotto, C.; Borsò, M.; Rugnini, L.; Bruno, L.; Sanità di Toppi, L. Eukaryotic and Prokaryotic Phytochelatin Synthases Differ Less in Functional Terms than Previously Thought: A Comparative Analysis of *Marchantia polymorpha* and *Geitlerinema* Sp. PCC 7407. *Plants* **2020**, *9*, 914–12.
- (14) Rawlings, N. D.; Waller, M.; Barrett, A. J.; Bateman, A. MEROPS: The Database of Proteolytic Enzymes, Their Substrates and Inhibitors. *Nucleic Acids Res.* **2014**, *42*, D503–D509.
- (15) Rawlings, N. D.; Barrett, A. J.; Thomas, P. D.; Huang, X.; Bateman, A.; Finn, R. D. The MEROPS Database of Proteolytic Enzymes, Their Substrates and Inhibitors in 2017 and a Comparison with Peptidases in the PANTHER Database. *Nucleic Acids Res.* **2018**, *46*, D624–D632.
- (16) Barrett, A. J.; Rawlings, N. D. Evolutionary Lines of Cysteine Peptidases. *Biol. Chem.* **2001**, *382*, 727–733.
- (17) Rea, P. A. Phytochelatin Synthase: Of a Protease a Peptide Polymerase Made. *Physiol. Plant.* **2012**, *145*, 154–164.
- (18) Rea, P. A. Phytochelatin Synthase. *eLS* **2020**, *3*, 1–15.
- (19) Vivares, D.; Arnoux, P.; Pignol, D. A Papain-like Enzyme at Work: Native and Acyl-Enzyme Intermediate Structures in Phytochelatin Synthesis. *Proc. Natl. Acad. Sci. U.S.A.* **2005**, *102*, 18848–18853.
- (20) Drenth, J.; Kalk, K. H.; Swen, H. M. Binding of Chloromethyl Ketone Substrate Analogs to Crystalline Papain. *Biochemistry* **1976**, *15*, 3731–3738.
- (21) Vernet, T.; Tessier, D. C.; Chatellier, J.; Plouffe, C.; Lee, T. S.; Thomas, D. Y.; Storer, A. C.; Ménard, R. Structural and Functional Roles of Asparagine 175 in the Cysteine Protease Papain. *J. Biol. Chem.* **1995**, *270*, 16645–16652.
- (22) Romanyuk, N. D.; Rigden, D. J.; Vatamaniuk, O. K.; Lang, A.; Cahoon, R. E.; Jez, J. M.; Rea, P. A. Mutagenic Definition of a Papain-like Catalytic Triad, Sufficiency of the N-Terminal Domain for Single-Site Core Catalytic Enzyme Acylation, and C-Terminal Domain for Augmentative Metal Activation of a Eukaryotic Phytochelatin Synthase. *Plant Physiol.* **2006**, *141*, 858–869.
- (23) Tsuji, N.; Nishikori, S.; Iwabe, O.; Matsumoto, S.; Shiraki, K.; Miyasaka, H.; Takagi, M.; Miyamoto, K.; Hirata, K. Comparative Analysis of the Two-Step Reaction Catalyzed by Prokaryotic and Eukaryotic Phytochelatin Synthase by an Ion-Pair Liquid Chromatography Assay. *Planta* **2005**, *222*, 181–191.
- (24) Li, M.; Barbaro, E.; Bellini, E.; Saba, A.; Sanità di Toppi, L.; Varotto, C. Ancestral Function of the Phytochelatin Synthase C-Terminal Domain in Inhibition of Heavy Metal-Mediated Enzyme Overactivation. *J. Exp. Bot.* **2020**, *71*, 6655–6669.
- (25) Ruotolo, R.; Peracchi, A.; Bolchi, A.; Infusini, G.; Amoresano, A.; Ottonello, S. Domain Organization of Phytochelatin Synthase. Functional Properties of Truncated Enzyme Species Identified by Limited Proteolysis. *J. Biol. Chem.* **2004**, *279*, 14686–14693.
- (26) Clemens, S.; Peřšoh, D. Multi-Tasking Phytochelatin Synthases. *Plant Sci.* **2009**, *177*, 266–271.
- (27) Clay, N. K.; Adio, A. M.; Denoux, C.; Jander, G.; Ausubel, F. M. Glucosinolate Metabolites Required for an Arabidopsis Innate Immune Response. *Science* **2009**, *323*, 95–101.
- (28) Kaneko, T.; Nakamura, Y.; Wolk, C. P.; Kuritz, T.; Sasamoto, S.; Watanabe, A.; Iriguchi, M.; Ishikawa, A.; Kawashima, K.; Kimura, T.; et al. Complete Genomic Sequence of the Filamentous Nitrogen-Fixing Cyanobacterium *Anabaena* Sp. Strain PCC 7120. *DNA Res.* **2001**, *8*, 205–213.
- (29) Culka, M.; Gisdon, F. J.; Ullmann, G. M. Computational Biochemistry-Enzyme Mechanisms Explored. *Advances in Protein Chemistry and Structural Biology*, 1st ed.; Elsevier Inc., 2017; Vol. 109.
- (30) Laskowski, R. A.; Swindells, M. B. LigPlot+: Multiple Ligand-Protein Interaction Diagrams for Drug Discovery. *J. Chem. Inf. Model.* **2011**, *51*, 2778–2786.
- (31) Foerster, J. M.; Poehner, I.; Ullmann, G. M. MCMAP-A Computational Tool for Mapping Energy Landscapes of Transient Protein-Protein Interactions. *ACS Omega* **2018**, *3*, 6465–6475.
- (32) Harrison, M. J.; Burton, N. A.; Hillier, I. H. Catalytic Mechanism of the Enzyme Papain: Predictions with a Hybrid Quantum Mechanical/Molecular Mechanical Potential. *J. Am. Chem. Soc.* **1997**, *119*, 12285–12291.
- (33) Grill, E.; Löffler, S.; Winnacker, E.-L.; Zenk, M. H. Phytochelatin, the heavy-metal-binding peptides of plants, are synthesized from glutathione by a specific γ -glutamylcysteine dipeptidyl transpeptidase (phytochelatin synthase). *Proc. Natl. Acad. Sci. U.S.A.* **1989**, *86*, 6838–6842.
- (34) Zechmann, B.; Tomašić, A.; Horvat, L.; Fulgosi, H. Subcellular Distribution of Glutathione and Cysteine in Cyanobacteria. *Protoplasma* **2010**, *246*, 65–72.
- (35) Eser, M.; Masip, L.; Kadokura, H.; Georgiou, G.; Beckwith, J. Disulfide bond formation by exported glutaredoxin indicates glutathione’s presence in the *E. coli* periplasm. *Proc. Natl. Acad. Sci. U.S.A.* **2009**, *106*, 1572–1577.
- (36) Mondal, J.; Friesner, R. A.; Berne, B. J. Role of Desolvation in Thermodynamics and Kinetics of Ligand Binding to a Kinase. *J. Chem. Theory Comput.* **2014**, *10*, 5696–5705.
- (37) Diaz-Mochon, J. J.; Planonh, S.; Bradley, M. From 10,000 to 1: Selective Synthesis and Enzymatic Evaluation of Fluorescence Resonance Energy Transfer Peptides as Specific Substrates for Chymopapain. *Anal. Biochem.* **2009**, *384*, 101–105.
- (38) Almagro Armenteros, J. J.; Tsirigos, K. D.; Sønderby, C. K.; Petersen, T. N.; Winther, O.; Brunak, S.; von Heijne, G.; Nielsen, H. SignalP 5.0 Improves Signal Peptide Predictions Using Deep Neural Networks. *Nat. Biotechnol.* **2019**, *37*, 420–423.
- (39) Bock, T.; Luxenburger, E.; Hoffmann, J.; Schütza, V.; Feiler, C.; Müller, R.; Blankenfeldt, W. AibA/AibB Induces an Intramolecular Decarboxylation in Isovalerate Biosynthesis by *Myxococcus xanthus*. *Angew. Chem., Int. Ed.* **2017**, *56*, 9986–9989.
- (40) Mueller, U.; Darowski, N.; Fuchs, M. R.; Förster, R.; Hellmig, M.; Paithankar, K. S.; Pühringer, S.; Steffien, M.; Zocher, G.; Weiss, M. S. Facilities for Macromolecular Crystallography at the Helmholtz-Zentrum Berlin. *J. Synchrotron Radiat.* **2012**, *19*, 442–449.
- (41) Kabsch, W. XDS. *Acta Crystallogr., Sect. D: Biol. Crystallogr.* **2010**, *66*, 125–132.

- (42) Potterton, E.; Briggs, P.; Turkenburg, M.; Dodson, E. A graphical user interface to the CCP4 program suite. *Acta Crystallogr. Sect. D: Biol. Crystallogr.* **2003**, *59*, 1131–1137.
- (43) Karplus, P. A.; Diederichs, K. Linking Crystallographic Model and Data Quality. *Science* **2012**, *336*, 1030–1033.
- (44) Adams, P. D.; Afonine, P. V.; Bunkóczi, G.; Chen, V. B.; Davis, I. W.; Echols, N.; Headd, J. J.; Hung, L.-W.; Kapral, G. J.; Grosse-Kunstleve, R. W.; et al. PHENIX: A Comprehensive Python-Based System for Macromolecular Structure Solution. *Acta Crystallogr. Sect. D Biol. Crystallogr.* **2010**, *66*, 213–221.
- (45) Emsley, P.; Lohkamp, B.; Scott, W. G.; Cowtan, K. Features and development of Coot. *Acta Crystallogr. Sect. D Biol. Crystallogr.* **2010**, *66*, 486–501.
- (46) Bernstein, F. C.; Koetzle, T. F.; Williams, G. J. B.; Meyer, E. F.; Brice, M. D.; Rodgers, J. R.; Kennard, O.; Shimanouchi, T.; Tasumi, M. The Protein Data Bank: A Computer-Based Archival File for Macromolecular Structures. *J. Mol. Biol.* **1977**, *112*, 535–542.
- (47) Herrera, I.; Winnik, M. A. Differential Binding Models for Isothermal Titration Calorimetry: Moving beyond the Wiseman Isotherm. *J. Phys. Chem. B* **2013**, *117*, 8659–8672.
- (48) Delaglio, F.; Grzesiek, S.; Vuister, G.; Zhu, G.; Pfeifer, J.; Bax, A. NMRPipe: A Multidimensional Spectral Processing System Based on UNIX Pipes. *J. Biomol. NMR* **1995**, *6*, 277–293.
- (49) Brooks, B. R.; Brucoleri, R. E.; Olafson, B. D.; States, D. J.; Swaminathan, S.; Karplus, M. CHARMM: A program for macromolecular energy, minimization, and dynamics calculations. *J. Comput. Chem.* **1983**, *4*, 187–217.
- (50) MacKerell, A. D.; Bashford, D.; Bellott, M.; Dunbrack, R. L.; Evanseck, J. D.; Field, M. J.; Fischer, S.; Gao, J.; Guo, H.; Ha, S.; et al. All-Atom Empirical Potential for Molecular Modeling and Dynamics Studies of Proteins. *J. Phys. Chem. B* **1998**, *102*, 3586–3616.
- (51) Bashford, D.; Gerwert, K. Electrostatic Calculations of the PKa Values of Ionizable Groups in Bacteriorhodopsin. *J. Mol. Biol.* **1992**, *224*, 473–486.
- (52) Bashford, D. An object-oriented programming suite for electrostatic effects in biological molecules An experience report on the MEAD project. In *Lecture Notes in Computer Science*; Ishikawa, Y., Oldehoeft, R. R., John, V. W., Reynders, M. T., Eds.; SpringerBerlin Heidelberg, 1997; pp 233–240.
- (53) Ullmann, R. T.; Ullmann, G. M. GMCT : A Monte Carlo simulation package for macromolecular receptors. *J. Comput. Chem.* **2012**, *33*, 887–900.
- (54) Beroza, P.; Fredkin, D. R.; Okamura, M. Y.; Feher, G. Protonation of Interacting Residues in a Protein by a Monte Carlo Method: Application to Lysozyme and the Photosynthetic Reaction Center of Rhodospirillum rubrum. *Proc. Natl. Acad. Sci. U.S.A.* **1991**, *88*, 5804–5808.
- (55) Ullmann, G. M.; Knapp, E.-W. Electrostatic Models for Computing Protonation and Redox Equilibria in Proteins. *Eur. Biophys. J.* **1999**, *28*, 533–551.
- (56) Yamamoto, D.; Matsumoto, K.; Ohishi, H.; Ishida, T.; Inoue, M.; Kitamura, K.; Mizuno, H. Refined x-ray structure of papain.E-64-c complex at 2.1-Å resolution. *J. Biol. Chem.* **1991**, *266*, 14771–14777.
- (57) Arad, D.; Langridge, R.; Kollman, P. A. A simulation of the sulfur attack in catalytic pathway of papain using molecular mechanics and semiempirical quantum mechanics. *J. Am. Chem. Soc.* **1990**, *112*, 491–502.
- (58) Baker, N. A.; Sept, D.; Joseph, S.; Holst, M. J.; McCammon, J. A. Electrostatics of Nanosystems: Application to Microtubules and the Ribosome. *Proc. Natl. Acad. Sci. U.S.A.* **2001**, *98*, 10037–10041.
- (59) Field, M. J. The PDynamo Program for Molecular Simulations Using Hybrid Quantum Chemical and Molecular Mechanical Potentials. *J. Chem. Theory Comput.* **2008**, *4*, 1151–1161.
- (60) Neese, F. The ORCA Program System. *Wiley Interdiscip. Rev.: Comput. Mol. Sci.* **2012**, *2*, 73–78.
- (61) Neese, F. Software update: the ORCA program system, version 4.0. *Wiley Interdiscip. Rev.: Comput. Mol. Sci.* **2018**, *8*, No. e1327.
- (62) Ditchfield, R.; Hehre, W. J.; Pople, J. A. Self-Consistent Molecular-Orbital Methods. IX. An Extended Gaussian-Type Basis for Molecular-Orbital Studies of Organic Molecules. *J. Chem. Phys.* **1971**, *54*, 724–728.
- (63) Francl, M. M.; Pietro, W. J.; Hehre, W. J.; Binkley, J. S.; Gordon, M. S.; DeFrees, D. J.; Pople, J. A. Self-consistent molecular orbital methods. XXIII. A polarization-type basis set for second-row elements. *J. Chem. Phys.* **1982**, *77*, 3654–3665.
- (64) Hehre, W. J.; Ditchfield, R.; Pople, J. A. Self-Consistent Molecular Orbital Methods. XII. Further Extensions of Gaussian-Type Basis Sets for Use in Molecular Orbital Studies of Organic Molecules. *J. Chem. Phys.* **1972**, *56*, 2257–2261.
- (65) Stephens, P. J.; Devlin, F. J.; Chabalowski, C. F.; Frisch, M. J. Ab Initio Calculation of Vibrational Absorption and Circular Dichroism Spectra Using Density Functional Force Fields. *J. Phys. Chem.* **1994**, *98*, 11623–11627.
- (66) Gisdon, F. J.; Culka, M.; Ullmann, G. M. PyCPR - a python-based implementation of the Conjugate Peak Refinement (CPR) algorithm for finding transition state structures. *J. Mol. Model.* **2016**, *22*, 242.
- (67) Peters, B.; Heyden, A.; Bell, A. T.; Chakraborty, A. A Growing String Method for Determining Transition States: Comparison to the Nudged Elastic Band and String Methods. *J. Chem. Phys.* **2004**, *120*, 7877–7886.
- (68) Mueller, U.; Förster, R.; Hellmig, M.; Huschmann, F. U.; Kastner, A.; Malecki, P.; Pühringer, S.; Röwer, M.; Sparta, K.; Steffien, M.; et al. The Macromolecular Crystallography Beamlines at BESSY II of the Helmholtz-Zentrum Berlin: Current Status and Perspectives. *Eur. Phys. J. Plus* **2015**, *130*, 141–150.




ACS
MATERIALS Au
AN OPEN ACCESS JOURNAL OF THE AMERICAN CHEMICAL SOCIETY

Editor-in-Chief: **Prof. Shelley D. Minteer**, University of Utah, USA

Deputy Editor:
Prof. Stephanie L. Brock
Wayne State University, USA

Open for Submissions 

pubs.acs.org/materialsau

 ACS Publications
Most Trusted. Most Cited. Most Read.

Publication IV

Modular synthesis of glutathione analogues to study peptidase
reactions in vitro and in vivo

Oxana Kempf,[†] G. Matthias Ullmann,[~] Olaf Stemmann,[⊥] Rainer Schobert,[‡] Karl Kempf,^{*} [‡]
and Elisa Bombarda^{*},[†]

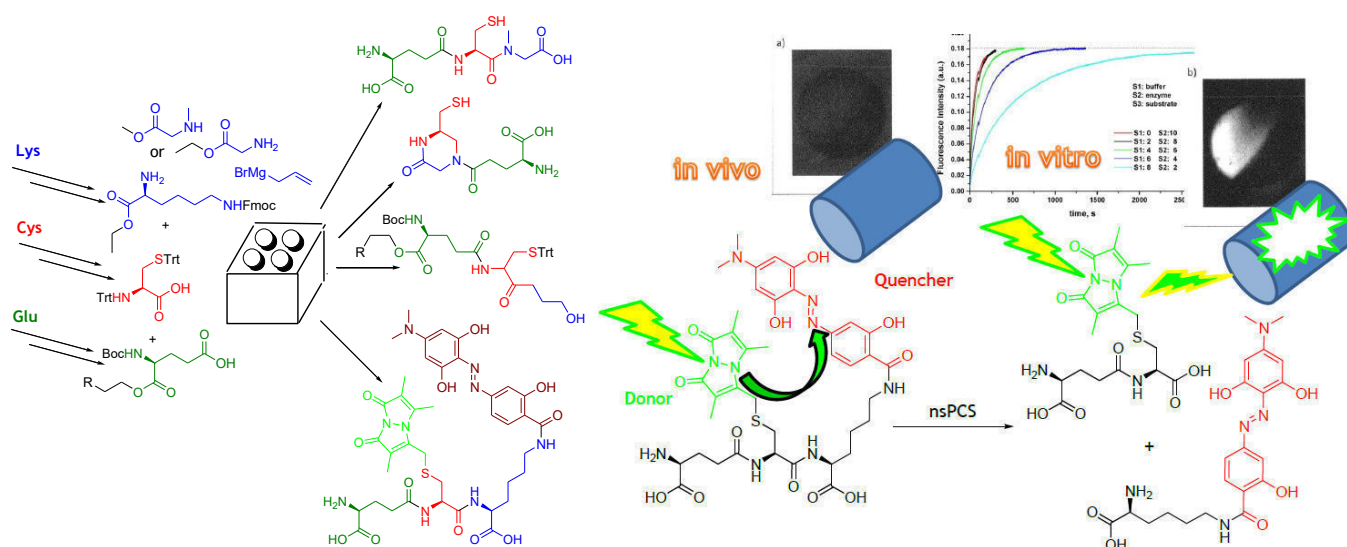
[†]Department of Biochemistry, [~]Computational Biochemistry, [⊥]Genetics and [‡]Organic
Chemistry Laboratory, University of Bayreuth, Universitätsstr. 30, 95440, Bayreuth,
Germany.

Closse to submission

Modular synthesis of glutathione analogues to study peptidase reactions *in vitro* and *in vivo*

Oxana Kempf,[†] G. Matthias Ullmann,[~] Olaf Stemmann,[⊥] Rainer Schobert,[‡] Karl Kempf,^{*,‡} and Elisa Bombarda^{*,†}

[†]Department of Biochemistry, [~]Computational Biochemistry, [⊥]Genetics and [‡]Organic Chemistry Laboratory, University of Bayreuth, Universitätsstr. 30, 95440, Bayreuth, Germany.



ABSTRACT

We developed a versatile reaction scheme consisting of mild and environmentally benign conversions allowing for the efficient solution phase synthesis of oligopeptides containing triple-functional group amino acids. We applied this strategy to synthesize and chemically modify glutathione. The double-labelled glutathione analogue showed successful applications in FRET-based activity tests of phytochelatin synthase from cyanobacterium *Nostoc sp.* (NsPCS), both *in vitro* and *in vivo*.

INTRODUCTION

Glutathione is the tripeptide γ -L-glutamyl-L-cysteinyl-glycine which bears an uncommon gamma bond between glutamate and cysteine and exists ubiquitously in all domains of life. GSH is the most abundant antioxidant in cells present at a 1-10 mM concentration¹. Glutathione exists in the thiol-reduced (GSH) and disulfide-oxidized (GSSG) forms², of which GSH is the predominant form and accounts for >98 % of total glutathione³⁻⁵. Eukaryotic cells have three major reservoirs of glutathione: most (80–85%) of the cellular glutathione are in the cytosol, 10–15 % is in the mitochondria and a small percentage is in the endoplasmic reticulum.

GSH serves several vital functions including antioxidant defence, detoxification of xenobiotics and/or their metabolites, iron-sulphur cluster biogenesis, regulation of cell cycle progression and apoptosis, storage of cysteine, maintenance of redox potential, modulation of immune function and fibrogenesis⁴⁻¹⁰. GSH also operates as cofactor for enzymes and participates in many pathways of primary metabolism¹¹.

The biosynthesis of GSH occurs via a two-step ATP-requiring enzymatic process. The first step consisting in the conjugation of cysteine with glutamate generating γ -glutamylcysteine (γ EC) is catalysed by glutamate-cysteine ligase. The second step is catalysed by GSH synthase, which adds glycine to γ EC to form γ -glutamylcysteinylglycine (GSH). GSH exerts a negative feedback inhibition on glutamate-cysteine ligase¹². Cellular GSH levels are maintained through a balance between its synthesis, degradation and utilization as a conjugating agent, and its recycling from the oxidized form, GSH disulfide (GSSG). In many organisms, the last process is carried out by GSH reductases with reducing equivalents from NADPH.

Glutathione have also a therapeutic importance. Many chronic and age-related diseases are associated with a decline in cellular GSH levels or impairment in the catalytic activity of the GSH biosynthetic enzyme glutamate cysteine ligase (GCL). Administration of γ -glutamylcysteine as precursor to glutathione (GSH), can replenish depleted GSH levels under oxidative stress conditions, by circumventing the regulation of GSH biosynthesis. γ -glutamylcysteine displays the protective role of up-regulating GSH¹³.

The structure of glutathione is unique in that the peptide bond linking glutamate and cysteine is through the γ -carboxyl group of glutamate rather than the conventional α -carboxyl group. This unusual γ -glutamyl bond favours the accumulation of GSH in the cell, in fact it confers on glutathione an exceptional stability, making it insensitive to the numerous peptidases in the cell, and requiring very specific enzymes for its degradation. The enzyme

that can hydrolyse this unusual bond is γ -glutamyltranspeptidase, which is only present on the external surfaces of certain cell types⁶ (e.g. at the plasma membrane in mammals and bacteria or at the vacuolar membrane in yeast and plants) and acts on extracellular or vacuolar pools. As a consequence, GSH was considered to be resistant to intracellular degradation and metabolized only extracellularly by cells that express γ -glutamyltranspeptidase. However, recently, few other enzymes able to attack this unusual bond have been identified in the cytosol¹⁴: the DUG enzymes (Defective in Utilization of Glutathione), which is present only in yeast and fungi¹⁵, and ChaC1, which, as a member of the γ -glutamylcyclotransferase family, acts to hydrolyse the corresponding γ -glutamyl compound (glutathione, γ -glutamyl-cysteinyl-glycine) leading to the formation of that compound devoid of the γ -glutamyl group (cysteinyl-glycine) and 5-oxoproline, while it lacks any significant activity against γ -Glu-aa dipeptides^{16,17} and against oxidized glutathione¹⁸.

The second peptide bond between cysteine and glycine is specifically converted by phytochelatase (PCS). In eukaryotes, PCS is ubiquitous in the plant kingdom^{19,20} and is also present in many invertebrates such as protozoa and nematodes²¹⁻²³, but it has not been found in vertebrates. This enzyme can act both as a peptidase, by cleaving off the glycine (Gly) from GSH, and as transpeptidase by transferring the remaining γ EC dipeptide onto another GSH molecule^{24,25}. The products with the general formula $[\gamma\text{Glu-Cys}]_n\text{-Gly}$ ($n=2-4$) are called phytochelatins (PCs)²⁶. The cleavage of glycine is also the first step in the degradation of GSH S-conjugates as a response to electrophilic toxins or drugs (a.k.a. xenobiotic metabolism)²⁷. Due to its absence in humans, PCS may be a suitable drug target for the treatment of diseases caused by pathogens expressing PCS. For example, its potential as a target for schistosomiasis treatment has been discussed²⁸⁻³⁰.

In the prokaryotic kingdom, a number of cyanobacteria and proteobacteria³¹ possess genes that encode for proteins that show similarity to the N-terminal catalytic domain of PCS. These bacterial proteins have been assigned as being PCS-like. Similar to PCS, PCS-like proteins use GSH as substrate. However, while they are able to cleave off the glycine residue to form γ -Glu-Cys (γ EC), the formation of PC in PCS-like proteins was detected only in low amounts and thus the transpeptidase activity of these proteins is still debated³²⁻³⁵. Nowadays, amounting evidence supports the hypothesis that PCS serves functions besides cadmium and arsenic detoxification, for example through roles in essential metal homeostasis²⁰ and in innate immunity³⁶. The role of the PCS-like proteins is even less clear, since they are seemingly not able to produce larger amounts of phytochelatins. In order to better identify the tasks of PCS-like proteins, their detailed mechanistic characterization is a priority³⁷.

The interest to shed light on the mechanism of PCS-like proteins prompted us to design substrate-based probes by chemically modifying glutathione. The synthesis of glutathione is challenging. An earlier protocol to synthesize GSH³⁸ and derivatives thereof³⁹ including lysine instead of glycine⁴⁰ relied on benzyl protecting groups. Since catalytic hydrogenolysis is not possible in the presence of sulphur atoms, the global deprotection was carried out with sodium dissolved in liquid ammonia. This procedure is not only time consuming, dangerous and inconvenient; the strongly basic conditions can lead to racemisation or degradation. Consequently, most GSH syntheses rely on acid labile tert butyl protecting groups⁴¹⁻⁴³. The preparation of *tert*-butyl ester or thio-ether, however, requires the handling with gaseous isobutene, which is also inconvenient. The trityl group in contrast, offers simple protection and selective deprotection⁴⁴. However, this strategy has not yet been applied for non-natural GSH derivatives, which can be useful for various biochemical and pharmacological applications.

In this work we describe the synthesis of a double-labelled fluorogenic probe as GSH-analogue. The modular and efficient reaction scheme is based on precursor “building blocks”, namely the appropriately protected amino acids glutamate, cysteine and lysine. The amino acids can be combined like LEGO[®]-bricks and can be easily exchanged, for example sarcosine at the place of lysine. This modular reaction scheme provides also the opportunity for the synthesis of natural GSH, γ -EC, or chemical modifications of the peptide bond, namely the reduced form “CH₂-amine” and the ketone. As an application of the fluorogenic probe synthesized herein, a FRET-based assay to monitor the cleavage of GSH *in vitro* and *in vivo* by the PCS-like enzyme from the cyanobacterium *Nostoc sp.* is described.

RESULTS AND DISCUSSION

Synthesis of a substrate-based fluorogenic probe.

When investigations on the mechanism involved in peptidase reactions (such as PCS) are intended, an appropriate labelling can allow for fast and highly sensitive spectroscopic measurements. The enzymatic hydrolysis of a peptide is usually monitored by functionalization of the two amino acids adjacent to the cleavage site with a fluorophore and a quencher, respectively. Previous physiological studies showed the conversion of S-alkyl GSH derivatives by PCS⁴⁵, which infer the opportunity of attaching chromophores on the thiol.

As donor fluorophore we chose bimane based on the fact that monobromobimane is a small fluorophore commercially available allowing for simple substitution on the thiol group^{46,47}. Bimane has the advantage to be comparatively small as compare to other commonly used fluorescence probes. Moreover, glutathione-bimane conjugates were already employed in previous assays involving PCS, and proved not to affect activity^{25,47-50}.

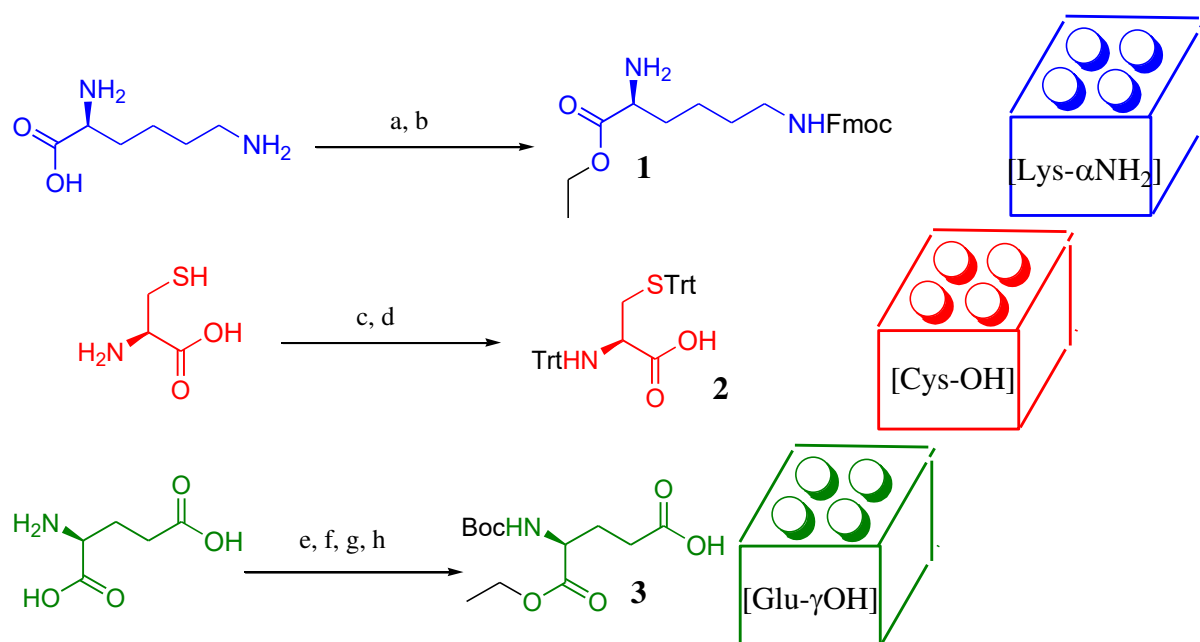
In order to create a fluorogenic probe⁵¹ suitable to monitor the cleavage of the peptide bond Cys-Gly in glutathione, a dark quencher chromophore needs to be attached to the glycine moiety. Originally we chose dabcyI since it is a commercially available quencher spectrally compatible with bimane. However, dabcyI is hardly soluble in water due to its hydrophobicity, which severely limits its use in biological system where water is the natural solvent. Even when this hydrophobicity can be partly compensated for by the hydrophilicity of the substrate to which dabcyI is linked (e.g., long DNA segments or peptide chains), it poses a real problem in the case of comparatively small substrates (e.g. a tripeptide). We have addressed this problem systematically⁵² and we designed and synthesized hydrodabcyI, a trihydroxy derivative of the parent dabcyI, which overcomes the problem of insolubility in aqueous media, doing away with the need of organic co-solvents^{53,54}. Due to the superiority of hydrodabcyI in aqueous media, this work relies on the use of hydrodabcyI in place of dabcyI.

The only functional group in the glycine moiety available for attaching the quencher would be the carboxylate. However, in all its multifunctional roles, GSH is in the globally monoanionic form GSH⁻ and the three charged groups (the positive amino group and the two negative carboxylate groups) are strongly involved with regard to the environment and particularly in the GSH⁻-enzyme interactions⁵⁵. Therefore, the intrinsic electrostatic properties of GSH are essential in the molecular mechanism of these interactions and cannot be modified. In the same line are the results of our study on the PCS-like enzyme, NsPCS³⁷. Calculations of the electrostatic potential on the surface of NsPCS reveal a significant clustering of positive charged amino acid residues around the binding pocket. This is a logic adaption to the negatively charged substrate GSH. In this case, the removal of the negative charge by functionalization with a chromophore would alter the interaction of the enzyme with its substrate.

Consequently, we decided to replace the glycine by an amino acid containing an amino group in the side chain, since the CH₂ group of the glycine is chemically inactive. The additional primary amino group was intended to be linked to the carboxyl group of hydrodabcyI *via* amide bond. In this manipulation of GSH we have been comforted by the fact that there are also different naturally existing congeners of GSH with other amino acids in

the place of glycine (e.g. γ -glutamylcysteinyl serine and γ -glutamylcysteinyl- β -alanine (homogluthathione)⁵⁶. The initial choice fell on ornithine, which is a precursor (before carbamoylation) of arginine. Unfortunately, the δ -amino group of ornithine attacked its own α -carbonyl ester to form a stable 6-membered lactame ring, preventing the coupling with hydrodabcy. To overcome this problem, we decided to substitute the Gly moiety with a lysine, motivated by the fact that lysine has one CH_2 - group more than ornithine and a 7-membered ring does not form so easily. As expected, coupling of hydrodabcy to lysine was successful.

Corresponding to this functional requirement, we established a modular reaction scheme based on three main building blocks **1-3**, namely the derivatives of lysine, cysteine and glutamate, protected on each two of the three functional groups (Scheme 1). Since these each three functional groups require selective and orthogonal protection; we had to face some challenging optimization.



Scheme 1. Synthesis of the **Lys building block**: **a.** 0.5 eq. $\text{Cu}(\text{OAc})_2$, Na_2CO_3 10 % solution, 1.1 eq. FmocONSu in H_2O /dioxane, 1.5 h r.t., quant.; **b.** 12 eq. SOCl_2 in EtOH, 3 h 80 °C, quant.; **Cys building block**: **c.** 3 eq. TrtCl, 0.5 eq ZnCl_2 in MeCN, 25 min at 40 °C then 1 h r.t., quant.; **d.** 0.5 eq. $\text{Cu}(\text{OAc})_2$ in DCM/MeOH, 4 h r.t., EDTA, 90 %; **Glu building block**: **e.** 13 eq. BnOH, 2 eq. $\text{HBF}_4 \cdot \text{OEt}_2$, Na_2SO_4 , overnight r.t., quant.; **f.** 1.1 eq. Boc_2O , 1 eq. NEt_3 in THF, overnight r.t., 76 %; **g.** 1.2 eq. EtOH, 1.1 eq. EDC, 1 eq. DMAP in DCM, 3 h 0 °C, 74 %; **h.** 5%Pd/C, MeOH, H_2 , 2h r.t., quant.

The Lys building block **1** was synthesized starting with L-lysine being transferred into its copper complex followed by selective ϵ -Fmoc protection in a one-pot procedure based on literature⁵⁷⁻⁵⁹. Decomplexation with aqueous hydrochloric acid and subsequent esterification

with thionyl chloride (SOCl₂) in ethanol left the lysine compound in quantitative yield after two steps in a storable form as salt.

The Cys building block **2** containing the free acid was synthesized starting with per-trityl protection followed by selective ester cleavage *via* the copper chelate⁴⁴ in 90 % yield after two steps.

The Glu building block **3** was synthesized in four steps from L-glutamic acid⁶⁰. In a previously patented straight-forward synthesis of GSH⁴⁴, a selective condensation of N-trityl-glutamate occurred only on the γ -carboxyl group, probably due to steric hindrance on the α position. Since the synthesis of N-trityl glutamate requires anyway further steps for protection and deprotection of the carboxyl groups, we instead employed a Boc-glutamate hemi-ester in order to generate always totally protected coupling products for convenient purification in the frame of the modular synthesis strategy. The differentiation between the carboxyl groups was achieved by esterification of the γ -carboxyl group with benzyl alcohol in the presence of tetrafluoroboric acid diethylether complex (HBF₄·Et₂O) which forms in situ a BF₂- complex between the α -carboxyl and the amino group as transient protection. Subsequently, the amino group was boc-protected and the α -carboxyl group esterified with ethanol and propylphosphonic anhydride T3P (2,4,6-Tripropyl-1,3,5,2,4,6-trioxatriphosphorinan-2,4,6-trioxid)^{61,62}. Hydrogenolysis of the benzyl ester gave the glutamic acid compound in 56 % yield after four steps in a storable form ready for coupling.

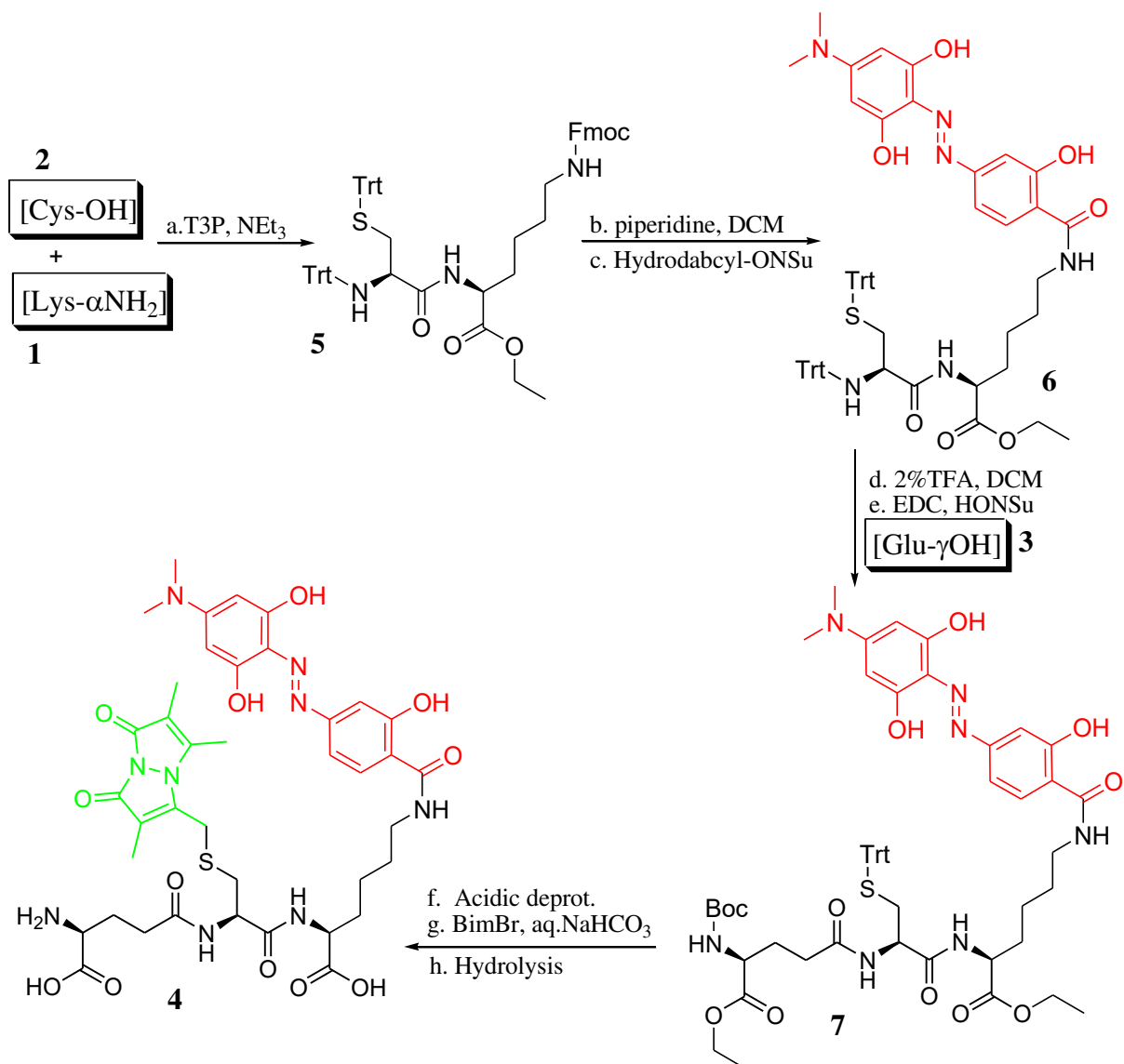
While preparing the glutamate building block, we observed racemization. That is consistent with the literature reporting that the esterification of amino acid derivatives with N,N'-dicyclohexylcarbodiimide and 4-(dimethylamino)pyridine (DCC/DMAP) can lead to racemization⁶³ when stirred, as conventionally⁶⁴, overnight. After 3 hours, however, complete conversion was reported without racemization. Consequently, we used EDC instead of DCC and limited the reaction to 3 h at 0 °C.

As key reagent for condensation reactions we used T3P⁶¹ which leaves water soluble by-products and thereby provides almost clean crude products in almost quantitative yields without necessity of chromatography. Most importantly it forms amide bonds with primary amines in only one hour at 0 °C which avoids the necessity for protection of alcohols and secondary amines which do not react under these conditions.

The synthesis of the double labelled GSH-analogue **4** (Scheme 2) starts by condensation of the above-described building blocks **2** and **3** with T3P followed by standard Fmoc deprotection of dipeptide **5** to liberate the amino group for coupling with Hydrodabcyln-NHS. The selective deprotection of the N-trityl group in the hydrodabcyln-labeled dipeptide **6**

was easily be achieved with 20 % trifluoroacetic acid (TFA)⁶⁵ in dichloromethane (DCM) because the S-trityl group is much more stable. During further experiments, we found out, that the amount of TFA can be reduced to 2 % and the N-detritylation still proceeds quantitatively. The so-formed free amine was reacted under analogous condensation conditions with the glutamic acid component and T3P to obtain the protected glutathione analogue **7** in 13 % yield after five steps starting from the building blocks.

The deprotection started with saponification of the ester groups carried out at 0 °C and under argon in order to avoid oxidative degradation of the phenolic hydrodabcy. Acidic deprotection of Boc- and S-trityl group proceeded with TFA and triethyl silane for quenching of the free trityl cations⁶⁶. The isolation of the polar and oxidation-sensitive compound was achieved by reversed phase column chromatography under acidic conditions. The free sulphur was functionalized selectively with monobromo bimane⁴⁶. HPLC- purification left the double-labeled hydrodabcy-bimane glutathione derivative **4** in 12 % yield after 8 steps. In order to optimize this procedure, we will carry out the saponification after the functionalization with bimane which takes place anyway in basic aqueous solution. Natural GSH can also be synthesized with the same strategy by employing commercially available glycine-ethyl ester instead of the protected lysine (see NMR spectra of fully protected GSH in SI).

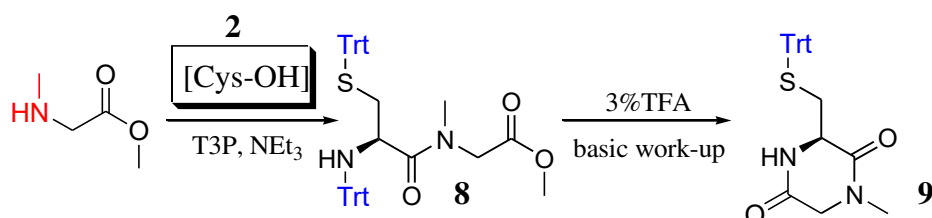


Scheme 2. Synthesis of the double labelled GSH-analogue: **a.** 2.5 eq. NEt₃, 1.15 eq. T3P, 50 % in THF 0 °C 1 h, 86 %; **b.** 20 % piperidine in DCM 10 min at 0 °C 1 h, quant; **c.** 1 eq. hydrodabcy1-ONSu in DMSO, 1.6 eq. NEt₃, in THF overnight at r.t., 85 %; **d.** 2 % TFA, DCM, EtOH; r.t. 1 h, quant.; **e.** 1 eq. **3** in DCM, 1.1 eq. EDC, 1 eq. HONSu, 1 eq. amine from step d, overnight at r.t., 53 %; **f.** 100 eq. TFA, 4.4 eq. HSiEt₃, r.t. 1 h; **g.** 1 eq. mono Br-Bimane, 3 eq. NaHCO₃, MeCN/H₂O 1:4, r.t. 1 h; **h.** 2 eq. K₂CO₃ pH 8, EtOH/H₂O 2:1 (degassed, argon), overnight at r.t., HPLC, 30 %.

N-methylated GSH derivative.

In view of studying the catalytic mechanism of PCS-like enzymes that catalyse the cleavage of the second peptide bond in GSH between Cys-Gly, we got interested in synthesizing glutathione analogues in which this peptide bond is non-cleavable. Such category of substrate turns to be useful when binding is desired to be kept separated from catalysis. The ideal and general non-cleavable peptide bond isoster does not exist, but literature shows some

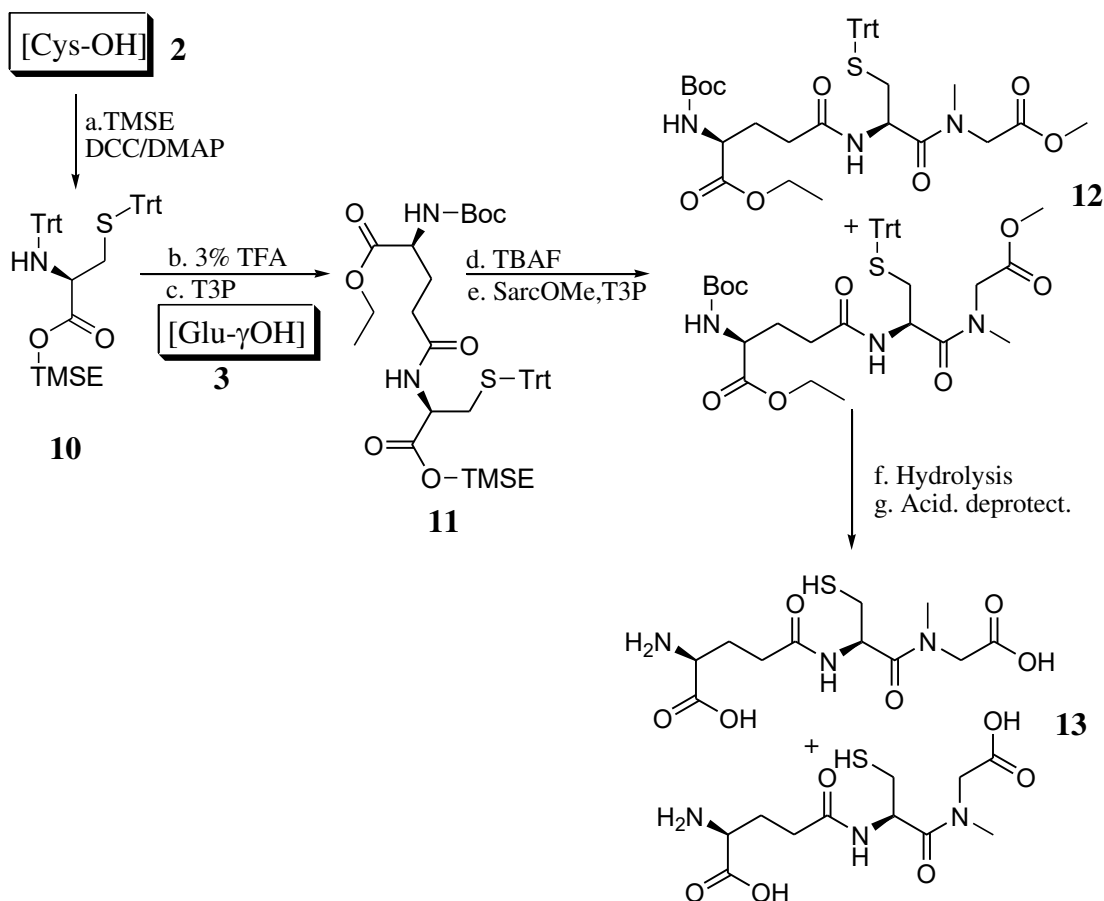
“imperfect options” depending on the purpose⁶⁷. N-methylated peptide bonds, for example, are known to be potentially resistant to proteolysis⁶⁸. In our reaction scheme, we can easily introduce sarcosine methyl ester by condensation with the cysteine building block **2**. Upon deprotection of the N-methylated dipeptide **8**, however, the formation of a six membered ring **9** occurred (Scheme 3).



Scheme 3. First unsuccessful trial for the synthesis of the N-methylated GSH derivative.

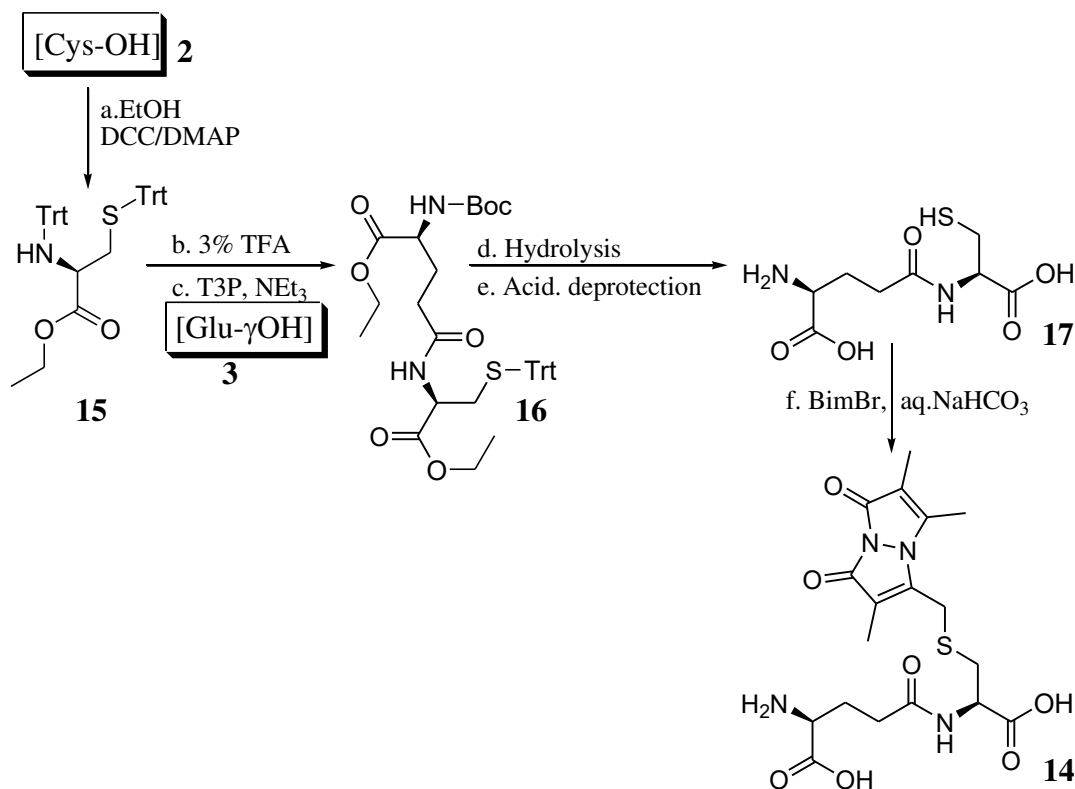
By changing the coupling sequence, we were able to circumvent the ring formation. For this purpose, we synthesized the cysteine building block with free amino group carrying as ester trimethylsilyl-ethyl (TMSE) **10** allowing for orthogonal ester cleavage (Scheme 4).

In this order, the cysteine amine **10** was firstly reacted with the glutamate **3**. The selective cleavage of the TMSE ester of cysteine but not the ethyl ester of glutamate was achieved with tetrabutyl ammonium fluoride TBAF⁶⁹. The usual saponification followed by acidic deprotection procedure left the N-methylated GSH derivative **13** in 29 % after six steps and final HPLC purification. Interestingly, all proton and carbon NMR spectra containing the N-methylated amide bond show two signal sets which are attributed to the presence of both E and Z amide because of the relatively large distance observed usually for E/Z isomers rather than diastereomers. The same effect occurred upon formation of another series of compounds containing secondary amides (Scheme 6).



Scheme 4. Synthesis of “non-cleavable” GSH-analogues with N-methylated amide bond: **a.** 1.1 eq. TMSEOH, 1 eq. DCC, 0.1 eq. DMAP, in DCM, at 0 °C then r.t. overnight, 71 %; **b.** 3 % TFA, DCM, EtOH; r.t. 2h, quant.; **c.** 1 eq. **3**, 2.5 eq. NEt₃, 1.15 eq. T3P, 50 % in THF 0 °C 1 h, 89 %; **d.** 3 eq. TBAF in THF, 0 °C 1 h, quant.; **e.** 2 eq. SarcOMe, 4 eq. NEt₃, 1.15 eq. T3P, 50 % in THF, overnight at r.t., 62 %; **f.** 1 eq. NaOH, MeOH/H₂O 2:1, 4 °C 6h; **g.** 100 eq. TFA, 4.4 eq. HSiEt₃, r.t. 1 h, HPLC, 73 %. The derivatives with N-methylated amide are present as a ~1:1 mixture of E and Z isomers as depicted exemplarily for **13**.

The same strategy can be used to synthesize the bimeane labelled γ EC dipeptide **14** (Scheme 5). In this case, ethyl ester **15** was synthesized as a cheap alternative, since orthogonal ester cleavage was not required.

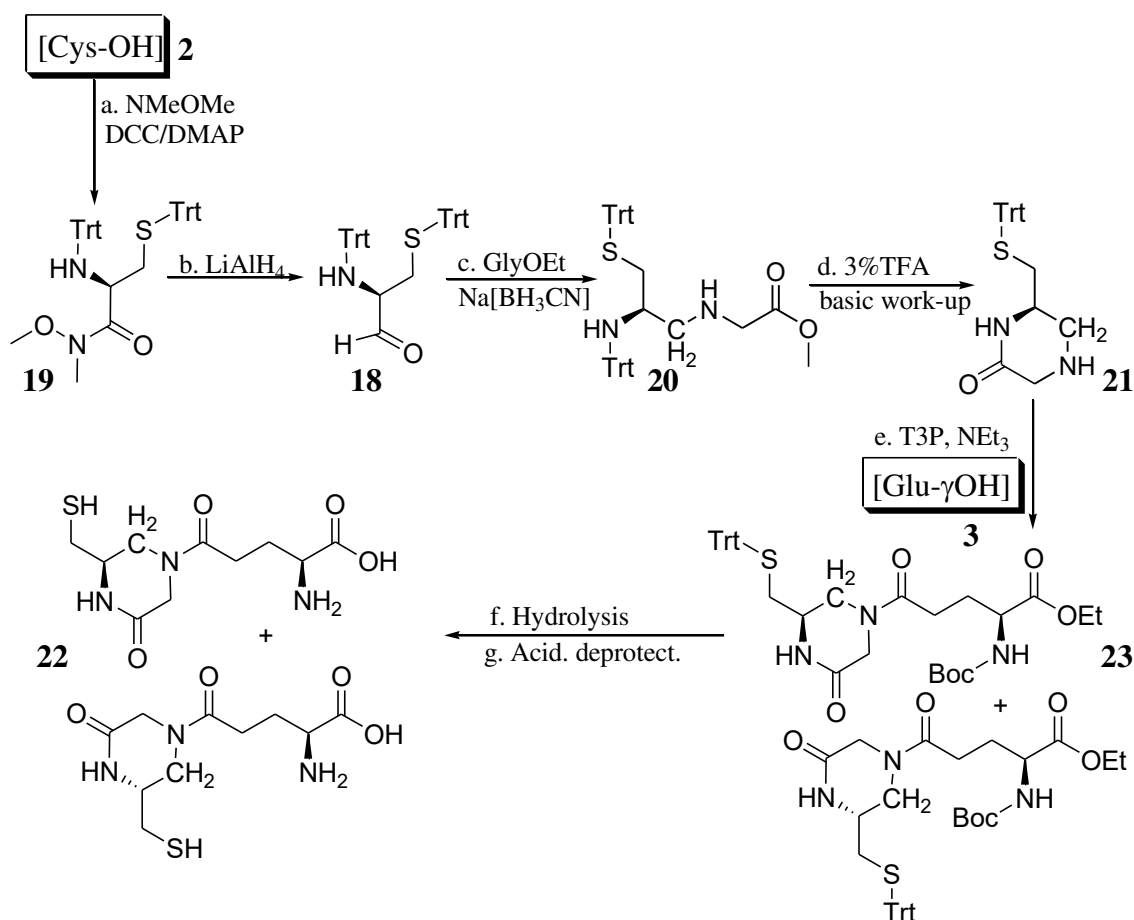


Scheme 5. Synthesis of labelled γ EC dipeptide: **a.** 5 eq. EtOH, 1 eq. DCC, 0.1 eq. DMAP, DCM, r.t. overnight, 96 %; **b.** 3 % TFA, DCM, EtOH; r.t. 2h, quant.; **c.** 1 eq. **3**, 2.5 eq. NEt₃, 1.15 eq. T3P, 50 % in THF 0 °C 1 h, 81 %; **d.** 1 eq. NaOH, MeOH/H₂O 2:1, 4 °C 6 h; **e.** 100 eq. TFA, 4.4 eq. HSiEt₃, r.t. 1 h; **f.** 1 eq. mono Br-Bimane, 3 eq. NaHCO₃, MeCN/H₂O 1:4, r.t. 1 h, HPLC, 40 %.

GSH derivative with the “reduced amide bond” (amino linkage) between Cys and Gly.

Another non-cleavable derivative is the reduced form CH₂-amine⁷⁰. The absence of a carbonyl group offers the advantage to be absolutely non-cleavable in the course of a peptidase mechanism. This secondary amino linkage, however, is not an amide isoster due to the increased rotational flexibility, the positive charge at physiologic pH and the lack of planar mesomeric delocalization. The CH₂-amino derivative is accessible *via* reductive amination of the cysteine aldehyde **18** (Scheme 6). Our strategy allowed us to simply convert the cysteine building block **2** into its Weinreb amide **19** which was reduced with lithium aluminium hydride to the desired aldehyde **18**. The latter was reacted with ethylglycinate and sodium cyanoborohydride under standard conditions to achieve eventually the protected reduced pseudo-dipeptide **20**. N-trityl deprotection was carried out as usually with TFA. The removal of this concurrence carboxylic acid by aqueous basic workup is mandatory prior to condensation with the glutamic acid. Upon evaporation of the solvent, however, the free amine directly attacked the ester to form a stable six membered lactam, formal a substituted piperazinone **21**. All attempts to isolate the free amine under low-temperature extraction and

evaporation at 0 °C failed. Condensation of the secondary amine **21** with the glutamate component **3** followed by the usual deprotection gave the N-acyl-piperazinone **22**. Analogously to the N-methylated series of secondary amides (see Scheme 4), **23** and **22** exist as a ~ 1:1 mixture of E/Z amide isomers. The relatively large distance between the signals is observed usually for E/Z isomers rather than for diastereomers. This argumentation is further corroborated by the synthesis of the protected natural GSH (see NMR spectra in SI). The isomer of **8** derived from ethyl glycinate was N-detritylated and coupled with the glutamate building block without any ring formation.



Scheme 6. Synthesis of “non-cleavable“ GSH-analogues with reduced amide bond: **a.** 1.1 eq. NMeOMe·HCl, 1 eq. DCC, 1.1 eq. DMAP, DCM, r.t. overnight, 65 %; **b.** 1.25 eq. LiAlH₄, THF, r.t. 3 h, quant; **c.** 1 eq. GlyOEt·HCl, 2 eq. Na[BH₃CN], AcOH, EtOH, 0 °C 1.5 h, 89 %; **d.** 3 % TFA, DCM, EtOH; r.t. 2h, quant.; **e.** 1 eq. **3**, 2.5 eq. NEt₃, 1.15 eq. T3P, 50 % in THF 0 °C 1 h, 86 %; **f.** 1 eq. NaOH, MeOH/H₂O 2:1, 4 °C 6h; **g.** 100 eq. TFA, 4.4 eq. HSiEt₃, r.t. 1 h, HPLC, 47 %. The derivatives containing a secondary amide are present as a ~1:1 mixture of E and Z isomers as depicted exemplarily for **22**.

A proposed solution for synthesizing the reduced linear glycine derivative relies on blocking the nucleophilicity of an amino group by protonation. We made use of this effect in the synthesis of **1** (see scheme 1) when selectively esterifying without amide formation under

acidic conditions. The following sequence might also be used to synthesize **13** (see scheme 4) without additional TMSE protection: (i) N-trityl deprotection of **20** (Scheme 6) with a mineral acid, such as hydrochloric, (ii) evaporation, i.e. isolation as ammonium salt, (iii) mixing of glutamic acid building block with T3P and NEt₃, (iv) slow addition of the ammonium salt in DCM (+ DMF if necessary) solution at 0 °C.

The cyclic GSH- analogue N-acyl-piperazinone **22** fits surprisingly very well into the GSH- binding pocket of NsPCS by forming a disulphide bridge with the cysteine in the catalytic triad, as revealed by the high resolution crystal structure of this complex (Figure 4). This finding suggests that **22** bears the potential to be an inhibitor for cysteine peptidases.

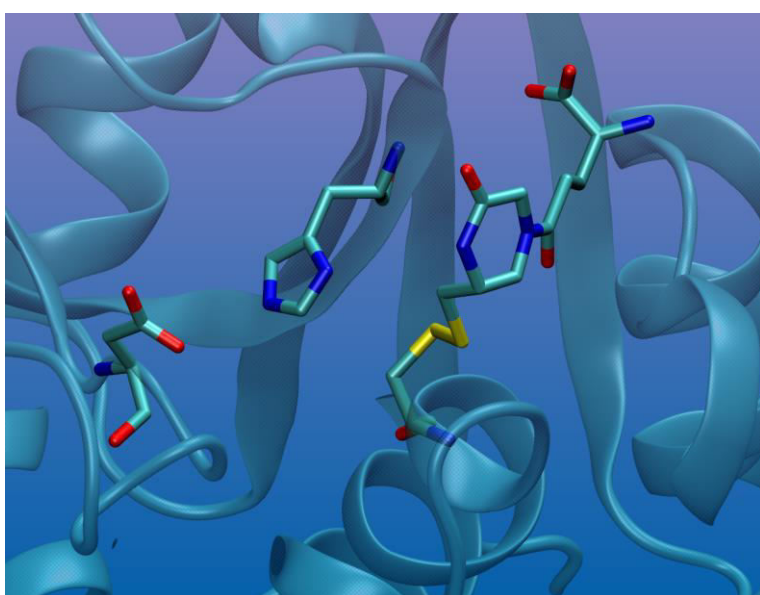


Figure 3. The crystal structure of cyclic GSH-analogue **22** bound to the active site cysteine via disulphide bond in NsPCS.

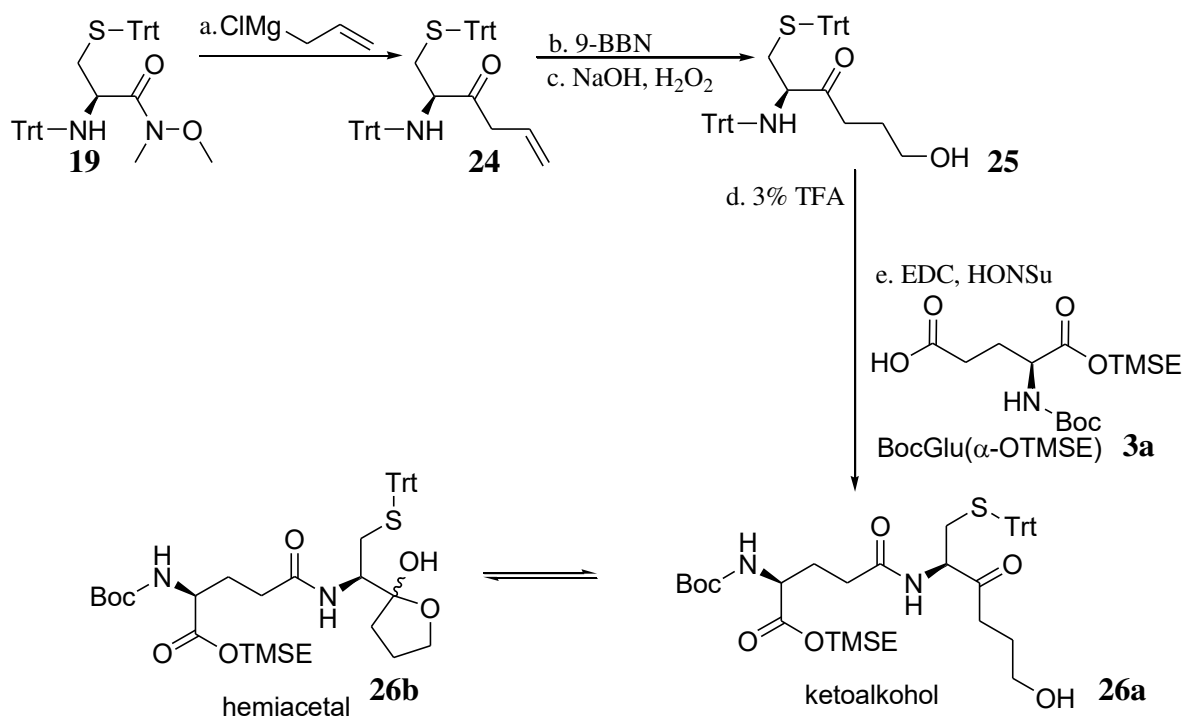
GSH-ketone- analogue.

The N-methylated GSH derivative was biologically unuseful to our purposes since it turned out to be a substrate for NsPCS and was cleaved enzymatically. The reduced form led to an unwanted ring formation and therefore requires further optimization. This effort might not be worth the additional costs, since the secondary amino linkage would introduce an additional positive charge changing the electrostatic properties of the compound, which could alter the results in binding studies. To overcome all these disadvantages we planned to synthesize another derivative, namely the ketone. Ketones can be attacked by the active site cysteine to form the oxyanion and are important protease inhibitors. However, they challenge organic

chemists with the use of hazardous reagents such as the toxic and highly explosive diazomethane still nowadays⁷¹.

Similarly to a previous Grignard-based approach⁷², we generated a ketone from our Cysteine building block **2** *via* Weinreb amide **19**, which reacted almost quantitatively with the commercially available allyl Grignard reagent (Scheme 7).

The hydroboration⁷³ of **24** with subsequent oxidative workup proceeded without racemization ($[\alpha]_{D}^{25} +100$) **25** and can be further optimized using shorter reaction time and less basic conditions. The optimal GSH-ketone would contain the carboxylic acid on the “glycine terminus of **25**. In order to rapidly assess the stability of ketone **25** under peptide coupling conditions, we skipped the oxidation and continued with standard N-trityl deprotection with TFA followed by an aqueous carbonate work-up without column chromatography. The crude product was directly subjected to peptide coupling with the TMSE-protected glutamate building block **3a**. Since ketone derivatives can easily undergo enolization under basic conditions, racemization or oligomerization by aldol reactions may occur. Consequently, we employed the TMSE-protected glutamate building block **3a** to avoid the necessity of ester saponification for final deprotection. Mass spectrometry indicated that the correct product had been formed in the coupling reaction. However, NMR spectroscopy showed two signal sets revealing the presence of an around 1:1 equilibrium between the expected product, ketoalcohol **26a** and its cyclic hemiacetal **26b**. We attributed the absence of this cyclisation product in the product **25** with the steric hindrance of two adjacent trityl groups preventing the alcohol to approach the ketone. Since the complete analysis of the NMR spectra would be complicated due to the additional presence of **26b** as two diastereomers, we decided not to go on with this derivative, but rather continue with optimization of the oxidation of alcohol **25**. Since direct oxidation to the acid with PDC did not yield the desired product, we tested the two- step process which is significantly milder and thus oxidative degradation of the thioether would be less probable.



Scheme 7. Synthesis of ketone: **a.** allyl magnesium chloride, r.t. 1 h, 93 %; **b.** 9-BBN, r.t. 1 h; **c.** NaOH, H₂O₂, 0 °C 1 h, 50 %; **d.** 3 % TFA, DCM, r.t. 1 h; **e.** 1.17 eq. **3a** in DCM, 1.2 eq. EDC, 1.2 eq. HONSu, 1 eq. amine from step d, overnight at r.t., 30 %;

The continued effort to finally synthesize the deprotected GSH ketone analogue in future is not only justified by its use for studying enzyme kinetics, but the applications of non-cleavable peptide derivatives are manifold. For instance, such compounds often act as inhibitor. Inhibitors for PCS may find an application as co-drugs against schistosomiasis²⁸⁻³⁰. Inhibitors against GSH synthetase are relevant against malaria⁷⁴. Furthermore, peptide drugs like GSH derivatives readily undergo enzymatic degradation in gastrointestinal fluids, lowering bioavailability⁷⁵. A decrease in endogenous GSH levels is associated with the onset and progression of many degenerative diseases including but not limited to Parkinson's, dementia and cataracts^{76,77}. Consequently, more stable GSH analogues could allow for oral application as antioxidant against degenerative diseases.

The synthesized GSH analogues prove to work both *in vitro* and *in vivo* assays.

The double labelled GSH derivative **4** has been originally designed to monitor the peptidase activity of PCS.

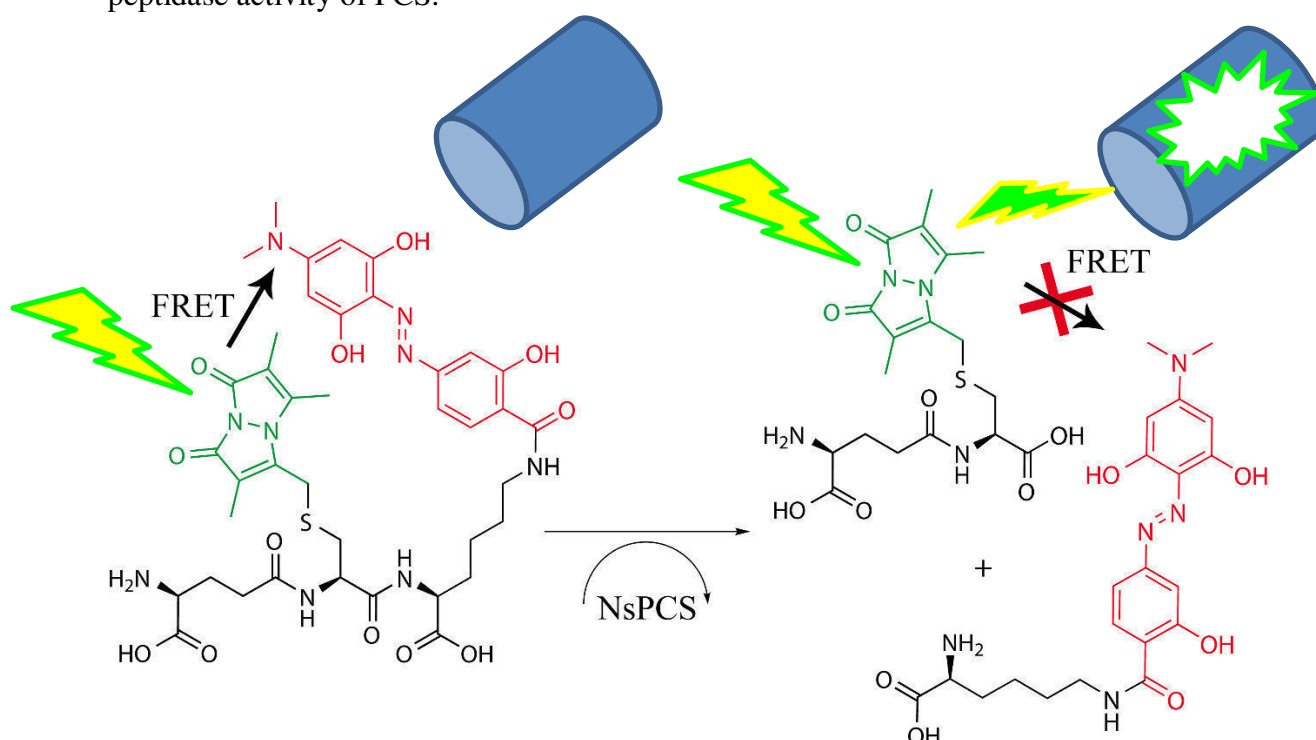


Figure 4. Schematic view of the experiment to monitor the peptidase activity of NsPCS with the fluorogenic substrated-based probed developed in this work. A signal is detected only after the quencher moiety gets far away upon cleavage.

In a qualitative proof of concept experiment, **4** was administered to *Xenopus* oocytes and irradiated at 391nm. As expected, no fluorescence was detected (Figure 5a). Upon addition of NsPCS, cleavage could be observed by a significant increase in fluorescence (Figure 5b). Interestingly, the growth of the embryos was not affected, indicating that the double-labelled construct is not cytotoxic and therefore ideal also for *in vivo* investigations. Furthermore, the cleavage occurred only after addition of NsPCS. Considering the presence of numerous proteases *in vivo*, this result indicates that the presented substrate has remarkable specificity towards NsPCS. Moreover, this result shows that the double-labelled GSH can be converted even in the presence of natural GSH.

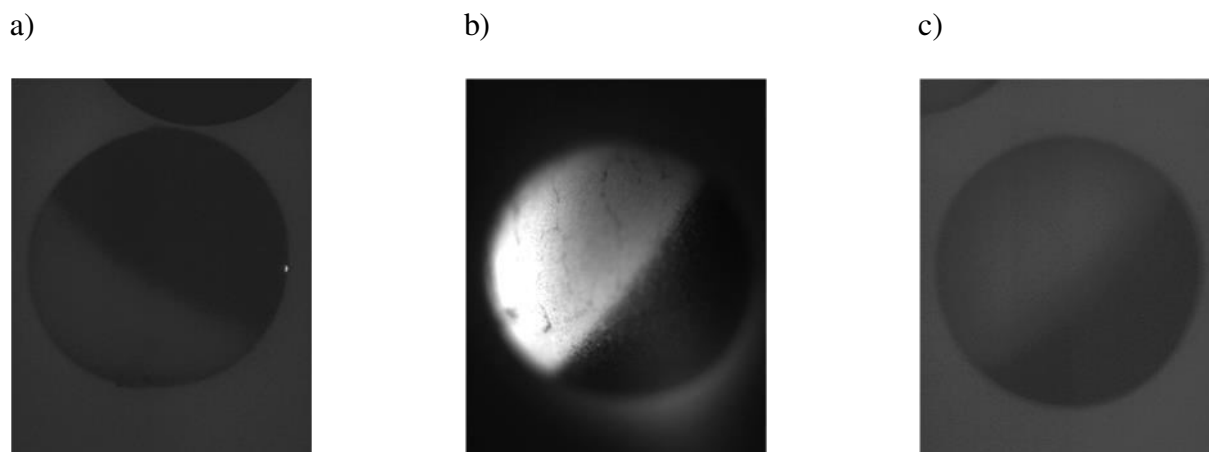


Figure 5. Cleavage reaction monitored by fluorescence microscopy. a) Oocyte microinjected with double-labeled GSH. b) NsPCS is microinjected to the oocytes containing double labelled GSH (picture taken 10 minutes after injection of the enzyme); c) control: microinjection of buffer.

In our previous activity assay by 1 h NMR³⁷ we observed complete cleavage of natural GSH in large excess by NsPCS after 1 h. Consequently, we started the first fluorescence-based quantitative kinetic experiment under the same conditions, using the double-labelled GSH in this work as substrate. As expected, an increase in fluorescence indicated the desired conversion. Its theoretical value of 100 % can be determined from the fluorescence intensity of an equimolar mixture of both chemically synthesized cleavage products, i.e., the γ GluCys(Bim) dipeptide **14** and the Lysine-Hydrodabcyyl fragment **28** (Figures 5 and 6). However, The fluorescence intensity in the kinetic saturation phase reached only ~12 % of the level denoting complete conversion. Addition of the same amount of enzyme (i.e., total ratio 1:100) lead to a significant increase of fluorescence, which corresponds to at least 50 % conversion. A third addition after 22h (total enzyme to substrate ration 1:65) leads to a further increase of fluorescence but could not yet lead to the reaction completion. This can also be due to degradation of the components in aqueous solution at the relatively basic pH 8. Even though the enzyme was added freshly, the chromophores are not stable overnight in aqueous basic solutions.

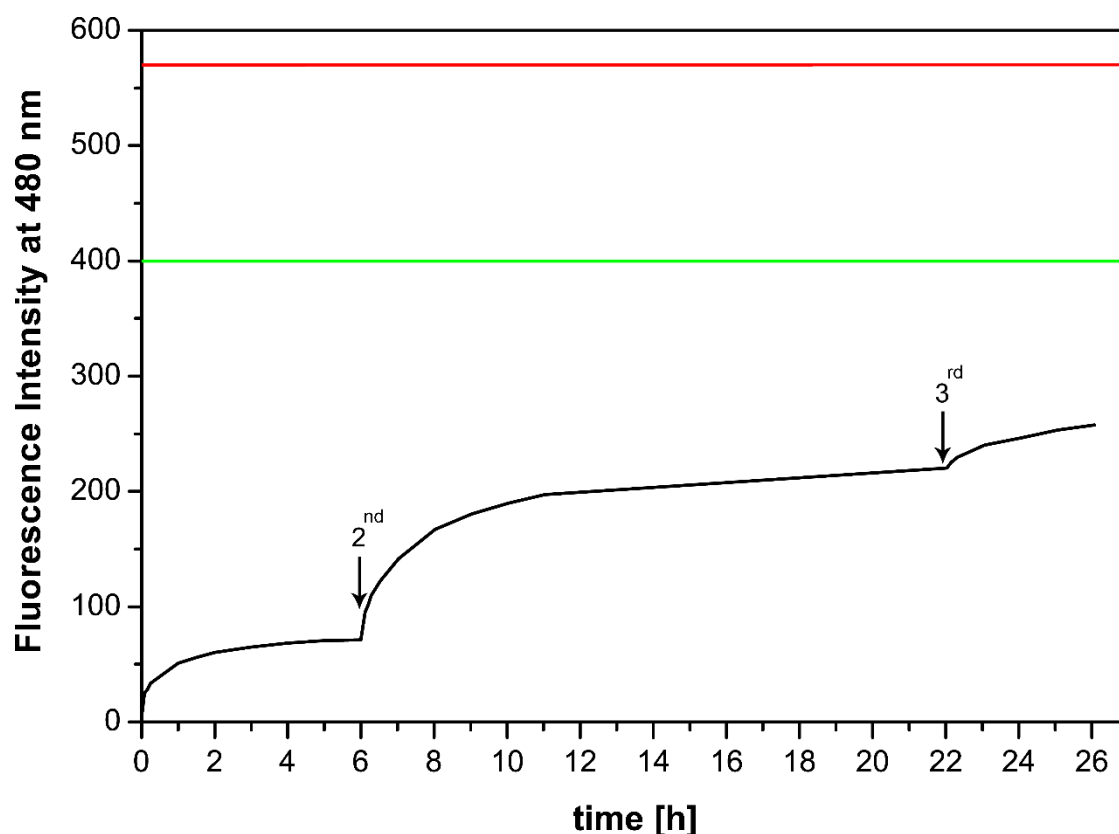


Figure 6. Kinetics of cleavage of the double-labelled GSH analogue **4** (20 μ M) by NsPCS (black line). The reaction is triggered by addition of the enzyme NsPCS in reaction tube containing the GSH analogue **4**. Enzyme to substrate ratios: 1:200 (1st addition at time zero), 1:100 (2nd addition) and 1:65 (3rd addition). (λ_{Ex} = 391nm, λ_{Em} = 480 nm, T = 35 °C, pH 8). The green line is the fluorescence level of an equimolar mix of the chemically synthesized cleavage products **14** and **28** (Fig.5) simulating the signal of full conversion. Red line is the signal of **14** bearing the fluorophore in absence of quencher-containing **28**.

This experiment shows that NsPCS is able to cleave the double labelled GSH analogue and that this reaction can be monitored by restoration of the donor fluorescence upon cleavage-off of the quencher moiety. However, the turnover compared to the reaction with natural GSH is significantly reduced. We can explain this finding by considering that the double-labelled GSH analogues interfere with the catalytic process due to its steric demand and different distribution of polar groups, such as hydrogen bond donors/ acceptors. Consequently, the affinity of the substrate and the velocity of dissociation of the products can be decreased.

Since a reasonable timescale for a kinetics experiment with oxidation- sensitive components (the free thiol of the enzyme is necessary for catalysis) does not exceed several hours, the second fluorescence-based quantitative kinetic experiment was carried out starting from an equimolar mixture of enzyme and substrate, ratio 1:1, up to a 1:5 ratio (Figure 7). The

fluorescence climbs to the same level in all the time-traces indicating complete conversion without inhibition.

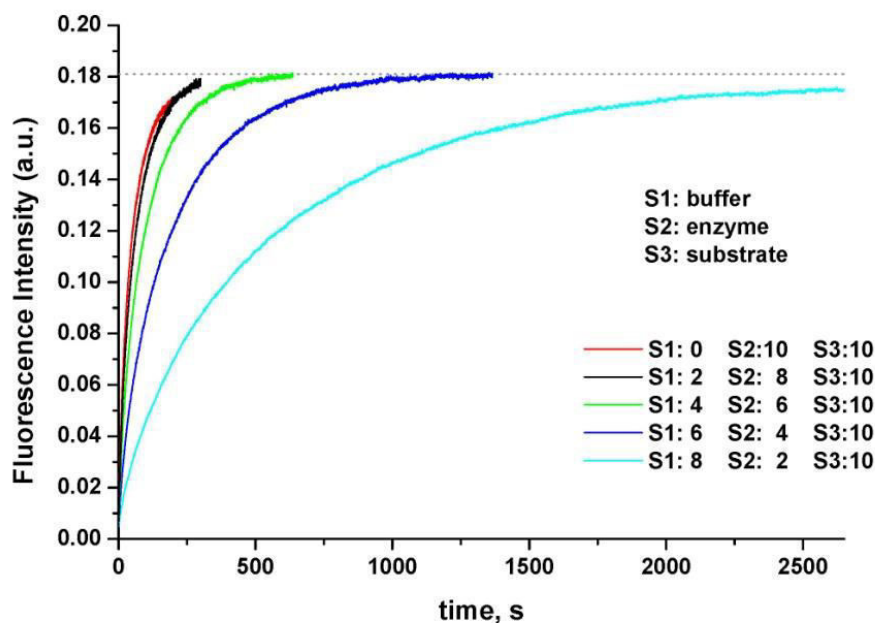


Figure 7. Kinetics of the cleavage of the double-labelled GSH analogue 4 by NsPCS measured with a stopped-flow apparatus. $\lambda_{Ex} = 391$ nm, $\lambda_{Em} = 480$ nm, $T = 35$ °C, pH 8. Enzyme to substrate ratios: 1:1 (red), 1:1.25 (black), 1:1.67 (green), 1:2.5 (blue) and 1:5 (cyan).

CONCLUSION

We have developed a modular and versatile strategy for the solution phase synthesis of oligopeptides consisting of amino acids bearing three functional groups. The synthetic advances reported herein offer an unprecedented access to highly functionalized chromophore labelled oligopeptide analogues. This modular and efficient reaction scheme allows us to synthesize GSH and various derivatives thereof from simple and cheap precursors in large laboratory scale with good to excellent yields. These results will facilitate the mechanistic study of peptidase reactions. As an example, we have prepared several GSH derivatives. Moreover, due to the various and fundamental roles of GSH in the metabolism of basically all the organisms, a versatile strategy to synthesize and manipulate glutathione is of general interest.

ASSOCIATED CONTENT

Supporting Information

Synthetic protocols and NMR spectra of new compounds (PDF). The Supporting Information is available free of charge on the ACS Publications website.

AUTHOR INFORMATION

Corresponding Authors

* elisa.bombarda@uni-bayreuth.de

* karl.kempf@u-bordeaux.fr

Notes

The authors declare no competing financial interests.

ACKNOWLEDGMENT

We are very thankful to Johannes M. Förster and Florian Gisdon for fruitful discussions.

The present work was supported by the DFG Grant BO 3578/1 and by the SFB 1357 (Project C03).

REFERENCES

- (1) Meister, A. *Methods Enzymol.* **1995**, 251 (C), 3.
- (2) Kaplowitz, N.; Aw, T. Y.; Ookhtens, M. *Annu. Rev. Pharmacol. Toxicol.* **1985**, VOL. 25, 715.
- (3) Akerboom, T. P. M.; Bilzen, M.; Sies, H. *J. Biol. Chem.* **1982**, 257 (8), 4248.
- (4) Ballatori, N.; Krance, S. M.; Notenboom, S.; Shi, S.; Tieu, K.; Hammond, C. L. *Biol. Chem.* **2009**, 390, 191.
- (5) Forman, H. J.; Zhang, H.; Rinna, A. *Mol. Aspects Med.* **2009**, 30 (1–2), 1.
- (6) Meister, A.; Anderson, M. E. *Annu. Rev. Biochem.* **1983**, 52, 711.
- (7) Suthanthiran, M.; Anderson, M. E.; Sharmatt, V. K.; Meister, A. *Proc. Natl. Acad. Sci. USA* **1990**, 87 (3343–3347).
- (8) Lu, S. C. *Mol. Aspects Med.* **2009**, 30 (1–2), 42.
- (9) Liu, R. M.; Gaston Pravia, K. A. *Free Radic. Biol. Med.* **2010**, 48 (1), 1.
- (10) Deponte, M. *Antioxidants Redox Signal.* **2017**, 27 (15), 1130.
- (11) Lushchak, V. I. *J. Amino Acids* **2012**, 2012, 1.

- (12) Lu, S. C. *Biochim. Biophys. Acta - Gen. Subj.* **2013**, *1830* (5), 3143.
- (13) Braidy, N.; Zarka, M.; Jugder, B. E.; Welch, J.; Jayasena, T.; Chan, D. K. Y.; Sachdev, P.; Bridge, W. *Front. Aging Neurosci.* **2019**, *11*, 1.
- (14) Bachhawat, A. K.; Kaur, A. *Antioxidants Redox Signal.* **2017**, *27* (15), 1200.
- (15) Kaur, H.; Ganguli, D.; Bachhawat, A. K. *J. Biol. Chem.* **2012**, 287, 8920.
- (16) Crawford, R. R.; Prescott, E. T.; Sylvester, C. F.; Higdon, A. N.; Shan, J.; Kilberg, M. S.; Mungrue, I. N. *J. Biol. Chem.* **2015**, *290*, 15878.
- (17) Kumar, A.; Tikoo, S.; Maity, S.; Sengupta, S.; Sengupta, S.; Kaur, A.; Bachhawat, A. K. *EMBO Rep.* **2012**, *13*, 1095.
- (18) Tsunoda, S.; Avezov, E.; Zyryanova, A.; Konno, T.; Mendes-Silva, L.; Melo, E. P.; Harding, H. P.; Ron, D. *Elife* **2014**, *3*, e03421.
- (19) Gekeler, W.; Grill, E.; Winnacker, E. L.; Zenk, M. H. *Zeitschrift fur Naturforsch. - Sect. C J. Biosci.* **1989**, *44* (5–6), 361.
- (20) Filiz, E.; Saracoglu, I. A.; Ozyigit, I. I.; Yalcin, B. *Biotechnol. Biotechnol. Equip.* **2019**, *33* (1), 178.
- (21) Clemens, S.; Kim, E. J.; Neumann, D.; Schroeder, J. I. *Embo J.* **1999**, *18* (12), 3325.
- (22) Cazalé, A. C.; Clemens, S. *FEBS Lett.* **2001**, *507*, 215.
- (23) Vatamaniuk, O. K.; Bucher, E. A.; Ward, J. T.; Rea, P. A. *Trends Biotechnol.* **2002**, *20* (2), 61.
- (24) Grill, E.; Löffler, S.; Winnacker, E. L.; Zenk, M. H. *Proc. Natl. Acad. Sci. U S A* **1989**, *86* (18), 6838.
- (25) Clemens, S.; Peršoh, D. *Plant Sci.* **2009**, *177* (4), 266.
- (26) Cobbett, C.; Goldsbrough, P. *Annu. Rev. Plant. Biol.* **2002**, *53*, 159.
- (27) Bleuel, C.; Wesenberg, D.; Meyer, A. J. *Plant Cell Physiol.* **2011**, *52* (7), 1153.
- (28) Rigouin, C.; Nylin, E.; Cogswell, A. A.; Schaumlöffel, D.; Dobritsch, D.; Williams, D. L. *PLoS Negl. Trop. Dis.* **2013**, *7* (1), e2037.
- (29) Ray, D.; Williams, D. L. *PLoS Negl. Trop. Dis.* **2011**, *5* (5), e1168.
- (30) Huang, H.-H.; Rigouin, C.; Williams, D. L. *Curr. Pharm. Des.* **2012**, *18* (24), 3505.
- (31) Clemens, S. *J. Plant Physiol.* **2006**, *163* (3), 319.
- (32) Harada, E.; von Roepenack-Lahaye, E.; Clemens, S. *Phytochemistry* **2004**, *65* (24), 3179.
- (33) Tsuji, N.; Nishikori, S.; Iwabe, O.; Shiraki, K.; Miyasaka, H.; Takagi, M.; Hirata, K.; Miyamoto, K. *Biochem. Biophys. Res. Commun.* **2004**, *315* (3), 751.
- (34) Rea, P. A. *Proc. Natl. Acad. Sci. U. S. A.* **2006**, *103* (3), 507.

- (35) Bellini, E.; Varotto, C.; Borsò, M.; Rugnini, L.; Bruno, L.; Di Toppi, L. S. *Plants* **2020**, *9* (7), 1.
- (36) Clay, N. K.; Adio, A. M.; Denoux, C.; Jander, G.; Ausubel, F. M. *Science* (80-.). **2009**, *323* (5910), 95.
- (37) Gisdon, F. J.; Feiler, G. C.; Kempf, O.; Foester, J. M.; Haiss, J.; Blankenfeldt, W.; Ullmann, G. M.; Bombarda, E. *ACS Chem. Biol.* **2022**, *17* (4), 883.
- (38) Adang, A. E. P.; Brussee, J.; Meyer, D. J.; Coles, B.; Ketterer, B.; Van der Gen, A.; Mulder, G. J. *Biochem. J.* **1988**, *255* (2), 721.
- (39) Adang, A. E.; Duindam, A. J.; Brussee, J.; Mulder, G. J.; van der Gen, A. *Biochem. J.* **1988**, *255* (2), 715.
- (40) Adang, A. E. P.; Brussee, J.; Van Der Gen, A.; Mulder, G. J. *Biochem. J.* **1990**, *269* (1), 47.
- (41) Pastuszak, J. J.; Chimiak, A. *J. Fur Prakt. Chemie* **1980**, *322* (3), 495.
- (42) Minchev, S.; Sofroniev, N. V. *Liebigs Ann. Der Chemie* **1987**, No. 1, 69.
- (43) Zeng, W.; Hemmasi, B. *Liebigs Ann. der Chemie* **1992**, *1992* (4), 311.
- (44) Maltese, M. Tritylation reactions based on metallic catalysts. WO 2007/009944 A1, 2007.
- (45) Vatamaniuk, O. K.; Mari, S.; Lang, A.; Chalasani, S.; Demkiv, L. O.; Rea, P. A. *J. Biol. Chem.* **2004**, *279* (21), 22449.
- (46) Radkowsky, A. E.; Kosower, E. M. *J. Am. Chem. Soc.* **1986**, *108* (13), 4527.
- (47) Grzam, A.; Tennstedt, P.; Clemens, S.; Hell, R.; Meyer, A. J. *FEBS Lett.* **2006**, *580* (27), 6384.
- (48) Meyer, A. J.; May, M. J.; Fricker, M. *Plant J.* **2001**, *27* (1), 67.
- (49) Ohkama-Ohtsu, N.; Zhao, P.; Xiang, C.; Oliver, D. J. *Plant J.* **2007**, *49* (5), 878.
- (50) Grzam, A.; Martin, M. N.; Hell, R.; Meyer, A. J. *FEBS Lett.* **2007**, *581* (17), 3131.
- (51) Johansson, M. K.; Cook, R. M. *Chem. Eur. J.* **2003**, *9* (15), 3466.
- (52) Kempf, O.; Ullmann, G. M.; Schobert, R.; Kempf, K.; Bombarda, E. *ACS Omega* **2021**, *6* (48), 32896.
- (53) Bombarda, E.; Kempf, O.; Kempf, K.; Schobert, R.; Ullmann, G. M. Hydrodabcyll. WO 2016/083611 A1, 2016.
- (54) Kempf, O.; Kempf, K.; Schobert, R.; Bombarda, E. *Anal. Chem.* **2017**, *89* (22), 11893.
- (55) Broch, H.; Ellem, M.; Viani, R.; Vasilescu, D. *Int. J. Quantum Chem.* **1993**, *48*, 49.
- (56) Noctor, G.; Mhamdi, A.; Chaouch, S.; Han, Y.; Neukermans, J.; Marquez-Garcia, B.; Queval, G.; Foyer, C. H. *Plant, Cell Environ.* **2012**, *35* (2), 454.
- (57) Rosowsky, A.; Vaidya, C. M.; Bader, H.; Wright, J. E.; Teicher, B. A. *J. Med. Chem.*

- 1997, 40 (3), 286.
- (58) Wiejak, S.; Masiukiewicz, E.; Rzeszotarska, B. *Chem. Pharm. Bull.* **1999**, 47 (10), 1489.
- (59) Wiejak, S.; Masiukiewicz, E.; Rzeszotarska, B. *Chem. Pharm. Bull.* **2001**, 49 (9), 1189.
- (60) Albert, R.; Danklmaier, J.; Hönig, H.; Kandolf, H. *Synth.* **1987**, 1987 (7), 635.
- (61) Wissmann, H.; Kleiner, H. -J. *Angew. Chemie Int. Ed. English* **1980**, 19 (2), 133.
- (62) Escher, R.; Bünning, P. *Angew. Chemie Int. Ed. English* **1986**, 25 (3), 277.
- (63) Dhaon, M. K.; Olsen, R. K.; Ramasamy, K. *J. Org. Chem.* **1982**, 47, 1962.
- (64) Neises, B.; Steglich, W. *Angew. Chemie Int. Ed. English* **1978**, 17 (7), 522.
- (65) Kim, Y.; Ebright, Y. W.; Goodman, A. R.; Reinberg, D.; Ebright, R. H. *Nucleic Acids Res.* **2008**, 36 (19), 6143.
- (66) Inguibert, N.; Coric, P.; Dhotel, H.; Llorens-Cortes, C.; Fournié-Zaluski, M. C.; Roques, B. P. *J. Label. Compd. Radiopharm.* **2004**, 47 (13), 997.
- (67) Choudhary, A.; Raines, R. T. *ChemBioChem* **2011**, 12, 1801.
- (68) Miller, S. M.; Simon, R. J.; Ng, S.; Zuckermann, R. N.; Kerr, J. M.; Moos, W. H. *Drug Dev. Res.* **1995**.
- (69) Borsuk, K.; Van Delft, F. L.; Eggen, I. F.; Ten Kortenaar, P. B. W.; Petersen, A.; Rutjes, F. P. J. T. *Tetrahedron Lett.* **2004**, 45 (18), 3585.
- (70) Haffar, B. M.; Hocart, S. J.; Coy, D. H.; Mantey, S.; Chiang, H. C. V.; Jensen, R. T. *J. Biol. Chem.* **1991**.
- (71) Joshi, D.; Milligan, J. C.; Zeisner, T. U.; O'Reilly, N.; Diffley, J. F. X.; Papageorgiou, G. *RSC Adv.* **2021**, 11 (33), 20457.
- (72) Garrett, G. S.; Emge, T. J.; Lee, S. C.; Fischer, E. M.; Dyehouse, K.; McIver, J. M. *J. Org. Chem.* **1991**, 56 (16), 4823.
- (73) McIntosh, J. M.; Cassidy, K. C.; Matassa, L. C. *Tetrahedron* **1989**, 45 (17), 5449.
- (74) Kumar, Y.; Jeyakodi, G.; Thulasibabu, R.; Gunasekaran, K.; Jambulingam, P. *Comb. Chem. High Throughput Screen.* **2015**, 18 (5), 492.
- (75) Liu, M.; Sharma, M.; Lu, G. L.; Yin, N.; Gailani, M. Al; Sreebhavan, S.; Wen, J. *Drug Dev. Ind. Pharm.* **2020**, 46 (5), 717.
- (76) Flagg, E. W.; Coates, R. J.; Jones, D. P.; Byers, T. E.; Greenberg, R. S.; Gridley, G.; Mclaughlin, J. K.; Blot, W. J.; Haber, M.; Preston-martin, S.; Schoenberg, J. B.; Austin, D. F.; Fraumeni, J. F. *Am. J. Epidemiol.* **1994**, 139 (5), 453.
- (77) Giblin, F. J. *J. Ocul. Pharmacol. Ther.* **2000**, 16 (2), 121.

Modular synthesis of glutathione analogues to study peptidase reactions *in vitro* and *in vivo*

Oxana Kempf, Matthias Ullmann, Olaf Stemmann, Rainer Schobert, Karl Kempf* and Elisa Bombarda*

Supporting Information

List of abbreviations:

$[\alpha]_D^{25}$	optical rotation at 25 °C
AcOEt	ethyl acetate
ATR	attenuated total reflection
Boc ₂ O	di ^{tert} butyl dicarbonate
CH	cyclohexane
CHCl ₃	chloroform
DCM	dichloromethane
DMSO	dimethyl sulfoxide
EDTA	ethylenediamine tetraacetic acid
EtOH	ethanol
FmocONSu	N-(9-H-Fluoren-9-ylmethoxycarbonyloxy) succinimide
H ₂ O	water
HCOOH	formic acid
HONSu	N-hydroxysuccinimide
HPLC	high pressure chromatography
HSiEt ₃	triethylsilane
IR	infrared
lit. ref.	literature reference
m. p.	melting point
MeCN	acetonitrile
MeOH	methanol
Na ₂ CO ₃	sodium carbonate
Na ₂ SO ₄	sodium sulphate
NaHSO ₄	sodium hydrogensulfate
NEt ₃	triethyl amine
NH ₄ Cl	ammonium chloride
NMR	nuclear magnetic resonance
Pd/C	palladium on activated charcoal
pH	negative decadic logarithm of proto concentration
R _f	ratio of fronts
RP	reversed phase
r.t.	room temperature
SOCl ₂	thionyl chloride
THF	tetrahydrofurane
TLC	thin layer chromatography
t _R	retention time
UV	ultraviolet
Vis	visible
λ	wavelength

Experimental Data

General Information. Double beam Perkin Elmer Lambda 750 UV/Vis spectrophotometer equipped with a thermostated cuvette holder was used to record the absorption spectra over a wavelength range 270–650 nm at 20 °C. The quartz cuvettes with 1 cm light path were from Hellma. Fluorescence was tested with a Cary Eclipse fluorimeter equipped with a thermostated cuvette holder. The pH was measured with the Mettler Toledo micro-electrode.

Chemical Synthesis. All chemicals were purchased from commercial vendors and used without further purification, unless indicated otherwise. All nonaqueous reactions were carried out under a nitrogen atmosphere in oven-dried glassware. Reaction progress was monitored by Thin Layer Chromatography (TLC) on pre-coated silica plates (Merck TLC Silica gel 60 F254) and spots were visualized by UV light and stained with ceric ammonium molybdate (CAM) solution. Chromatography was carried out using Macherey-Nagel 60 silica gel (230-400 mesh). The ^1H and ^{13}C NMR spectra were taken on a Bruker Avance 300 MHz spectrometer. Chemical shifts are reported in parts per million (ppm) referenced with respect to residual solvent ($\text{CHCl}_3 = 7.26/77.16$ ppm, $\text{DMSO} = 2.50/39.52$ ppm¹). IR spectra were recorded with a FT-IR spectrometer PerkinElmer S100 equipped with an Attenuated Total Reflection (ATR) unit. HPLC was performed on Bischoff ProntoSIL RP 200-5-C18, 250 x 4.6 mm (analytical) and 250 x 20 mm (preparative) columns.

General procedure A, T3P-coupling².

To a stirred solution of acid 1 Eq and amine 1 Eq in anhydrous DCM (10 mL/1mmol) was cooled to 0 °C. After addition of NEt_3 2.5 Eq the solution of T3P, 50 % in THF 1.15 Eq was added dropwise. The reaction mixture was stirring for 1 h at 0 °C and then was allowed to warm to r.t. The reaction was quenched with water and then water layer was extracted with DCM 3 times. The organic layer was dried over anhydrous Na_2SO_4 and evaporated *in vacuo*. The residue was purified by column chromatography (silica gel 60; $\text{CH}_2\text{Cl}_2/\text{AcOEt}$).

General procedure B, (N)Trt-deprotection³.

To a stirred solution of (N)Trt-protected amine 1Eq in DCM (10 mL/1mmol) at room temperature were added trifluoroacetic acid 1-3 % and EtOH (5 mL/1mmol). The reaction mixture was stirring for 2 h at r.t. and then cooled on the ice bath. Water was added and the mixture was basified with saturated potassium carbonate. The water layer was extracted with

ethyl acetate 3 times. The organic layer was dried over anhydrous Na_2SO_4 and evaporated *in vacuo*. The residue was purified by column chromatography (silica gel 60; CH/AcOEt + 0.5 % NEt_3).

General procedure C, hydrolysis.

The substance 1 Eq was dissolved in MeOH (10 mL/1mmol) and then H_2O (5 mL/1mmol) was introduced slowly. NaOH 1 Eq was added and reaction mixture was stirring for 6 h at 4 °C. The pH of the mixture then was adjusted till 7 and evaporated *in vacuo* at 30 °C. The remainder was partitioned between ethyl acetate and acidic water and then extracted with ethyl acetate 3 times. The organic layer was dried over anhydrous Na_2SO_4 and evaporated *in vacuo*. Product was used without further purification.

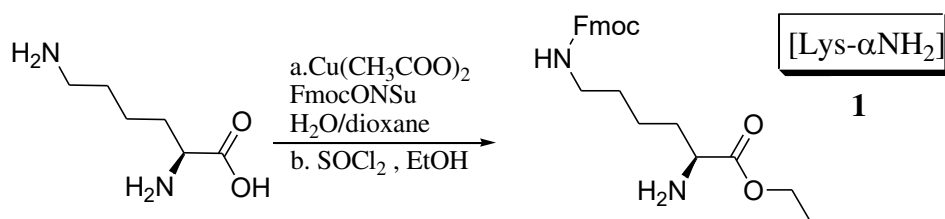
General procedure D, acidic deprotection⁴, HPLC.

To a stirred solution of protected peptide 1 Eq in DCM (20 ml/1mmol) at room temperature were added trifluoroacetic acid 100 Eq and HSiEt_3 4.4 Eq. The reaction mixture was stirring for 1 h at r.t. The mixture was evaporated *in vacuo* at 25 °C. The remainder was dissolved in degassed solution of MeOH/ H_2O (0.1 % HCOOH) and filtered through RP silica C_{18} . Mercaptoethanol (100 μL) was added (in case of free -SH) and the residue was purified by preparative HPLC. The fraction was carefully evaporated using high vacuum pump and liquid N_2 . The residue was dry by lyophilisation. The substance is O_2 -sensitive; keep in the fridge under Argon.

General procedure E. Bimane attachment⁵.

Peptide with free thiol group (0.08 mmol) was dissolved in degassed water (6 mL) under argon. After addition of NaHCO_3 (20.2 mg, 0.24 mmol) the solution of monobromo-Bimane (21.8 mg, 0.08 mmol) in acetonitrile (1.5 mL) was added. The reaction mixture was stirring for 1 h at r.t., then acidify with HCOOH, add H_2O (0.1 % HCOOH) and acetonitrile to get appropriate mixture for preparative HPLC.

Lysin building block (1):



a. (9H-fluoren-9-yl) methyl (S)-5-(ethoxycarbonyl)-5-aminopentylcarbamate hydrochloride.

This step was performed based on the literature⁶. To a mixture of L-lysine (8.77 g, 60 mmol), copper (II) acetate monohydrate (5.97 g, 30 mmol) in 10 % Na₂CO₃ solution (180 mL) was stirring for 45 min at room temperature. Then the mixture of H₂O (400 mL) and dioxane (500 mL) was added. Afterwards the solution of FmocONSu (22.3 g, 66 mmol) in dioxane (300 mL) was slowly introduced into reaction mixture. After 45 min stirring at room temperature the reaction mixture was acidified by half concentrated hydrochloric acid and washed twice with ethyl ether and twice with ethyl acetate. The water phase was concentrated *in vacuo* and put overnight into the fridge. The precipitate was filtered on Buchner funnel, washed with water and dried under vacuum. The white powder was used without purification.

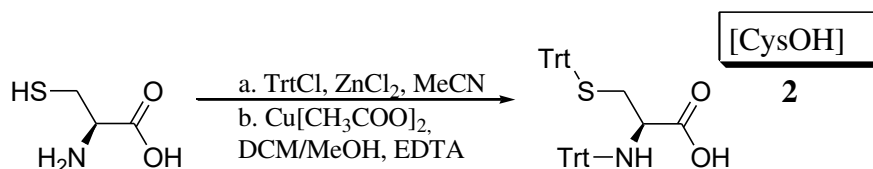
b. (9H-fluoren-9-yl)methyl (S)-5-(ethoxycarbonyl)-5-aminopentylcarbamate hydrochloride (N ϵ -Fmoc-L-lysine ethyl ester) 1 .

To a stirred cooled solution of L-Lysine(ϵ -Fmoc) hydrochloride salt (24.3 g, 60 mmol) in anhydrous EtOH (600 mL) under argon was slowly added SOCl₂ (52 ml, 720 mmol) at 0 °C. The reaction mixture was refluxed for 3 h (at 80 °C). Then the solvent was evaporated *in vacuo* and the remainder dispersed in diethyl ether, filtered and washed with diethyl ether. The product was dried *in vacuo* and used directly without further purification. Yield: 23.8 g (quantitative) as white solid of m.p. 156-157 °C.

IR (ATR): IR (ATR): 3361, 2869, 1743, 1687, 1586, 1525, 1475, 1462, 1447, 1409, 1314, 1273, 1256, 1227, 1195, 1168, 1139, 1102, 1031, 1012, 978, 860, 797, 764, 740 cm⁻¹.

[M+H]⁺ calc 397.21218 for C₂₃H₂₉N₂O₄⁺, [M+H]⁺ found 397.21120.

Cysteine building block (2):



a. (R)-trityl 2-(tritylamino)-3-(tritylthio)propanoate (N,S,O-tritrityl-L-cysteine).

This step was performed based on the literature⁷. The mixture of trityl chloride (33.8g, 121 mmol) and zinc chloride (2.75 g, 20 mmol) in anhydrous acetonitrile (370 mL) was stirring for 5 min. Then L-cysteine (4.9 g, 40.4 mmol) was added and the final mixture was stirring for 25 min at 40 °C until clear solution. The solution was allowed to cool to room

temperature and NEt_3 (16.9 g, 121 mmol) was added and was stirring for 1 h at room temperature. Then the mother liquor was pouring into the water (3.67 L) with stirring. The white suspension was filtered on the Buchner funnel and washed with water. The dried crude product was dissolved in diethyl ether, dried over anhydrous Na_2SO_4 and evaporated *in vacuo*. The product (thrityl ester N,S-ditritylcysteine) was used directly without further purification. Yield: 34.3 g (quantitative) as white foam⁶.

b. (R)-2-(tritylamino)-3-(tritylthio)propanoic acid (N, S-ditrityl-L-cysteine) 2.

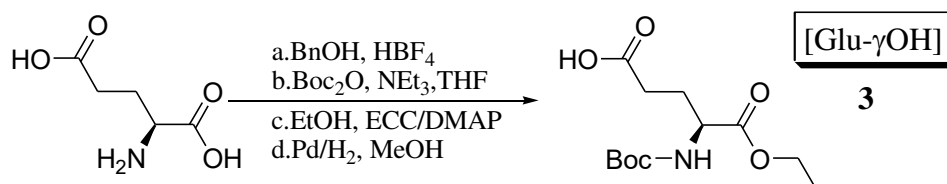
To a stirring solution of thrityl ester N,S-ditritylcysteine (34.3 g, 40.4mmol) in DCM (400 mL) was added copper (II) acetate monohydrate (4.03 g, 20.2 mmol) in methanol (700 mL) during 1 h. The reaction mixture was stirring for 4h at r.t. and then evaporated. The residue was dissolved in toluene and added to a freshly prepared solution of disodium EDTA (53.7 mmol). The emulsion was stirring for 30 min at room temperature and then the fractions were separated. The water layer was extracted 3 times with toluene. The organic layer was dried over anhydrous Na_2SO_4 and evaporated *in vacuo*. The residue was purified by column chromatography (silica gel 60; CH/AcOEt 3:1, R_f 0.3). Yield: 22 g (90 %) as white foam of m.p. 93 °C (lit. ref. for characterisation⁸).

¹h NMR (300 MHz, CHLOROFORM-*d*) δ ppm 2.37 (dd, $J=11.8, 6.3$ Hz, 1 H), 2.63 (dd, $J=11.8, 4.7$ Hz, 1 H), 3.42 (dd, $J=6.3, 4.7$ Hz, 1 H), 7.09 - 7.36 (m, 26 H), 7.42 - 7.48 (m, 5 H)
¹³C NMR (75 MHz, CHLOROFORM-*d*) δ 177.4, 145.3 ($\times 3$), 144.6 ($\times 3$), 129.7 ($\times 6$), 128.9 ($\times 6$), 128.1 ($\times 12$), 127.0 ($\times 6$), 71.5, 66.9, 55.7, 36.5.

IR (ATR): 3058, 2925, 2850, 1709, 1595, 1489, 1446, 1211, 1184, 1157, 1115, 1083, 1032, 1002, 939, 901, 847, 741, 696, 645, 616 cm^{-1} .

$[\text{M}-\text{H}]^-$ calc 604.23157 for $\text{C}_{41}\text{H}_{34}\text{NO}_2\text{S}^-$, $[\text{M}-\text{H}]^-$ found 604.23205.

Glutamic building block (3):



a. (S)-4-((benzyloxy)carbonyl)-2-aminobutanoic acid ammonium salt (L-Glu- γ -OBn NEt_3).

This step was performed according to the literature⁹.

b. tert-butyl (S)-3-((benzyloxy)carbonyl)-propylcarbamate (N-Boc-Glu- γ -OBn).

To a stirred solution of L-Glu(γ -OBn) triethylamine salt (8.16 g, 24 mmol) in THF (100 mL) at r.t. was added NEt₃ (3.34 mL, 24 mmol). The reaction mixture was cooled on an ice bath and then was added Boc₂O (5.76 g, 26.4 mmol). The reaction mixture was stirring overnight at room temperature. THF was evaporated *in vacuo*. The remainder was partitioned between ethyl acetate and H₂O and then cooled. 1 M NaHSO₄ was added at 0 °C and then water layer was extracted with ethyl acetate 3 times. The organic layer was dried over anhydrous Na₂SO₄ and evaporated *in vacuo*. The residue was purified by column chromatography (silica gel 60; CH/AcOEt 1:1, R_f 0.2). Yield: 4.1 g (76 %) (lit. ref. for characterisation¹⁰).

¹H NMR (300 MHz, CHLOROFORM-*d*) δ ppm 1.39 (s, 9 H), 1.86 - 2.03 (m, 1 H), 2.11 - 2.29 (m, 1 H), 2.33 - 2.55 (m, 2 H), 4.16 - 4.34 (m, 1 H), 5.08 (s, 2 H), 7.24 - 7.35 (m, 5 H).

¹³C NMR (75 MHz, CHLOROFORM-*d*) δ 177.2, 173.1, 155.8, 135.7, 128.4, 128.1, 128.0, 79.8, 66.3, 53.5, 30.3, 28.2, 27.5.

IR (ATR): 3326, 2979, 2557, 1729 1712, 1499, 1454, 1392, 1368, 1241, 1156, 1046, 1028, 850, 779, 735, 697, cm⁻¹.

c. tert-butyl (S)-3-((benzyloxy)carbonyl)-1-(ethoxycarbonyl)propylcarbamate (N-Boc-Glu- α -OEt- γ -OBn).

This step was performed based on the literature¹¹. To a stirred solution of L-(N)Boc-Glu(γ -OBn) (5.13 g, 15.2 mmol) in anhydrous DCM (150 mL) under argon were added EDC (3.2 g, 16.7 mmol), anhydrous EtOH (1.1 mL, 18.2 mmol) and DMAP (0.19 g, 1.52 mmol) at 0°C. The mixture then was stirred for 3 h at 0°C. 1M NaHSO₄ was added at 0°C and then water layer was extracted with DCM 3 times. The organic phases were washed with water and then dried over anhydrous Na₂SO₄ and evaporated *in vacuo*. The residue was purified by column chromatography (silica gel 60; CH/AcOEt 3:1, R_f 0.54). Yield: 4.1 g (74 %) as a white solid of m.p. 67 °C (lit. ref. for characterisation¹²).

¹H NMR (300 MHz, CHLOROFORM-*d*) δ ppm 1.27 (t, *J*=7.1 Hz, 3 H), 1.43 (s, 9 H), 1.91 - 2.02 (m, 1 H), 2.13 - 2.27 (m, 1 H), 2.36 - 2.56 (m, 2 H), 4.18 (dd, *J*=14.3, 7.1 Hz, 2 H), 4.26 - 4.37 (m, 1 H), 5.12 (s, 2 H), 7.35 (s, 5 H).

¹³C NMR (75 MHz, CHLOROFORM-*d*) δ 172.7, 172.3, 155.5, 135.9, 128.6 (×2), 128.4 (×3), 128.2, 80.1, 66.6, 61.7, 53.1, 30.5, 28.4 (×3), 28.0, 14.3.

IR (ATR): 3369, 2980, 2929, 1729, 1709, 1516, 1450, 1390, 1366, 1253, 1214, 1157, 1092, 1050, 1027, 980, 906, 860, 783, 735, 697, cm⁻¹.

d. (S)-3-((benzyloxy)carbonyl)-1-(ethoxycarbonyl)propylcarbamate (N-BocGlu- α OEt) 3.

To a stirred solution of N-Boc-Glu- α -OEt- γ -OBn (8.76 g, 24 mmol) in anhydrous MeOH (200 mL) under argon was added 5 % Pd/C (0.438 g, 5 %). The reaction flask first was filled with H₂ and then the reaction mixture was slowly bubbled with H₂ for 2 h at r.t.. Then the mixture was filtered through Celite and filtrate was concentrated *in vacuo*. Product was used without further purification. Yield: 6.6 g (quantitative) as transparent oil.

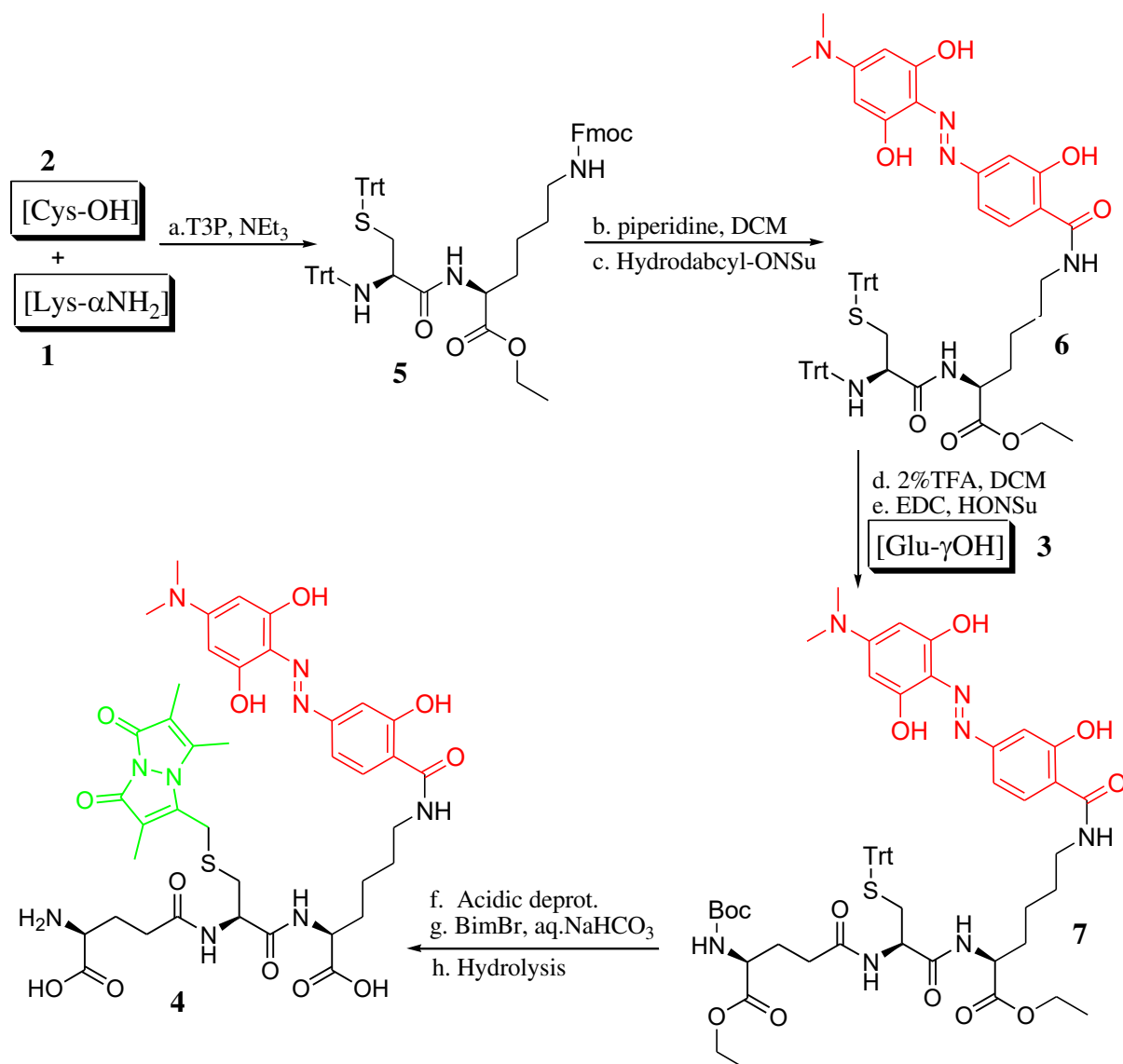
¹H NMR (300 MHz, CHLOROFORM-*d*) δ ppm 1.26 (t, *J*=7.1 Hz, 3 H), 1.41 (s, 9 H), 1.85 - 1.99 (m, 1 H), 2.07 - 2.22 (m, 1 H), 2.32 - 2.51 (m, 2 H), 4.17 (dd, *J*=14.3, 7.1 Hz, 2 H), 4.23 - 4.35 (m, 1 H), 5.18 - 5.34 (m, 1 H).

¹³C NMR (75 MHz, CHLOROFORM-*d*) δ 177.0, 172.4, 155.7, 80.2, 61.7, 53.0, 30.3, 28.4 ($\times 3$), 27.8, 14.2.

IR (ATR): 3341, 2980, 2934, 2582, 1736, 1707, 1513, 1450, 1393, 1367, 1248, 1212, 1158, 1050, 1025, 853, 777, 735, 702, cm⁻¹.

[M-H]⁻calc for C₁₂H₂₀NO₆⁻ 274.12961, [M-H]⁻found 274.12987

Synthesis of the double labelled GSH-analogue (γ -GluCys(Bim)Lys-HydrodabcyI) 4:



a. N, S-ditrityl-L-cysteinyl-N ϵ -Fmoc-L-lysine ethyl ester (5).

T3P coupling was performed according to general procedure A. The protected tripeptide was purified by column chromatography (silica gel 60; CH/AcOEt 2:1, R_f 0.49). Yield: 7.0 g (86 %) new substance as white foam of m.p. 79-81°C, $[\alpha]_D^{25} = + 29.6$ (c = 0.1, dichloromethane).

¹H NMR (300 MHz, CDCl₃) δ ppm 1.27 (t, J=7.2 Hz, 3 H), 1.31 - 1.48 (m, 2 H), 1.53 (m, 2 H), 1.74 (m, 1 H), 1.80 - 1.91 (m, 1 H), 1.96 (dd, J=12.0, 4.9 Hz, 1 H), 2.77 (d, J=3.5 Hz, 1 H), 2.97 (dd, J=12.0, 2.9 Hz, 1 H), 3.03 - 3.22 (m, 2 H), 3.39 (ddd, J=4.9, 3.5, 2.9 Hz, 1 H), 4.06 - 4.53 (m, 6 H), 4.93 (t, J=5.6 Hz, 1 H), 7.14 - 7.44 (m, 34 H), 7.61 (d, J=7.5 Hz, 2 H), 7.71 (d, J=7.3 Hz, 1 H), 7.78 (d, J=7.5 Hz, 2 H).

¹³C NMR (75 MHz, CDCl₃) δ 172.8, 171.5, 156.4, 145.2 (x3), 144.5 (x3), 144.1 (x2), 141.3 (x2), 129.7 (x6), 129.0 (x6), 128.0 (x6), 127.9 (x6), 127.7 (x2), 127.1 (x2), 126.9 (x3), 126.8

(×3), 125.1 (×2), 120.0 (×2), 71.9, 66.8, 66.5, 61.3, 56.7, 52.0, 47.4, 40.9, 36.5, 32.7, 29.3, 22.3, 14.7.

IR (ATR): 3322, 2927, 2850, 1722, 1664, 1491, 1446, 1372, 1243, 1185, 1031, 902, 740, 698 cm^{-1} .

$[\text{M}+\text{H}]^+$ calc 984.44047 for $\text{C}_{64}\text{H}_{62}\text{N}_3\text{O}_5\text{S}^+$, $[\text{M}+\text{H}]^+$ found 984.44269.

b. N, S-ditrityl-L-cysteinyl-L-lysine ethyl ester.

Fmoc-deprotection: To a stirred solution **5** (0.8 g, 0.8 mmol) in DCM (4 mL) at 0 °C was added solution of piperidine (1.6 mL) in DCM (2.4 mL). The reaction mixture was stirring for 10 min at 0 °C and then evaporated *in vacuo* at 25 °C. The residue was purified by column chromatography (AcOEt/EtOH + 0.5 % NEt_3 , R_f 0.05), evaporated *in vacuo* and used directly for the coupling. Yield: 0.61 g (quantitative).

c. N, S-ditrityl-L-cysteinyl-N ϵ -HydrodabcyL-L-lysine ethyl ester (6).

Coupling with hydrodabcyL-ONSu: To a stirred solution of amino compound (0.3 g, 0.4 mmol) in THF (20 mL) a solution of hydrodabcyL-ONSu ester (0.166 g, 0.4 mmol) in DMSO (1.5 mL) was added at room temperature. Then NEt_3 (0.100 mL, 0.7 mmol) was added. The reaction mixture was stirred overnight at room temperature. Thereafter, THF was evaporated and residue diluted with dichloromethane (100 mL), washed with brine (3 × 25 mL). The aqueous phases were extracted with dichloromethane (2 × 100 mL). The organic layer was dried over anhydrous Na_2SO_4 and evaporated *in vacuo*. The crude product was purified by column chromatography by column chromatography (silica gel 60; AcOEt, R_f 0.74) to afford **6** (360 mg, 85 %) new substance as a dark red foam of m.p. 114-115 °C.

^1H NMR (300 MHz, CDCl_3) δ ppm 1.23 (t, $J=6.7$ Hz, 3 H), 1.40 - 1.87 (m, 6 H), 1.95 (dd, $J=11.9, 5.0$ Hz, 1 H), 2.73 (d, $J=3.8$ Hz, 1 H), 2.87 (dd, $J=11.9, 3.5$ Hz, 1 H), 3.07 (s, 6 H), 3.30 - 3.45 (m, 3 H), 4.12 (s, 2 H), 4.19 - 4.27 (m, 1 H), 5.58 (d, $J=2.2$ Hz, 1 H), 5.92 (d, $J=2.2$ Hz, 1 H), 6.78 (dd, $J=8.5, 1.6$ Hz, 1 H), 7.01 (t, $J=4.5$ Hz, 1 H), 7.11 - 7.21 (m, 25 H), 7.25 - 7.32 (m, 6 H), 7.54 (d, $J=8.5$ Hz, 1 H), 7.71 (d, $J=7.5$ Hz, 1 H), 12.89 (s, 1 H).

^{13}C NMR (75 MHz, CDCl_3) δ 173.3, 171.4, 169.8, 165.6, 162.8, 158.8, 157.1, 150.7, 145.1 (×3), 144.4 (×3), 129.6 (×6), 129.0 (×6), 128.0 (×12), 127.4, 126.9 (×6), 123.8, 112.5, 109.8, 106.2, 92.5, 90.9, 71.9, 66.8, 61.5, 56.7, 51.8, 40.5 (×2), 39.7, 36.4, 33.1, 28.2, 22.6, 14.2.

IR (ATR): 3335, 2921, 2852, 1736, 1639, 1594, 1489, 1445, 1372, 1234, 1202, 1149, 1030, 890, 844, 810, 742, 697 cm^{-1} .

$[\text{M}+\text{H}]^+$ calc 1061.46300 for $\text{C}_{64}\text{H}_{65}\text{N}_6\text{O}_7\text{S}^+$, $[\text{M}+\text{H}]^+$ found 1061.45961.

d. S-trityl-L-cysteinyl-N ϵ -Hydrodabacyl-L-lysine ethyl ester.

Trt(N)deprotection on compound **6** was performed according to general procedure B. The dipeptide containing the free amino group was purified by column chromatography (silica gel 60; DCM/MeOH + 0.5 % NEt₃, R_f 0.5), evaporated *in vacuo* and used directly for the coupling. Yield: 0.22 g (quantitative).

e. N-Boc- α -ethyl- γ -L-glutamyl-S-ditrityl-L-cysteinyl-N ϵ -Hydrodabacyl-L-lysine ethyl ester (7).

To a stirred solution of **3** (52 mg, 0.188 mmol) in anhydrous DCM (10 mL) under argon were added EDC (40 mg, 0.207 mmol) and HONSu (22 mg, 0.19 mmol) at 0°C. After 5 min freshly deprotected compound **6** (154 mg, 0.188 mmol from step **d**) was added at 0°C and the reaction mixture was stirred overnight at r.t.. Thereafter saturated NH₄Cl was added and the water layer was extracted with DCM 3 times. The organic phases were washed with water and then dried over anhydrous Na₂SO₄ and evaporated *in vacuo*. The protected tripeptide was purified by column chromatography (silica gel 60; DCM/MeOH + 0.5 % NEt₃, R_f 0.5) to afford **7** (108 mg, 53 %) new substance as a dark red foam of m.p. 126-128 °C.

¹H NMR (300 MHz, CDCl₃) δ ppm 1.16 - 1.25 (m, 6 H), 1.36 - 1.45 (m, 11 H), 1.55 - 1.92 (m, 6 H), 2.11 - 2.20 (m, 2 H), 2.59 (dd, J=13.5, 5.0 Hz, 1 H), 2.70 - 2.86 (m, 1 H), 3.11 (s, 6 H), 3.19 - 3.31 (m, 1 H), 3.46 (dt, J=13.0, 6.3 Hz, 1 H), 3.57 - 3.72 (m, 1 H), 4.08 - 4.19 (m, 4 H), 4.22 - 4.35 (m, 1 H), 4.44 - 4.55 (m, 1 H), 5.23 - 5.37 (m, 1 H), 5.62 (d, J=2.0 Hz, 1 H), 5.83 - 5.97 (m, 1 H), 6.36 (d, J=5.9 Hz, 1 H), 6.52 (d, J=7.9 Hz, 1 H), 6.95 (d, J=8.2 Hz, 1 H), 7.14 (d, J=1.5 Hz, 1 H), 7.19 - 7.31 (m, 10 H), 7.42 (d, J=7.6 Hz, 6 H), 7.67 (d, J=8.2 Hz, 1 H), 12.78 (br. s., 1 H).

¹³C NMR (75 MHz, CDCl₃) δ 172.5, 172.3, 171.8, 170.1, 169.9, 165.3, 162.7, 159.0, 157.4, 156.0, 150.7, 144.4 (\times 3), 130.0 (\times 6), 128.2 (\times 6), 127.9, 127.1 (\times 3), 123.9, 112.9, 109.8, 106.4, 92.6, 91.1, 80.4, 67.5, 61.8, 61.6, 53.1, 52.9, 52.0, 40.6 (\times 2), 39.2, 33.0, 32.3, 31.6, 29.2, 28.4 (\times 3), 28.2, 22.2, 14.2 (\times 2).

IR (ATR): 3291, 2931, 1736, 1714, 1640, 1493, 1444, 1418, 1392, 1367, 1243, 1205, 1156, 1107, 1028, 970, 891, 840, 808, 740, 699 cm⁻¹.

[M+H]⁺calc 1076.47977 for C₅₇H₇₀N₇O₁₂S⁺, [M+H]⁺found 1076.48108.

f, g and h. γ -L-glutamyl-S-Bimane-L-cysteinyl-N ϵ -HydrodabcyL-L-lysine (4).

Acidic deprotection of **7** was performed according to general procedures D without further purification. The residue was evaporated *in vacuo* at 30 °C, dried on HV pump and used directly for the coupling with monobromo-Bimane according to general procedure E without further purification. The reaction mixture was directly used for hydrolysis by addition of 4 mL degassed EtOH and K₂CO₃ (30 mg) till pH 8 (degassed solutions under argon) and was allowed to stir overnight under argon. The crude mixture purified by preparative HPLC (flow rate 10 mL/min, 55 % MeOH/45 % H₂O + 0.1% HCOOH) t_R = 15 min. Yield: 25 mg, (at least 30 % yield after 3 steps and preparative HPLC) as a dark red solid of m.p. 229 °C.

¹H NMR (500 MHz, DMSO-*d*₆) δ ppm 1.26 - 1.37 (m, 2 H), 1.43 - 1.62 (m, 4 H), 1.67 - 1.76 (m, 2 H), 1.71 (s, 3 H), 1.79 (s, 3 H), 1.82 - 1.92 (m, 1 H), 1.98 - 2.01 (m, 1 H), 2.25 - 2.36 (m, 2 H), 2.39 (s, 3 H), 2.74 (dd, *J*=13.4, 10.1 Hz, 1 H), 3.02 (dd, *J*=13.4, 4.4 Hz, 1 H), 3.07 (s, 6 H), 3.90 (s, 2 H), 3.31 - 3.38 (m under water signal, 1 H), 4.10 - 4.14 (m, 1 H), 4.50 (td, *J*=8.9, 4.7 Hz, 1 H), 5.71 (br. s., 2 H), 7.18 (dd, *J*=8.5, 1.8 Hz, 1 H), 7.34 (d, *J*=1.8 Hz, 1 H), 8.00 (d, *J*=8.5 Hz, 1 H), 8.41 (d, *J*=8.2 Hz, 1 H), 8.45 (d, *J*=7.3 Hz, 1 H), 9.26 (t, *J*=5.2 Hz, 1 H).

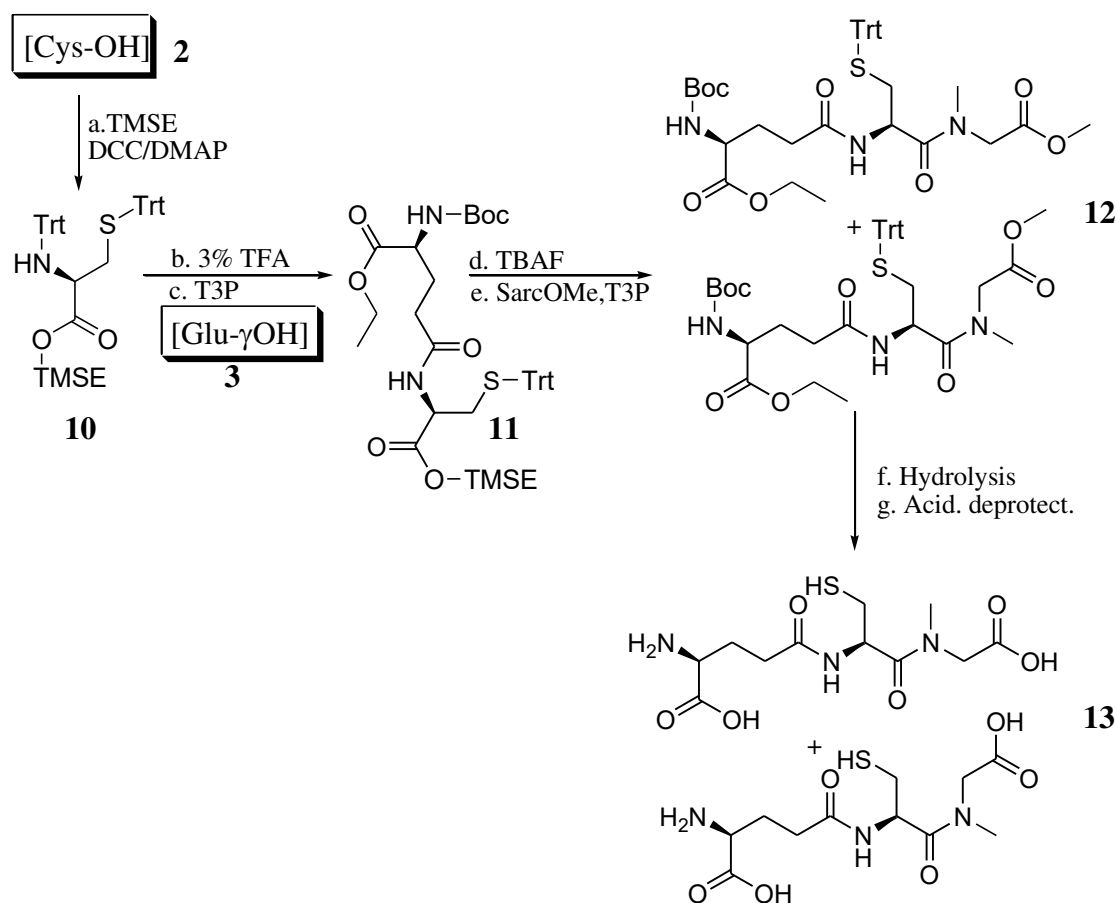
¹³C NMR (125.8 MHz, CDCl₃) δ 173.4, 171.9, 170.5, 170.3, 168.8, 161.8, 160.2, 159.8, 157.7 ($\times 2$), 151.1, 147.6, 146.9, 129.0, 124.3 ($\times 2$), 112.9, 112.8, 110.8, 110.0, 106.0, 91.4 ($\times 2$), 53.0, 52.7, 52.1, 40.1 ($\times 2$), 40.0, 33.7, 31.6, 30.4, 28.5, 26.9, 24.6, 22.9, 11.3, 6.8, 6.5.

IR (ATR): 3270, 2928, 2872, 1739, 1631, 1594, 1543, 1504, 1412, 1239, 1159, 1107, 1088, 1026, 891, 810, 739 cm⁻¹.

[M-H]⁻ calc 866.31376 for C₃₉H₄₈N₉O₁₂S⁻, [M-H]⁻ found 866.31614.

“Non-cleavable” amide bond isosters

N-methylated amide bond (γ -GluCysSarc) 13:



a. (R)-2-(trimethylsilyl)ethyl 2-(tritylamino)-3-(tritylthio)propanoate (N, S-ditrityl-L-cysteinyl-OTMSE) 10.

To a stirred solution of **2** (2 g, 3.3 mmol) in anhydrous DCM (30 mL) under argon were added DCC (0.68 g, 3.3 mmol) in DCM (10 mL), DMAP (0.04 g, 0.33 mmol) in DCM (10 mL) and trimethylsilylethanol (0.52 mL, 3.63 mmol) at 0 °C. The mixture then was stirred for 5 min at 0°C and at r.t. overnight. Precipitated urea was then filtered off and the filtrate evaporated *in vacuo*. The residue was purified by column chromatography (silica gel 60; cyclohexane / ethyl acetate 3:1, R_f 0.8). Yield: 1.64 g (71 %) as white foam of m.p. 58-59 °C, $[\alpha]_D^{25} = +48$ (c = 0.1, dichloromethane) (known substance, but no lit. ref. for characterisation).

^1H NMR (300 MHz, CDCl_3) δ ppm -0.02 (s, 9 H), 0.70 (dt, $J=11.1$, 5.4 Hz, 2 H), 2.47 (dd, $J=11.0$, 6.5 Hz, 1 H), 2.53 (dd, $J=11.0$, 4.5 Hz, 1 H), 3.36 (dd, $J=6.5$, 4.5 Hz, 1 H), 3.50 (dtd, $J=11.0$, 6.9, 6.9, 4.7 Hz, 1 H), 3.63 (dt, $J=11.1$, 6.9 Hz, 1 H), 7.16 - 7.30 (m, 20 H), 7.45 (t, $J=6.6$ Hz, 10 H).

^{13}C NMR (75 MHz, CDCl_3) δ 173.4, 145.8 ($\times 3$), 144.7 ($\times 3$), 129.7 ($\times 6$), 128.8 ($\times 6$), 127.9 ($\times 6$), 127.8 ($\times 6$), 126.6 ($\times 3$), 126.3 ($\times 3$), 71.2, 67.1, 63.0, 55.4, 37.3, 16.9, -1.6 ($\times 3$).

IR (ATR): 3054, 2955, 1729, 1595, 1489, 1446, 1249, 1168, 1121, 1033, 931, 902, 835, 742, 696 cm^{-1} .

$[\text{M}+\text{H}]^+$ calc for $\text{C}_{46}\text{H}_{47}\text{NO}_2\text{SSi}^+$ 322.10673, $[\text{M}+\text{H}]^+$ found 322.10630.

b. Trt(N)deprotection on compound **10** was performed according to general procedure B. The dipeptide containing the free amino group was purified by column chromatography (silica gel 60; CH/AcOEt 3:1 + 0.5 % NEt_3 , R_f 0.3), evaporated *in vacuo* and used directly for the coupling. Yield: 1.07 g (quantitative).

c. **tert-butyl (S)-3-((R)-1-((2-(trimethylsilyl)ethoxy)carbonyl)-2-(tritylthio)ethyl carbamoyl)-1-(ethoxycarbonyl)propylcarbamate (N-Boc- α -ethyl- γ -L-glutamyl-S-ditrityl L-cysteinyl-OTMSE) 11.**

T_3P coupling was performed according to general procedure A. The protected dipeptide was purified by column chromatography (silica gel 60; cyclohexane/AcOEt 3:1, R_f 0.28). Yield: 1.38 g (89 %).

d. N-Boc- α -ethyl- γ -L-glutamyl-S-ditrityl-L-cysteine.

TMSE-deprotection: The stirred solution of **11** (1.55 g, 2.15 mmol) in anhydrous THF (20 mL) was cooled to 0°C . After addition of (3 Eq) TBAF, 1M in THF (6.45 ml, 6.45 mmol) the reaction mixture was stirring for 1 h at 0°C . Afterward THF was evaporated at 30°C and the crude product was purified by column chromatography (silica gel 60; DCM/MeOH 9:1, R_f 0.4). Evaporate the fraction with toluol. Yield: 1.33 g (quantitative) and use directly for the next step.

e. N-Boc- α -ethyl- γ -L-glutamyl-S-ditrityl-L-cysteinyl-L-sarcosine methyl ester (12).

T_3P coupling was performed according to general procedure A (2 eq. SarcOMe, 4eq. NEt_3 , the reaction mixture was stirring overnight at room temperature). The protected tripeptide was purified by column chromatography (silica gel 60; DCM/MeOH 9:1, R_f 0.67). Yield: 1.55 g (62 %).

f, g. γ -GluCysSarc (13).

Hydrolysis, total deprotection and HPLC were performed according to general procedures C and D. The final dipeptide was purified by preparative HPLC (flow rate 18 mL/min 3 % MeOH/ 97 % H_2O (0.1 % HCOOH) isocratic), $t_R = 15$ min, $[\alpha]_D^{25} = -21$. Yield: 264 mg (73 %) white solid.

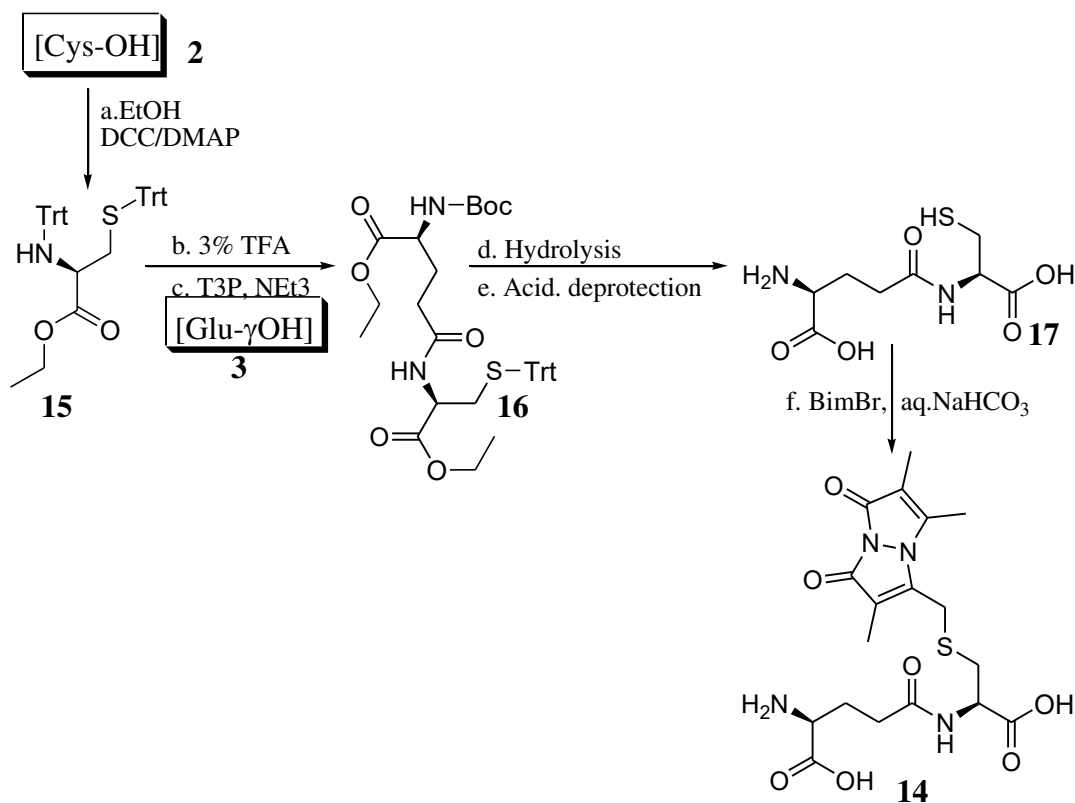
^1H NMR (300 MHz, DMSO- d_6) δ ppm 1.82 (td, $J=14.4, 7.7$ Hz, 2 H)/ 1.96 (td, $J=13.2, 7.0$ Hz, 2 H), 2.20 - 2.35 (m, 2+2 H), 2.45 - 2.60 (m, 2 H), 2.76 (dd, $J=12.6, 7.1$ Hz, 2 H), 2.84 (s, 3 H)/ 3.08 (s, 3 H), 3.41 (t, $J=6.4$ Hz, 1 H)/ 3.63 (dd, $J=7.7, 5.2$ Hz, 1 H), 3.89 (d, $J=17.2$ Hz, 1 H, $\text{CH}_2\text{S}^{\text{a}}$)/ 3.89 (d, $J=18.1$ Hz, 1 H, $\text{CH}_2\text{S}^{\text{a}}$), 4.06 (d, $J=17.2$ Hz, 1 H, $\text{CH}_2\text{S}^{\text{b}}$)/ 4.22 (d, $J=18.1$ Hz, 1 H, $\text{CH}_2\text{S}^{\text{b}}$), 4.72 (dt, $J=9.1, 7.1$ Hz, 1 H)/ 4.84 (dt, $J=8.3, 7.0$ Hz, 1 H), 8.38 (d, $J=9.1$ Hz, 1 H)/ 8.43 (d, $J=8.3$ Hz, 1 H).

^{13}C NMR (75 MHz, , DMSO- d_6) δ 171.5/ 171.4, 171.2/ 171.1, 170.9/ 170.5, 169.8, 53.1/ 52.5, 51.5/ 49.7, 51.0/ 50.7, 36.1/ 34.7, 31.4/ 30.5, 27.1/ 27.0, 25.8/ 25.5.

IR (ATR): 2940, 1622, 1489, 1404, 1212, 629, 591, 568 cm^{-1} .

$[\text{M}+\text{Na}]^+$ calc for $\text{C}_{46}\text{H}_{47}\text{NO}_2\text{SSiNa}^+$ 728.29890, $[\text{M}+\text{Na}]^+$ found 728.29825.

Dipeptide γ -GluCys (γ -GluCysBim) 14:



a. (R)-ethyl 2-(tritylamino)-3-(tritylthio)propanoate (N, S-ditrityl-L-cysteinyl-OEt) 15.

To a stirred solution of N,S-ditritylcysteine (6.06 g, 10 mmol) in anhydrous DCM (20mL) under argon were added DCC (2.06 g, 10 mmol) in DCM (10 ml), anhydrous ethanol (2.92 mL, 50 mmol) and DMAP (0.112 g, 1 mmol) in DCM (10 ml) at 0°C. The mixture then was stirred for 5 min at 0 °C and at 20 °C overnight. Precipitated urea was then filtered off and the filtrate evaporated *in vacuo*. The residue was purified by column chromatography

(silica gel 60; cyclohexane / ethyl acetate 10:1, R_f 0.46). Yield: 6.1g (96%) new substance as white foam of m.p. 175°C, $[\alpha]_D^{25} = +63$ (c = 0.1, dichloromethane).

^1H NMR (300 MHz, CHLOROFORM-*d*) δ ppm 1.01 (t, $J=7.1$ Hz, 3 H), 2.49 (dd, $J=11.8, 7.4$ Hz, 1 H), 2.56 (dd, $J=11.8, 4.9$ Hz, 1 H), 2.85 (d, $J=9.9$ Hz, 1 H), 3.38 (ddd, $J=9.9, 7.4, 4.9$ Hz, 1 H), 3.51 (dq, $J=10.7, 7.1$ Hz, 1 H), 3.66 (dq, $J=10.6, 7.1$ Hz, 1 H), 7.11 - 7.35 (m, 20 H), 7.44 - 7.50 (m, 10 H).

^{13}C NMR (75 MHz, CHLOROFORM-*d*) δ 173.3, 145.7 ($\times 3$), 144.7 ($\times 3$), 129.6 ($\times 6$), 128.8 ($\times 6$), 127.8 ($\times 6$), 127.7 ($\times 6$), 126.6 ($\times 3$), 126.3 ($\times 3$), 71.2 ($\times 2$), 60.7, 55.3, 37.3, 13.8.

IR (ATR): 3058, 2925, 1732, 1595, 1489, 1446, 1183, 1113, 1028, 906, 729, 697 cm^{-1} .

$[\text{M}+\text{Na}]^+$ calc 656.25937 for $\text{C}_{43}\text{H}_{39}\text{NNaO}_2\text{S}^+$, $[\text{M}+\text{Na}]^+$ found 656.26001.

b. (R)-ethyl 3-(tritylthio)propanoate.

Trt(N)deprotection on compound **15** was performed according to general procedure B. The dipeptide containing the free amino group was purified by column chromatography (silica gel 60; CH/AcOEt 1:1 + 0.5% NEt_3 , R_f 0.5), evaporated *in vacuo* Yield: 1.85 g (quantitative).

c. tert-butyl (S)-3-((R)-1-(ethoxycarbonyl)-2-(tritylthio)ethylcarbamoyl)-1-(ethoxycarbonyl)propylcarbamate (N-Boc- α -ethyl- γ -L-glutamyl-S-ditryl-L-cysteinyl-OEt) 16.

T_3P coupling was performed according to general procedure A. The protected dipeptide was purified by column chromatography (silica gel 60; cyclohexane/AcOEt 1:1, R_f 0.58). Yield: 0.77 g (81 %) new substance.

^1H NMR (300 MHz, CHLOROFORM-*d*) δ ppm 1.20 (t, $J=7.1$ Hz, 6 H), 1.38 - 1.42 (m, 9 H), 1.78 - 1.93 (m, 1 H), 2.04 - 2.28 (m, 3 H), 2.56 (dd, $J=12.3, 4.7$ Hz, 1 H), 2.65 (dd, $J=12.3, 6.3$ Hz, 1 H), 4.11 (s, 4 H), 4.17 - 4.36 (m, 1 H), 4.47 (ddd, $J=7.4, 6.3, 4.7$ Hz, 1 H), 5.28 (d, $J=8.0$ Hz, 1 H), 6.25 (d, $J=7.4$ Hz, 1 H), 7.15 - 7.27 (m, 9 H), 7.31 - 7.39 (m, 6 H).

^{13}C NMR (75 MHz, CHLOROFORM-*d*) δ 172.4, 172.2, 155.9, 144.5 ($\times 3$), 129.6 ($\times 6$), 128.8 ($\times 6$), 126.8 ($\times 3$), 80.1, 66.7, 61.5, 53.29, 51.9, 51.6, 45.5, 33.9, 32.4, 28.4 ($\times 3$), 14.2, 13.7.

d, e. (S)-4-((R)-1-carboxy-2-mercaptoethylcarbamoyl)-2-aminobutanoic acid (γ -GluCys) 17.

Hydrolysis, total deprotection and HPLC were performed according to general procedures C and D. The final dipeptide was purified by preparative HPLC (10 mL/min): 3% MeOH/97% H_2O (0.1% HCOOH), $t_R = 7.4$ min. (lit. ref. for characterisation^{13,14}).

^1H NMR (300 MHz, DEUTERIUM OXIDE) δ ppm 2.09 - 2.25 (m, 2 H), 2.49 - 2.57 (m, 2 H), 2.92 (dd, $J=14.3, 6.3$ Hz, 1 H), 2.98 (dd, $J=14.3, 4.9$ Hz, 1 H), 3.91 (t, $J=6.3$ Hz, 1 H), 4.58 (dd, $J=6.3, 4.9$ Hz, 1 H)

^{13}C NMR (75 MHz, DEUTERIUM OXIDE) δ 174.5, 173.8, 172.8, 55.0, 53.2, 31.1, 25.9, 25.1.

f. (S)-4-((R)-1-carboxy-2-(((1,7-dihydro-2,3,6-trimethyl-1,7-dioxopyrazolo[1,2-a] pyrazol 5-yl)methyl)sulfanyl)ethylcarbamoyl)-2-aminobutanoic acid (γ -GluCysBim) 14.

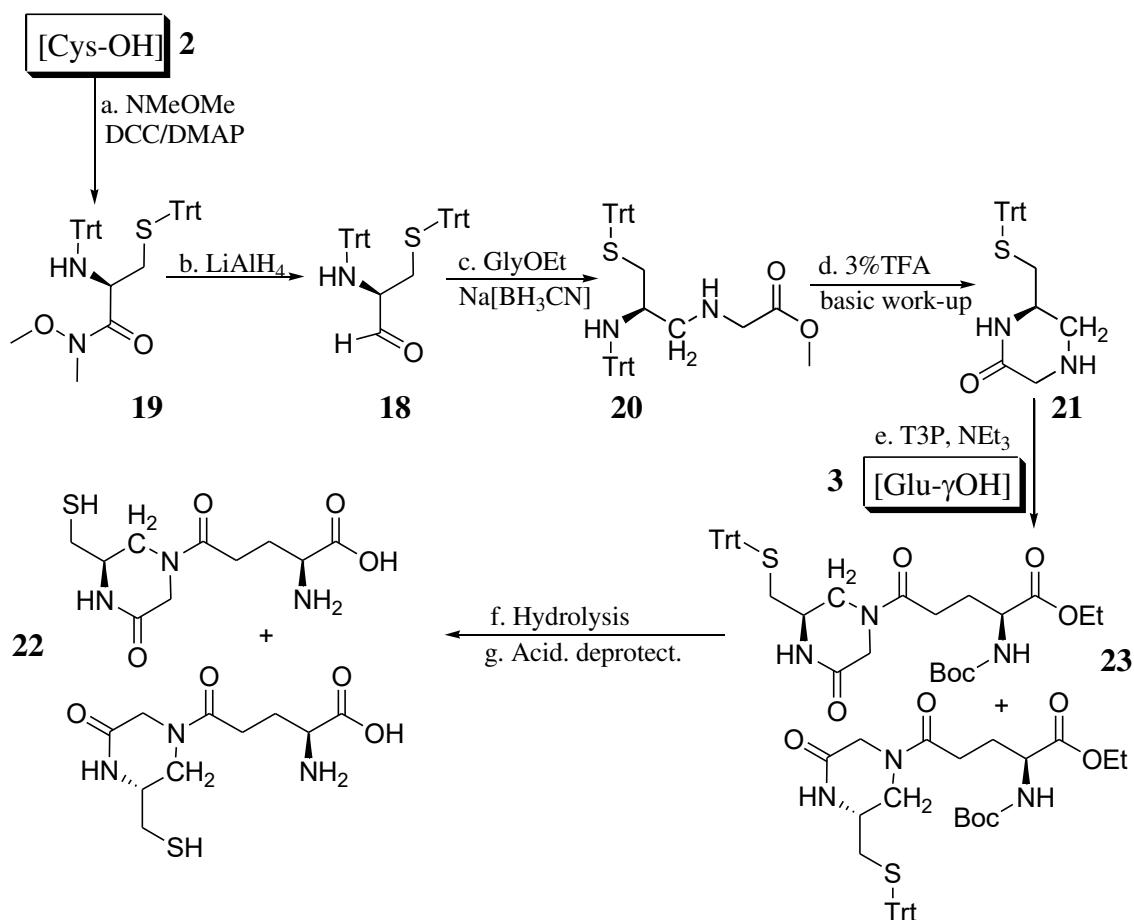
Coupling with monobromo-Bimane was performed according to general procedure E (room temperature overnight) without additional hydrolysis before with NaOH. The crude mixture purified by preparative HPLC (flow rate 10 mL/min, 10 % MeOH/90 % H_2O + 0.1% HCOOH) $t_{\text{R}} = 14.5$ min. Yield: 18 mg, (at least 40 % yield after preparative HPLC) as a yellow solid.

^1H NMR (300 MHz, DEUTERIUM OXIDE) δ ppm 1.68 - 1.76 (m, 3 H), 1.76 - 1.85 (m, 3 H), 1.98 - 2.10 (m, 2 H), 2.30 - 2.47 (m, 5 H), 2.85 - 2.93 (m, 1 H), 3.04 - 3.11 (m, 1 H), 3.67 (t, $J=5.8$ Hz, 1 H), 3.83 (d, $J=2.7$ Hz, 2 H), 4.28 - 4.32 (m, 1 H).

^{13}C NMR (75 MHz, DEUTERIUM OXIDE) δ 171.9, 169.6, 168.7, 160.1, 160.0, 147.6, 146.9, 112.8, 110.7, 53.3, 51.8, 33.3, 31.9, 27.1, 24.5, 11.3, 6.7, 6.4.

TOF MS ES⁺: $[\text{M}+\text{H}]^+$ calc 441.14385 for $\text{C}_{18}\text{H}_{25}\text{N}_4\text{O}_7\text{S}^+$, $[\text{M}+\text{H}]^+$ found 441.32.

Reduced form of amide bond (nc γ -GluCysGly) 22:



a. (R)-N-methoxy-N-methyl-2-(tritylamino)-3-(tritylthio)propanamide (N, S-ditrityl-L-cysteinyl-NMeOMe) 19.

To a stirred solution of N,S-ditritylcysteine (6.1 g, 10 mmol) in anhydrous DCM (40 mL) under argon were added DCC (2.1g, 10 mmol) in DCM (15 mL), DMAP (1.2 g, 11 mmol) in DCM (15 mL) and N,O-Dimethylhydroxylamine hydrochloride (1.2 g, 11 mmol) at 0°C. The mixture then was stirred for 5 min at 0 °C and at 20 °C overnight. Precipitated urea was then filtered off and the filtrate evaporated *in vacuo*. The residue was purified by column chromatography (silica gel 60; cyclohexane / ethyl acetate 3:1, R_f 0.48). Yield: 4.2 g (65 %) new substance as white foam of m.p. 197 °C, $[\alpha]_D^{25} = +65$ (c = 0.1, dichloromethane).

¹H NMR (300 MHz, CHLOROFORM-*d*) δ 2.42 (dd, $J=11.7, 4.9$ Hz, 1 H), 2.55 (dd, $J=11.7, 4.9$ Hz, 1 H), 2.67 (s, 3 H), 3.18 (s, 3 H), 3.36 (d, $J=9.6$ Hz, 1 H), 3.99 (dt, $J=9.6, 4.9$ Hz, 1 H), 7.16 - 7.36 (m, 20 H), 7.56 (m, 10 H).

¹³C NMR (75 MHz, CHLOROFORM-*d*) δ 173.4, 146.1 ($\times 3$), 144.9 ($\times 3$), 129.8 ($\times 6$), 129.0 ($\times 6$), 127.9 ($\times 6$), 127.7 ($\times 6$), 126.6 ($\times 3$), 126.2 ($\times 3$), 71.2, 66.3, 60.6, 51.4, 37.8, 32.4.

IR (ATR): 3296, 3057, 2928, 1660, 1594, 1488, 1445, 1377, 1319, 1265, 1182, 1082, 1031, 999, 956, 939, 902, 846, 742, 697, cm^{-1} .

Elem. Anal. Calculated for $\text{C}_{43}\text{H}_{40}\text{N}_2\text{O}_2\text{S}$: C, 79.60; H, 6.21; N, 4.32; O, 4.93; S, 4.94. Found: C, 79.51; H, 6.29; N, 4.23; S, 4.73.

b. (R)-2-(tritylamino)-3-(tritylthio)propanal (N, S-ditrityl-L-cysteinal) 18.

This step was performed based on the literature¹⁵. To a stirred solution of N-methoxy-N-methyl-2-(tritylamino)-3-(tritylthio)propanamide (3.86 g, 6 mmol) in anhydrous THF (60 mL) under argon were added lithiumaluminiumhydride (0.285 g, 7.5 mmol). The reaction mixture was stirring for 3 h at room temperature, then reaction was quenched with K, Na-tartrat and extracted three times with diethyl ether. The combined organic phases were washed with NaHSO_4 , NaHCO_3 and brine. The organic layer was dried over anhydrous Na_2SO_4 evaporated *in vacuo*. Product was used without further purification (cyclohexane / ethyl acetate 10:1, R_f 0.45). Yield: 2.05 g (100 %) new substance as white foam of m.p. 140 °C, $[\alpha]_D^{25} = +48.4$ (c = 0.1, dichloromethane).

^1H NMR (300 MHz, CHLOROFORM-*d*) δ ppm 2.43 (d, $J=1.1$ Hz, 1 H), 2.45 (s, 1 H), 3.19 (br. s, 1 H), 3.40 (t, $J=5.5$ Hz, 1 H), 7.26 - 7.38 (m, 20 H), 7.45 - 7.54 (m, 10 H), 8.80 (d, $J=0.8$ Hz, 1 H).

^{13}C NMR (75 MHz, CHLOROFORM-*d*) δ 201.4, 145.7 ($\times 3$), 144.4 ($\times 3$), 129.5 ($\times 6$), 128.6 ($\times 6$), 128.0 ($\times 6$), 127.9 ($\times 6$), 126.7 ($\times 3$), 126.6 ($\times 3$), 71.1, 66.9, 60.6, 34.45.

IR (ATR): 3054, 3025, 1723, 1594, 1488, 1445, 1318, 1183, 1157, 1082, 1032, 1001, 901, 829, 741, 697, cm^{-1} .

$[\text{M}+\text{Na}]^+$ calc 612.23316 for $\text{C}_{41}\text{H}_{35}\text{NONaS}^+$, $[\text{M}+\text{Na}]^+$ found 612.23446

Elem. Anal. Calculated for $\text{C}_{41}\text{H}_{35}\text{NOS}$: C, 83.49; H, 5.98; N, 2.37; O, 2.71; S, 5.44. Found: C, 82.37; H, 6.01; N, 2.38; S, 4.49.

c. ethyl 2-((R)-2-(tritylamino)-3-(tritylthio)propylamino)acetate (20).

To a stirred solution of 2-(tritylamino)-3-(tritylthio)propanal (1.85 g, 3.14 mmol) and glycine ethyl ester hydrochloride GlyOEt*HCl (1.85 g, 3.14 mmol) in pA EtOH (60 mL) at 0°C were added glacial acetic acid (0.361 mL) and $\text{Na}[\text{BH}_3\text{CN}]$ (0.395 g, 6.28 mmol). The reaction mixture was stirring for 1.5 h at 0°C and then the solvent was evaporated. The remainder was partitioned between ethyl acetate and diluted potassium carbonate and then extracted with ethyl acetate 3 times. The organic layer was dried over anhydrous Na_2SO_4 and evaporated *in*

vacuo. The residue was purified by column chromatography (silica gel 60; cyclohexane / ethyl acetate 3:1, R_f 0.53), $[\alpha]_D^{25} + 97$, m.p.: 60°C. Yield: 1.9 g (89 %) new substance as white foam of m.p. 60 °C.

^1H NMR (300 MHz, CHLOROFORM-*d*) δ ppm 1.29 (t, $J=7.1$ Hz, 3 H), 1.81 (dd, $J=12.1$, 5.0 Hz, 1 H), 2.26 - 2.37 (m, 3 H), 2.58 - 2.69 (m, 1 H), 3.00 (d, $J=17.3$ Hz, 1 H), 3.07 (d, $J=17.3$ Hz, 1 H), 4.18 (q, $J=7.1$ Hz, 2 H), 7.21 - 7.34 (m, 18 H), 7.42 - 7.48 (m, 6 H), 7.52 - 7.59 (m, 6 H).

^{13}C NMR (75 MHz, CHLOROFORM-*d*) δ 172.2, 146.7 ($\times 3$), 144.8 ($\times 3$), 129.5 ($\times 6$), 128.6 ($\times 6$), 127.7 ($\times 12$), 126.4 ($\times 3$), 126.1 ($\times 3$), 71.1, 66.1, 60.4, 51.3, 51.0, 50.8, 36.0, 14.1.

IR (ATR): 3057, 3023, 1736, 1595, 1488, 1446, 1371, 1200, 1155, 1082, 1031, 906, 853, 729, 698, cm^{-1} .

Elem. Anal. Calculated for $\text{C}_{45}\text{H}_{44}\text{N}_2\text{O}_2\text{S}$: C, 79.85; H, 6.55; N, 4.14; O, 4.73; S, 4.74. Found: C, 78.61; H, 6.61; N, 4.19; S, 4.48.

d. (R)-6-((tritylthio)methyl)piperazin-2-one (21).

Trt(N)deprotection on compound **20** was performed according to general procedure B. The residue was purified by column chromatography (silica gel 60; DCM/MeOH 9:1, R_f 0.33), $[\alpha]_D^{25} + 1$. Yield: 1.04 g (100 %) of **21** new substance as white foam of m.p. 55 °C.

^1H NMR (300 MHz, CHLOROFORM-*d*) δ ppm 2.28 (dd, $J=12.9$, 7.4 Hz, 1 H), 2.41 (dd, $J=12.9$, 5.5 Hz, 1 H), 2.45 - 2.55 (m, 1 H), 2.73 (br. s, 1 H), 2.80 - 2.91 (m, 2 H), 3.27 (d, $J=17.3$ Hz, 1 H), 3.36 (d, $J=17.6$ Hz, 1 H), 5.94 - 6.05 (m, 1 H), 7.16 - 7.29 (m, 9 H), 7.34 - 7.42 (m, 6 H).

^{13}C NMR (75 MHz, CHLOROFORM-*d*) δ 169.3, 144.2 ($\times 3$), 129.5 ($\times 6$), 128.0 ($\times 6$), 127.0 ($\times 3$), 67.3, 51.5, 49.0, 46.5, 35.8.

IR (ATR): 3232, 3057, 2924, 1649, 1594, 1487, 1443, 1407, 1336, 1262, 1203, 1175, 1128, 1082, 1033, 1001, 885, 837, 800, 740, 721, 697, 675, cm^{-1} .

$[\text{M}+\text{Na}]^+$ calc 411.15016 for $\text{C}_{24}\text{H}_{24}\text{N}_2\text{OSNa}^+$, $[\text{M}+\text{Na}]^+$ found 411.14875.

e. tert-butyl (S)-1-(ethoxycarbonyl)-4-oxo-4-((R)-3-oxo-5-((tritylthio)methyl)piperazin-1-yl)butylcarbamate (23).

The T3P coupling was performed according to general procedure A. The residue was purified by column chromatography (silica gel 60; AcOEt/5 % EtOH, R_f 0.58), $[\alpha]_D^{25} - 22$. Yield: 1.14 g (86 %) product **23** new substance as white foam of m.p. 70 °C.

^1H NMR (300 MHz, CHLOROFORM-*d*) δ ppm 1.20 - 1.30 (m, 6 H), 1.37 - 1.46 (m, 18 H), 1.83 - 2.02 (m, 2 H), 2.12 - 2.52 (m, 10 H), 2.54 - 2.65 (m, 1 H), 2.70 - 2.81 (m, 1 H), 3.21 (dd, $J=13.4, 5.8$ Hz, 1 H), 3.33 - 3.48 (m, 2 H), 3.60 (dd, $J=13.4, 3.6$ Hz, 1 H), 3.93 (d, $J=3.8$ Hz, 2 H), 3.99 - 4.11 (m, 1 H), 4.11 - 4.22 (m, 5 H), 4.22 - 4.33 (m, 2 H), 5.26 - 5.36 (m, 2 H), 6.32 (br. s, 1 H), 6.38 (br. s, 1 H), 7.18 - 7.34 (m, 20 H), 7.38 - 7.45 (m, 10 H).

^{13}C NMR (75 MHz, CHLOROFORM-*d*) 175.8, 172.2, 170.5, 166.0, 155.5, 144.2, 144.0, 129.5, 129.4, 128.2, 128.1, 127.1, 127.0, 61.5, 53.2, 52.9, 50.4, 49.9, 48.3, 45.7, 45.5, 42.1, 35.4, 34.6, 28.9, 28.3, 27.6, 14.1.

IR (ATR): 3274, 2981, 1734, 1699, 1652, 1489, 1444, 1392, 1367, 1308, 1247, 1163, 1051, 1028, 907, 853, 726, 700, 675, cm^{-1} .

$[\text{M}+\text{H}]^+$ calc for $\text{C}_{36}\text{H}_{44}\text{N}_3\text{O}_6\text{S}^+$ 646.29453, $[\text{M}+\text{H}]^+$ found 646.29436

$[\text{M}+\text{Na}]^+$ calc 668.27648 for $\text{C}_{36}\text{H}_{43}\text{N}_3\text{NaO}_6\text{S}^+$, $[\text{M}+\text{Na}]^+$ found: 668.27605 $\text{C}_{36}\text{H}_{43}\text{N}_3\text{O}_6\text{S}$

f, g. (S)-2-amino-5-((R)-3-(mercaptomethyl)-5-oxopiperazin-1-yl)-5-oxopentanoic acid (22).

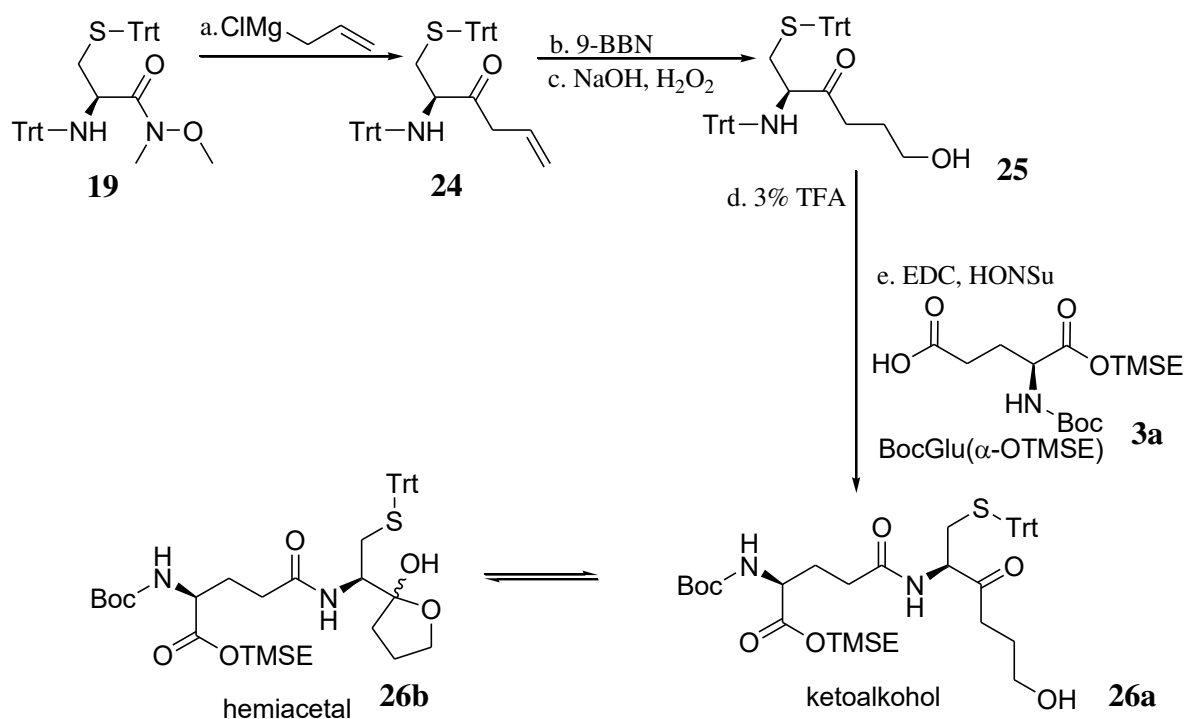
Hydrolysis, acidic deprotection and HPLC were performed according to general procedures C and D. The final dipeptide was purified by preparative HPLC (flow rate 10 mL/min of 3 % MeOH, 97 % H_2O (0.1 % HCOOH), $t_{\text{R}} = 6$ min, $[\alpha]_{\text{D}}^{25} - 19$. Yield: 200 mg (at least 47 % yield after preparative HPLC) new substance as white crystals of m.p. 95 °C. The substance is O_2 -sensitive; keep in the fridge under argon.

^1H NMR (300 MHz, DEUTERIUM OXIDE) δ ppm 2.20 (q, $J=6.9$ Hz, 4 H) 2.62 - 2.83 (m, 8 H) 3.58 - 3.69 (m, 2 H) 3.69 - 3.76 (m, 1 H) 3.78 - 3.90 (m, 2 H) 3.93 (qt, $J=3.6, 2.7$ Hz, 2 H) 4.06 - 4.35 (m, 5 H).

^{13}C NMR (75 MHz, DEUTERIUM OXIDE) δ 173.0, 172.9, 170.0, 169.2, 53.3, 53.2, 52.4, 52.3, 47.8, 45.3, 44.4, 40.71, 28.8, 28.7, 26.4, 26.1, 25.3, 25.2.

IR (ATR): 3027, 2936, 2547, 1623, 1446, 1411, 1327, 1235, 1197, 1175, 1123, 1076, 1002, 831, 797, 719, cm^{-1} .

Synthesis of ketone:



Compound **19** was described above.

Compound **3a** was synthesised according to compound **3** (lit. ref. for characterisation of **3a**¹⁶)

a. (R)-2-(tritylamino)-1-(tritylthio)hex-5-en-3-one (24)

To a stirred solution of **19** (0.76 g, 1.17 mmol) in anhydrous THF (10mL) was added allyl magnesium chloride (2 M in THF, 0.565 mL, 1.17 mmol). The reaction mixture was stirring for 1 h at room temperature then diluted with ethyl acetate (60 mL) and washed once with saturated ammonium chloride (40 mL) and once with brine (40 mL). The aqueous phases were extracted with ethyl acetate (3×50 mL). The organic layer was dried over anhydrous Na₂SO₄ and evaporated *in vacuo*. The residue was purified by column chromatography (silica gel 60; CH/AcOEt 5:1, R_f 0.68), [α]²⁵_D + 100.2. Yield: 0.73 g (99 %) new substance as white foam of m.p. 60 °C.

¹ H NMR (300 MHz, CHLOROFORM-*d*) δ ppm 2.09 (dd, *J*=18.1, 6.6 Hz, 1 H), 2.48 (dd, *J*=12.1, 4.9 Hz, 1 H), 2.55 (dd, *J*=12.1, 6.3 Hz, 1 H), 2.63 (dd, *J*=18.1, 6.6 Hz, 1 H), 3.38 (d, *J*=8.2 Hz, 1 H), 3.49 (ddd, *J*=8.2, 6.1, 4.9 Hz, 1 H), 4.80 (dd, *J*=17.2, 1.2 Hz, 1 H), 5.01 (dd, *J*=10.2, 1.2 Hz, 1 H), 5.47 (ddt, *J*=17.2, 10.2, 6.6, 6.6 Hz, 1 H), 7.17 - 7.36 (m, 21 H), 7.47 - 7.52 (m, 11 H).

¹³C NMR (75 MHz, CHLOROFORM-*d*) δ 209.1, 146.3 (×3), 144.7 (×3), 130.4, 129.8 (×6), 129.1 (×6), 128.1 (×6), 128.0 (×6), 126.8 (×3), 126.6 (×3), 118.4, 71.5, 66.8, 60.3, 45.2, 36.4.

IR (ATR): cm⁻¹. 3058, 3029, 2924, 2850, 1714, 1642, 1595, 1489, 1446, 1388, 1319, 1206, 1184, 1156, 1082, 1058, 1033, 1001, 919, 902, 850, 741, 697, 676, 643, 616, 584, 567 cm⁻¹.

[M+Na]⁺ calcd for C₄₄H₃₉NNaOS⁺ 652.26446 [M+Na]⁺ found 652.26265.

b. To a solution of **24** (0.73 g, 1.16 mmol) in THF (5 mL) at 0 °C was added 9-BBN (0.5 M in THF, 5.8 mL, 2.9 mmol) dropwise. The reaction mixture was then warmed to room temperature over 4 h and then left to stir overnight.

c. (R)-6-hydroxy-2-(tritylamino)-1-(tritylthio)hexan-3-one (25).

After 20 h, EtOH (2 mL), a solution of aqueous NaOH (6 M, 2 mL) and H₂O₂ (33 %, 4 mL) were added at 0°C, and the reaction mixture was stirred for 3 h at 0°C. After that, the reaction mixture was diluted with ethyl acetate (100 mL) and washed once with saturated Na₂CO₃ (40 mL) and once with brine (40 mL). The aqueous phases were extracted with ethyl acetate (3×50 mL). The organic layer was dried over anhydrous Na₂SO₄ and evaporated *in vacuo*. The crude product was purified by column chromatography (silica gel 60; CH/AcOEt 1:1, R_f 0.59), [α]_D²⁵ = +121.5. Yield: 0.390 g (52 % over 2 steps) new substance as white foam.

¹H NMR (300 MHz, CHLOROFORM-*d*) δ ppm 1.21 - 1.37 (m, 3 H), 1.53 (br. s., 1 H), 1.88 - 2.02 (m, 1 H), 2.40 (dd, *J*=11.8, 4.7 Hz, 1 H), 2.45 (dd, *J*=11.9, 6.3 Hz, 1 H), 3.26 - 3.31 (m, 2 H), 3.38 (ddd, *J*=8.0, 6.3, 4.7 Hz, 1 H), 7.09 - 7.29 (m, 19 H), 7.36 - 7.44 (m, 11 H).

¹³C NMR (75 MHz, CHLOROFORM-*d*) δ 211.7, 146.3 (×3), 144.6 (×3), 129.8 (×6), 129.1 (×6), 128.1 (×6), 127.8 (×6), 126.9 (×3), 126.6 (×3), 71.5, 66.9, 62.0, 60.5, 37.4, 36.6, 26.1

IR (ATR): 3426, 3056, 2931, 1712, 1595, 1489, 1446, 1402, 1370, 1319, 1266, 1208, 1184, 1157, 1082, 1055, 1032, 1002, 939, 902, 848, 742, 697, 676, 643, 621, 584, 567 cm⁻¹.

[M+Na]⁺ calc for C₄₄H₄₁NNaO₂S⁺ 670.27502, [M+Na]⁺ found 670.27376

d. Trt(N)deprotection on compound **25** was performed according to general procedure B and used directly for the coupling without chromatographic purification.

e. tert-butyl (S)-1-((2-(trimethylsilyl)ethoxy)carbonyl)-3-((R)-6-hydroxy-3-oxo-1(tritylthio) hexan-2-ylcarbamoyl)propylcarbamate (26).

To a stirred solution of **3a** (0.41 g, 1.17mmol) in anhydrous DCM (10 mL) under argon were added EDC (0.27 g, 1.4 mmol) and HONSu (0.16 g, 1.4 mmol). The mixture then was stirred overnight at r.t.. Freshly deprotected compound **25** (0.4 g, 1 mmol from step **d**) was added at 0°C and reaction mixture was stirred 3 h at r.t.. Thereafter saturated NH₄Cl was added and

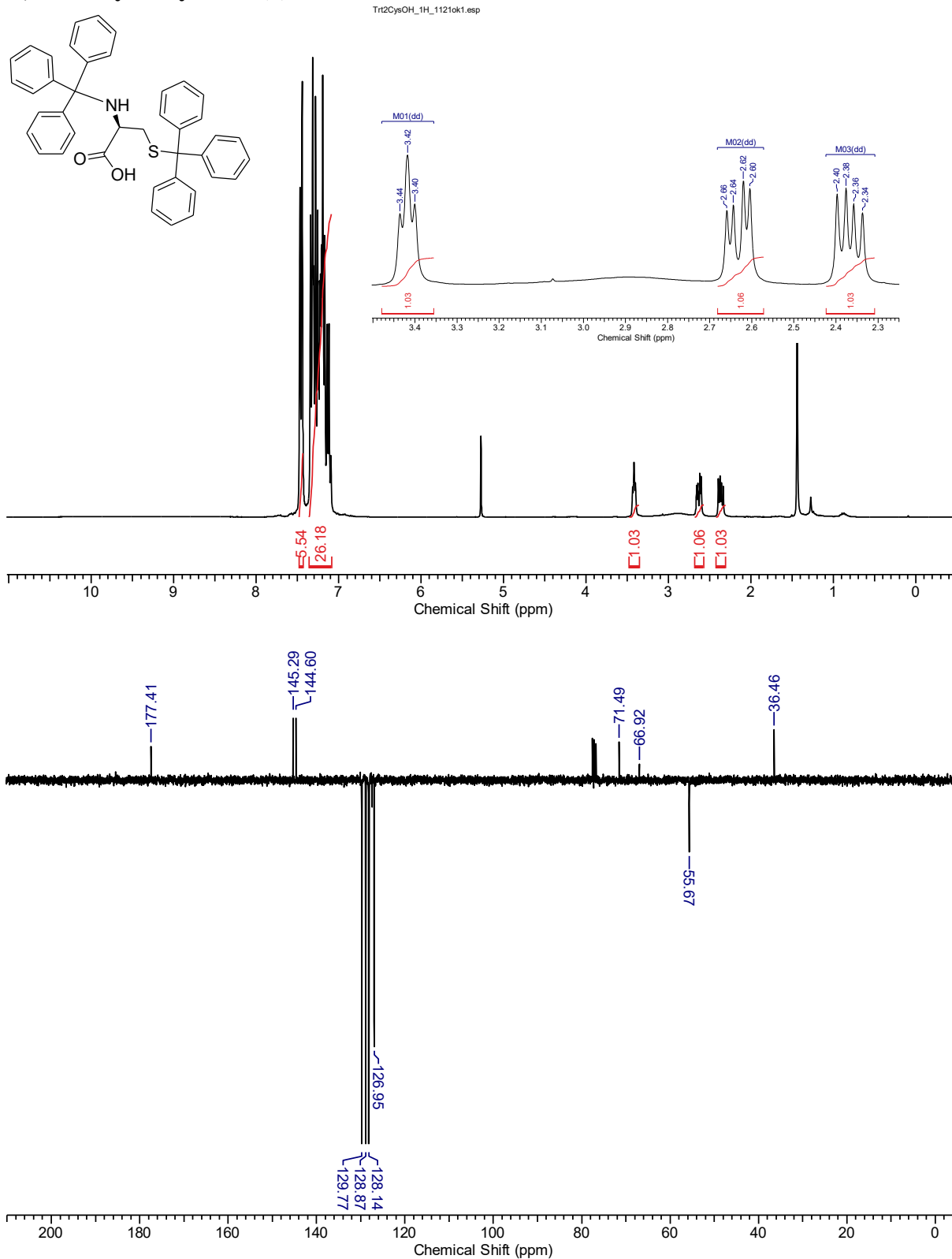
then water layer was extracted with DCM 3 times. The organic phases were washed with water and then dried over anhydrous Na_2SO_4 and evaporated *in vacuo*. The residue was purified by column chromatography (silica gel 60; CH/AcOEt 1:1, R_f 0.22). Yield: 220 mg (30 %) as a white solid 1/1 mixture of ketoalcohol/hemiacetal.

IR (ATR): 3345, 3059, 2956, 1783, 1716, 1661, 1492, 1445, 1392, 1367, 1250, 1220, 1164, 1057, 1035, 909, 859, 837, 730, 699 cm^{-1} .

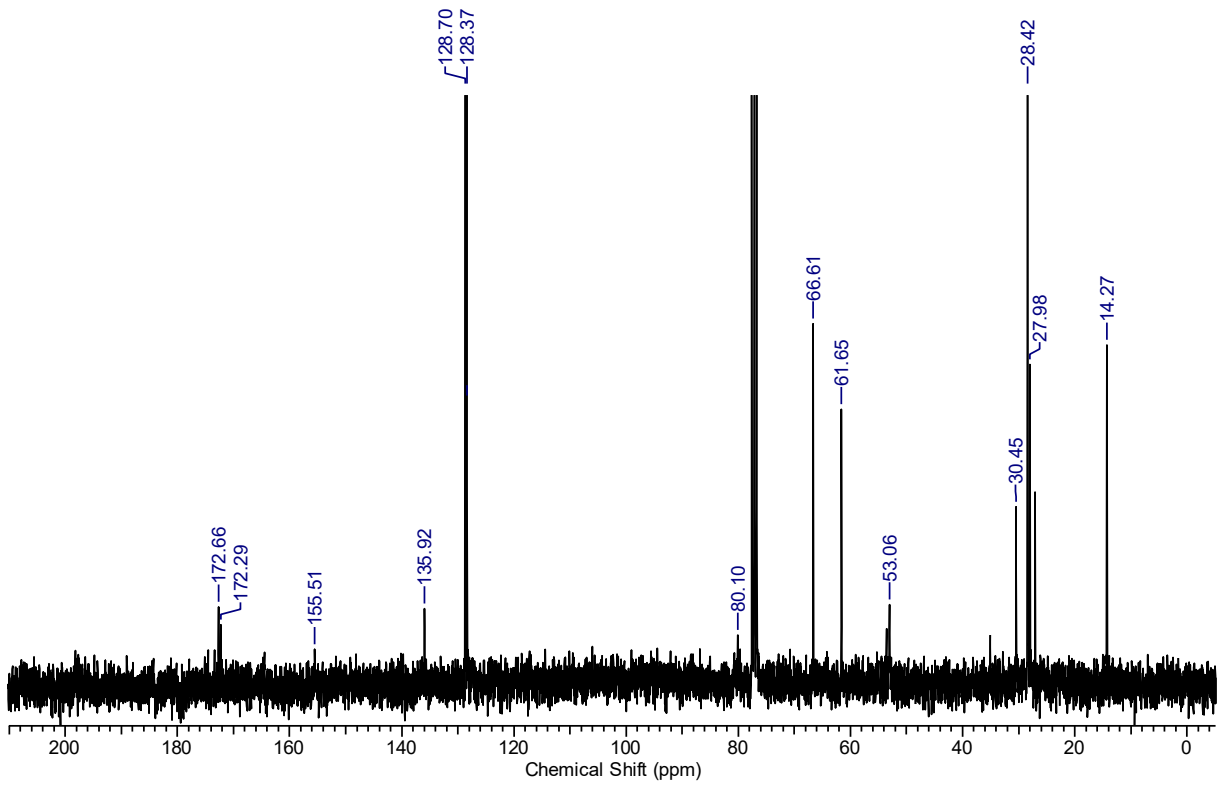
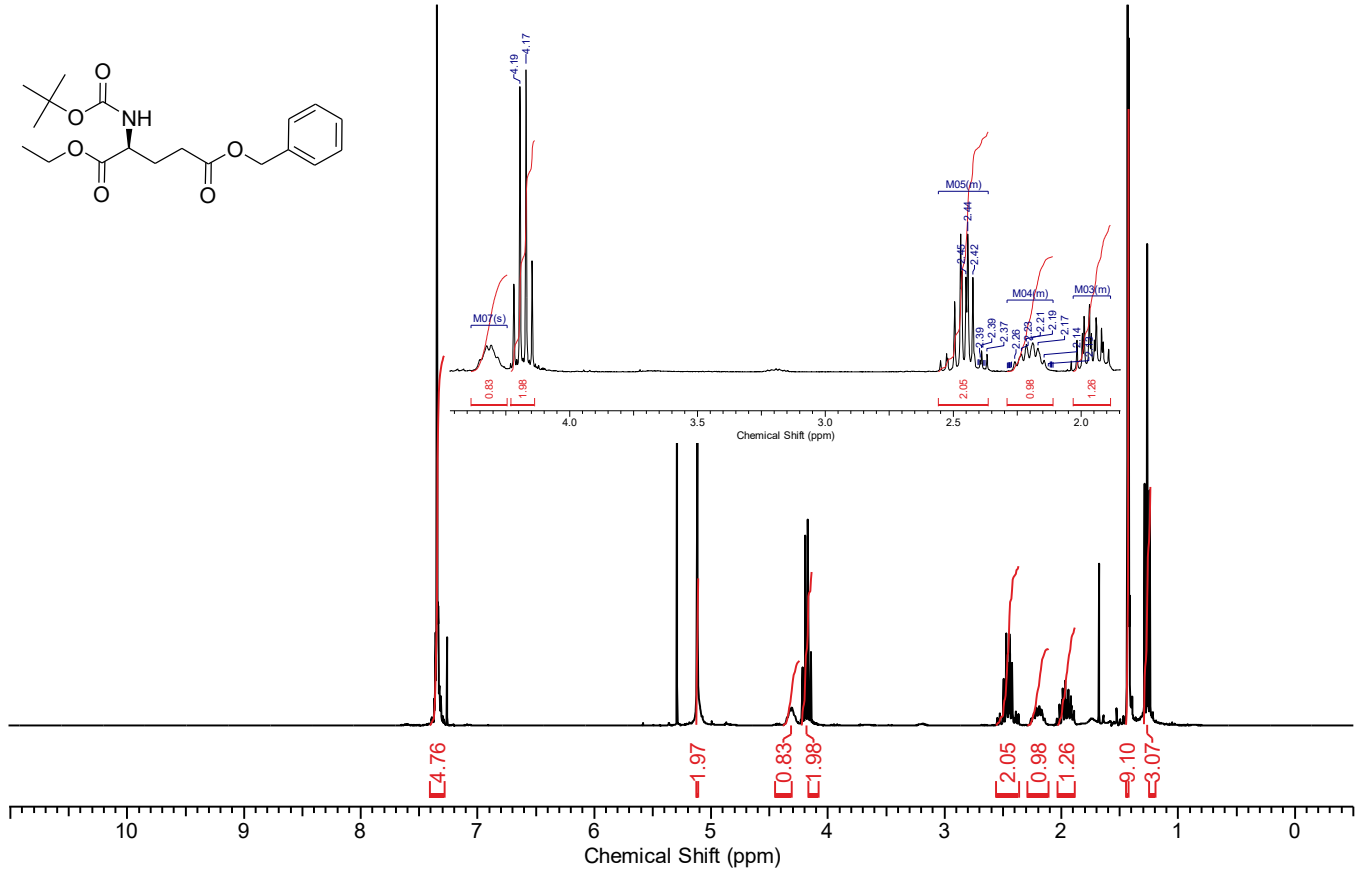
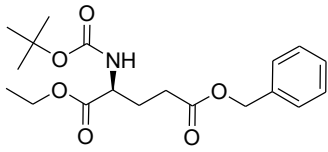
$[\text{M}+\text{Na}]^+$ calc for $\text{C}_{40}\text{H}_{54}\text{N}_2\text{NaO}_7\text{SSi}^+$ 757.33132, $[\text{M}+\text{Na}]^+$ found 757.33987.

NMR Spectra

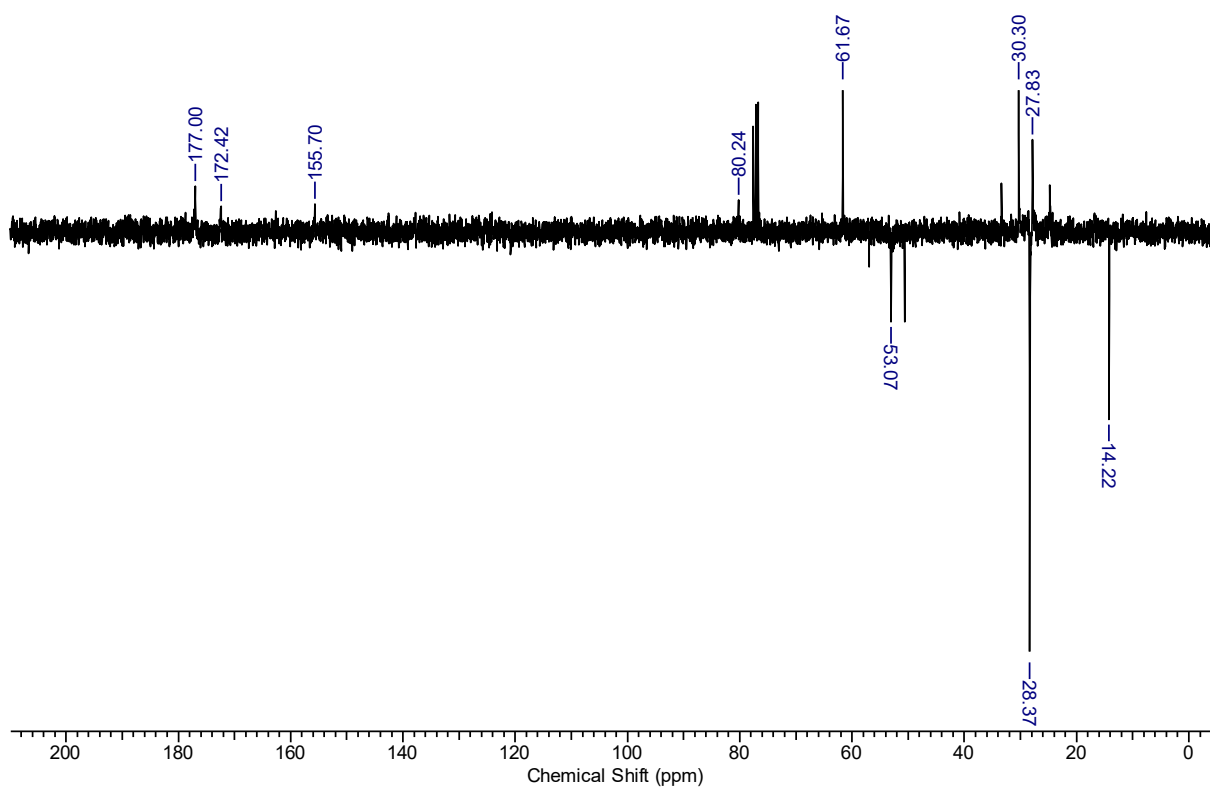
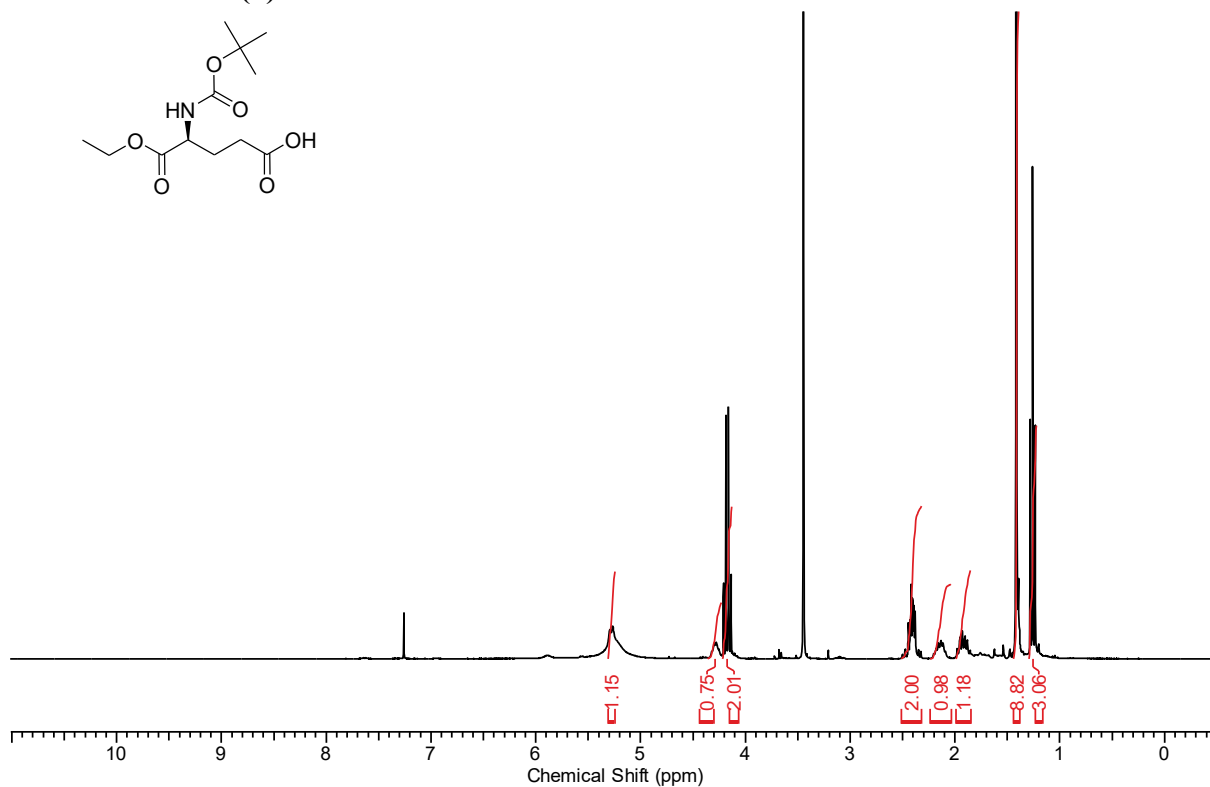
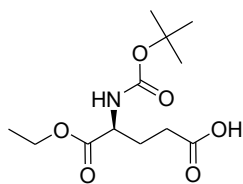
N, S-ditrityl-L-cysteine (2).



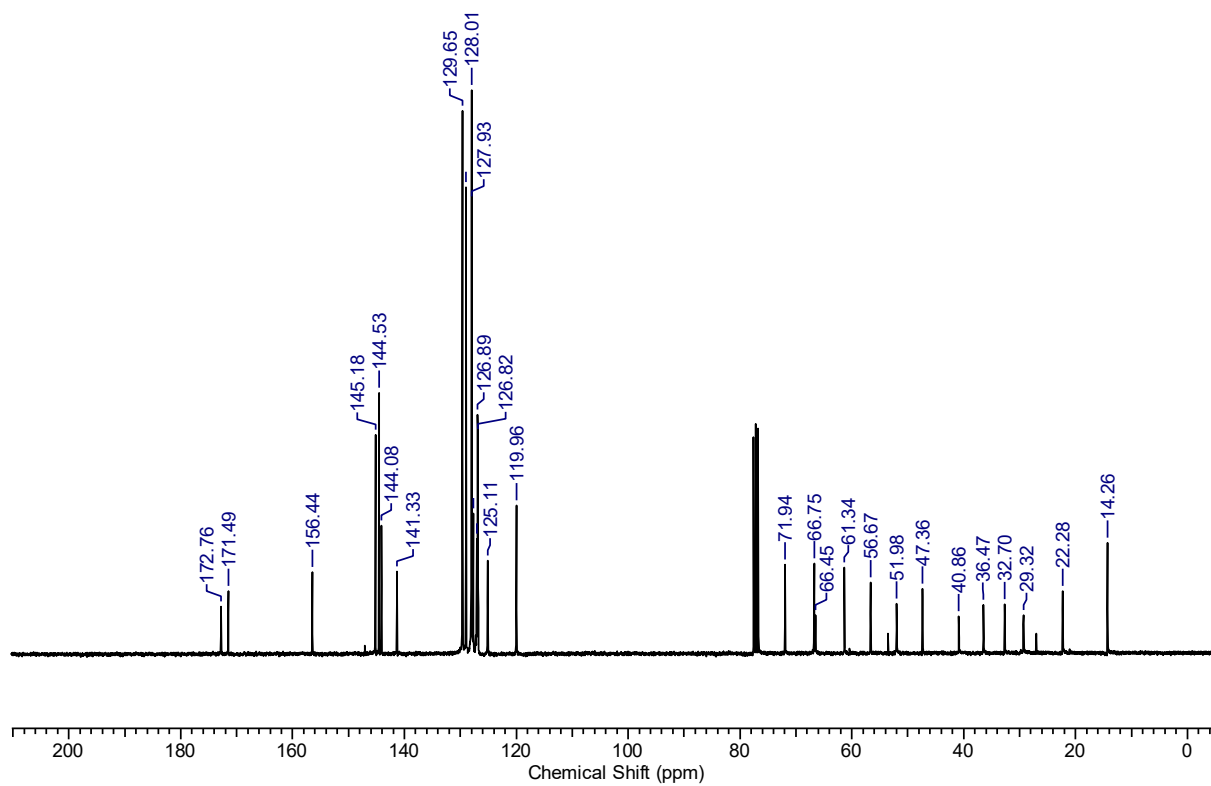
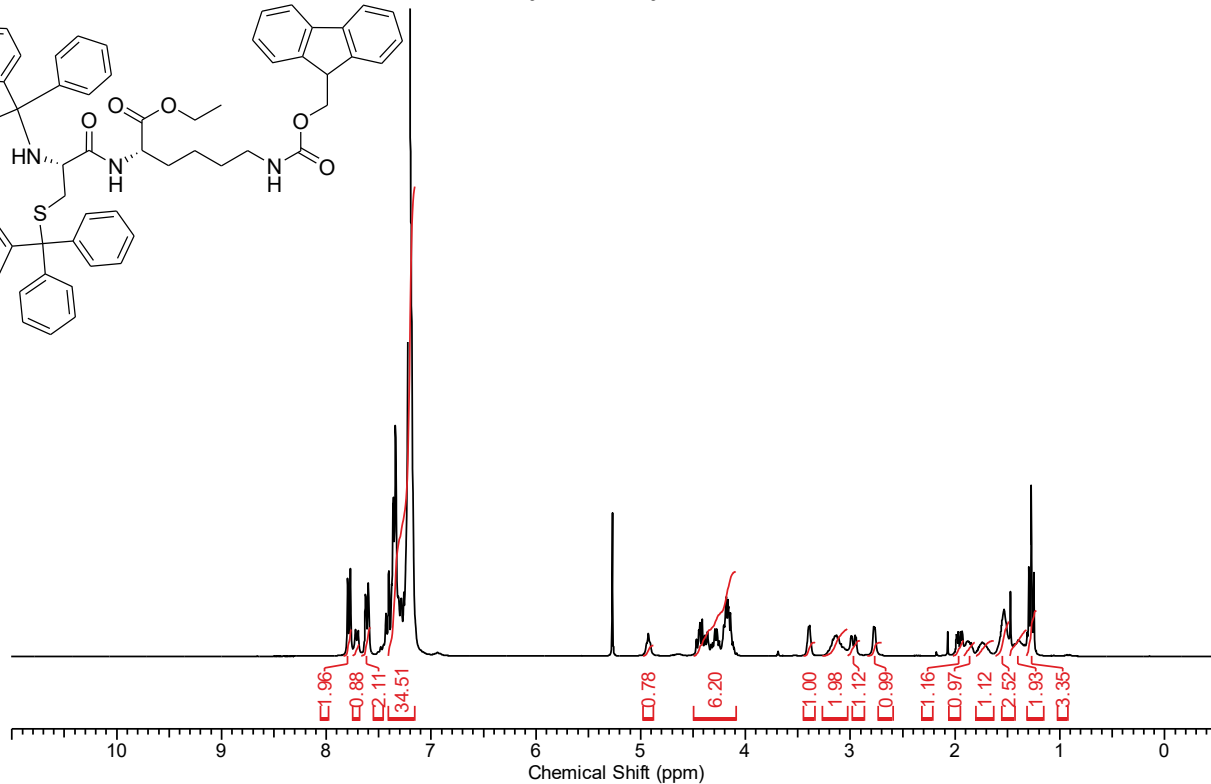
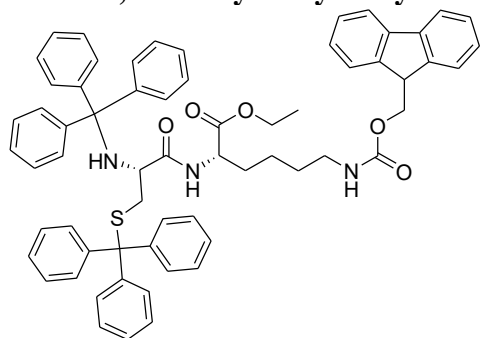
N-Boc-Glu- α -OEt- γ -OBn.



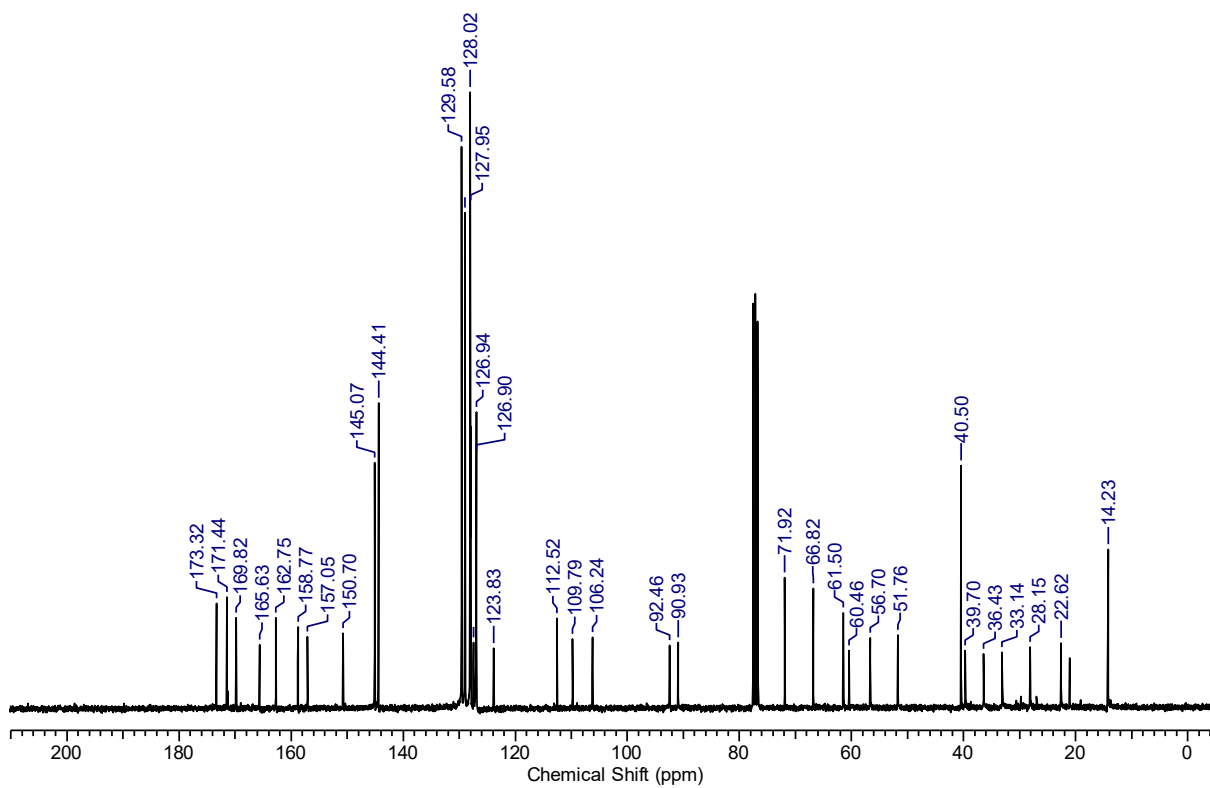
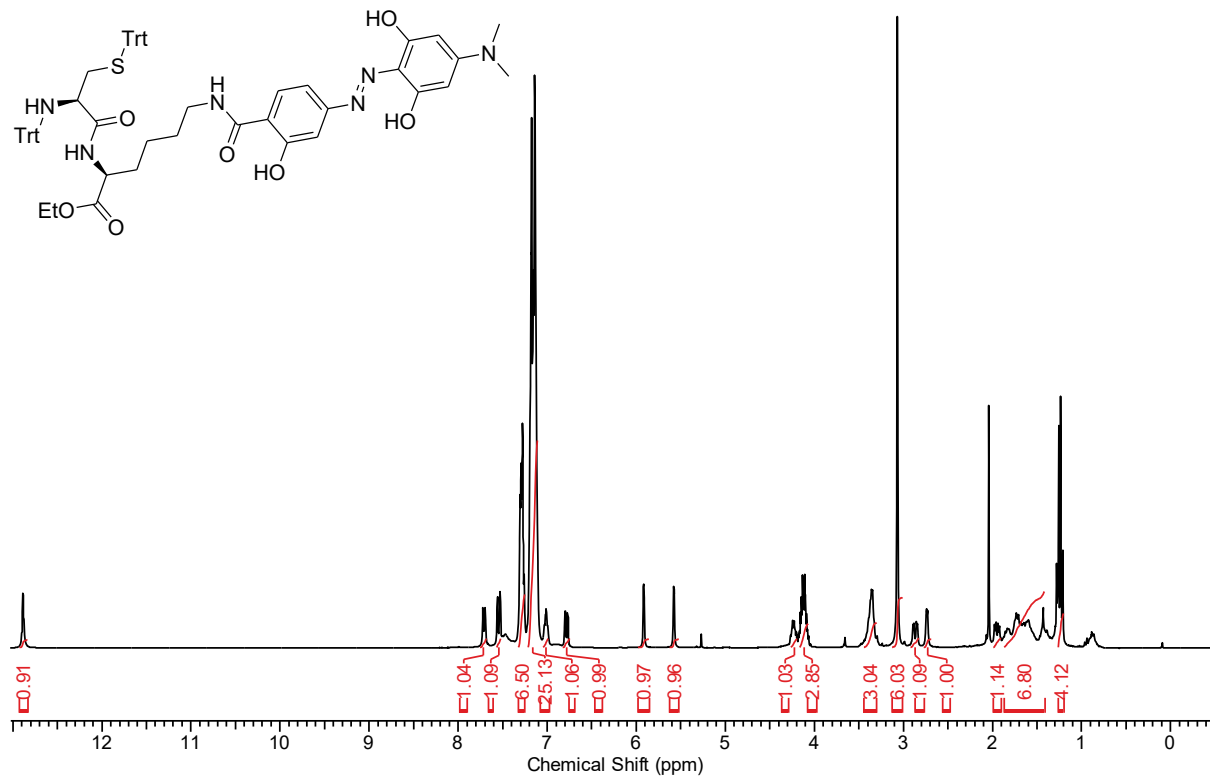
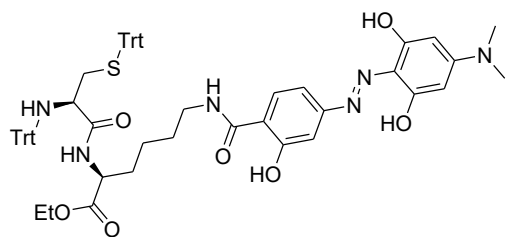
N-BocGlu- α OEt (3).



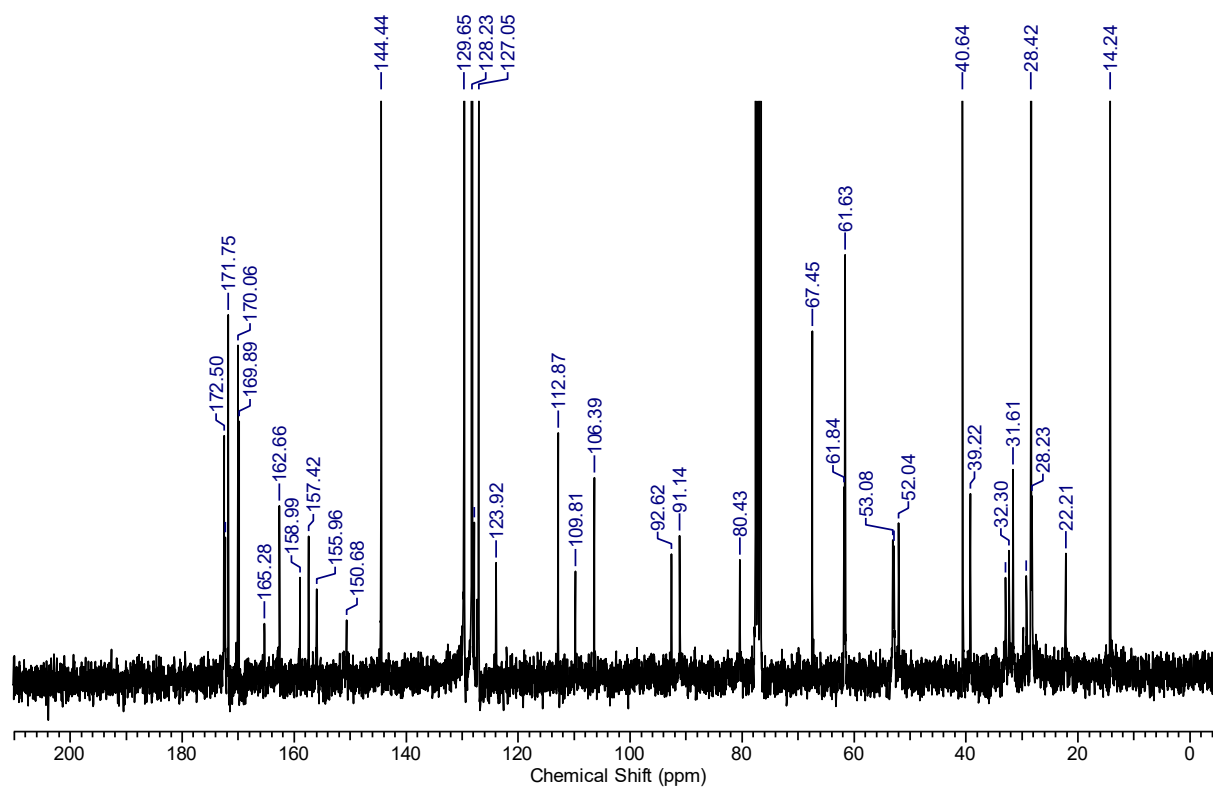
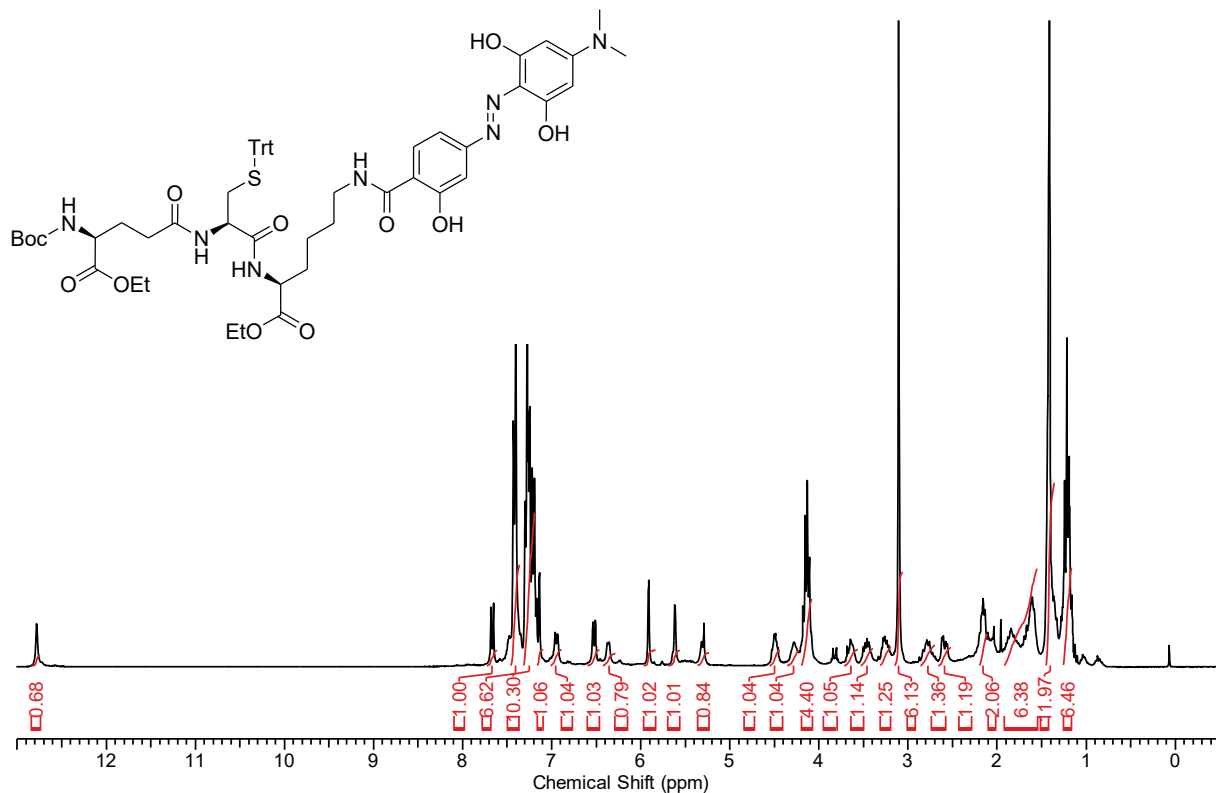
N, S-ditrityl-L-cysteinyl-N ϵ -Fmoc-L-lysine ethyl ester (5).



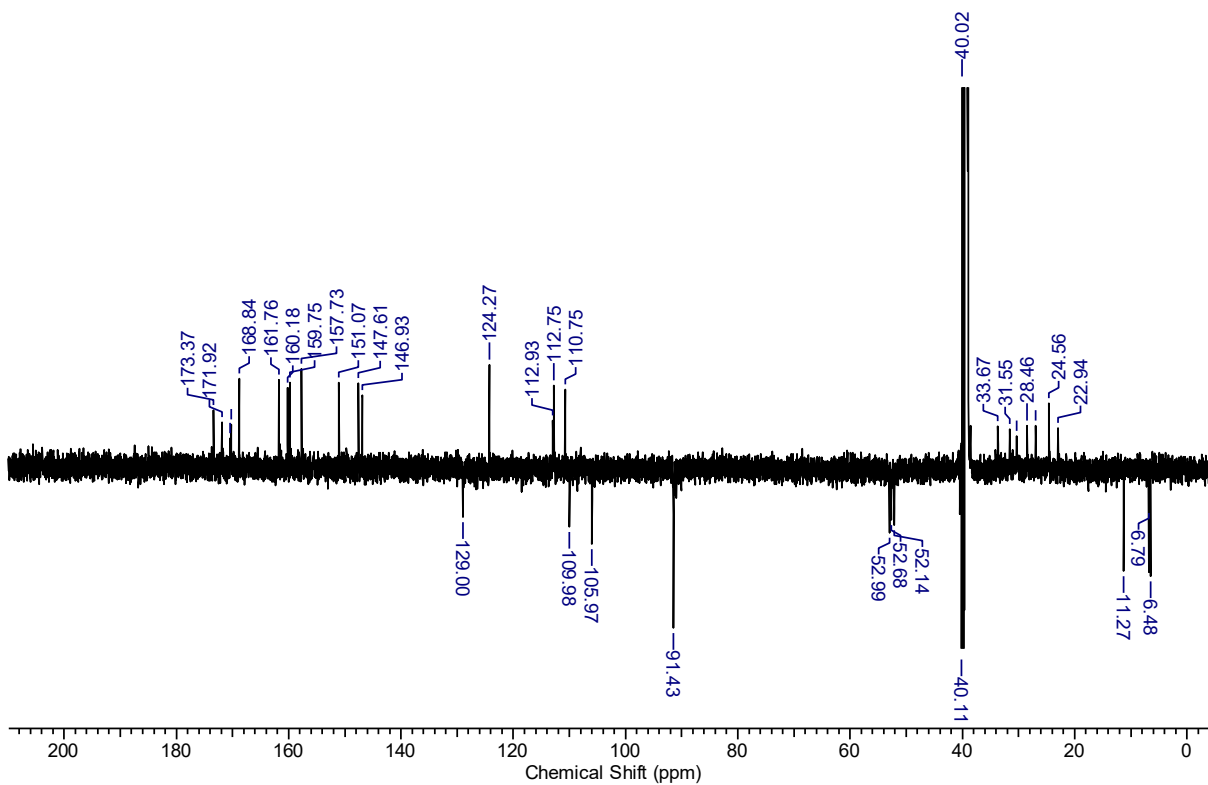
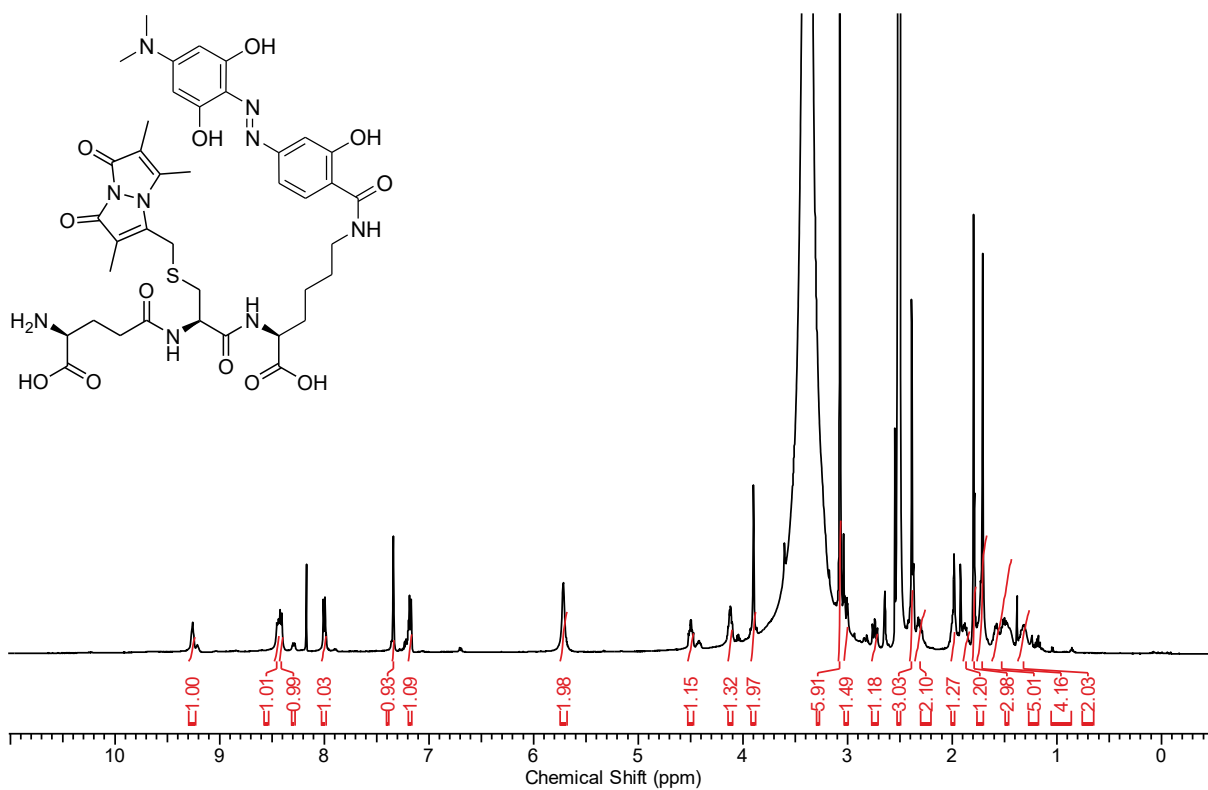
N, S-ditrityl-L-cysteinyl-N ϵ -Hydrodabacyl-L-lysine ethyl ester (6).



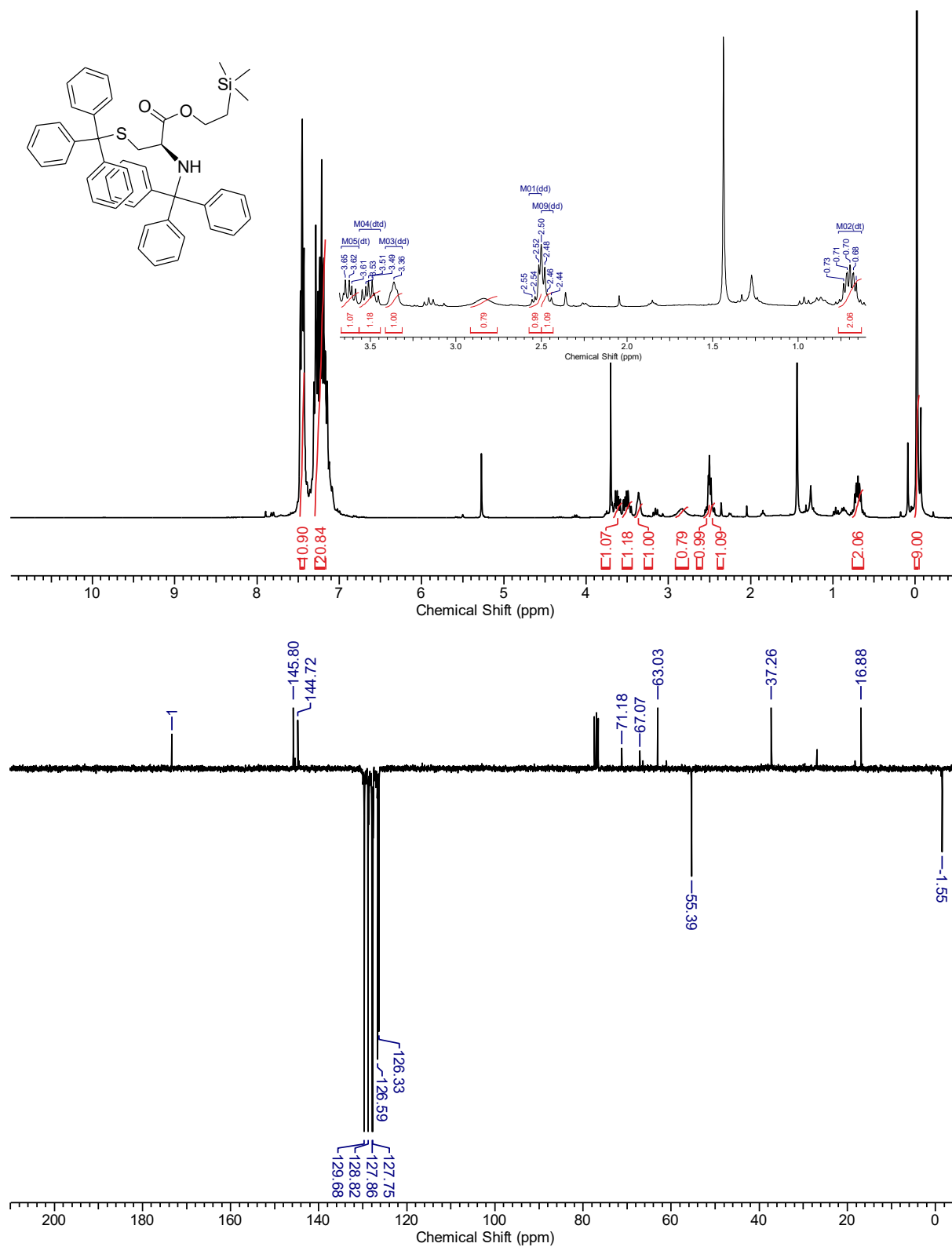
N-Boc- α -ethyl- γ -L-glutamyl-S-ditrityl-L-cysteinyl-N ϵ -Hydrodabcylyl-L-lysine ethyl ester (7).



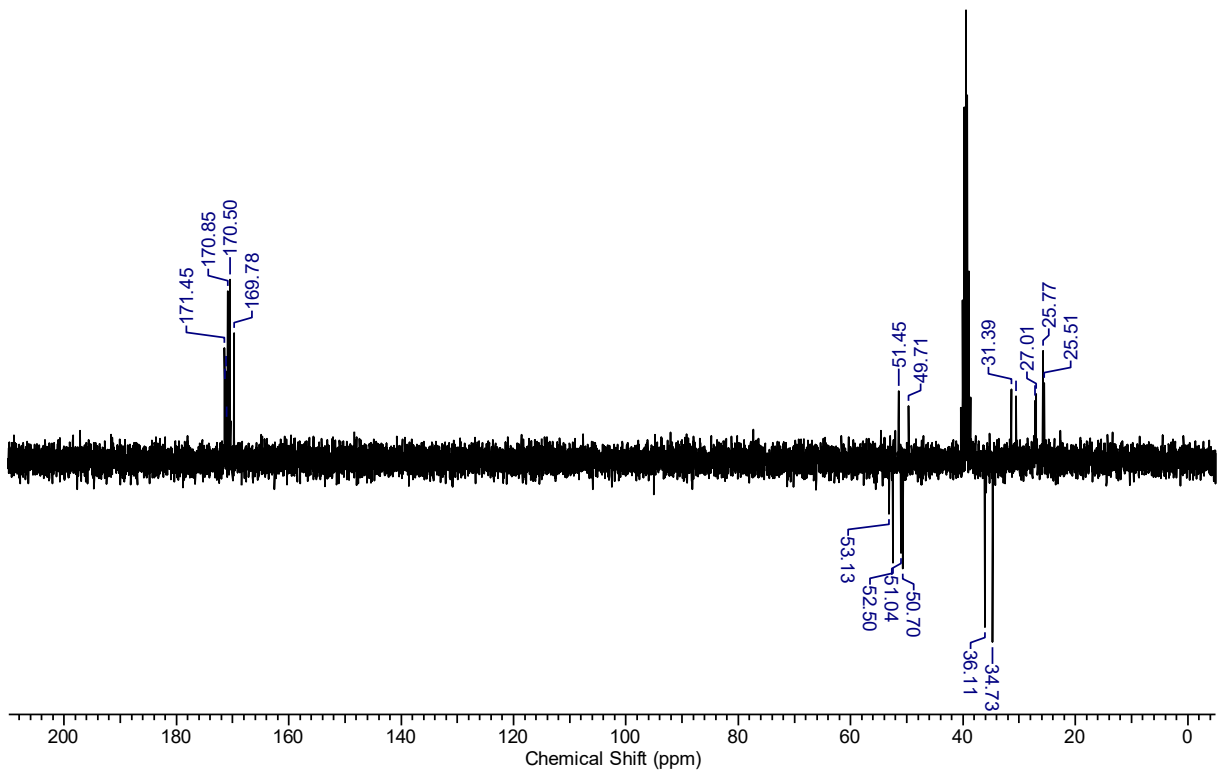
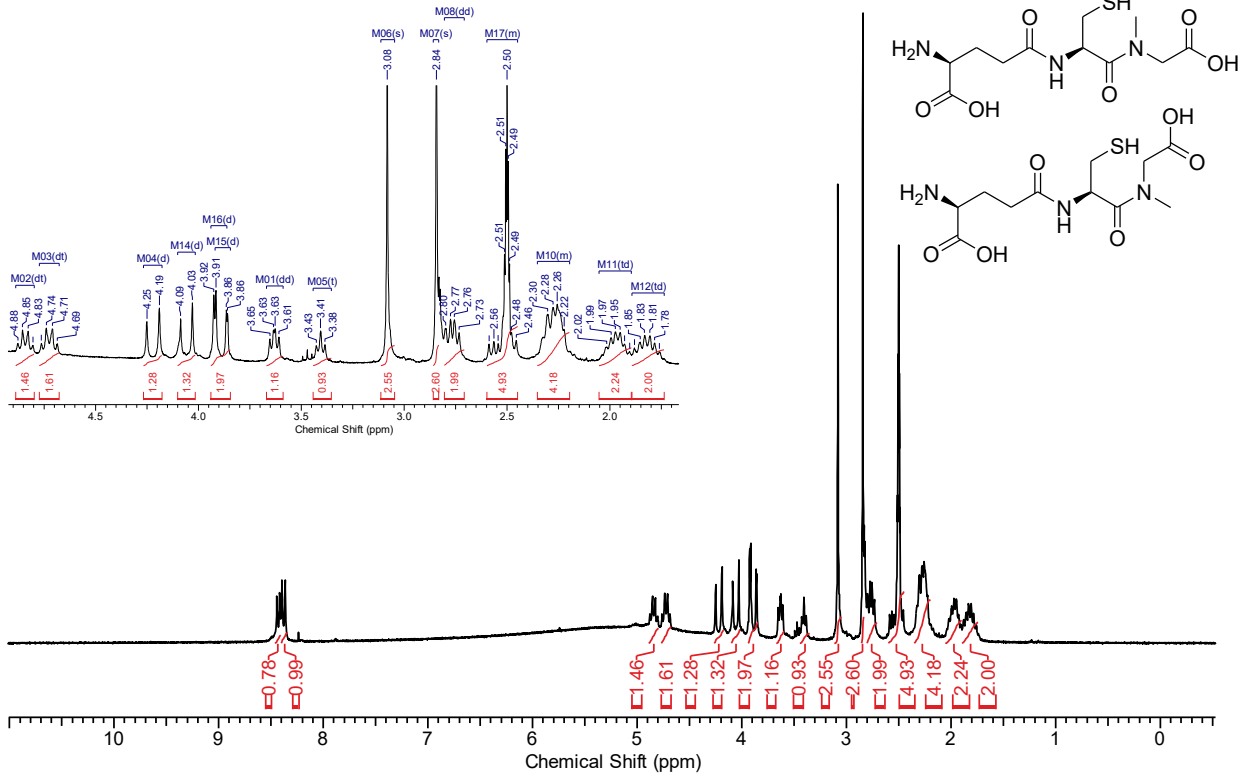
γ -L-glutamyl-S-Bimane-L-cysteinyl-N ϵ -Hydrodabicyl-L-lysine (4).



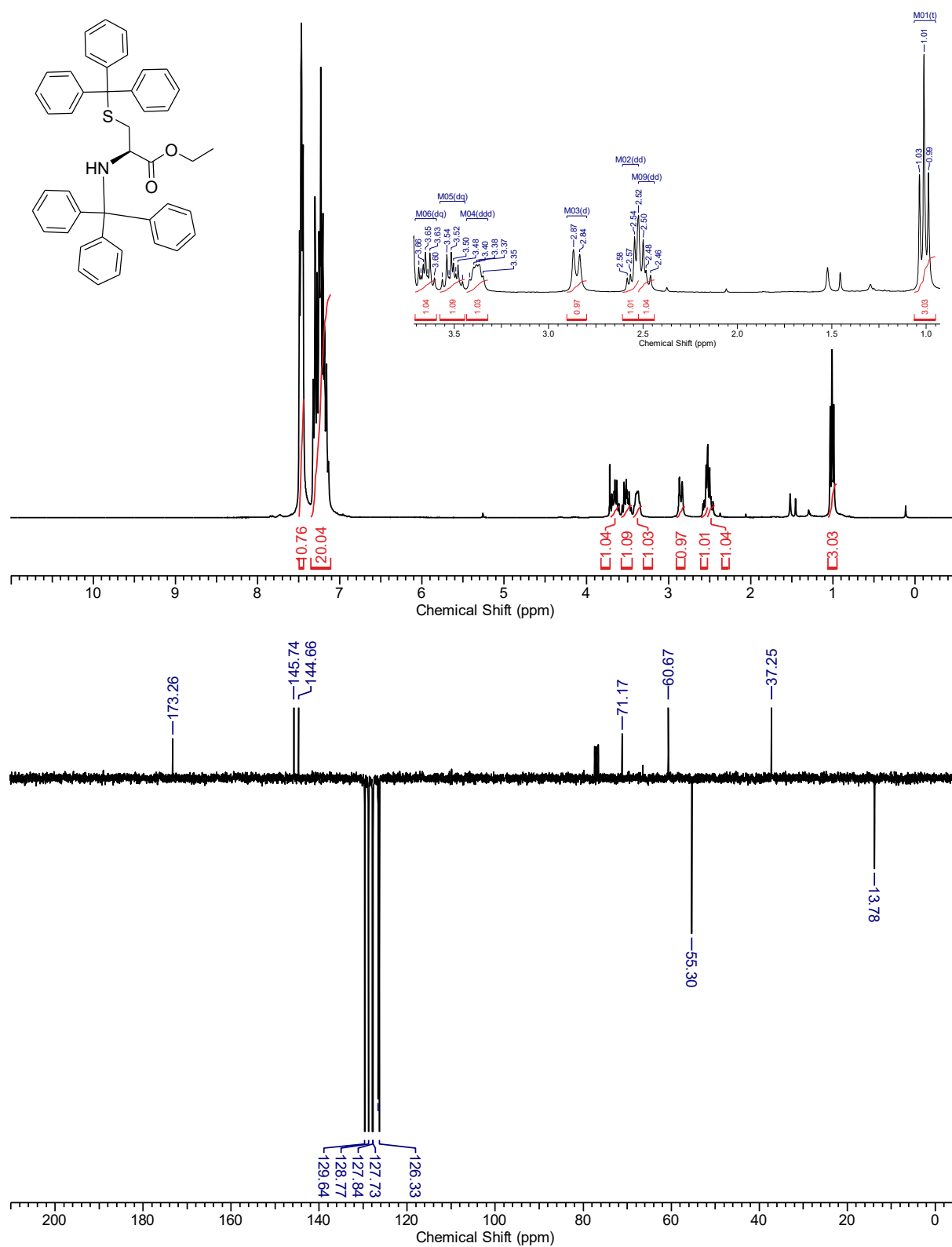
N, S-ditrityl-L-cysteinyl-OTMSE (10).



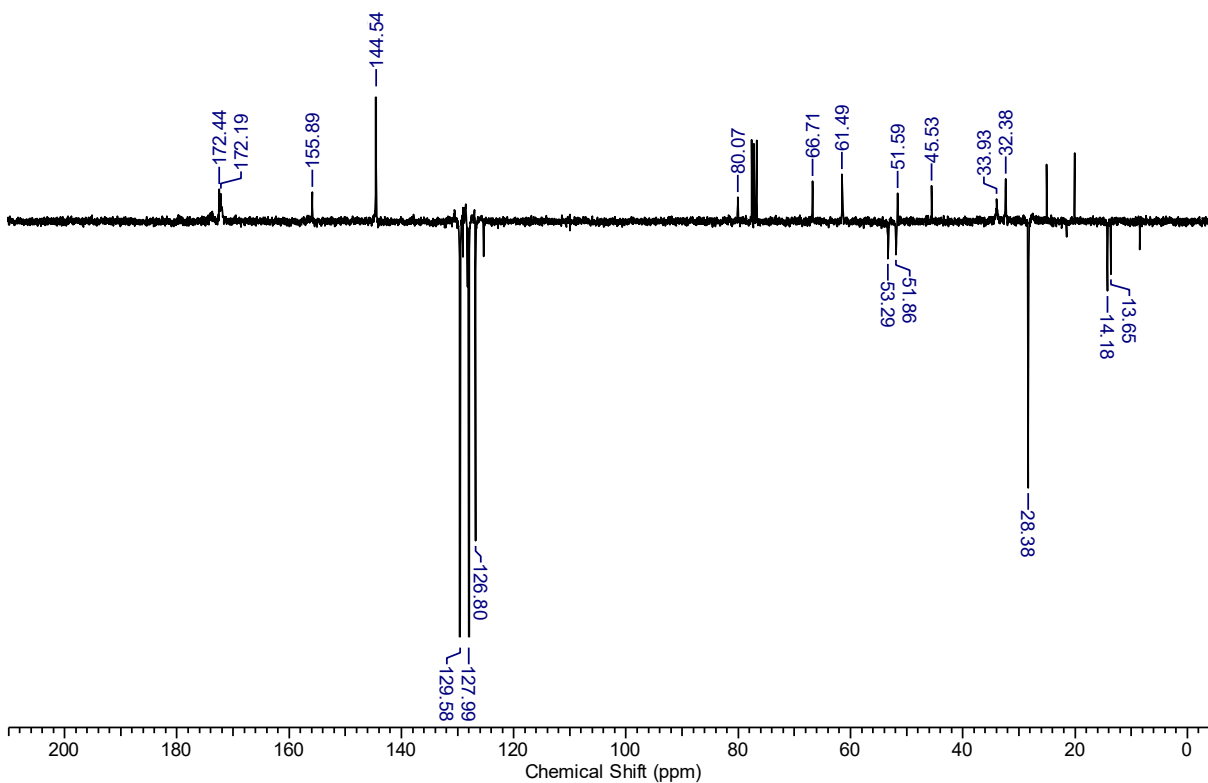
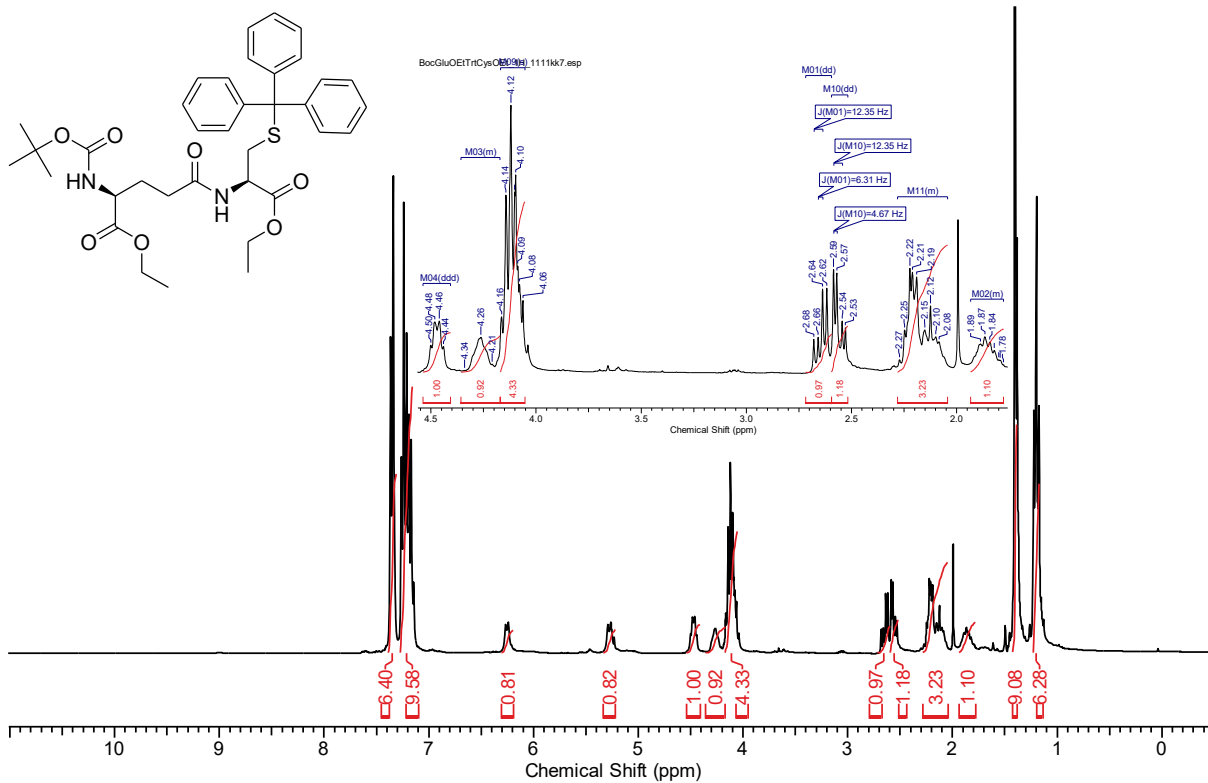
γ -GluCysSarc (13).



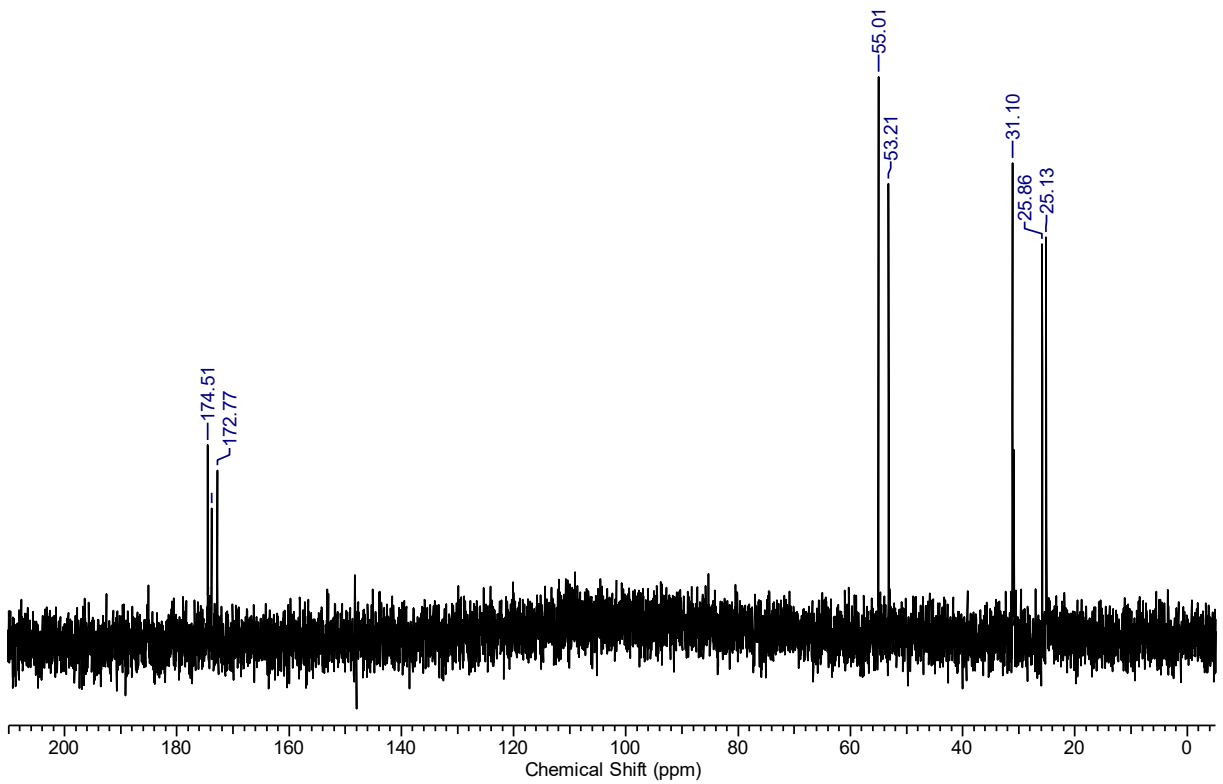
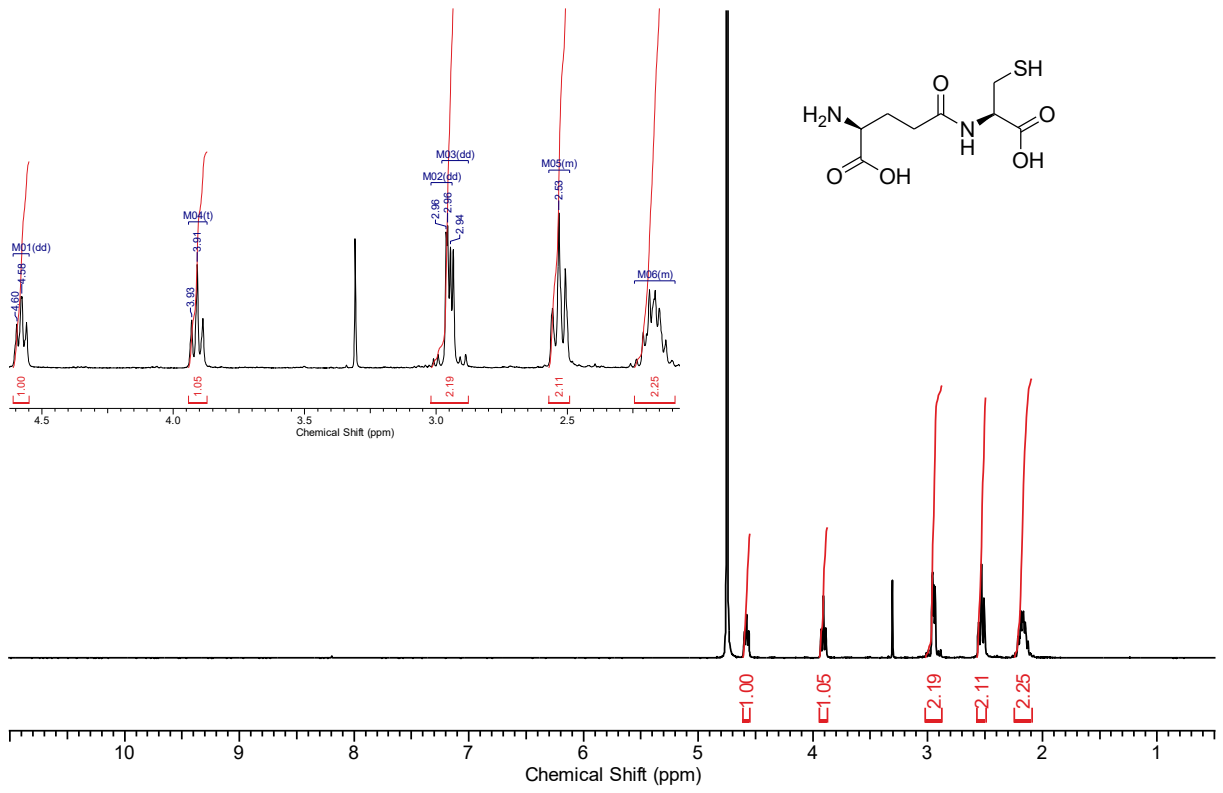
N, S-ditrityl-L-cysteinyl-OEt (15).



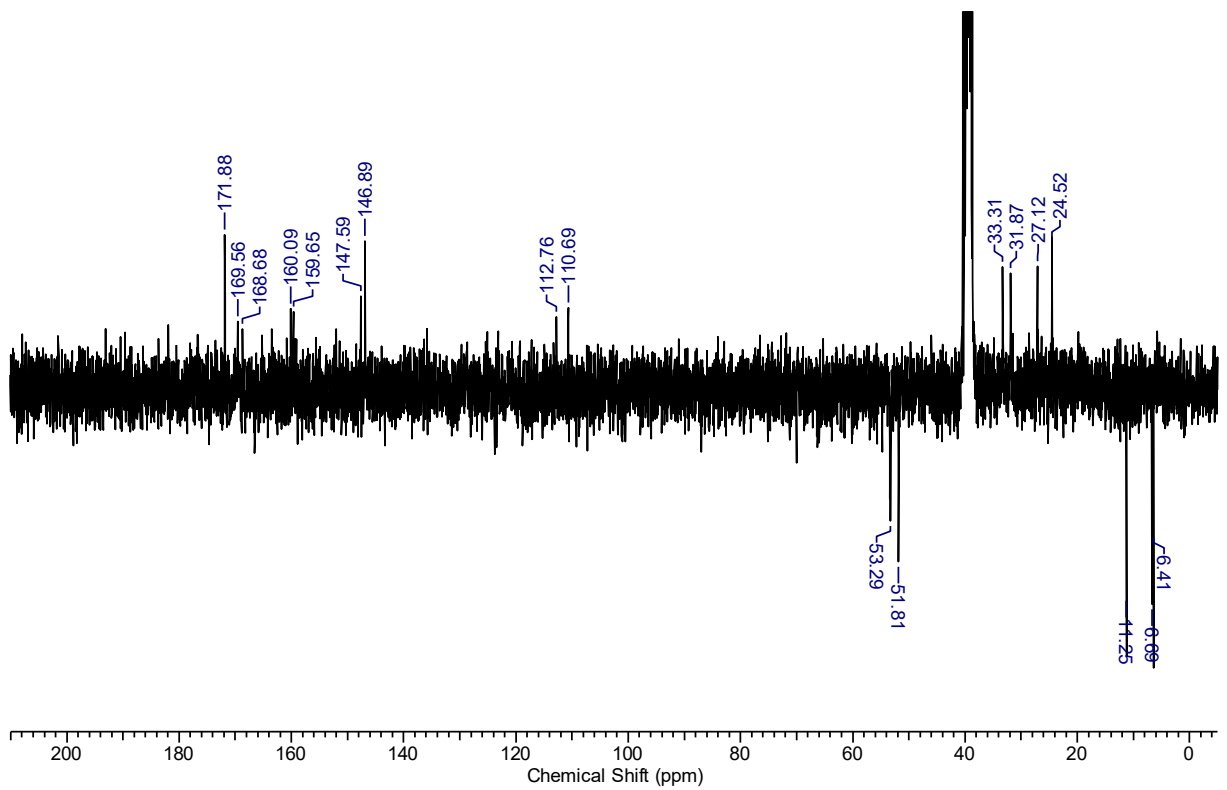
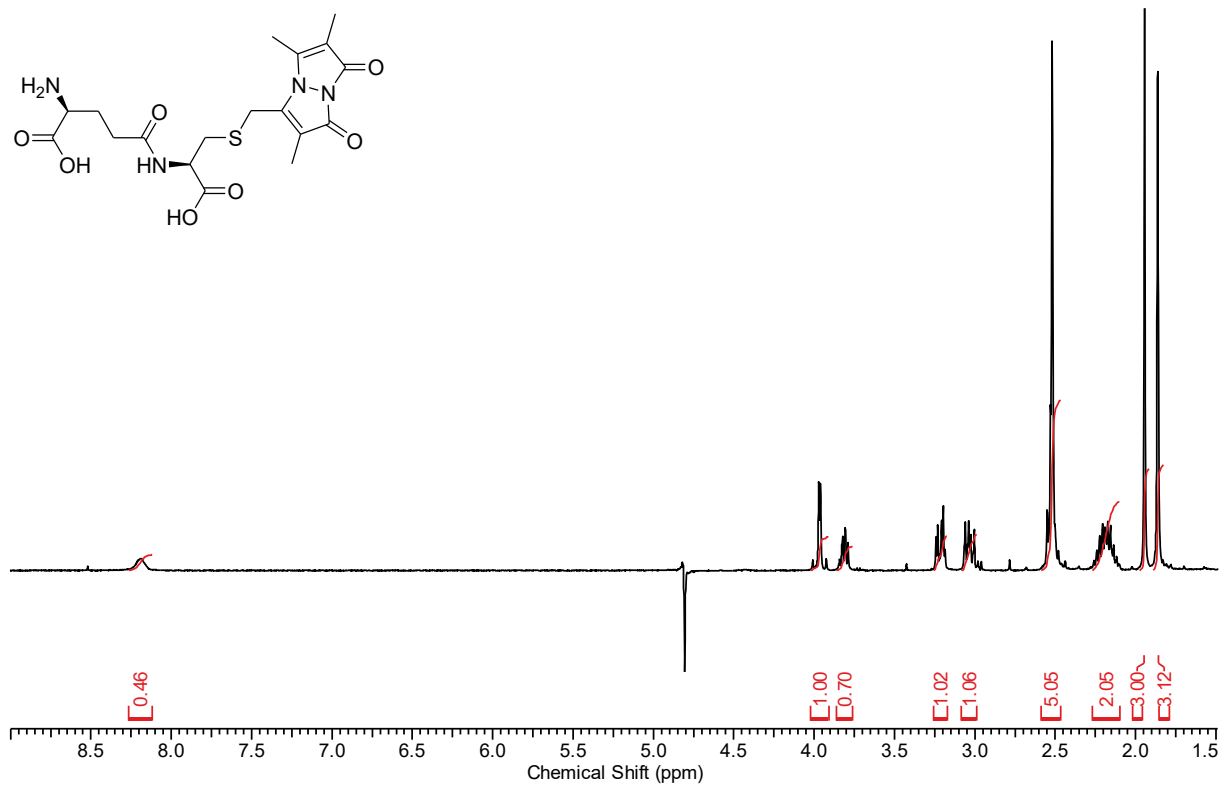
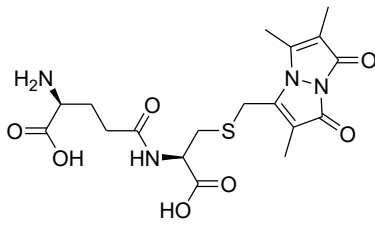
N-Boc- α -ethyl- γ -L-glutamyl-S-ditrityl-L-cysteinyl-OEt (16).



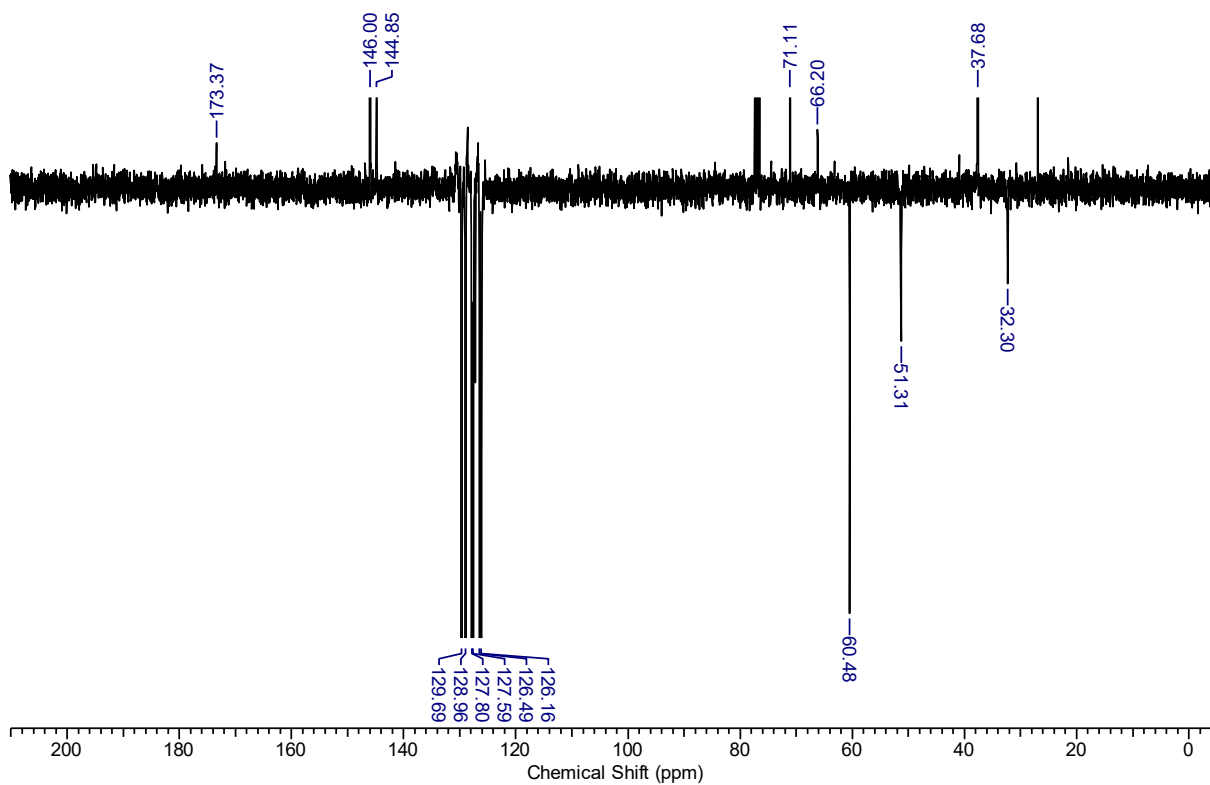
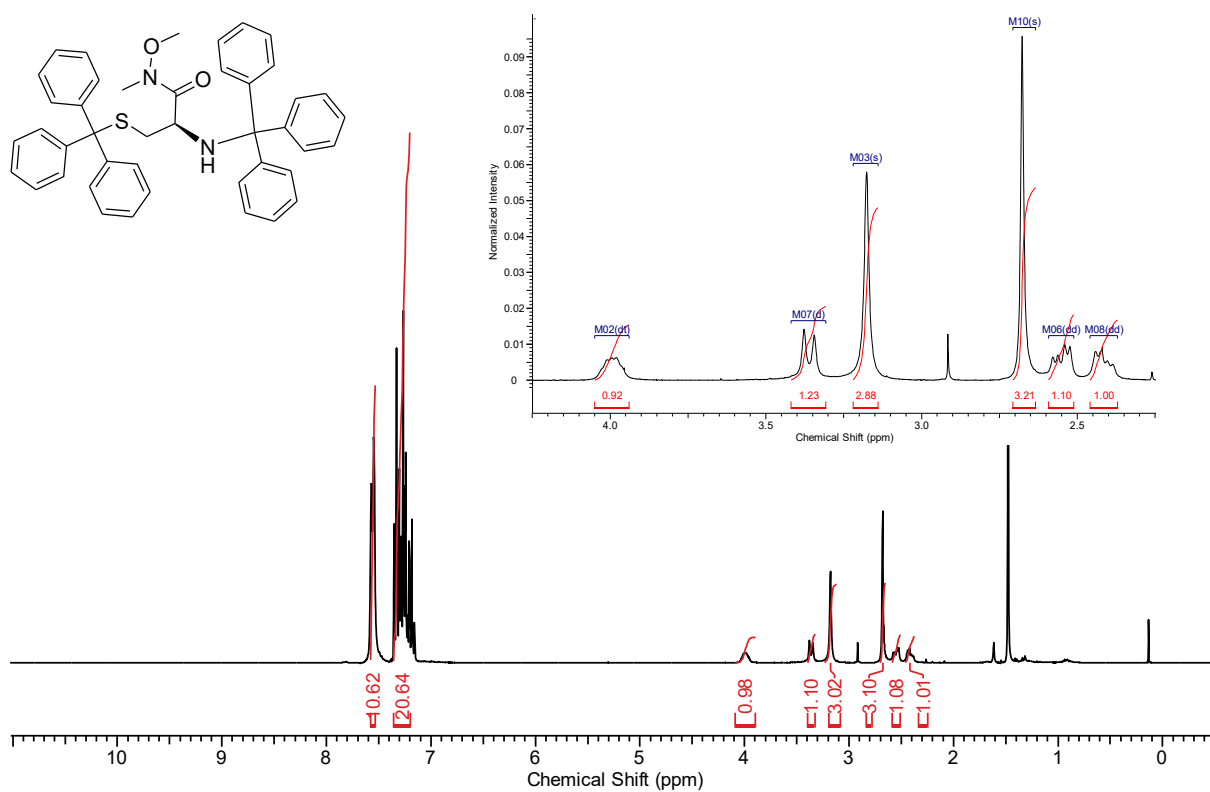
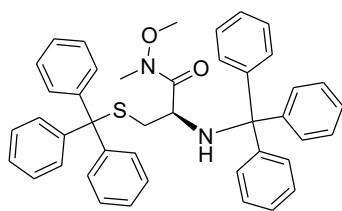
γ -GluCys (17).



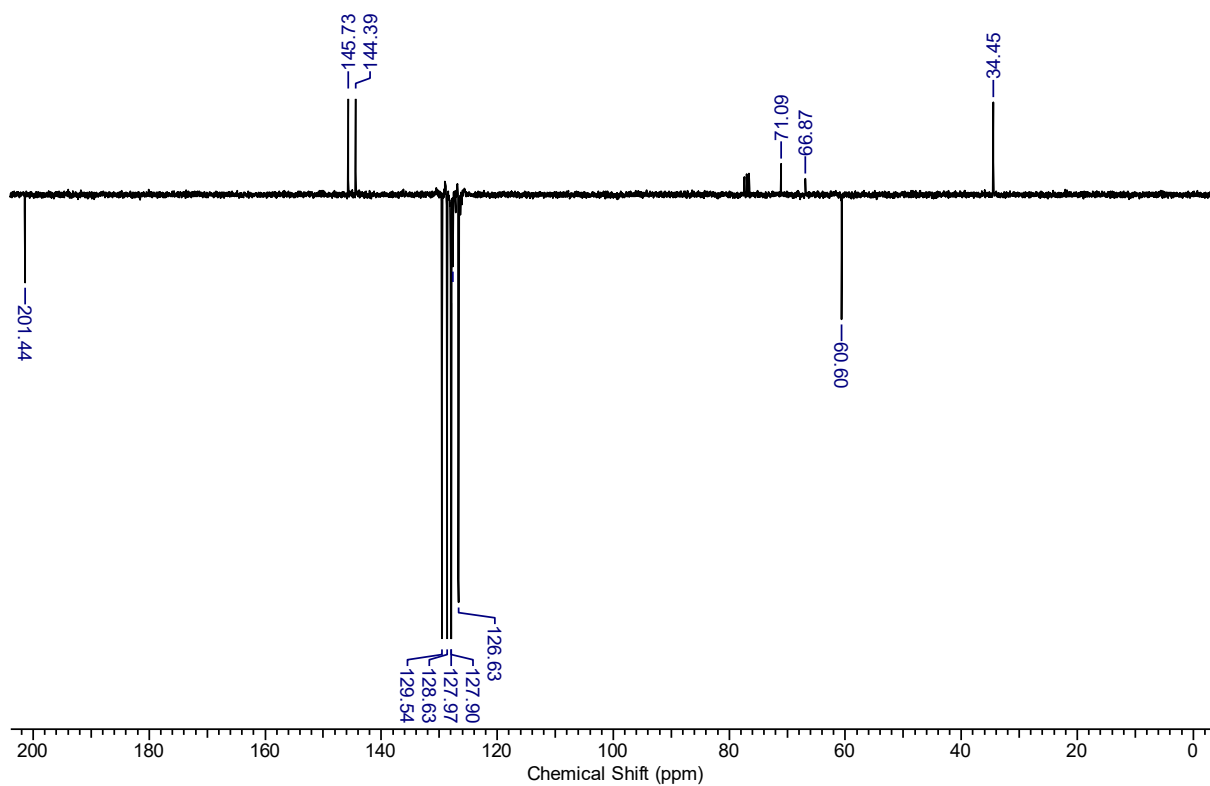
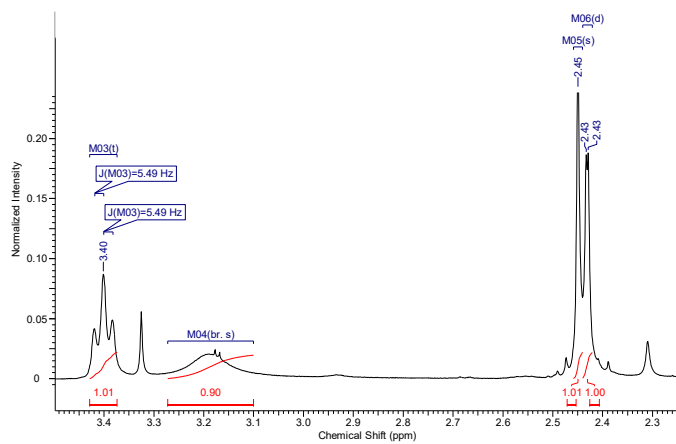
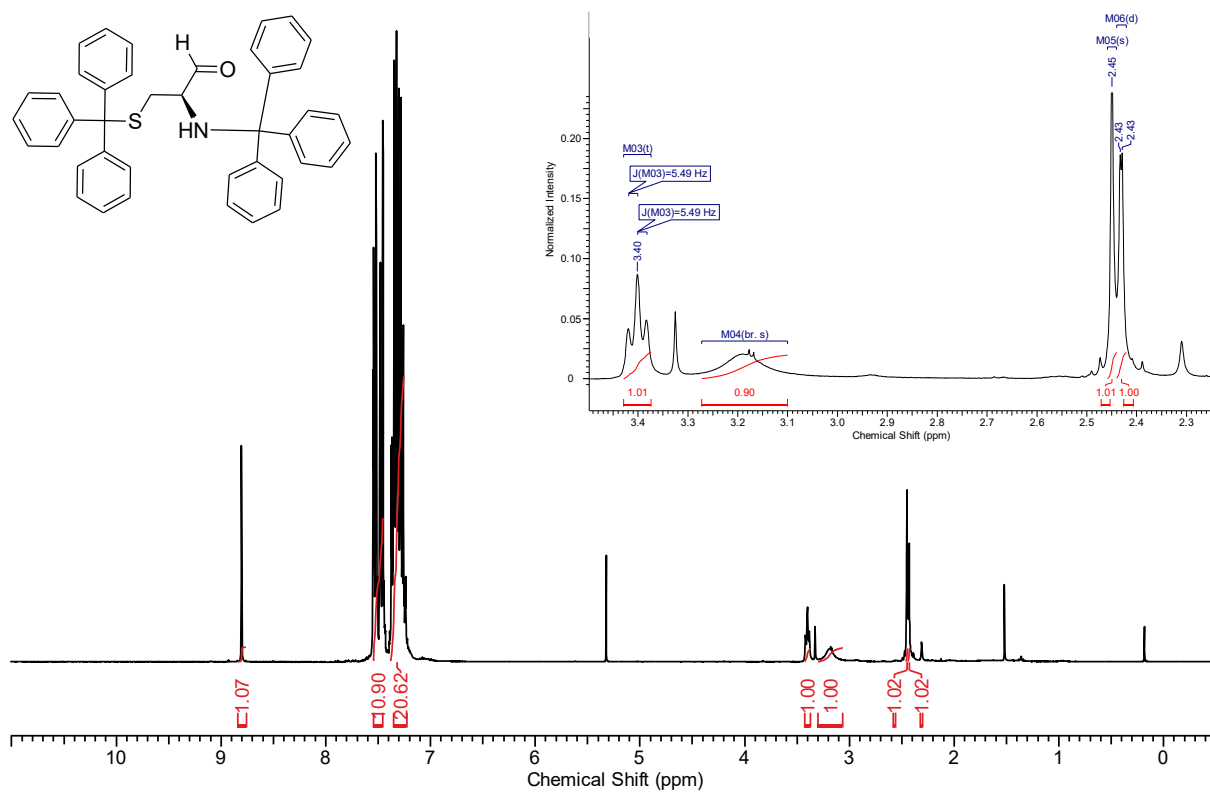
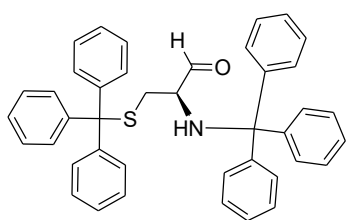
γ -GluCysBim (14).



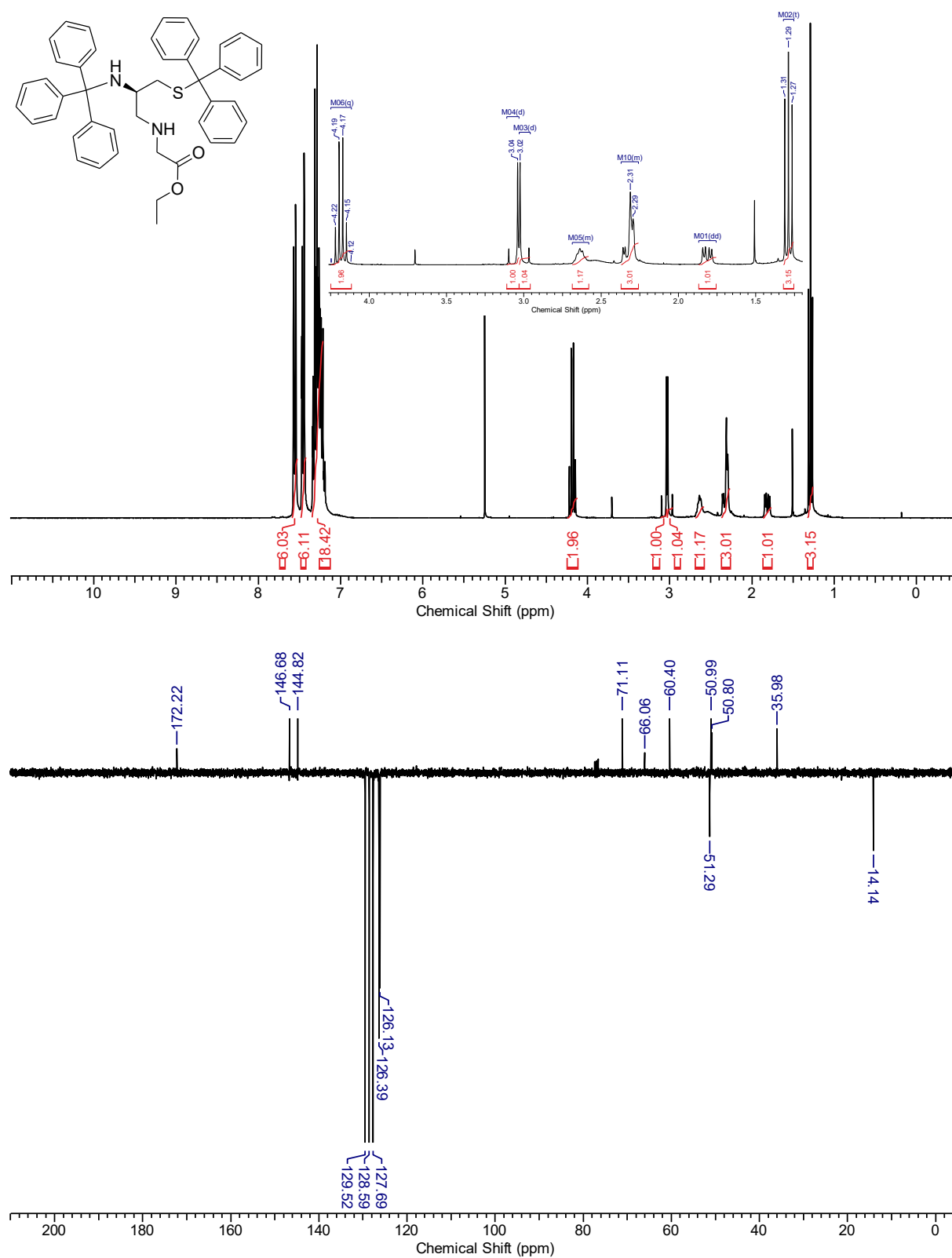
N, S-ditrityl-L-cysteinyl-NMeOMe (19).



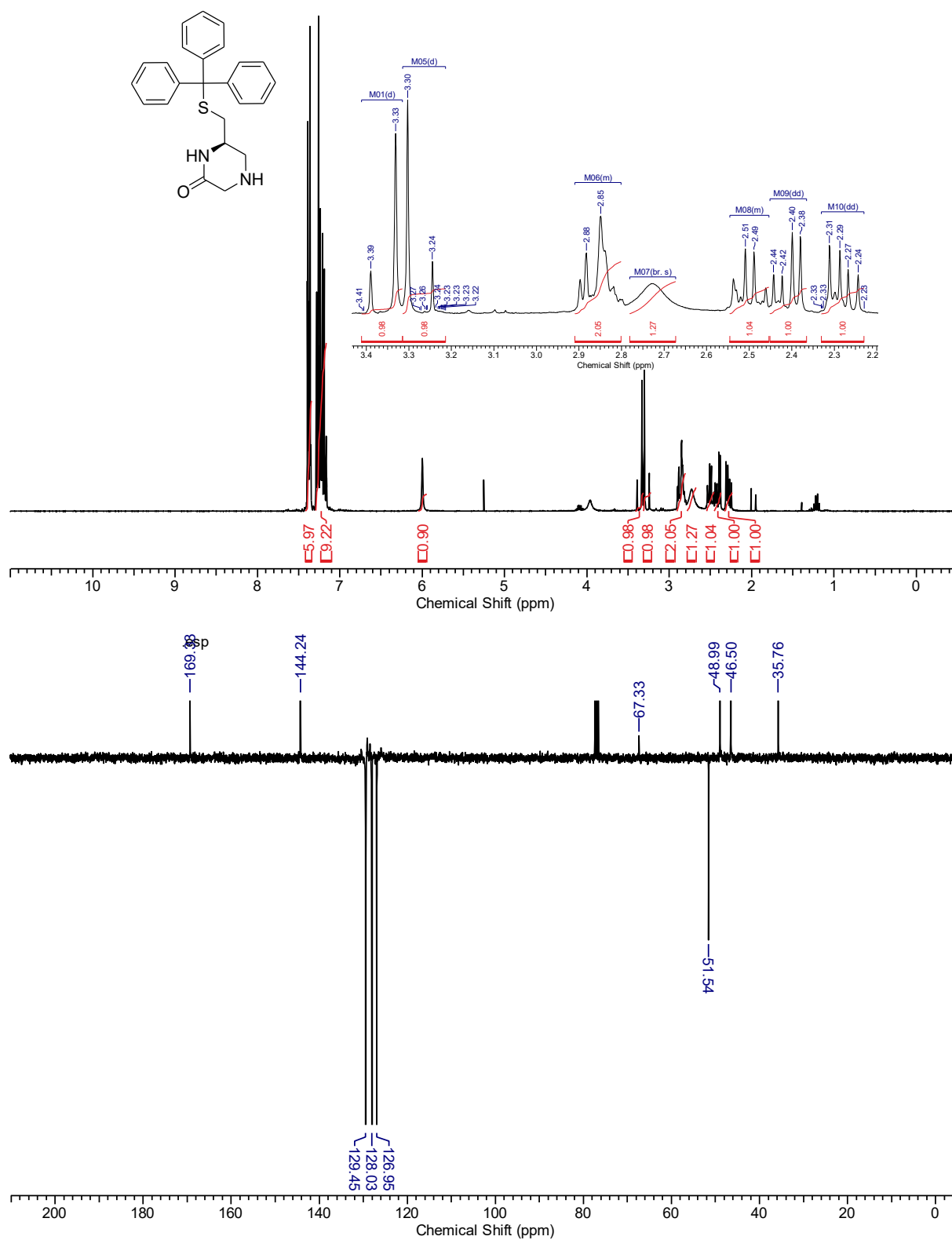
N, S-ditrityl-L-cysteinyl (18).



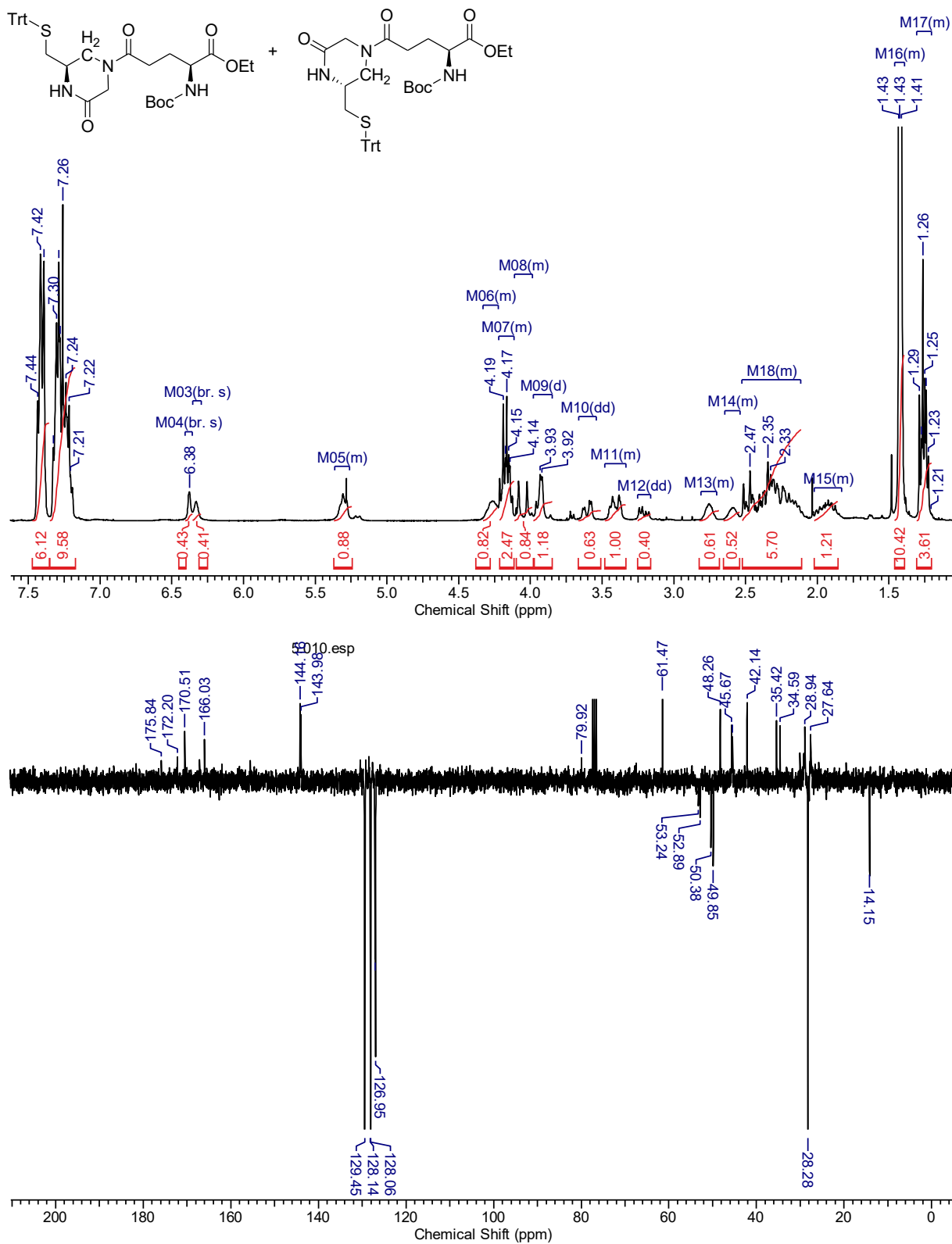
ethyl 2-((R)-2-(tritylamino)-3-(tritylthio)propylamino)acetate (20).



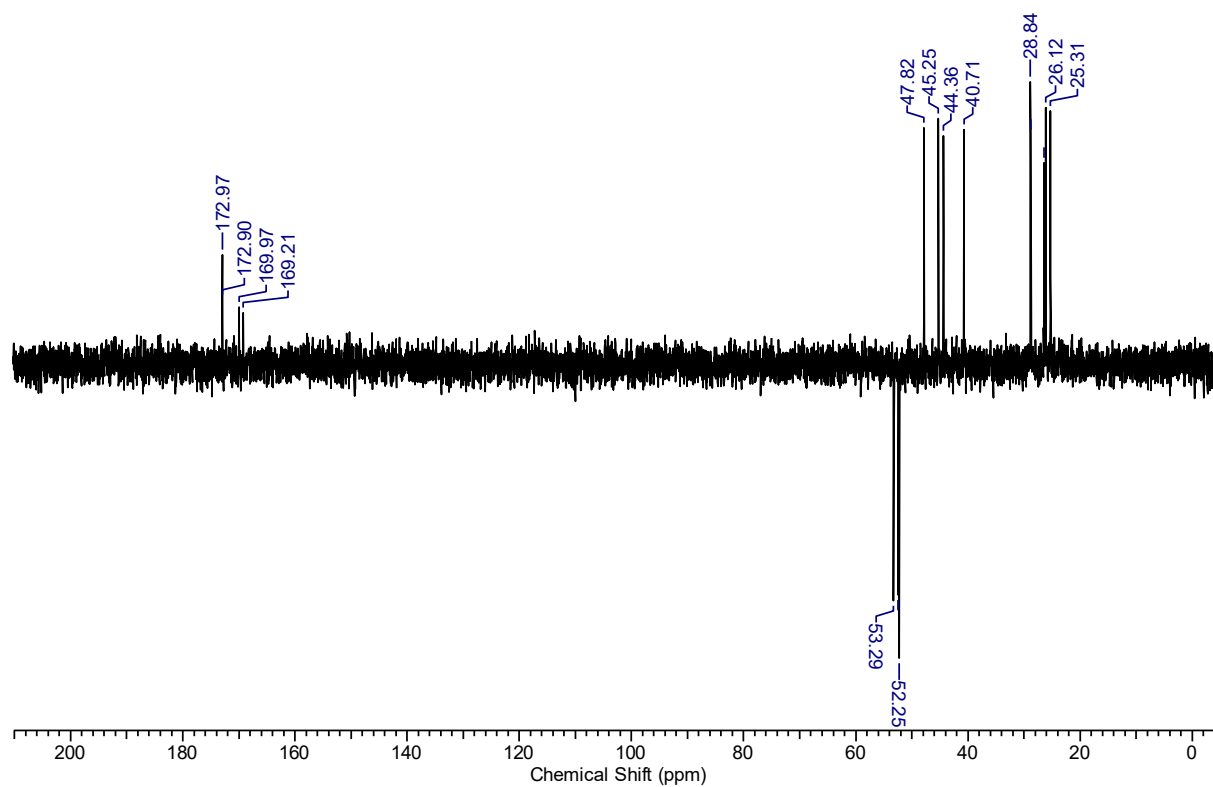
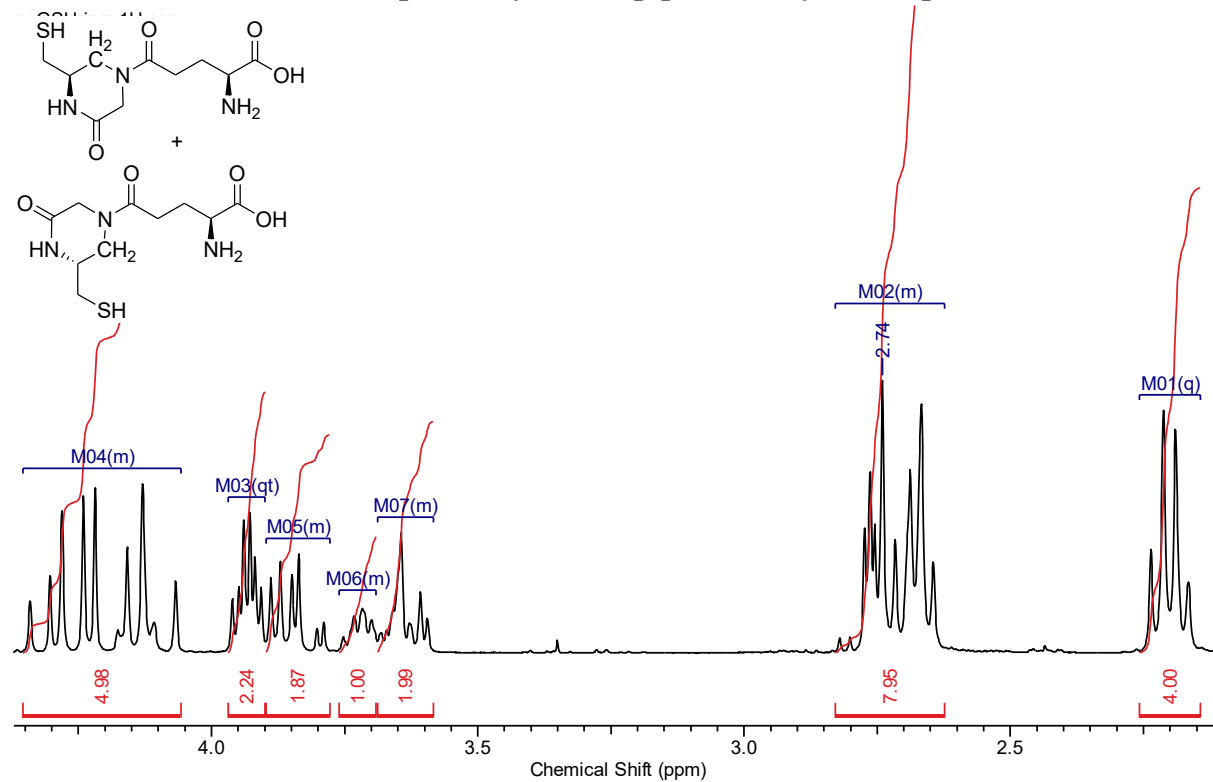
(R)-6-((tritylthio)methyl)piperazin-2-one (21).



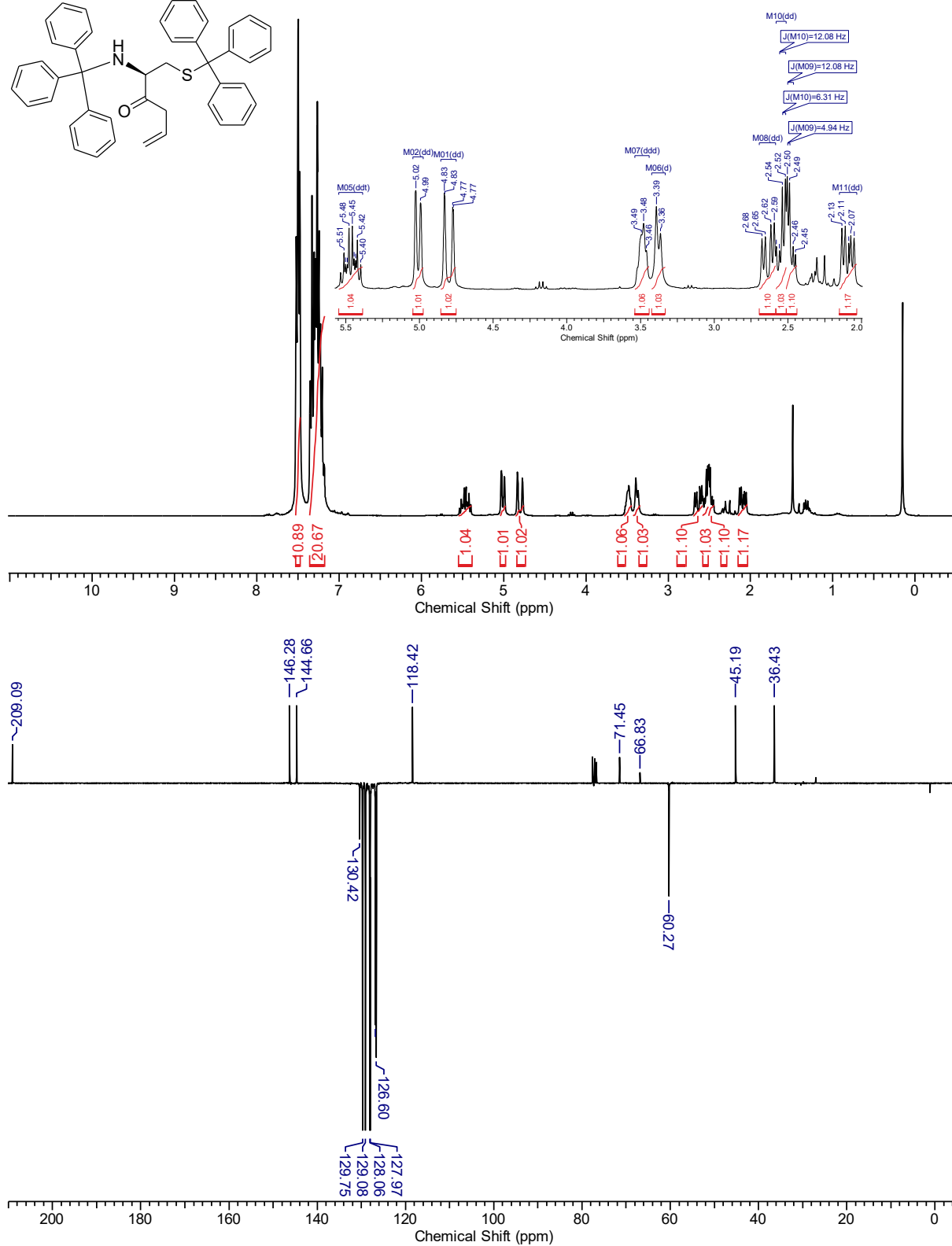
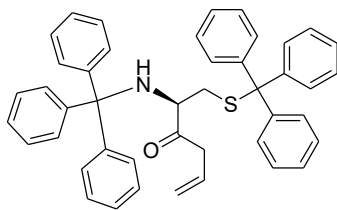
tert-butyl (S)-1-(ethoxycarbonyl)-4-oxo-4-((R)-3-oxo-5-((tritylthio)methyl)piperazin-1-yl)butylcarbamate (23).



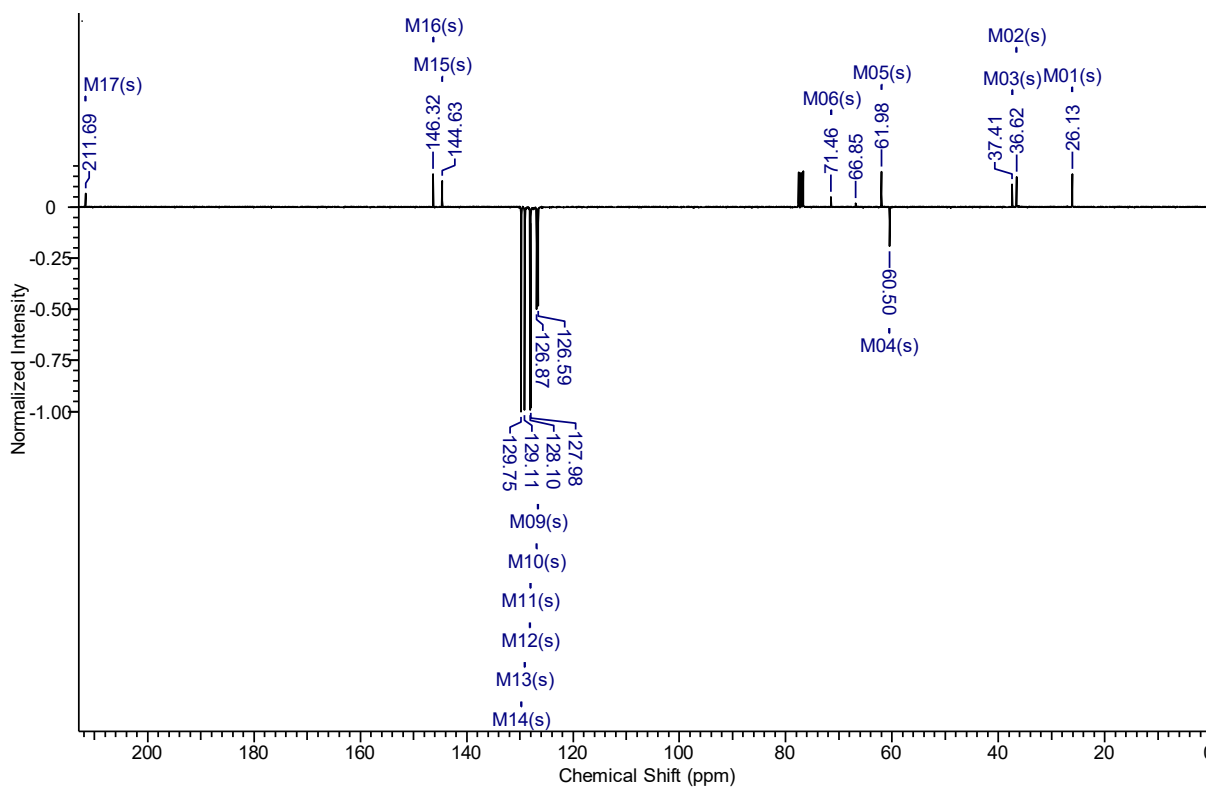
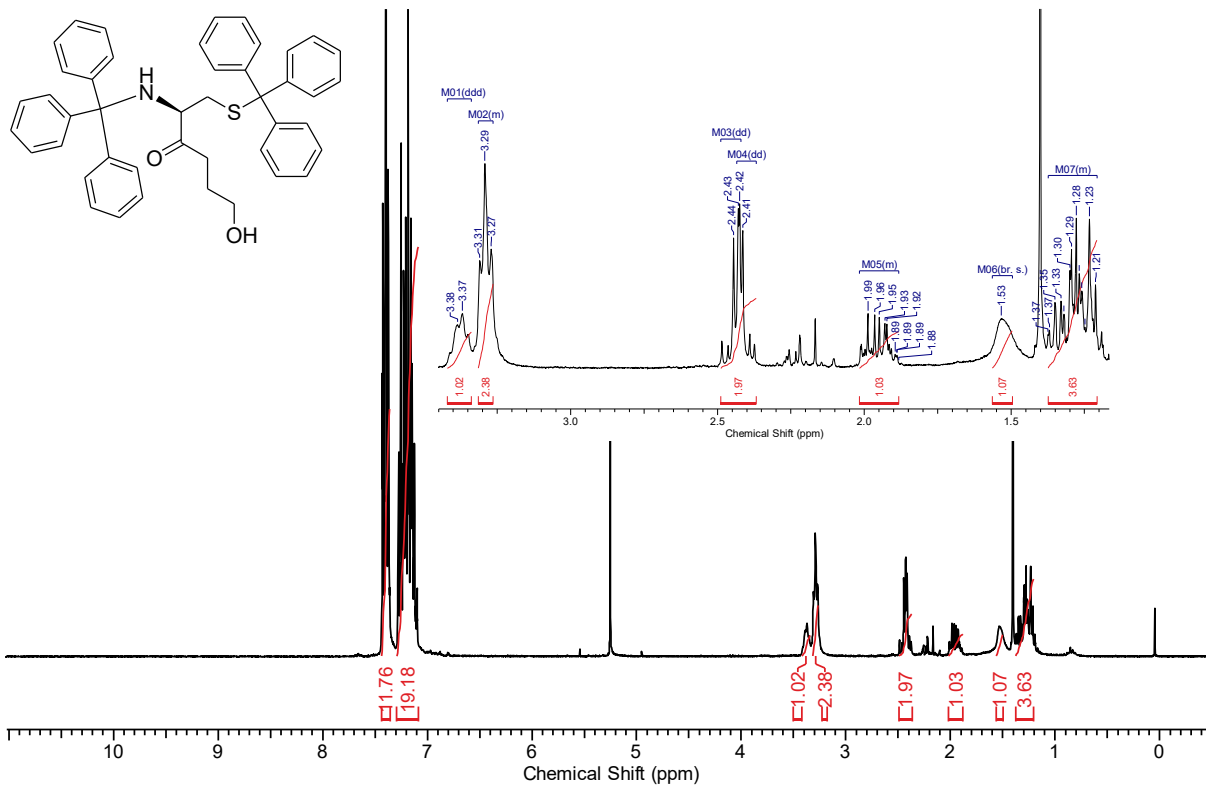
(S)-2-amino-5-((R)-3-(mercaptomethyl)-5-oxopiperazin-1-yl)-5-oxopentanoic acid (22).



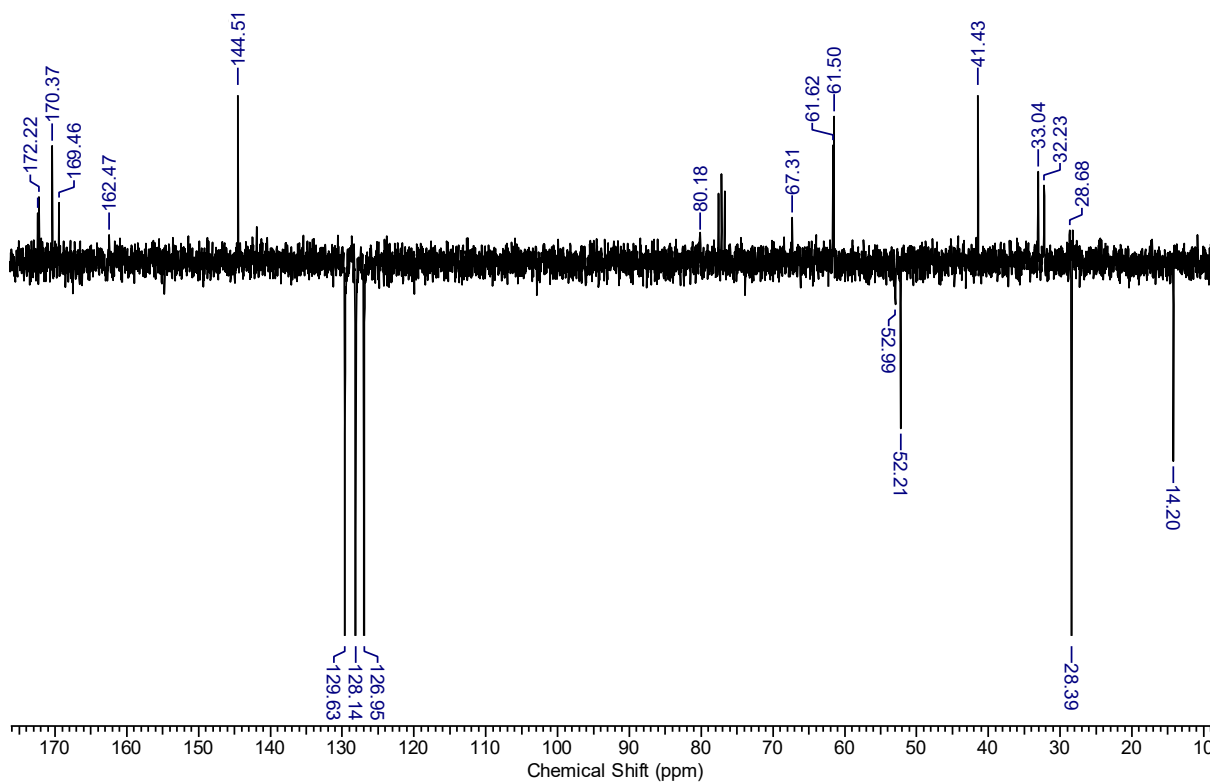
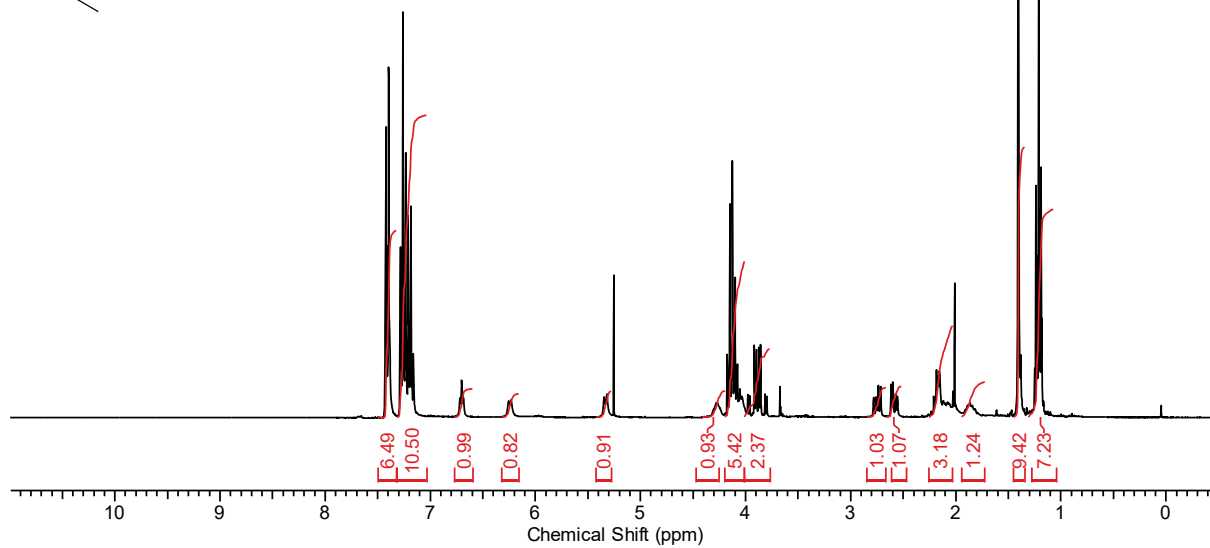
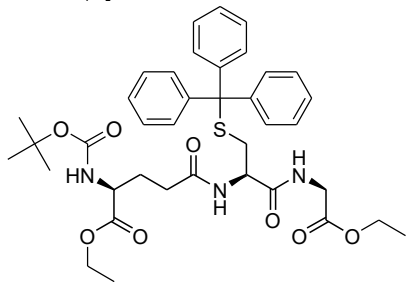
(R)-2-(tritylamino)-1-(tritylthio)hex-5-en-3-one (24).



(R)-6-hydroxy-2-(tritylamino)-1-(tritylthio)hexan-3-one (25).



Fully protected GSH.



-
- ¹ H. E. Gottlieb, V. Kotlyar and A. Nudelman, *J. Org. Chem.*, **1997**, *62*, 7512-751.
- ² ARCHIMICA CONFIDENTIAL INFORMATION. T3P® - A Unique Reagent for Selective Transformations of Multifunctional Molecules. 1. Peptide Couplings and Amide Formation. Standard Procedure for Peptide and Amide Couplings. Recommended General Reaction Procedure.
- ³ Y. Kim, Y. W. Ebright, A. R. Goodman, D. Reinberg, R. H. Ebright, *Nucleic Acids Research*, **2008**, *36*, 6143–6154.
- ⁴ N. Inguibert, P. Coric, H. Dhotel, C. Llorens-Cortes, M.-C. Fournie'-Zaluski and B.P. Roques, *J Label Compd Radiopharm*, **2004**, *47*, 997–1005.
- ⁵ A. Radkowsky, E. M. Kosower, *J. Am. Chem. Soc. Chem Soc.*, **1986**, *108*, 4527–4531.
- ⁶ a) A. Rosowsky, Ch. M. Vaidya, H. Bader, J. E. Wright, B. A. Teicher, *J. Med. Chem.*, **1997**, *40*, 286–299.
- b) S. Wiejak, E. Masiukiewicz and B. Rzeszotarska, *Chem. Pharm. Bull.*, **2001**, *49*, 1189–1191.
- ⁷ Tritylation reactions based on metallic catalysts Patent WO 2007/009944 A1.
- ⁸ Zervas, Leonidas, *Journal of the American Chemical Society*, **1962**, *84*, 3887-97.
- ⁹ A. Rainer, J. Danklmaier, H. Hoenig, H. Kandolf, *Synthesis*, **1987**, *7*, 635–637.
- ¹⁰ N. S. Trotter, S. Nicholas, *Bioorganic & Medicinal Chemistry*, **2004**, *13*, 501-517.
- ¹¹ M. K. Dhaon, R. K. Olsen, K. Ramasamy, *J. Org. Chem.*, **1982**, *47*, 1962-1965.
- ¹² Min, Tao, *Medicinal Chemistry Research*, **2009**, *18*, 495-510.
- ¹³ Delalande, Olivier, *FEBS Journal*, **2010**, *277*, 5086-5096.
- ¹⁴ Sheehan, John C., *Journal of the American Chemical Society*, **1958**, *80*, 1158-64.
- ¹⁵ J.-A. Fehrentz, B. Castro, *Synthesis*, 1983, 676-678.
- ¹⁶ D. L. Bertuzzi, G. Perli, C. B. Braga and C. Ornelas, *New J. Chem.*, **2020**, *44*, 4694-4703.

Eidesstattliche Versicherung

Hiermit versichere ich an Eides statt, dass ich die vorliegende Arbeit selbstständig verfasst und keine anderen als die von mir angegebenen Quellen und Hilfsmittel verwendet habe.

Weiterhin erkläre ich, dass ich die Hilfe von gewerblichen Promotionsberatern bzw. -vermittlern oder ähnlichen Dienstleistern weder bisher in Anspruch genommen habe, noch künftig in Anspruch nehmen werde.

Zusätzlich erkläre ich hiermit, dass ich keinerlei frühere Promotionsversuche unternommen habe.

Bayreuth, den

Unterschrift